Hanna Maria Kauko

Light response and acclimation of microalgae in a changing Arctic

Hanna Maria Kauko

Doctoral thesis

NTNU
Norwegian University of
Science and Technology

NTNU
Norwegian University of
Science and Technology

NTNU

Hanna Maria Kauko

Light response and acclimation of microalgae in a changing Arctic

NTNU
Norwegian University of
Science and Technology

Acknowledgements

First and foremost I would like to thank my supervisor at the Norwegian Polar Institute, Philipp Assmy. He created and led the project (Boom or bust) which my PhD position was part of, so without that I couldn't have joined the N-ICE2015 project. He is very nice to work with, passionate about algae and truly cared about his group, and was absolutely essential in carrying out the biological part of N-ICE2015. Geir Johnsen, my supervisor at NTNU, gave the possibility to complete a PhD within the project by having long experience both in bio-optics and in supervising PhD students. I appreciated his enthusiasm and care for his students. Mats Granskog has not only been guiding me through the PhD journey but was also the chief scientist of N-ICE2015. His interests span across physics, biology and chemistry, which bridges the groups.

In my PhD period, I have been lucky to have been surrounded by many post docs, that had N-ICE2015 as their main task and consequently we had the same goals and received a lot of help from each other. I have learned a lot from all of you, and it has been a great 'family' to grow up in. I worked tightly with Alexey Pavlov, again, a very nice person to work with, who shares my bio-optical interests. If I had a problem or a question, whether about the subject or on some practical matters about the different sides of academic research, I would walk to his office. Mar Fernández-Méndez and Lasse Mork Olsen on the biology side were my group and we together carried out the field sampling in the biologically most active time period. Mar has many resources, not least in presenting, about which I have learned a lot. Lasse has long experience in various aspects of algal ecology, and if I had a question about topics in my second paper, I would go to him. Others in the biology group, Pedro Duarte, Anette Wold and Haakon Hop, have also greatly contributed to this journey. Without Anette, nothing practical would work, and Pedro has done pretty much everything and consequently can help e.g. with coding, statistics, ecological theory, or laboratory methods.

The physics post docs, Amelie Meyer, Anja Rösel, Polona Itkin, Lana Cohen, Jennifer King and Rob Graham have also been a central force in N-ICE2015, part of the 'family' I mentioned and I'm happy to have gotten to know you. Steve Hudson was essential for

Abstract

This thesis investigates ice-associated and under-ice algal communities, and the controlling role of light in the Arctic pack ice region. Changes in the light regime are a consequence of the substantial environmental changes happening in the Arctic. To this end the research vessel *Lance* was frozen into the pack ice north of Svalbard (80.2–82.8 °N) for nearly half a year from January to June 2015 during the Norwegian young sea ICE (N-ICE2015) expedition to study the new, thinner sea ice regime and associated environmental and ecosystem processes. The presented results from the spring and early summer season (April–June) suggest that an under-ice phytoplankton bloom can develop and grow under the opaque ice cover because open and refrozen leads acted as light conduits into the water column. The ratio of photoprotective (PPC) to photosynthetic (PSC) carotenoids indicated that the bloom was low-light acclimated, which supports the conclusion of in situ growth under the ice pack. The pigment ratios were in addition related to the slope of in situ absorption measurements between 488 and 532 nm (affected by absorption by PPC and PSC, respectively) to evaluate a method to assess the photoacclimation state of phytoplankton blooms in situ. We also studied the young ice in a refrozen lead which had a thin ice and snow cover and high light transmittance of up to 0.41. Under-ice irradiance, E_d(PAR) (photosynthetically active radiation, 400 to 700 nm) was up to 350 µmol photons $m^{-2} s^{-1}$, and the high light conditions resulted in accumulation of cellular photoprotective pigments (mycosporine-like amino acids (MAAs) and PPC). Biomass in the lead ice (mg Chl *a* m^{-2}) did not exceed the surrounding older and thicker ice with low light availability (E_d(PAR) <20 µmol photons $m^{-2} s^{-1}$), owing likely to several factors such as time and energy needed for photoacclimation, nutrient limitation and time needed for recruitment of ice algae into the new ice habitat (the refrozen lead). The algal community in the young ice was in the beginning composed of ciliates, flagellates and dinoflagellates, and over one month developed towards dominance of typical ice-associated pennate diatoms (e.g. *Nitzschia frigida* and *Navicula* spp.). Environmental conditions such as irradiance levels did not affect the species succession to a great degree, based on multivariate statistical testing with the main environmental drivers and comparison to the surrounding older and thicker ice. This suggests that species traits and adaptations to the ice environment play an important role for algal community dynamics

in sea ice. These studies improve our understanding on ice algal ecology in a high-light habitat and offer new insights into community development in newly formed sea ice in spring. The origin of the sea ice diatoms in the young lead ice was in the surrounding older ice. We also discuss the observed patterns – algal blooms in the different habitats – with respect to the physical changes in the icescape. Thinning and increased drifting speed of the sea ice affects the dynamics in the icescape and may lead to more frequent lead formation, increasing the importance of these habitats in the future Arctic.

List of papers

The thesis is based on the following four papers, referred to as Paper I–IV in bold throughout the text.

I. Assmy P, Fernández-Méndez M, Duarte P, Meyer A, Randelhoff A, Mundy CJ, Olsen LM, **Kauko HM** et al (2017) Leads in Arctic pack ice enable early phytoplankton blooms below snow-covered sea ice. Sci Rep 7:40850. doi:10.1038/srep40850

II. **Kauko HM**, Taskjelle T, Assmy P, Pavlov A, Mundy CJ, Duarte P, Fernández-Méndez M, Olsen LM, Hudson SR, Johnsen G, Elliott A, Wang F, Granskog MA (2017) Windows in Arctic sea ice – light transmission and ice algae in a refrozen lead. J Geophys Res Biogeosciences 122:1486-1505. doi:10.1002/2016JG003626

III. **Kauko HM**, Olsen LM, Duarte P, Peeken I, Granskog MA, Johnsen G, Fernández-Méndez M, Pavlov AK, Mundy CJ, Assmy P (2018) Algal colonization of young Arctic sea ice in spring. Front Mar Sci. 5:199. doi: 10.3389/fmars.2018.00199

IV. **Kauko HM**, Pavlov AK, Johnsen G, Granskog MA, Peeken I, Assmy P. Assessing photoacclimation state of an Arctic under-ice phytoplankton bloom using in situ absorption measurements. *Manuscript*

Other co-authored papers that are referred to in the thesis:

Duarte P, Meyer A, Olsen LM, **Kauko HM**, Assmy P, Rösel A, Itkin P, Hudson SR, Granskog MA, Gerland S, Sundfjord A, Steen H, Hop H, Cohen L, Peterson AK, Jeffery N, Eliott SM, Hunke EC, Turner AK (2017) Sea-ice thermohaline-dynamics and biogeochemistry in the Arctic Ocean: empirical and model results. J Geophys Res Biogeosciences 122:1632-1654. doi:10.1002/2016JG003660

Fernández-Méndez M, Olsen LM, **Kauko HM**, Meyer A, Rösel A, Merkouriadi I, Mundy CJ, Ehn JK, Johansson AM, Wagner PM, Ervik Å, Sorrell BK, Duarte PM, Wold A, Hop H, Assmy P (2018) Algal hot spots in a changing Arctic Ocean: Sea-ice ridges and the snow-ice interface. Front Mar Sci 5:75. doi:10.3389/fmars.2018.00075

Olsen LM, Laney SR, Duarte P, **Kauko HM**, Fernández-Méndez M, Mundy CJ, Rösel A, Meyer A, Itkin P, Cohen L, Peeken I, Tatarek A, Różańska M, Wiktor J, Taskjelle T, Pavlov A, Hudson SR, Granskog MA, Hop H, Assmy P (2017) The seeding of ice-algal blooms in Arctic pack ice: the multiyear ice seed repository hypothesis. J Geophys Res Biogeosciences 122:1529-1548. doi:10.1002/2016JG003668

Pavlov A, Taskjelle T, Hamre B, **Kauko HM**, Hudson SR, Assmy P, Duarte P, Fernández-Méndez M, Mundy CJ, Granskog MA (2017) Altered inherent optical properties and estimates of the underwater light field during an Arctic under-ice bloom of *Phaeocystis pouchetii*. J Geophys Res Oceans 122:4939-4961. doi:10.1002/2016JC012471

Table of Contents

1. Preface

With respect to the observed climate changes in the Arctic, the trends and dynamics in Arctic marine primary production are of major research focus. Through photosynthesis, autotrophic algae convert inorganic carbon dioxide (CO_2) to organic biomass (hence primary production) and by this form the basis of the marine food web. The rate at which they are able to photosynthetize and grow determines the energy flow through the marine ecosystem. Algae need especially two resources to be able to perform photosynthesis: light energy from the sun and nutrients.

One of the most profound effects of the ongoing climatic changes is the reduction in the extent and thickness of the Arctic sea-ice cover. As a consequence light availability for ice algae and phytoplankton is expected to increase. Therefore, questions arise: How do the algae respond to this? Are growth or community composition affected by the increased light availability? Are the algae able to protect themselves from excess light? But also: How can we retain more information from this logistically challenging study area?

"Science is always a work in progress and our publications mere progress reports on an endless journey toward understanding." (Behrenfeld and Boss 2018)

2. Scope of thesis

This work was part of the Norwegian young sea ICE (N-ICE2015) expedition (Granskog et al. 2016, 2018), during which the research vessel *Lance* was frozen into the pack ice north of Svalbard for nearly 6 months (January–June 2015; Figure 1). A multidisciplinary science team studied the physical and biological processes of the new, thinner Arctic sea ice regime. The expedition included in total four drifts (four ice floes), and this thesis focuses on the spring time, i.e. Floes 3 and 4 (22 April until 22 June 2015).

In this thesis, I have concentrated on refrozen leads and their impact on ice algal growth and community development, under-ice phytoplankton bloom dynamics and algal photoacclimation. I present two cases: young ice that formed in an open lead next to Floe 3 (Figure 2), and an under-ice phytoplankton bloom that was observed in the water column. The main objectives of the individual papers that the thesis builds upon were:

Paper I: To understand how an under-ice phytoplankton bloom developed despite the thick snow cover.

Paper II: To describe the bio-optical properties of newly formed sea ice in a refrozen lead, and to quantify the ultraviolet (UV) -protective pigments of the ice algae and the role of algae in light transmission through thin sea ice.

Paper III: To describe the succession of the ice algal community in the early stages of sea ice growth in a refrozen lead, and to understand the origin of the ice algal community and the effect of environmental drivers such as irradiance on community composition.

Paper IV: Evaluation of a method to use in situ absorption measurements to assess the photoacclimation state of an under-ice phytoplankton bloom.

Algal responses to the light transmitted through the thin ice in the leads, and consequences of the changing sea ice regime are unifying themes of the papers included in this thesis. The leads acted like windows, channelling light into the water column for phytoplankton growth (paper I and IV). Refrozen leads also act as high-light habitats for ice algae (Figure 3; paper II and III). In addition, the co-authored papers (Duarte et al. 2017, Olsen et al. 2017, Fernández-Méndez et al. 2018) investigated other, adjacent sea-ice habitats, that is,

thicker first-year and second-year ice, sea ice ridges and snow infiltration communities. Together these papers give a comprehensive picture of algal habitats and ecology in spring Arctic pack ice. Algal responses such as biomass accumulation (growth), cellular photoprotective pigment accumulation, and species composition were investigated (Figure 4). The methods applied are described in the respective papers. In the thesis, first an introduction to the topic is given in chapter 3. The thesis papers are discussed in chapters 4–6, in connection with related papers from the N-ICE2015 expedition (including the co-authored papers) and other relevant literature. The co-authored paper by Fernández-Méndez et al. (2018) is discussed in chapter 4.5.
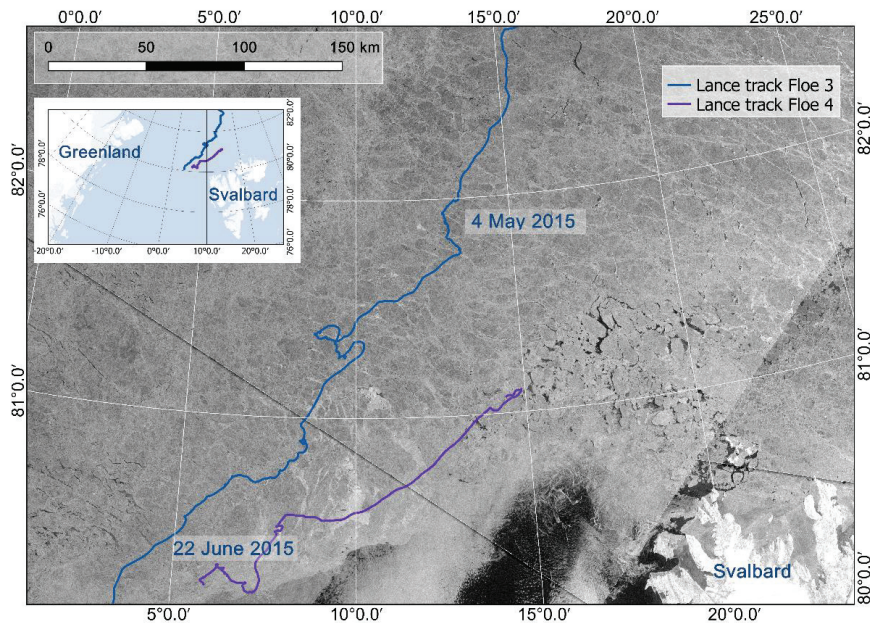
Figure 1 Map showing the drift tracks of R/V Lance when anchored to Floes 3 and 4, i.e. the study period covered in this thesis. Sampling on the refrozen lead started on 4 May and lasted until 3 June. The under-ice bloom was encountered 25 May and was sampled until 22 June, which was the end of the campaign. Map modified from **paper II**. Satellite image (from 25 May 2015) source: RADARSAT-2 image provided by NSC/KSAT under the Norwegian-Canadian RADARSAT agreement. RADARSAT-2 Data and Products © MacDonald, Dettwiler and Associates Ltd (2013). All Rights Reserved. RADARSAT is an official mark of the Canadian Space Agency. Map created by the Norwegian Polar Institute/Max König.
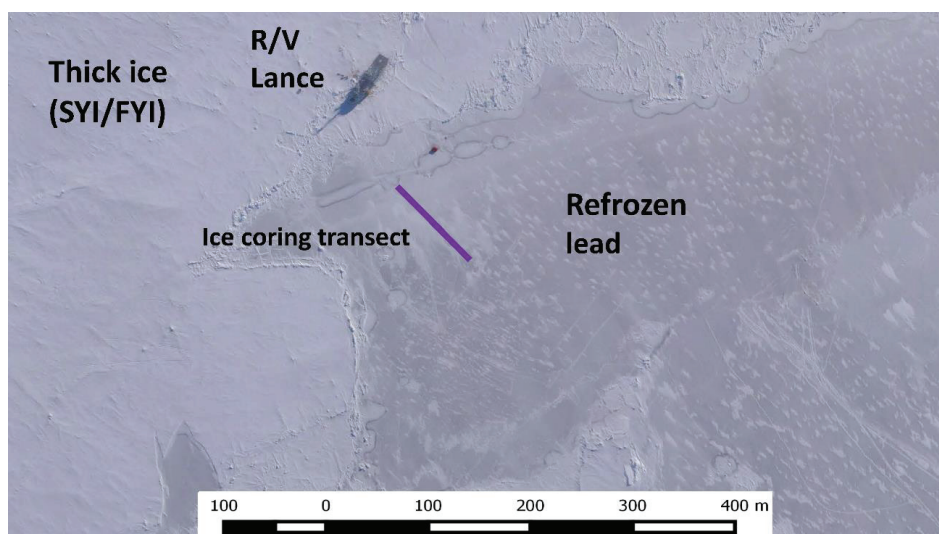
Figure 2 Map showing the R/V Lance attached to Floe 3 during N-ICE2015 and the studied refrozen lead (the grey area on the right part of the image) with the ice coring (sampling) transect. SYI: second-year ice, FYI: first-year ice. Modified from **paper II**. See papers II and III for more details on sampling. Aerial image (from 23 May 2015) source: Vasily Kustov and Sergey Semenov (Arctic and Antarctic Research Institute, St. Petersburg, Russia).
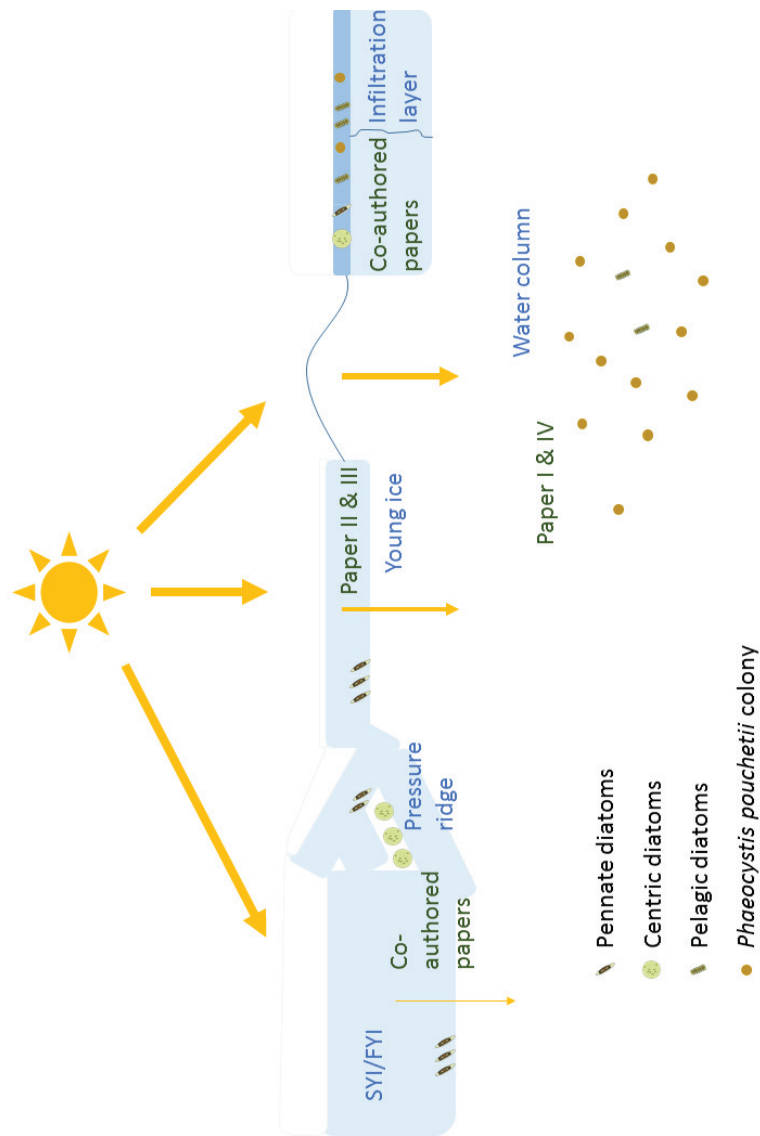
Figure 3 The different algal habitats included in this thesis. From left: thick first-year (FYI) or second-year ice (SYI) and a pressure ridge (the former discussed mainly in chapter 4.2 and the latter in chapter 4.5, based on co-authored papers). Thin, young ice in a refrozen lead and under-ice water column are the focus of this thesis (papers I–IV). On the right a snow infiltration community (discussed in chapter 4.5, based on a co-authored paper). Light transmittance varied between the ice types and open water (yellow arrows). Different algal groups were dominant in the different habitats during the bloom phase (see legend).
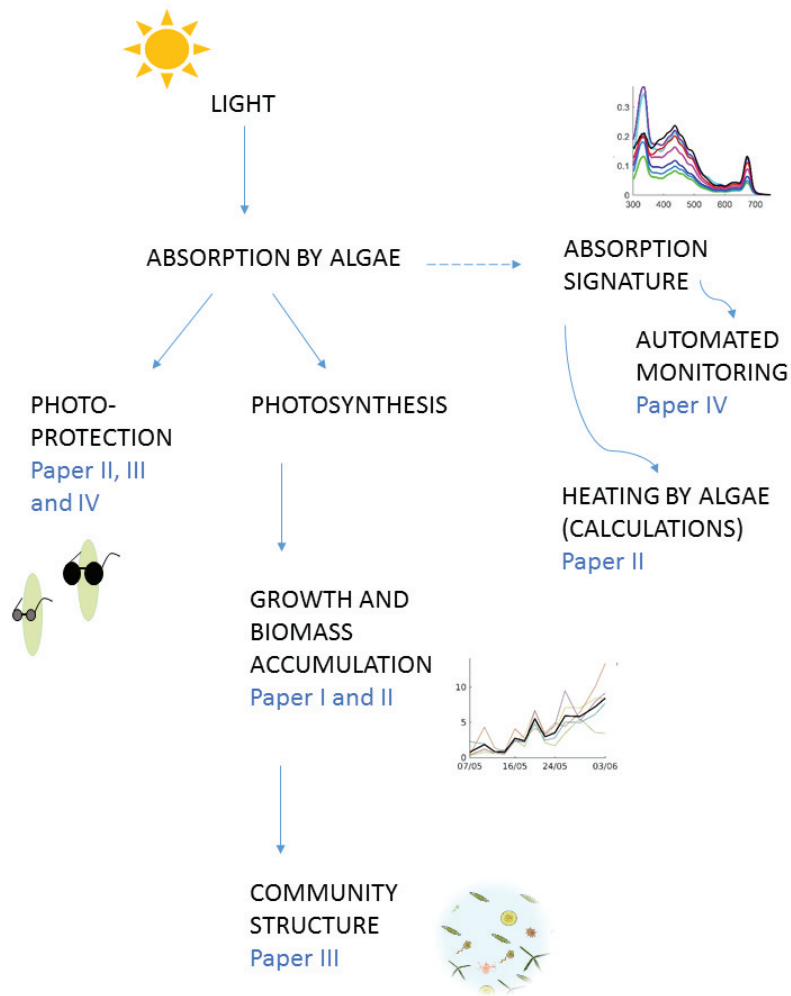
Figure 4 Graphical presentation of the different topics of algal bio-optics and ecology studied in this thesis. Growth and biomass accumulation are discussed in chapters 4.1 and 4.2, community structure in chapter 4.3, photoprotection in chapter 4.4, heating by algae in chapter 5 and automated monitoring applications in chapter 6. Source of the small figures: absorption spectrum from Figure 5 in **paper II**; biomass plot from Figure 2 in **paper II**; community structure from Figure 10 **in paper III**.

3. Introduction

3.1 General marine optics

Light is the common term for irradiance (E) in the visible part of the electromagnetic radiation (400–700 nm, also called photosynthetically active radiance, PAR). Light is a prominent environmental cue in most ecosystems and the marine environment is no exception. A comprehensive overview of aquatic optics is given for example in Jerlov (1976), Mobley (1994) and Kirk (2011). Incoming solar irradiance (E) can be measured and described in a variety of ways: in energy scale (W m^{-2}) or quanta (photon) scale (μmol photons m^{-2} s^{-1}). Further, it can be measured with a spherical sensor measuring from all angles, giving scalar irradiance E_o (360° detection angle, 4π light collector), or with a planar sensor (180° detection angle, 2π light collector, cosine corrected) measuring either downwelling (E_d) or upwelling (E_u) irradiance.

The behaviour of light in seawater (or sea ice) is for humans visible as differences in colour and transparency of the medium. The colour of sea water has been recorded also for the Arctic as part of expeditions already since the 16th century (Scoresby 1820; de Veer 1876; Nansen 1906).

When light enters a medium, it is attenuated i.e. it can either be absorbed or scattered (direction change; Kirk 2011). These are called the inherent optical properties (IOP) that only depend on the properties of the constituents. The total absorption (a) of sea water consists of, in addition to dissolved salts and gases, absorption by coloured dissolved organic matter (CDOM, also called gilvin or gelbstoff; a_{CDOM}), algal pigments (a_ϕ) and detrital (or non-algal pigments) matter (a_d), all with characteristic absorption spectra (unit m^{-1}) altering the colour of the water body. In addition, high particle concentrations lead to high scattering resulting in turbid waters (Kirk 2011). The IOPs are measured with "active sensors" having their own light source. Apparent optical properties (AOP) are dependent also on the current light field (e.g. solar angle, cloud cover) and are measured with "passive sensors", i.e. using the ambient light from the sun as a light source. An example of an AOP is the diffuse attenuation coefficient K_d which describes the total vertical light attenuation (m^{-1}).

The light regime comprises different aspects of light, both the intensity, spectral composition and day length. In the Arctic, the light regime is characterized by the extensive ice cover reducing light transmission to the water column, and the high latitudes resulting in polar night in the winter (the sun is permanently below the horizon) and midnight sun period in the summer (the sun is permanently above the horizon). In this thesis I mainly concentrate on light propagation through sea ice (mainly concerning the intensity), algal absorption properties and pigments, and their role in algal ecology and monitoring (Figure 4).

3.2 Algal optics and pigments

As mentioned above, microalgae are one of the optically active constituents, IOPs, in the water column and in sea ice. This means they absorb and scatter light and contribute to the total light attenuation. Scattering characteristics depend on species morphology such as mineralized cell walls or gas vacuoles (Kirk 2011). Absorption characteristics are determined by the pigment suite in the particular algae (Falkowski and Raven 2007; Johnsen et al. 2011; Kirk 2011) which differs between algal groups (Jeffrey et al. 2011). A typical algal absorption spectrum for e.g. diatoms is shown in Figure 5. Magnitude and "flatness" of the chlorophyll (Chl) *a* specific absorption spectra are dependent on pigment packaging in the cells (pigment "density"), which again is affected by cell size and photoacclimation state (Johnsen et al. 2011; Kirk 2011).
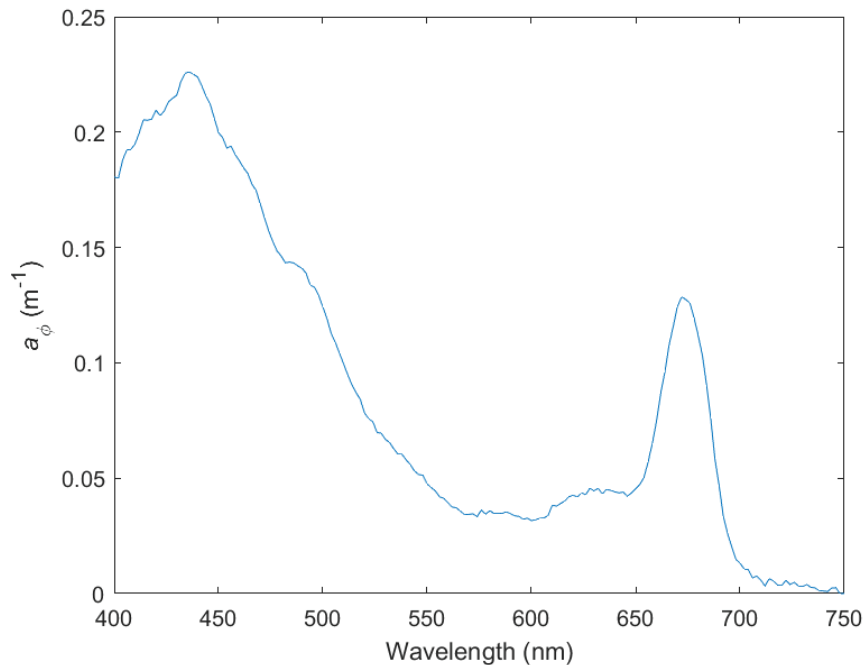
Figure 5 Algal absorption a_ϕ in the PAR range in the refrozen lead on 26 May (see also Figure 3 in **paper II**), showing the main Chl *a* absorption peaks at 440 and 674 nm and absorption peaks/shoulders by carotenoids between 450 and 550 nm (especially fucoxanthin) and by different chlorophylls between 550 and 640 nm (especially Chl *c*).

Algae are exposed to a highly variable light regime that on different time scales depends on for example snow cover (especially in the case of ice algae; see next chapter), solar angle, vertical mixing, cloud cover or waves (Kirk 2011). This means that at times algae need to maximize light absorption and the corresponding utilization, whereas at other times light is available in excess and absorbing and channelling too much of it to photosynthesis would damage the photosynthetic machinery and the molecules involved in photosynthesis. Balancing the amount of light absorbed and used in photosynthesis is therefore a major component in algal photophysiology and involves several mechanisms that span over time scales of seconds to weeks (Brunet et al. 2011). Algae can for example alter the pigment pool and the fraction of photoprotective and photosynthetic pigments and thus alter the relation of light absorbed (all cellular pigments) and utilized for

11

photosynthesis (all light harvesting pigments). Photoprotective pigments absorb light efficiently but dissipate it directly as heat instead of passing the energy on to photosystem (PS) II and I for photosynthesis. Photoprotective carotenoids (PPC) absorb mainly in the blue-green part of the visible radiation (350–500 nm) (Johnsen et al. 2011) and mycosporine-like amino acids (MAAs) have absorption maxima in the UV range (309–360 nm) (Carreto et al. 2011). These processes are part of the photoacclimation capabilities of algae, which means physiological adjustments in the algal cell, whereas adaptation refers to long-term, genetic changes on evolutionary timescales (Brunet et al. 2011).

Separating, identifying and quantifying algal pigments by means of high-performance liquid chromatography (HPLC) is a widely used method to gain information on the algal community (Jeffrey et al. 1997; Higgins et al. 2011). Firstly, pigment composition varies between algal groups, as mentioned above, and some pigments are specific to certain groups, thus taxonomic information can be retrieved from knowing the pigments in a sample. For example, peridinin indicates the presence of dinoflagellates and alloxanthin is specific for cryptophytes (Jeffrey et al. 2011). Secondly, fractions of photoprotective pigments indicate photoacclimation status. The carotenoids diadino- and diatoxanthin are the main photoprotective pigments of most chromophytes (Chl c -containing algae) such as diatoms (Brunet et al. 2011). Because the in vivo algal absorption spectrum comprises individual pigment signatures, relating pigments and algal absorption characteristics has also been a field of study aiming both to model algal absorption spectra from individual pigments, and to decompose algal absorption spectra to individual pigments (reviewed in Johnsen et al. (2011)). The better the dependency of the sum absorption spectrum on the individual constituents is known, the more information can be retrieved from the absorption spectra, which has relevance e.g. for remote sensing applications (e.g. Organelli et al. 2013).

3.3 Light transmission through sea ice

Transmittance (T) denotes the fraction of incoming irradiance that passed through the snow and ice pack, whereas albedo describes the fraction that is reflected from the surface. Light transmission through sea ice cover is largely determined by the presence

of snow cover, because snow attenuates light stronger than the sea ice itself (Grenfell and Maykut 1977; Perovich 1990; Hamre et al. 2004) and has a high albedo (e.g. 0.85; Nicolaus et al. 2010; Perovich and Polashenski 2012). Even a snow cover of a few centimetres effectively reduces the light transfer (twofold to sevenfold increase in transmittance after snow removal; **paper II**). Further, light transmission is modified by ice properties such as ice crystal structure (Grenfell and Maykut 1977; Uusikivi et al. 2010; **paper II**). Also the organic constituents in ice, such as CDOM and ice algae, reduce light transmission and affect the spectral shape, i.e. quality of transmitted light (Zeebe et al. 1996; Perovich et al. 1998; Belzile et al. 2000; Mundy et al. 2007; Uusikivi et al. 2010; **paper II**). Melt ponds have a high impact on the light transmission in the melting season (Nicolaus et al. 2012); for example for melting first-year ice, transmittance through melt ponds was on average two to four times higher than through white ice (Hudson et al. 2013). Light transmission through snow and sea ice has a direct consequence on algal physiology by mediating the access to light energy. It also influences the habitat by warming up and melting the ice.

3.4 Role of light for Arctic primary production

3.4.1 Ice algae

An overview of sea ice algal ecology is presented in Arrigo et al. (2010) and von Quillfeldt et al. (2009). Bottom ice algal communities typically live under low-light conditions because of the presence of snow cover (see previous chapter), and are able to photosynthetize and grow at very low irradiance, E(PAR) of <1–9 µmol photons $m^{-2} s^{-1}$ (Horner and Schrader 1982; Gosselin et al. 1986; Hegseth 1992; Olsen et al. 2017). Field and experimental studies show however that they are also able to acclimate to and protect against high irradiances (E(PAR) 100–250 or even 400 µmol photons $m^{-2} s^{-1}$) on time scale of hours or days (Hegseth 1992; Robinson et al. 1997; Petrou et al. 2011; Galindo et al. 2017). The Chl a specific maximum rate of photosynthesis, P_{max}, is nevertheless usually lower in ice algae compared to polar phytoplankton (usually ≤1 versus up to 8 µg C µg Chl $a^{-1} h^{-1}$, respectively) due to the light and temperature conditions in sea ice (Cota and Smith 1991; van Leeuwe et al. 2018). The photosynthetic efficiency in the light limited (i.e. linear) part of a photosynthesis vs. irradiance (PE) curve, α, in ice algae can

13

be 2 to 3 -fold higher compared to comparable measurements of phytoplankton (Cota and Smith 1991). One of the open questions of sea ice algal ecology is when and under which light conditions growth starts in the spring, after the long dark period. Recently, Hancke et al. (2018) observed that ice algae could initiate growth under extremely low irradiance, below 0.17 µmol photons $m^{-2} s^{-1}$. They showed that temperature changes in the snow pack caused changes in the morphology and optical properties of the snow grains and triggered the (albeit very modest) biomass increase.

Ice algal contribution to Arctic primary production varies greatly between seasons and regions. In total, ice algae are estimated to contribute 7.5% to annual primary production (PP) in the Arctic (Dupont 2012). The ice algal share can be up to 60% of PP in the Central Arctic Ocean (Gosselin et al. 1997; Fernández-Méndez et al. 2015) and ≤5% in areas such as Greenland fjords or the Chukchi Sea (Gosselin et al. 1997; Rysgaard and Nielsen 2006). The importance of ice algae depends at least as much on the timing; usually, the ice algal bloom precedes the phytoplankton bloom and thus provides an early, concentrated food source that matches e.g. certain phases in zooplankton life cycles (Søreide et al. 2010). Ice algae are also crucial in the diet of ice-associated amphipods (Kohlbach et al. 2016; Brown et al. 2017).

3.4.2 Phytoplankton

Due to the strong light attenuation caused by the ice and snow cover, water column production in ice-covered waters was considered negligible. Accumulating evidence on under-ice phytoplankton blooms challenge this view (Fortier et al. 2002; Mundy et al. 2009, 2014; Arrigo et al. 2012, 2014; **paper I**) and call for including the different under-ice bloom scenarios into modelling and estimates of Arctic primary production (Johnsen et al. 2018). In open water areas, where large scale monitoring is possible due to satellite remote sensing of ocean colour, reduction in sea ice cover and subsequent increase in light availability has triggered an increase in annual net primary production (Arrigo and van Dijken 2015). However, nutrient availability will eventually set the upper limit for the increase in Arctic primary production and in general determines the trophic status in different regions (Hill et al. 2013; Tremblay et al. 2015). The shelf seas contribute more to primary production in the Arctic Ocean (75% of depth integrated primary production)

than the Central Arctic Ocean due to differences e.g. in persistence of ice cover (Hill et al. 2013) and nutrient inventories (Codispoti et al. 2013).

3.5 Changing Arctic

Before one can hypothesise about the changes in the biological components of the Arctic, we need to have a look at the physical environment. The main limiting factors for algal growth are light and nutrients, whereby biotic interactions with grazers, parasites and pathogens (viruses) control mortality. Stratification is an important factor in determining nutrient availability as it limits the supply from the nutrient reservoir below the mixed layer to the photic zone (drivers for nutrient patterns reviewed in Tremblay et al. (2015)). Stratification can be altered in the future Arctic because of changes in precipitation and runoff i.e. freshwater input, altering the density of the surface layer, and because of changes in mixing due to declined ice cover (increase in e.g. wind fetch). Also changes in the frequency and severity of storms can affect the wind mixing. In the case of light, trends in the amount, timing and nature of precipitation are important in addition to changes in the ice cover itself. Whether the precipitation falls as snow or rain will have a major impact on light transmission through the ice pack. Further, whether the snow falls before or after ice formation in the autumn will determine how much snow will accumulate on the sea ice (Hezel et al. 2012). Regarding all of these aspects, high uncertainty remains and limits the possibility to predict future changes in primary production and other ecosystem processes. Nevertheless, prominent changes in the Arctic icescape are seen already and it seems evident that they will affect the ecosystem.

When it comes to changes in the icescape itself, thinning of the ice and loss of multiyear ice are apparent (Meier et al. 2014). The ice is also drifting faster (Kwok et al. 2013) and is more vulnerable to deformation by storms (Itkin et al. 2017). All of these emerging physical properties of the new sea ice regime will change the ice habitat and the growing conditions for ice algae. Loss of multiyear ice may have profound effects on ice algal habitats (Lange et al. 2017a), and species dispersion and dominance (Olsen et al. 2017). Changes in the timing of ice algal and phytoplankton blooms can affect higher trophic levels due to mismatch with grazer phenology (Leu et al. 2011). All in all, climate change impacts all aspects of the biogeochemical and ecological system (reviewed in Meier et al.

(2014) and Wassmann et al. (2011)), reaching the top of the food web where species rely on sea ice as a platform and on the sea-ice associated primary and secondary production for food supply. For many processes and regions, however, lack of data prevents quantifying the effects and hampers identifying a baseline status prior to changes, and calls for enhanced research efforts (Wassmann et al. 2011). In the following chapters, our new results from the Arctic pack ice region are discussed in connection with other relevant literature from polar regions and the occurring environmental changes.

4. Algal light responses and acclimation

4.1 Under-ice phytoplankton bloom

One fascinating light response we observed during the N-ICE2015 expedition was the development of an under-ice phytoplankton bloom. This bloom was growing under thick ice with thick snow cover and consequently very low irradiances (<1% of incoming light) in the water column underlying this ice type. It was therefore first suspected that this bloom was advected from open waters, or alternatively, a bloom that had been growing in open waters that later was covered by drifting sea ice. In **paper I**, we showed how the bloom could grow in situ under the very opaque ice cover thanks to open and refrozen leads, which enabled enough light to pass to the water column (transmittance up to 40% through the studied refrozen lead; **paper II**) so that the total under-ice irradiance was sufficient for phytoplankton in situ growth below the mosaic of ice floes.

The under-ice phytoplankton bloom was dominated by the haptophyte *Phaeocystis pouchetii* (**paper I**), which is known to have a high physiological plasticity regarding growth irradiances (Schoemann et al. 2005), and not by diatoms that often dominate the Arctic spring bloom (Degerlund and Eilertsen 2010). The conditions leading to either diatom or *P. pouchetii* dominance are not well understood and probably depend on many factors, light conditions possibly being one of them. In the Ross Sea in Antarctica, the sibling species *P. antarctica* dominated blooms in the Ross Sea polynya characterised by a deep mixed layer and variable light regime, whereas the shelf seas with a shallower mixed layer and more constant light regime were dominated by diatoms like *Fragilariopsis cylindrus* (Arrigo et al. 2000). *Phaeocystis antarctica* and *F. cylindrus* had different photoacclimation strategies and photoinhibition responses (Kropuenske et al. 2009, 2010). One can speculate, whether *P. pouchetii* is a more likely species to dominate the type of under-ice blooms we observed because of the variable light regime they encounter.

Another aspect of under-ice phytoplankton blooms able to grow below the ice cover is whether they are a fairly new phenomenon or just understudied and under-observed. Recently, there have been several reports of under-ice blooms (Mundy et al. 2009, 2014,

Arrigo et al. 2012, 2014) in addition to ours. However, because they cannot be observed from space, and field observations in the Arctic pack ice especially outside summer months are relatively scarce, it seems likely that they have gone unnoticed rather than being new for the Arctic. Pomeroy (1997) used measurements of dissolved oxygen as evidence for water column primary production in the Central Arctic, and there are for example reports of high phytoplankton production (73–2570 mg C m^{-2} d^{-1}) under partial ice cover of 55–90% (Gosselin et al. 1997) and blooms following early snow melt in the Canadian archipelago (Fortier et al. 2002). Lowry et al. (2014) argue based on satellite remote sensing of areas after ice retreat in spring that in the Chukchi Sea under-ice blooms have been common in the study period 1998–2012. Whether the frequency of under-ice blooms is increasing, is another question. Light availability for the primary producers is increasing in the melting season as the ice gets younger and thinner (Nicolaus et al. 2012), which could enable more blooms to happen. Horvat et al. (2017) suggest that light conditions suitable for under-ice blooms have increased in frequency in the past 30 years, based on modelling. When it comes to the early under-ice bloom below snow-covered sea ice we observed (**paper I**), increasing ice dynamics could cause higher lead frequencies and therefore more suitable conditions for under-ice blooms during the pre-melt season, given that the mixed layer is shallow enough (Lowry et al. 2018). Further, if these phenomena become more frequent in the future, and are often dominated by *P. pouchetii*, it could have implications for higher trophic levels and the biological carbon pump. The bloom would use up nutrients before the "typical" diatom spring bloom, but alters the grazing pathway (Vernet et al. 2017), and does not sink as effectively than a diatom bloom (Reigstad and Wassmann 2007), unless ballasted by mineral particles (Wollenburg et al. 2018).

The calculations in **paper I** that led us to conclude that the bloom was growing below the opaque ice cover, were as follows. From sea ice satellite remote sensing scenes, the fraction of thick ice, thin ice (refrozen leads) and open water in the study area were quantified. Light transmission through the different ice types was based on our field measurements of the study ice floe during N-ICE2015. Work and results of **paper II** were the basis for the optical properties used to describe refrozen leads in the modelling of light regime and bloom dynamics. This and measurements of the incoming irradiance allowed

to calculate an 'aggregate (total) light availability' for the bloom, that is to estimate the average amount of light the algae encountered considering that they were drifting past the different ice types or open water leads and received different intensities while drifting below the variable ice pack. Based on the light regime and photosynthesis versus irradiance relationship of *Phaeocystis* the possible growth response was modelled that showed that thin ice and open water in the leads allowed enough light to pass into the water column for growth to happen (**paper I**). Another important aspect in the evidence chain was that the ocean currents in the region showed low current speeds on the Yermak plateau (2.2 cm s^{-1} at 20–30 m depth), and current direction towards (and not from) open water areas in the southwest (**paper I**). This ruled out the advective origin, in contrast to areas further west with higher northward current speeds, i.e. 5-10 cm s^{-1} (Johnsen et al. 2018). Further, physiological measurements (pulse amplitude modulated (PAM) fluorometry) confirmed that the algae were in a healthy condition (**paper I**).

In summary, expertise from a wide range of disciplines was used to reveal this new scenario for under-ice blooms happening before the sea-ice melting season, which illustrates that understanding ecosystem processes requires knowledge of the coupled bio-physical system.

4.2 Growth in young ice

Chl *a* standing stocks (indication of ice algal biomass) increased on average from 0.14 to 1.43 mg Chl *a* m^{-2} in the young ice of the refrozen lead over the study period but did not exceed those in the surrounding second-year (SYI) and first-year (FYI) ice despite large differences in light availability (**paper II**). This case exemplifies how algal growth rates are controlled by several factors and simply adding light does not necessarily lead to greater areal production. In **paper II** we discuss several possible factors responsible for the observed patterns, and those are summarized in Table 1 and described in the following paragraphs.

Table 1 Summary of factors regulating ice algal biomass accumulation in the different ice types. Upward facing arrow indicates enhancing role whereas downward facing arrow indicates suppressing role of the factor (hyphen indicates that the factor likely did not have a controlling role). Both ice types had similar Chl a standing stocks at the end of the study period (**paper II**).

	Thick old ice	Thin young ice
Light availability	↓	↑
Photoprotection costs	–	↓
Photoinhibition	–	↓
Seeding stock	↑	↓
Nutrient limitation (Duarte et al. 2017)	↓	↓
Standing stock	≤2.4 mg Chl a m^{-2} ≈	≤2.31 mg Chl a m^{-2}

As already mentioned, the irradiance was higher under the thin young ice with thin snow cover with E_d(PAR) averaging 114 µmol photons m^{-2} s^{-1} (**paper II**), compared to under SYI and FYI with E_d(PAR) <20 µmol photons m^{-2} s^{-1} (Olsen et al. 2017). This led to at times high concentrations of photoprotective pigments (MAA and PPC) in the young ice samples (**paper II and III;** chapter 4.4), which possibly had some metabolic cost as the synthesis of MAAs is estimated to be as costly as that of Chl a (Shick and Dunlap 2002). Photoinhibition (defined as decreasing photosynthetic rates in the PE curves at irradiances >P$_{max}$) was observed only at E_d(PAR) higher than the algae usually were exposed to (**paper II**), but we did not have PE curves from the beginning of the sampling period when the young ice was forming and the algal cells had newly arrived, thus some photoinhibition possibly occurred in low-light acclimated cells early during their incorporation in the young ice.

Furthermore, the surrounding SYI and FYI ice had a seeding stock of algal cells available (Olsen et al. 2017), which refers to cells present in older sea ice that had survived the previous melt season and can initiate growth and bloom development as soon as environmental conditions become favourable. The young ice in contrast had to "start from

scratch" with very low initial algal biomass (**paper II;** Olsen et al. 2017). Even with high growth rates, biomass accumulation could therefore not happen faster (Olsen et al. 2017). Finally, a companion study modelling the biogeochemistry in the different ice types observed more severe nutrient (silicate) limitation in the young ice case (Duarte et al. 2017). Silicate was however present in excess in the water column as the under-ice bloom observed was not formed by diatoms (**paper I**) and presumably the bottom ice had exchange with sea water (Olsen et al. 2017), but the details of nutrient transport in the brine channels still need further research, and on the other hand also the sea ice biogeochemical modelling in general still needs improvement (Duarte et al. 2017).

From this discussion it seems that the ice algae, and especially the typical ice algal species such as *Nitzschia frigida, Fragilariopsis cylindrus* and *Navicula* spp. (**paper III; Figure 6**), grew well in the young ice once cells became acclimated to the ambient irradiance levels and growth seemed not to be hampered by the high light directly (but possibly indirectly via photoprotection costs) or not to a large degree (exponential increase in dominant pennate diatoms; **paper III**). But biomass per unit area was not enhanced, which suggests that overall productivity of the study area was not increased by this high-light environment. Another aspect of the biomass accumulation is that the young ice could be followed only for a month, until it was destroyed by ice movement (**paper II**), and further studies are needed to reveal the development of the ice algal community beyond that time span.

In summary, our results (**paper I and II**) suggest that refrozen leads and possibly other high-light habitats formed in the new, more dynamic ice regime will not necessary become hot spots for ice algal areal production, but they can contribute to phytoplankton production since they act like windows into the underlying water column.
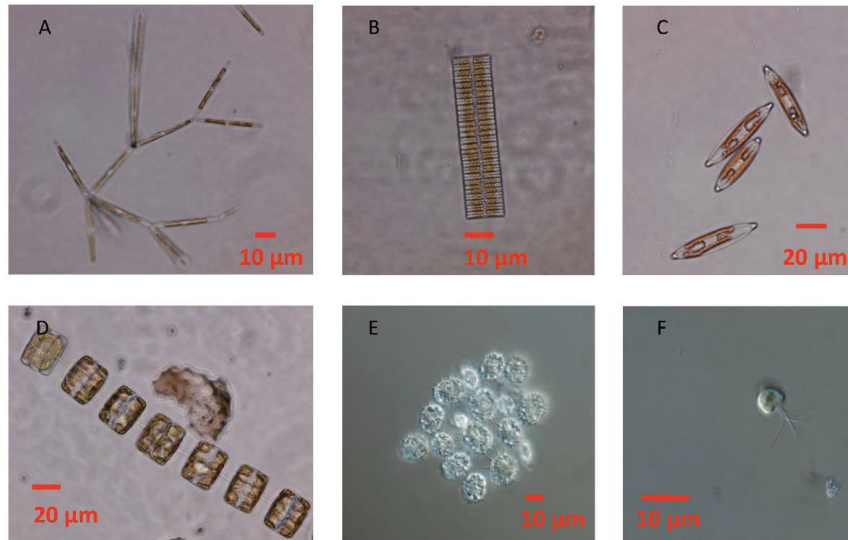
Figure 6 Micrographs showing (A) *Nitzschia frigida*, (B) *Fragilariopsis cylindrus*, (C) *Navicula* sp., (D) *Thalassiosira* sp., (E) cysts of dinoflagellate *Polarella glacialis*, and (F) prasinophyte *Pyramimonas* sp. Figure from **paper III**.

4.3 Algal community development in young ice

Another aspect of the young ice study is how the newly formed ice was colonized by ice algae and if species succession was driven by the environmental factors, namely high irradiances in thin ice in spring, with under-ice E_d(PAR) averaging 114 µmol photons m^{-2} s^{-1} (**paper II**)). In **paper III**, we concluded that the algal cell source habitat was different for different algal groups and that the typical ice-associated pennate diatoms originated from the surrounding older ice (**Figure 7**), based on species abundances in the different ice types and the water column during the refreezing of the lead. This highlights the importance of older ice for the seeding of the ice algal bloom as it is usually dominated by ice-associated pennate diatoms (Poulin et al. 2011; Leu et al. 2015; van Leeuwe et al. 2018), and supports the hypothesis by Olsen et al. (2017) about the seeding repository and colonization of *N. frigida* from the older ice. Other sources of ice algae are the

underlying water column (Syvertsen 1991; Lund-Hansen et al. 2017) or benthic habitats (Ratkova and Wassmann 2005).
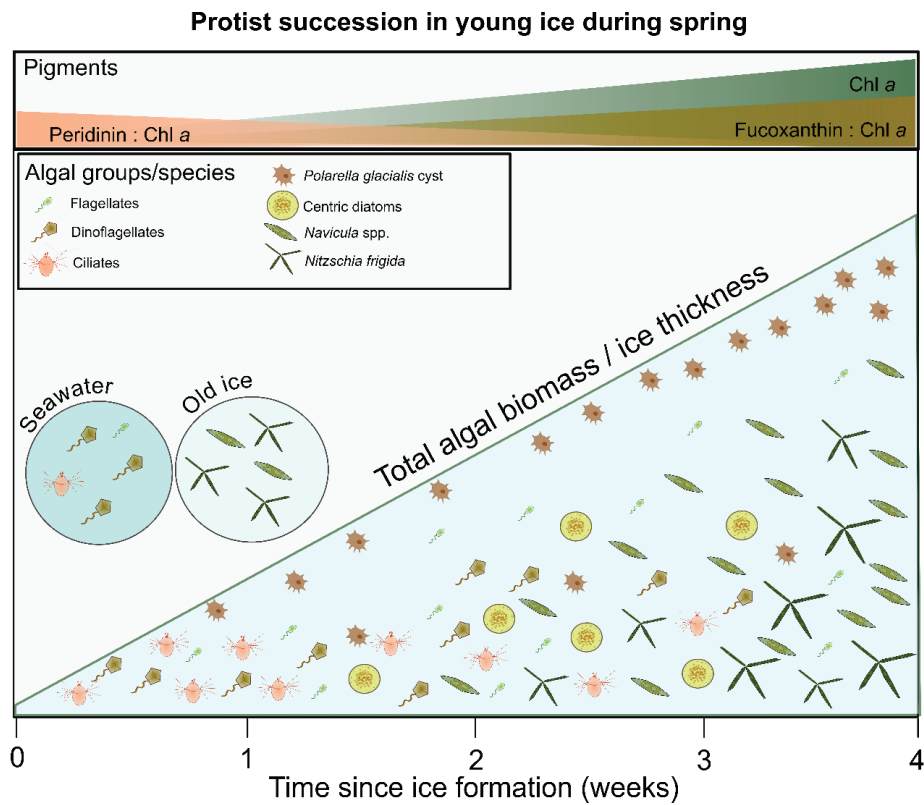
Figure 7 The main successional patterns in the young ice (the triangle) and species composition in the source habitats old ice and seawater (circles on the left). At the beginning, the young ice community had low biomass and was characterized by ciliates, dinoflagellates and flagellates. During four weeks, it developed towards dominance of pennate diatoms (especially *Navicula* spp. and *Nitzschia frigida*). Pennate diatoms eventually dominated also over centric diatoms. Cysts of the dinoflagellate *Polarella glacialis* were predominantly found in the top layer of the ice. Biomass in the bottom of the ice was typically higher than in the top part (coarsely indicated by the amount of icons within the young ice triangle), and increased over time (the diagonal line represents both increase in biomass and ice thickness in the young ice). In the top panel the main patterns of algal marker pigment to Chl *a* ratios are shown, which show the succession from dinoflagellates (type I, peridinin) to diatoms (fucoxanthin). Figure from **paper III.**

23

Once incorporated in sea ice, the pennate diatoms started their successful journey towards dominance of the ice algal community (**paper III; Figure 7**). This seemed to be little affected by the light environment or other abiotic factors: both comparison to the ice algal community of the adjacent older ice with low light, and multivariate statistical testing with the environmental variables available (snow thickness (representing in addition ice thickness and in-ice irradiance) and bulk salinity (representing in addition water column nitrate); **Figure 8**) did not indicate a strong controlling role of these variables (**paper III**). Instead, successional patterns are shaped by physiological, e.g. tolerance to a wide range of salinities, and morphological adaptation to the sea ice habitat, and likely species interactions.
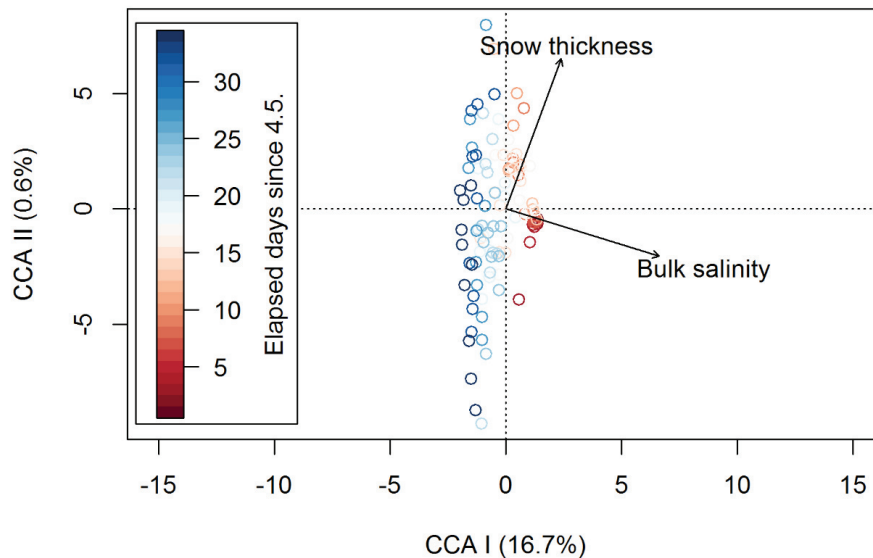
Figure 8 Canonical correspondence analysis (CCA) relating the young ice algal microscopy samples to main environmental drivers (snow thickness and bulk salinity representing also the co-varying in-ice irradiance & ice thickness and water column nitrate, respectively). The circles show the individual ice algal count samples and the colouring the time elapsed since sampling start (4 May). Environmental control was weak: low percentage of variance in the ice algal abundance was explained by the main axes, and especially snow thickness/irradiance did not have a strong role (alignment close to the second axis with 0.6 % variance accounted for). Figure from supplementary material of **paper III**.

Some studies have observed the dominance of centric diatoms over pennate diatoms during the post-bloom stage, and suggested nutrient limitation or increased irradiance to be the cause of it (Galindo et al. 2017; Campbell et al. 2018). In general, our understanding of ice algal ecology is hampered by the scarcity of long-term studies of the same patch of ice over several seasons. Clearly, more studies are needed to better understand ice algal community succession over the whole bloom cycle. In our study (**paper III**), we documented, possibly for the first time for the spring season, ice algal community succession in young ice in the Arctic.

4.4 Photoprotection and photoacclimation

We investigated photoprotection and photoacclimation of the algae, particularly dynamics in MAA (**paper II**) and PPC concentrations (**paper III**). In this thesis, I have concentrated on the light penetration provided by leads to the water column, and a high-light environment i.e. young ice with little snow cover, where under-ice E_d(PAR) ranged between 30 and 350 µmol photons m^{-2} s^{-1} (**paper II**). Whereas in the under-ice phytoplankton bloom study the research question was whether the bloom could grow with the amount of light available under the ice cover (**paper I**), in the young ice case in the refrozen lead irradiance reached levels that are photo-inhibiting for unacclimated cells (**paper II**; Kühl et al. 2001; Juhl and Krembs 2010).

MAAs (shinorine, palythine, porphyra-334), that provide protection from UV light (Karentz 2001; Carreto et al. 2011), were observed in high concentrations in the young ice samples (**paper II**): the MAA to Chl *a* ratios (w:w) were in fact the highest ever reported for sea ice, up to 6.3. This indicates that the UV exposure in the lead was high enough to trigger a substantial investment in photoprotection and that MAAs are an important protection mechanism for ice algae (**paper II**). MAA absorption peaks were highly evident in the UV region of the in vivo absorption spectra of the algae (**Figure 9**). One aspect that possibly led to increased UV exposure is that the young ice was formed from waters low in CDOM. CDOM absorbs mainly in the UV region and therefore high concentrations of it result in an additional protection for algae (**paper II; Figure 10**). Arctic waters are often rich in CDOM (Granskog et al. 2012; Pavlov et al. 2015), whereas our study area was influenced by Atlantic water low in CDOM (Pavlov et al. 2017). Also

changing algal community composition may play a role in the high MAA concentrations as the highest concentrations occurred variable in time.
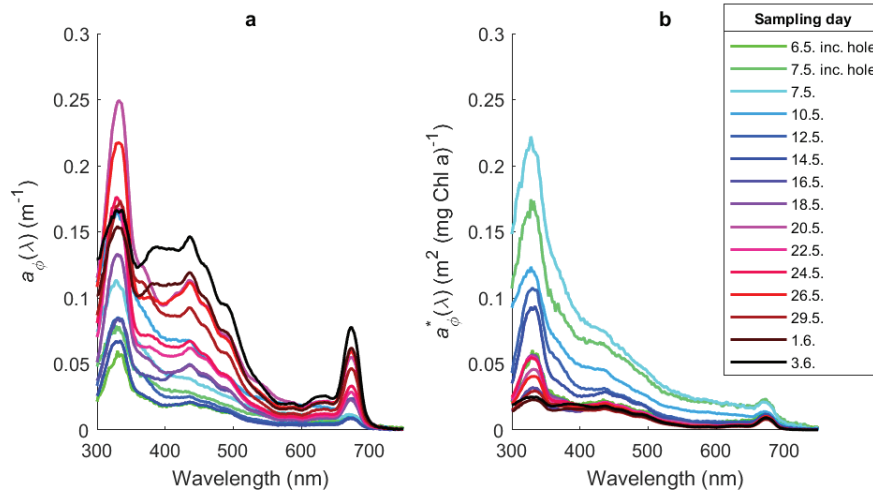
Figure 9 a) Algal (a_ϕ) and b) Chl *a* -specific algal absorption (a_ϕ^*) coefficients in young ice in the refrozen lead over the study period. Absorption at 300–400 nm is highly affected by mycosporine-like amino acids (MAA), while absorption at 400–700 nm indicates the total absorption of light harvesting pigments (LHP) and photoprotective carotenoids (PPC) of the algal cells present. The lines are averages of the five coring sites and after 18 May volumetric averages of ice core bottom and top section values. Inc. hole refers to an ice coring location outside the coring transect. See **paper II** for more details. Figure modified from **paper II**.
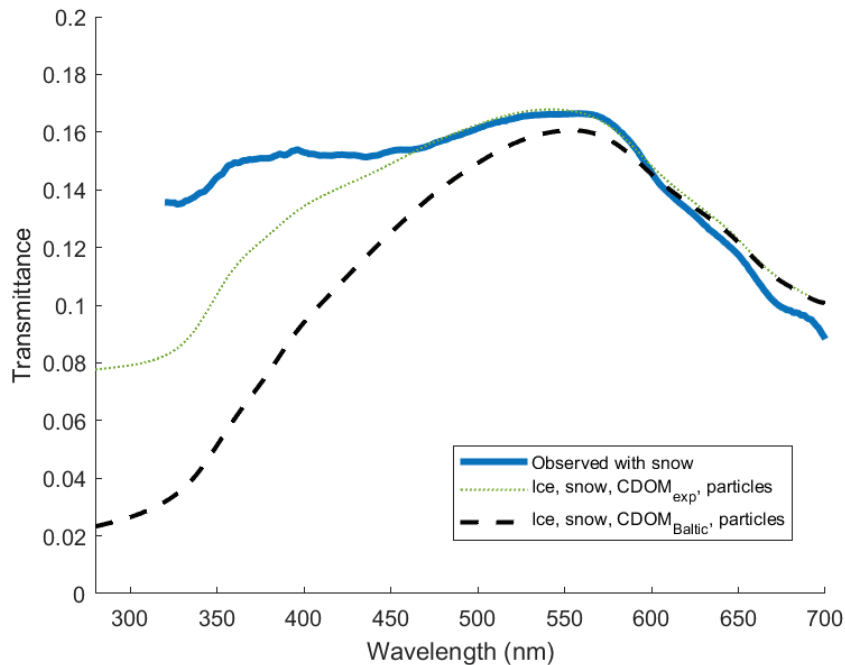
Figure 10 Observed (measured with a spectroradiometer, providing $E_d(\lambda)$) and modelled transmittance through the young ice in the refrozen lead on site 3 on 26 May. Modelling with in-ice CDOM concentration as observed in the Baltic Sea (Uusikivi et al. 2010) results in much higher light attenuation in the UV range than observed in the young ice, or modelled with CDOM concentration measured from young ice samples (MAA peaks removed; see **paper II**). Figure modified from **paper II**.

Photoacclimation with regard to differences in cellular concentrations and ratios of PPC was also observed in the young ice samples (**paper III**). The carotenoids involved in the xanthophyll cycle, specifically diadino- and diatoxanthin (DD+DT), showed an increase from 0.01 to 0.87 mg m^{-3} over the study period and reached levels ((DD+DT):Chl *a* up to 0.26) measured in other habitats with high light conditions, such as sea ice under thin snow cover (Alou-Font et al. 2013). Surprisingly, the DD+DT to Chl *a* ratio in the surrounding FYI with about 20 cm of snow cover was on average similar to that measured in the young ice (**paper III**). Further studies investigating the relationship between the pigment ratio and irradiance levels could reveal whether the pigment expression reaches

27

a plateau at a certain irradiance or if a threshold needs to be exceeded for the PPC to Chl *a* ratio to increase.

Not surprisingly, in the water column, the ratio of photoprotective to photosynthetic carotenoids (PPC:PSC) and (DD+DT):Chl *a* were low (<0.44 and <0.06, respectively; **paper IV**). An increase in the ratio could however be seen over time, which indicates that the algae adjusted the pigment pool when needed through active photoacclimation.

Information on photoacclimation can be further extracted from the in vivo Chl *a* -specific absorption spectra characteristics of algae. Pigment packaging (intra- and intercellular self-shading) and consequently the "flattening" of the spectra are affected by the light acclimation state because low-light acclimated cells contain high amounts of light harvesting pigments to enhance absorption of available light. The package effect is however also controlled by cell size, thylakoid stacking, chloroplast number and size (Johnsen et al. 2011; Kirk 2011), and the young ice case showed that packaging patterns over the study period were affected by species succession and that it was not straightforward to draw conclusions about photoacclimation from the absorption spectra (**paper II; Figure 9b**). In the under-ice bloom case, high pigment packaging was likely caused by low-light acclimation (Pavlov et al. 2017).

4.5 Other ice habitats and their light regime

We observed algal communities both in pressure ridges and at the snow-ice interface, which were investigated in the co-authored study by Fernández-Méndez et al. (2018). Both of these habitats had higher diatom biomass than the level ice (young ice, SYI, FYI; **paper II**; Olsen et al. 2017) and thus seemed to offer good growth conditions (Fernández-Méndez et al. 2018). This may imply that the importance of these ice-associated habitats increases as a result of the changing physical properties of the Arctic ice scape – thinner ice cover and higher drift speeds. The increasing dynamics of the ice field possibly result in more frequent leads, but also on the other hand in more frequent ridging when ice floes are colliding. A consequence of the thinning of the ice pack is that the snow to ice thickness ratio increases which results in more frequent occurrence of negative freeboard (the surface of the ice is below the water surface due to the excess weight of the snow

cover) and flooding at the snow-ice interface. These conditions are a prerequisite for the formation of snow infiltration communities (e.g. Buck et al. 1998; Kristiansen et al. 1998; McMinn and Hegseth 2004).

Light likely controlled algal growth also in these habitats, among other environmental variables like water current direction and physical structure of the habitats (Fernández-Méndez et al. 2018). In the snow infiltration layer, the irradiance was higher than in the water column as in the former the algae were located above the ice. Diatoms, that were observed in the water column at low abundances and as solitary cells, were forming long chains in the infiltration layer and were actively growing (Fernández-Méndez et al. 2018). Light measurements or modelling in ridges are challenging due to the complex geometry and difficulties of under-ice measurements, but due to often low snow cover on top of the ridge (e.g. Liston et al. 2018) light transmittance can be higher than in the surrounding ice and consequently provide a suitable habitat for ice algae, as observed for multi-year ice hummocks (Lange et al. 2017a). In addition, the ridge we studied was adjacent to the refrozen lead with high light transmittance (**paper II**) and therefore received additional light. Also other field studies have observed elevated biomass in pressure ridges (Lange et al. 2017b), whereas a modelling study (Castellani et al. 2017) concluded similar or lower biomass in ridges compared to level ice and later bloom onset in ridges.

5. The other way – bio-optical feedbacks

In the previous chapters, I have concentrated on the responses of algae to light intensity i.e. "how does the light regime affect algae". In this (5) and the next chapter (6), I turn it around and ask "how do algae affect the light regime", both in terms of integrated light energy absorption, wavelength-specific absorption and scattering. Besides having interesting ecological and bio-physical implications, as discussed in this chapter (**paper II** and other N-ICE2015 related papers), it is also the basis of bio-optical monitoring methods like ocean colour remote sensing or the approaches discussed in next chapter (including **paper IV**).

In **paper II**, we quantified the effect algae have on ice melting by absorbing light and dissipating it as heat. Heat loss happens at all stages of algal physiology; part of the absorbed irradiance is lost as heat and fluorescence, and heat is released also in respiration (Lin et al. 2016; see also discussion in Zeebe et al. (1996)). By radiative transfer modelling in **paper II** (**Figure 11**) we estimated the fraction of incoming spectral irradiance that was absorbed by the ice algae within a week (end of May), and approximated that the algae present in the refrozen lead could melt about 1 cm of pure ice within a week. While this is not remarkable compared to melting by ocean or atmospheric heat fluxes, it is a relevant thickness considering the ice algal habitat. Most of the biomass is situated in the bottom of the ice, and even in the lower most centimetre (Smith et al. 1990). The effect of algal heating depends however also on position of algal cells within the ice (how concentrated the biomass is) (Zeebe et al. 1996). Thus more detailed (modelling) studies are needed to quantify this effect, taking into account the algal concentration and sea ice thermodynamics as done in the study by Zeebe et al. (1996) for thick ice with thick snow cover. A large-scale ice algal modelling study for the Arctic (Castellani et al. 2017) estimated the integrated summer melting (April–September) caused by algae to be between 0.1 and 1.5 cm. It is nevertheless evident that even though biomass is low, with high incoming irradiance (as in the case of refrozen leads with thin ice and snow (**paper II**), or other high-light habitats) algal melting can potentially occur because of higher light absorption.
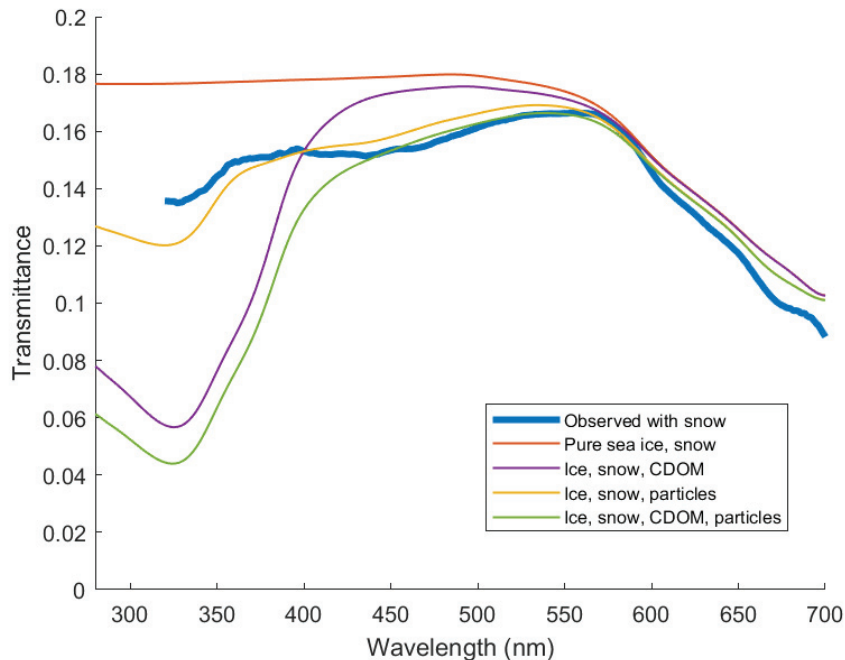
Figure 11 Observed and modelled light transmittance through the young ice in the refrozen lead on site 3 on 26 May. Different combinations of the optically active components were included in the model runs (see legend). The model agrees with observations (in the visible range) when the absorption by particles (including ice algae) is included in the model components (yellow and green lines). The different model runs allow separating the energy absorption between the components. For reasons for the discrepancy between observations and model results in the UV range see **paper II**. Figure modified from **paper II**. Transmittance is the fraction of incoming light passing through the snow and ice cover (maximum value 1).

During the N-ICE2015 expedition, algal contribution to heating was estimated also for the water column by Taskjelle et al. (2017). The under-ice bloom caused an increase in light absorption in the upper water column, and by radiative transfer modelling it was estimated that 35 % more energy was deposited in the upper 10 m after the bloom started compared to pre-bloom conditions. This could again affect the bottom ice algal habitat, by potentially melting 2.7 cm of pure ice over 25 days.

32

Another interesting aspect of the under-ice bloom was its effect on the under-ice light field. The high amount of algal cells caused a tenfold increase in light scattering (at visible wavelengths) in the upper 20 m of the water column compared to the pre-bloom situation (Pavlov et al. 2017). This resulted also in higher backscattering of ambient light – the water column thus became "brighter" when looking from above – which in turn resulted in higher light availability at the ice-ocean interface and bottom ice algal habitat (Pavlov et al. 2017). While the relevance of this effect for ice algal blooms needs to be confirmed (is the light increase caused by the under-ice bloom counteracted by the nutrient drawdown by the bloom?), it is a fascinating case of bio-physical feedbacks and also showed how ice as a highly scattering surface adds complexity, as compared to the open water case. Ice algae on the other hand can shade the water column due to their light absorption and suppress phytoplankton growth (Mundy et al. 2014; Castellani et al. 2017).

6. Future perspectives – automated monitoring

The optical fingerprint of algal pigments can be detected as spectral differences in reflected or transmitted light, due to varying algal pigment spectral absorption (see **Figures 4, 9a and 11**). In **paper IV**, in situ absorption measurements from light absorption and beam attenuation meter (ac-9) vertical profiles were related to the ratio of PPC to PSC from water samples. The slope of the absorption measurements between 488 and 532 nm (the former corresponding to PPC absorption and the latter to PSC) was found to have a significant linear relationship with the pigment ratios (**Figure 12**). This relationship could enable predicting the carotenoid ratio from additional absorption measurements. The slope was calculated as a_{ph} slope = $(a_{ph}(488) - a_{ph}(532)) / (a_{ph}(676) (488$ nm - 532 nm)) (Eisner et al. 2003).
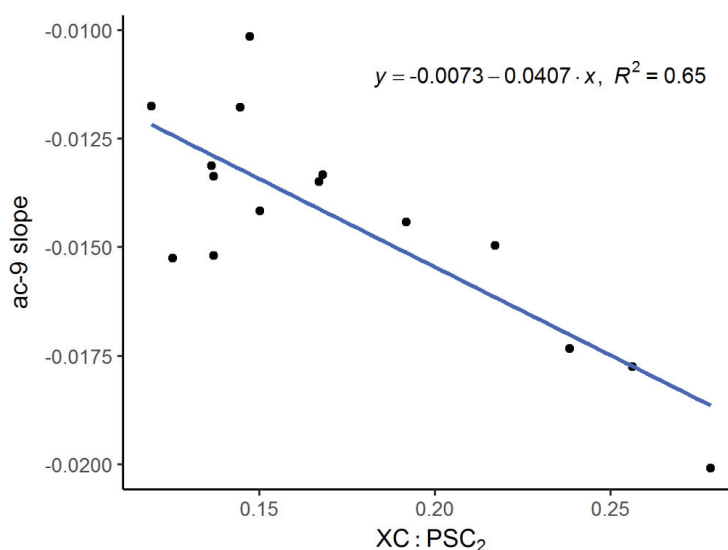
Figure 12 Relationship between the normalized absorption spectrum (a_ϕ) slopes from ac-9 measurements and the ratio of xanthophyll cycle carotenoids (XC) to photosynthetic carotenoids (PSC$_2$). Figure modified from **paper IV**.

The Arctic is facing profound changes in the physical properties like ice and snow cover, yet our ability to study and monitor the ecosystem is limited. Traditional data collection from research vessels and ice camps, while immensely valuable, is very time-consuming and logistically challenging and at best should be supplemented by autonomous data collection from various platforms. For the biological variables, however, this is in its infancy, since satellite remote sensing of ice algae and under-ice phytoplankton blooms is not possible in ice-covered waters and other autonomous platforms have just recently emerged. Ice-tethered buoys, buoyancy driven gliders, remotely operated vehicles (ROV) or propeller driven autonomous underwater vehicles (AUV) all offer new opportunities to increase sampling frequency both in time and space and link local measurements to a larger scale (e.g. Johnsen et al. 2018). These platforms can be equipped with bio-optical sensors like Chl *a* and CDOM fluorometers and radiometers. Developing applications for the type of data that can be retrieved will give new information on the biological processes and broaden the use of the measurements.

The measurements in our study (**paper IV**) were made during the ship campaign, but this study indicates how additional information could be obtained from an under-ice bloom that is otherwise hard to observe, if suitable sensors are mounted for example on AUVs. We investigated a method first used off the West Coast of the United States (Eisner et al. 2003) and obtained similar results in our ice-covered ocean setting and with a different bloom community composition. More work is needed to explore the wider applicability of the method and the pigment ratios used to indicate the photoacclimation state, but our study shows the potential in bio-optical measurements and how they could be used to study physiology and even the origin of the bloom. In 2010 an under-ice phytoplankton bloom was observed west of the Yermak Plateau and was studied with multiple platforms, including AUVs (Johnsen et al. 2018). The bloom was concluded to have advected under the ice, based on current speed and direction in the area, and observations of similar community composition in a phytoplankton bloom (comprising 32000 km^2) in open water areas south of the under-ice bloom (Johnsen et al. 2018). Also the high-light acclimation state of cells from the under-ice bloom, studied with PAM fluorometry and pigment measurements, was important in drawing the conclusion about the origin of the bloom.

The under-ice bloom of our study was low-light acclimated (**paper IV**), which is consistent with the conclusion of local growth under the ice pack.

Other interesting efforts to increase the palette of autonomous biological monitoring are estimating primary productivity from autonomous optical measurements of diel fluctuations of particulate organic carbon (from beam attenuation measurements) and dissolved oxygen (Briggs et al. 2018). Laney et al. (2014) demonstrated the use of ice-tethered profilers to monitor phytoplankton biomass in the Arctic.

There have been several attempts to remotely monitor ice algae by under-ice irradiance measurements. Algae living in the ice absorb mainly in the blue and red part of the visible spectrum of the sun light passing through the ice, and thus alter the spectral shape compared to the incoming irradiance above the ice. One method is based on calculating a suitable index from the spectral irradiance, validated by a set of concurrent under-ice irradiance measurements and ice core samples with Chl *a* laboratory measurements, and then predicting algal biomass on a larger area based on the index and additional irradiance measurements (Legendre and Gosselin 1991; Mundy et al. 2007). The equation for the normalized difference index (NDI) is $(T(\lambda_1) - T(\lambda_2)) / (T(\lambda_1) + T(\lambda_2))$, where T is light transmittance at wavelength λ_n (Mundy et al. 2007). This method has later been used to monitor the development of an ice algal community in spring in the Canadian Arctic (Campbell et al. 2014) and in spatial studies in the Antarctic (Melbourne-Thomas et al. 2015; Meiners et al. 2017; Wongpan et al. 2018). There has also been further method developments by McDonald et al. (2015) and Lange et al. (2016) by including further statistical tests like empirical orthogonal functions (EOF) to quantify the algal impact on transmitted irradiance. More information can be found in the recent review by Cimoli et al. (2017b), including the use of hyperspectral imaging (Cimoli et al. 2017a).

In our field campaign, we had extensive under-ice irradiance measurements from a ROV equipped with spectroradiometers. We made efforts to develop a NDI suitable for our study to expand biomass estimates beyond the ice coring locations, and to extract additional biological information by including other algal pigments besides Chl *a* in the analysis (the pigments presented in **paper III**)**.** The ice algal biomass in our study area (**paper II**), however, was low and did not enable for very robust relationships between

Chl *a* concentration in the ice core samples and corresponding irradiance measurements. One additional challenge is that the main pigments present in typical ice algae largely overlap in absorption properties. They also strongly correlate with Chl *a* which makes the use of single indices problematic if more information is to be retained. The wavelengths chosen in previous studies for the biomass index in fact carry information both from Chl *a* and different carotenoids. One multivariate method applied was the partial least squares regression (PLSR) analysis as done by Organelli et al. (2013), without obvious promising results. More work was thus needed to finalize these studies, which was beyond the timeline of the PhD project.

7. Summary and outlook

In this thesis I have concentrated on the spring period in the pack ice north of Svalbard and discussed the observed phenomena in light (!) of the emerging physical changes of the Arctic icescape and their possible implications for algal habitats. From the major controlling factors of algal growth I concentrated on irradiance and how that affects different aspects of algal ecology, such as biomass build-up (**paper I and II**), community composition (**paper III**) and photoprotection (**paper II and III**). Responses to the increased light intensities differed depending on the habitat and the above mentioned aspects of algal ecology. Increased underwater irradiance (because of leads) seemed to benefit *P. pouchetii*, which was able to form an under-ice phytoplankton bloom. Ice algal biomass in the young ice was not enhanced compared to the surrounding ice with lower irradiance, and community composition was not affected by irradiance. Other occurring changes in the icescape, such as disappearance of multiyear ice may however negatively affect the tightly ice-associated ice algal species that rely on multiyear ice for seeding and dispersion. I have also taken a look at how the interplay between light and algae is a two-way process, with algae at times having an impact, such as heating, on the physical environment (**paper II**). One practical application of the interplay is that the optical fingerprint algae leave in absorbed or transmitted light can be used to obtain information on their physiology and distribution (**paper IV**). Due to the constraints of the icescape, innovative new methods are needed to be able to extend the autonomous data collection into higher latitudes and into new variables for ecosystem monitoring.

New ice dynamics (thinner and younger ice) changes the ice algal habitats, yet there is still very limited information on the responses of the ecosystem. The majority of ice algal studies concentrate on multiyear and thick first-year ice where light often is limiting and reaches high levels only towards the melting season. Studies similar to **paper II and III** are needed to confirm the patterns in level ice under high light exposure during the bloom season. Further, a comprehensive view of ice algal phenology over the annual cycle is critically needed. Both the ice and under-ice habitats are inaccessible for biological remote sensing and extensive campaigns like the N-ICE2015 project are valuable in enhancing our understanding of the ecosystem in these times of great changes. In the

coming years, the Multidisciplinary drifting Observatory for the Study of Arctic Climate (MOSAiC) project will continue the efforts and conduct a year-long drift expedition in the Arctic pack ice. In general, long term monitoring is needed to be able to detect changes and baseline shifts. Understanding the patterns of Arctic primary production and its possible trends in the future form the basis for the management of the area, because with the photosynthetic capacity algae form the base of the food web of which heterotrophic organisms, including us, are dependent on.

8. References

Alou-Font E, Mundy CJ, Roy S, et al (2013) Snow cover affects ice algal pigment composition in the coastal Arctic Ocean during spring. Mar Ecol Prog Ser 474:89–104. doi: 10.3354/meps10107

Arrigo K, Perovich D, Pickart R, et al (2012) Massive phytoplankton blooms under Arctic sea ice. Science 336:1408. doi: 10.1007/BF02390423

Arrigo KR, DiTullio GR, Dunbar RB, et al (2000) Phytoplankton taxonomic variability in nutrient utilization and primary production in the Ross Sea. J Geophys Res 105:8827–8846. doi: 10.1029/1998JC000289

Arrigo KR, Mock T, Lizotte MP (2010) Primary producers and sea ice. In: Thomas DN, Dieckmann GS (eds) Sea ice, 2nd edition. Wiley-Blackwell, Oxford, pp 283–325

Arrigo KR, Perovich DK, Pickart RS, et al (2014) Phytoplankton blooms beneath the sea ice in the Chukchi sea. Deep Res Part II 105:1–16. doi: 10.1016/j.dsr2.2014.03.018

Arrigo KR, van Dijken GL (2015) Continued increases in Arctic Ocean primary production. Prog Oceanogr 136:60–70. doi: 10.1016/j.pocean.2015.05.002

Assmy P, Fernández-Méndez M, Duarte P, et al (2017) Leads in Arctic pack ice enable early phytoplankton blooms below snow-covered sea ice. Sci Rep 7:40850. doi: 10.1038/srep40850

Behrenfeld MJ, Boss ES (2018) Student's tutorial on bloom hypotheses in the context of phytoplankton annual cycles. Glob Chang Biol 24:55–77. doi: 10.1111/gcb.13858

Belzile C, Johannessen SC, Gosselin M, et al (2000) Ultraviolet attenuation by dissolved and particulate constituents of first-year ice during late spring in an Arctic polynya. Limnol Oceanogr 45:1265–1273. doi: 10.4319/lo.2000.45.6.1265

Briggs N, Guðmundsson K, Cetinić I, et al (2018) A multi-method autonomous assessment of primary productivity and export efficiency in the springtime North Atlantic. Biogeosciences Discuss. doi: https://doi.org/10.5194/bg-2017-534

Brown TA, Assmy P, Hop H, et al (2017) Transfer of ice algae carbon to ice-associated amphipods in the high-Arctic pack ice environment. J Plankton Res 39:664–674. doi: 10.1093/plankt/fbx030

Brunet C, Johnsen G, Lavaud J, Roy S (2011) Pigments and photoacclimation processes. In: Roy S, LLewellyn CA, Egeland ES, Johnsen G (eds) Phytoplankton Pigments -

Characterization, Chemotaxonomy and Applications in Oceanography, 1st edition. Cambridge University Press, Cambridge, pp 445–471

Buck KR, Nielsen TG, Hansen BW, et al (1998) Infiltration phyto- and protozooplankton assemblages in the annual sea ice of Disko Island, West Greenland, spring 1996. Polar Biol 20:377–381. doi: 10.1007/s003000050317

Campbell K, Mundy CJ, Barber DG, Gosselin M (2014) Remote estimates of ice algae biomass and their response to environmental conditions during spring melt. Arctic 67:375–387. doi: 10.14430/arctic4409

Campbell K, Mundy CJ, Belzile C, et al (2018) Seasonal dynamics of algal and bacterial communities in Arctic sea ice under variable snow cover. Polar Biol 41:41–58. doi: 10.1007/s00300-017-2168-2

Carreto JI, Roy S, Whitehead K, et al (2011) UV-absorbing "pigments": mycosporine-like amino acids. In: Roy S, Llewellyn CA, Egeland ES (eds) Phytoplankton Pigments - Characterization, Chemotaxonomy and Applications in Oceanography, 1st edition. Cambridge University Press, Cambridge, pp 412–441

Castellani G, Losch M, Lange BA, Flores H (2017) Modeling Arctic sea-ice algae: Physical drivers of spatial distribution and algae phenology. J Geophys Res Ocean 122:7466–7487. doi: 10.1002/2017JC012828

Cimoli E, Lucieer A, Meiners KM, et al (2017a) Towards improved estimates of sea-ice algal biomass: experimental assessment of hyperspectral imaging cameras for under-ice studies. Ann Glaciol 58:68–77. doi: 10.1017/aog.2017.6

Cimoli E, Meiners KM, Lund-Hansen LC, Lucieer V (2017b) Spatial variability in sea-ice algal biomass: an under-ice remote sensing perspective. Adv Polar Sci 28:268–296. doi: 10.13679/j.advps.2017.4.00268

Codispoti LA, Kelly V, Thessen A, et al (2013) Synthesis of primary production in the Arctic Ocean: III. Nitrate and phosphate based estimates of net community production. Prog Oceanogr 110:126–150. doi: 10.1016/j.pocean.2012.11.004

Cota GF, Smith RE (1991) Ecology of bottom ice algae: III. Comparative physiology. J Mar Syst 2:297–315

de Veer G (1876) The three voyages of William Barents to the Arctic regions (1594, 1595, and 1596). Hakluyt society, London

Degerlund M, Eilertsen HC (2010) Main species characteristics of phytoplankton spring

blooms in NE Atlantic and Arctic waters (68-80° N). Estuaries and Coasts 33:242–269. doi: 10.1007/s12237-009-9167-7

Duarte P, Meyer A, Olsen LM, et al (2017) Sea ice thermohaline dynamics and biogeochemistry in the Arctic Ocean: Empirical and model results. J Geophys Res Biogeosciences 122:1632–1654. doi: 10.1002/2016JG003660

Dupont F (2012) Impact of sea-ice biology on overall primary production in a biophysical model of the pan-Arctic Ocean. J Geophys Res Ocean 117:C00D17. doi: 10.1029/2011JC006983

Eisner LB, Twardowski MS, Cowles TJ, Perry MJ (2003) Resolving phytoplankton photoprotective : photosynthetic carotenoid ratios on fine scales using in situ spectral absorption measurements. Limnol Oceanogr 48:632–646. doi: 10.4319/lo.2003.48.2.0632

Falkowski PG, Raven JA (2007) Aquatic photosynthesis, 2nd edition. Princeton University Press, Princeton

Fernández-Méndez M, Katlein C, Rabe B, et al (2015) Photosynthetic production in the central Arctic Ocean during the record sea-ice minimum in 2012. Biogeosciences 12:3525–3549. doi: 10.5194/bg-12-3525-2015

Fernández-Méndez M, Olsen LM, Kauko HM, et al (2018) Algal hot spots in a changing Arctic Ocean: Sea-ice ridges and the snow-ice unterface. Front Mar Sci 5:75. doi: 10.3389/fmars.2018.00075

Fortier M, Fortier L, Michel C, Legendre L (2002) Climatic and biological forcing of the vertical flux of biogenic particles under seasonal Arctic sea ice. Mar Ecol Prog Ser 225:1–16. doi: 10.3354/meps225001

Galindo V, Gosselin M, Lavaud J, et al (2017) Pigment composition and photoprotection of Arctic sea ice algae during spring. Mar Ecol Prog Ser 585:49–69. doi: 10.3354/meps1239

Gosselin M, Legendre L, Therriault J-C, et al (1986) Physical control of the horizontal patchiness of sea-ice microalgae. Mar Ecol Prog Ser 29:289–298. doi: 10.3354/meps029289

Gosselin M, Levasseur M, Wheeler PA, et al (1997) New measurements of phytoplankton and ice algal production in the Arctic Ocean. Deep Res Part II 44:1623–1644. doi: 10.1016/S0967-0645(97)00054-4

Granskog MA, Assmy P, Gerland S, et al (2016) Arctic research on thin ice: Consequences of Arctic sea ice loss. Eos Trans AGU 97:22–26

Granskog MA, Fer I, Rinke A, Steen H (2018) Atmosphere-ice-ocean-ecosystem processes in a thinner Arctic sea ice regime: the Norwegian young sea ICE (N-ICE2015) expedition. J Geophys Res Ocean 123:1586-1594. doi: 10.1002/2017JC013328

Granskog MA, Stedmon CA, Dodd PA, et al (2012) Characteristics of colored dissolved organic matter (CDOM) in the Arctic outflow in the Fram Strait: Assessing the changes and fate of terrigenous CDOM in the Arctic Ocean. J Geophys Res Ocean 117:C12021. doi: 10.1029/2012JC008075

Grenfell TC, Maykut GA (1977) The optical properties of ice and snow in the Arctic basin. J Glaciol 18:445–463

Hamre B, Winther JG, Gerland S, et al (2004) Modeled and measured optical transmittance of snow-covered first-year sea ice in Kongsfjorden, Svalbard. J Geophys Res 109:C10006. doi: 10.1029/2003JC001926

Hancke K, Lund-Hansen LC, Lamare ML, et al (2018) Extreme low light requirement for algae growth underneath sea ice: A case study from Station Nord, NE Greenland. J Geophys Res Ocean 123:985–1000. doi: 10.1002/2017JC013263

Hegseth EN (1992) Sub-ice algal assemblages of the Barents Sea: Species composition, chemical composition, and growth rates. Polar Biol 12:485–496

Hezel PJ, Zhang X, Bitz CM, et al (2012) Projected decline in spring snow depth on Arctic sea ice caused by progressively later autumn open ocean freeze-up this century. Geophys Res Lett 39: L17505. doi: 10.1029/2012GL052794

Higgins HW, Wright SW, Schlüter L (2011) Quantative interpretation of chemotaxonomic pigment data. In: Roy S, LLewellyn CA, Egeland ES, Johnsen G (eds) Phytoplankton Pigments - Characterization, Chemotaxonomy and Applications in Oceanography, 1st edition. Cambridge University Press, Cambridge, pp 257–313

Hill VJ, Matrai P, Olson E, et al (2013) Synthesis of integrated primary production in the Arctic Ocean: II. In situ and remotely sensed estimates. Prog Oceanogr 110:107–125. doi: 10.1016/j.pocean.2012.11.005

Horner R, Schrader GC (1982) Relative contributions of ice algae, phytoplankton, and

benthic microalgae to primary production in nearshore regions of the Beaufort Sea. Arctic 35:485–503. doi: 10.14430/arctic2356

Horvat C, Jones DR, Iams S, et al (2017) The frequency and extent of sub-ice phytoplankton blooms in the Arctic Ocean. Sci Adv 3:e1601191. doi: 10.1126/sciadv.1601191

Hudson SR, Granskog MA, Sundfjord A, et al (2013) Energy budget of first-year Arctic sea ice in advanced stages of melt. Geophys Res Lett 40:2679–2683. doi: 10.1002/grl.50517

Itkin P, Spreen G, Cheng B, et al (2017) Thin ice and storms: a case study of sea ice deformation from buoy arrays deployed during N-ICE2015. J Geophys Res Ocean 122:4661–4674. doi: 10.1002/2016JC012403

Jeffrey SW, Mantoura RFC, Wright SW (1997) Phytoplankton pigments in oceanography: guidelines to modern methods. UNESCO Publishing, Paris

Jeffrey SW, Wright SW, Zapata M (2011) Microalgal classes and their signature pigments. In: Roy S, LLewellyn CA, Egeland ES, Johnsen G (eds) Phytoplankton Pigments - Characterization, Chemotaxonomy and Applications in Oceanography, 1st edition. Cambridge University Press, Cambridge, pp 3–77

Jerlov NG (1976) Marine optics, 2nd edition. Elsevier Scientific Publishing Company, Amsterdam

Johnsen G, Bricaud A, Nelson N, et al (2011) In vivo bio-optical properties of phytoplankton pigments. In: Roy S, LLewellyn CA, Egeland ES, Johnsen G (eds) Phytoplankton Pigments - Characterization, Chemotaxonomy and Applications in Oceanography, 1st edition. Cambridge University Press, Cambridge, pp 496–537

Johnsen G, Norli M, Moline M, et al (2018) The advective origin of an under-ice spring bloom in the Arctic Ocean using multiple observational platforms. Polar Biol. doi: 10.1007/s00300-018-2278-5

Juhl AR, Krembs C (2010) Effects of snow removal and algal photoacclimation on growth and export of ice algae. Polar Biol 33:1057–1065. doi: 10.1007/s00300-010-0784-1

Karentz D (2001) Chemical defenses of marine organisms against solar radiation exposure: UV-absorbing mycosporine-like amino acids and scytonemin. In: McClintock J, Baker W (eds) Marine Chemical Ecology. CRC Press, Inc., Boca

Raton, pp 481–520

Kauko HM, Taskjelle T, Assmy P, et al (2017) Windows in Arctic sea ice: Light transmission and ice algae in a refrozen lead. J Geophys Res Biogeosciences 122:1486–1505. doi: 10.1002/2016JG003626

Kirk JTO (2011) Light and Photosynthesis in Aquatic Ecosystems, 3rd edition. Cambridge University Press, Cambridge

Kohlbach D, Graeve M, Lange BA, et al (2016) The importance of ice algae-produced carbon in the central Arctic Ocean ecosystem: Food web relationships revealed by lipid and stable isotope analyses. Limnol Oceanogr 61:2027–2044. doi: 10.1002/lno.10351

Kristiansen S, Farbrot T, Kuosa H, et al (1998) Nitrogen uptake in the infiltration community, an ice algal community in Antarctic pack-ice. Polar Biol 19:307–315. doi: 10.1007/s003000050251

Kropuenske LR, Mills MM, van Dijken GL, et al (2009) Photophysiology in two major Southern Ocean phytoplankton taxa: photoprotection in *Phaeocystis antarctica* and *Fragilariopsis cylindrus*. Limnol Oceanogr 54:1176–1196. doi: 10.4319/lo.2009.54.4.1176

Kropuenske LR, Mills MM, Van Dijken GL, et al (2010) Strategies and rates of photoacclimation in two major southern ocean phytoplankton taxa: *Phaeocystis antarctica* (Haptophyta) and *Fragilariopsis cylindrus* (Bacillariophyceae). J Phycol 46:1138–1151. doi: 10.1111/j.1529-8817.2010.00922.x

Kwok R, Spreen G, Pang S (2013) Arctic sea ice circulation and drift speed: Decadal trends and ocean currents. J Geophys Res Ocean 118:2408–2425. doi: 10.1002/jgrc.20191

Kühl M, Glud RN, Borum J, et al (2001) Photosynthetic performance of surface-associated algae below sea ice as measured with a pulse-amplitude-modulated (PAM) fluorometer and O_2 microsensors. Mar Ecol Prog Ser 223:1–14. doi: 10.3354/meps223001

Laney SR, Krishfield RA, Toole JM, et al (2014) Assessing algal biomass and bio-optical distributions in perennially ice-covered polar ocean ecosystems. Polar Sci 8:73–85. doi: 10.1016/j.polar.2013.12.003

Lange BA, Flores H, Michel C, et al (2017a) Pan-Arctic sea ice-algal chl a biomass and

suitable habitat are largely underestimated for multiyear ice. Glob Chang Biol 23:4581–4597. doi: 10.1111/gcb.13742

Lange BA, Katlein C, Castellani G, et al (2017b) Characterizing spatial variability of ice algal chlorophyll a and net primary production between sea ice habitats using horizontal profiling platforms. Front Mar Sci 4:349. doi: 10.3389/fmars.2017.00349

Lange BA, Katlein C, Nicolaus M, et al (2016) Sea ice algae chlorophyll a concentrations derived from under-ice spectral radiation profiling platforms. J Geophys Res Ocean 121:8511–8534. doi: 10.1002/2016JC011991

Legendre L, Gosselin M (1991) In situ spectroradiometric estimation of microalgal biomass in first-year sea ice. Polar Biol 11:113–115. doi: 10.1007/BF00234273

Leu E, Mundy CJ, Assmy P, et al (2015) Arctic spring awakening – Steering principles behind the phenology of vernal ice algal blooms. Prog Oceanogr 139:151–170. doi: 10.1016/j.pocean.2015.07.012

Leu E, Søreide JE, Hessen DO, et al (2011) Consequences of changing sea-ice cover for primary and secondary producers in the European Arctic shelf seas: Timing, quantity, and quality. Prog Oceanogr 90:18–32. doi: 10.1016/j.pocean.2011.02.004

Lin H, Kuzminov FI, Park J, et al (2016) The fate of photons absorbed by phytoplankton in the global ocean. Science 351:264–267. doi: 10.1126/science.aab2213

Liston GE, Polashenski C, Rösel A, et al (2018) A distributed snow evolution model for sea ice applications (SnowModel). J Geophys Res Ocean. doi: 10.1002/2017JC013706

Lowry KE, Pickart RS, Selz V, et al (2018) Under-ice phytoplankton blooms inhibited by spring convective mixing in refreezing leads. J Geophys Res Ocean 123:90–109. doi: 10.1002/2016JC012575

Lowry KE, van Dijken GL, Arrigo KR (2014) Evidence of under-ice phytoplankton blooms in the Chukchi Sea from 1998 to 2012. Deep Res Part II 105:105–117. doi: 10.1016/j.dsr2.2014.03.013

Lund-Hansen LC, Hawes I, Nielsen MH, Sorrell BK (2017) Is colonization of sea ice by diatoms facilitated by increased surface roughness in growing ice crystals? Polar Biol 40:593–602. doi: 10.1007/s00300-016-1981-3

McDonald S, Koulis T, Ehn J, et al (2015) A functional regression model for predicting optical depth and estimating attenuation coefficients in sea-ice covers near Resolute

Passage, Canada. Ann Glaciol 56:147–154. doi: 10.3189/2015AoG69A004

McMinn A, Hegseth EN (2004) Quantum yield and photosynthetic parameters of marine microalgae from the southern Arctic Ocean, Svalbard. J Mar Biol Assoc United Kingdom 84:865–871. doi: 10.1017/S0025315404010112h

Meier WN, Hovelsrud GK, van Oort BEH, et al (2014) Actic sea ice in transformation: A review of recent observed changes and impacts on biology and human activity. Rev Geophys 51:185–217. doi: 10.1002/2013RG000431

Meiners KM, Arndt S, Bestley S, et al (2017) Antarctic pack ice algal distribution: Floe-scale spatial variability and predictability from physical parameters. Geophys Res Lett 44:7382–7390. doi: 10.1002/2017GL074346

Melbourne-Thomas J, Meiners KM, Mundy CJ, et al (2015) Algorithms to estimate Antarctic sea ice algal biomass from under-ice irradiance spectra at regional scales. Mar Ecol Prog Ser 536:107–121. doi: 10.3354/meps11396

Mobley CD (1994) Light and water: radiative transfer in natural waters. Academic press

Mundy CJ, Ehn JK, Barber DG, Michel C (2007) Influence of snow cover and algae on the spectral dependence of transmitted irradiance through Arctic landfast first-year sea ice. J Geophys Res Ocean 112:C03007. doi: 10.1029/2006JC003683

Mundy CJ, Gosselin M, Ehn J, et al (2009) Contribution of under-ice primary production to an ice-edge upwelling phytoplankton bloom in the Canadian Beaufort Sea. Geophys Res Lett 36:L17601. doi: 10.1029/2009GL038837

Mundy CJ, Gosselin M, Gratton Y, et al (2014) Role of environmental factors on phytoplankton bloom initiation under landfast sea ice in Resolute Passage, Canada. Mar Ecol Prog Ser 497:39–49. doi: 10.3354/meps10587

Nansen F (1906) Northern waters: captain Roald Amundsen's oceanographic observations in the Arctic seas in 1901, with a discussion of the origin of the bottom-waters of the northern seas. Fridtjof Nansens Fond, Christiania. Available at: http://www.clarityonthesea.org/files/pdf_archive/nansen-1906-northern waters.pdf

Nicolaus M, Gerland S, Hudson SR, et al (2010) Seasonality of spectral albedo and transmittance as observed in the Arctic Transpolar Drift in 2007. J Geophys Res Ocean 115:C11011. doi: 10.1029/2009JC006074

Nicolaus M, Katlein C, Maslanik J, Hendricks S (2012) Changes in Arctic sea ice result in increasing light transmittance and absorption. Geophys Res Lett 39:L24501. doi:

10.1029/2012GL053738

Olsen LM, Laney SR, Duarte P, et al (2017) The seeding of ice algal blooms in Arctic pack ice: The multiyear ice seed repository hypothesis. J Geophys Res Biogeosciences 122:1529–1548. doi: 10.1002/2016JG003668

Organelli E, Bricaud A, Antoine D, Uitz J (2013) Multivariate approach for the retrieval of phytoplankton size structure from measured light absorption spectra in the Mediterranean Sea (BOUSSOLE site). Appl Opt 52:2257–73. doi: 10.1364/AO.52.002257

Pavlov AK, Granskog MA, Stedmon CA, et al (2015) Contrasting optical properties of surface waters across the Fram Strait and its potential biological implications. J Mar Syst 143:62–72. doi: 10.1016/j.jmarsys.2014.11.001

Pavlov AK, Taskjelle T, Kauko HM, et al (2017) Altered inherent optical properties and estimates of the underwater light field during an Arctic under-ice bloom of *Phaeocystis pouchetii*. J Geophys Res Ocean 122:4939–4961. doi: 10.1002/2016JC012471

Perovich DK (1990) Theoretical estimates of light reflection and transmission by spatially complex and temporally varying sea ice covers. J Geophys Res 95:9557–9567. doi: 10.1029/JC095iC06p09557

Perovich DK, Polashenski C (2012) Albedo evolution of seasonal Arctic sea ice. Geophys Res Lett 39:L08501. doi: 10.1029/2012GL051432

Perovich DK, Roesler CS, Pegau WS (1998) Variability in Arctic sea ice optical properties. J Geophys Res 103:1193–1208

Petrou K, Hill R, Doblin MA, et al (2011) Photoprotection of sea-ice microalgal communities from the east Antarctic pack ice. J Phycol 47:77–86. doi: 10.1111/j.1529-8817.2010.00944.x

Pomeroy LR (1997) Primary production in the Arctic Ocean estimated from dissolved oxygen. J Mar Syst 10:1–8

Poulin M, Daugbjerg N, Gradinger R, et al (2011) The pan-Arctic biodiversity of marine pelagic and sea-ice unicellular eukaryotes: A first-attempt assessment. Mar Biodivers 41:13–28. doi: 10.1007/s12526-010-0058-8

Ratkova TN, Wassmann P (2005) Sea ice algae in the White and Barents seas: Composition and origin. Polar Res 24:95–110. doi: DOI 10.1111/j.1751-

8369.2005.tb00143.x

Reigstad M, Wassmann P (2007) Does *Phaeocystis* spp. contribute significantly to vertical export of organic carbon? Biogeochemistry 83:217–234. doi: 10.1007/s10533-007-9093-3

Robinson DH, Kolber Z, Sullivan CW (1997) Photophysiology and photoacclimation in surface sea ice algae from McMurdo Sound, Antarctica. Mar Ecol Prog Ser 147:243–256. doi: 10.3354/meps147243

Rysgaard S, Nielsen TG (2006) Carbon cycling in a high-arctic marine ecosystem - Young Sound, NE Greenland. Prog Oceanogr 71:426–445. doi: 10.1016/j.pocean.2006.09.004

Schoemann V, Becquevort S, Stefels J, et al (2005) *Phaeocystis* blooms in the global ocean and their controlling mechanisms: a review. J Sea Res 53:43–66. doi: 10.1016/j.seares.2004.01.008

Scoresby W (1820) An account of the Arctic regions, with a history and description of the northern whale-fishery. Archibald constable and co., Edinburgh. Available at: http://www.clarityonthesea.org/files/pdf_archive/scoresby-1820-account arctic regions 1.pdf ; http://www.clarityonthesea.org/files/pdf_archive/scoresby-1820-account arctic regions 2.pdf

Shick JM, Dunlap WC (2002) Mycosporine-like amino acids and related gadusols: biosynthesis, acumulation, and UV-protective functions in aquatic organisms. Annu Rev Physiol 64:223–262. doi: 10.1146/annurev.physiol.64.081501.155802

Smith REH, Harrison WG, Harris LR, Herman AW (1990) Vertical fine structure of particulate matter and nutrients in sea ice of the high Arctic. Can J Fish Aquat Sci 47:1348–1355. doi: 10.1139/f90-154

Syvertsen EE (1991) Ice algae in the Barents Sea: types of assemblages, origin, fate and role in the ice-edge phytoplankton bloom. Polar Res 10:277–288. doi: 10.1111/j.1751-8369.1991.tb00653.x

Søreide JE, Leu E, Berge J, et al (2010) Timing of blooms, algal food quality and *Calanus glacialis* reproduction and growth in a changing Arctic. Glob Chang Biol 16:3154–3163. doi: 10.1111/j.1365-2486.2010.02175.x

Taskjelle T, Granskog MA, Pavlov AK, et al (2017) Effects of an Arctic under-ice bloom on solar radiant heating of the water column. J Geophys Res Ocean 122:126–138.

doi: 10.1002/2016JC012187

Tremblay J-É, Anderson LG, Matrai P, et al (2015) Global and regional drivers of nutrient supply, primary production and CO_2 drawdown in the changing Arctic Ocean. Prog Oceanogr 139:171–196. doi: 10.1016/j.pocean.2015.08.009

Uusikivi J, Vähätalo A, Granskog MA, Sommaruga R (2010) Contribution of mycosporine-like amino acids and colored dissolved and particulate matter to sea ice optical properties and ultraviolet attenuation. Limnol Oceanogr 55:703–713. doi: 10.4319/lo.2009.55.2.0703

van Leeuwe MA, Tedesco L, Arrigo KR, et al (2018) Microalgal community structure and primary production in Arctic and Antarctic sea ice: A synthesis. Elem Sci Anthr 6:4. doi: 10.1525/elementa.267

Vernet M, Richardson TL, Metfies K, et al (2017) Models of plankton community changes during a warm water anomaly in Arctic waters show altered trophic pathways with minimal changes in carbon export. Front Mar Sci 4:160. doi: 10.3389/fmars.2017.00160

von Quillfeldt CH, Hegseth EN, Johnsen G, et al (2009) Ice algae. In: Sakshaug E, Johnsen G, Kovacs K (eds) Ecosystem Barents Sea. Tapir Academic Press, Trondheim, pp 285–302

Wassmann P, Duarte CM, Agustí S, Sejr MK (2011) Footprints of climate change in the Arctic marine ecosystem. Glob Chang Biol 17:1235–1249. doi: 10.1111/j.1365-2486.2010.02311.x

Wollenburg JE, Katlein C, Nehrke G, et al (2018) Ballasting by cryogenic gypsum enhances carbon export in a *Phaeocystis* under-ice bloom. Sci Rep 8:7703. doi: 10.1038/s41598-018-26016-0

Wongpan P, Meiners KM, Langhorne PJ, et al (2018) Estimation of Antarctic land-fast sea ice algal biomass and snow thickness from under-ice radiance spectra in two contrasting areas. J Geophys Res Ocean 123:1907–1923. doi: 10.1002/2017JC013711

Zeebe RE, Eicken H, Robinson DH, et al (1996) Modeling the heating and melting of sea ice through light absorption by microalgae. J Geophys Res 101:1163–1181. doi: 10.1029/95JC02687

Paper I

SCIENTIFIC REP⚙RTS

OPEN

Leads in Arctic pack ice enable early phytoplankton blooms below snow-covered sea ice

Philipp Assmy[1], Mar Fernández-Méndez[1], Pedro Duarte[1], Amelie Meyer[1], Achim Randelhoff[1,2], Christopher J. Mundy[3], Lasse M. Olsen[1], Hanna M. Kauko[1], Allison Bailey[1], Melissa Chierici[4], Lana Cohen[1], Anthony P. Doulgeris[5], Jens K. Ehn[3], Agneta Fransson[1], Sebastian Gerland[1], Haakon Hop[1,2], Stephen R. Hudson[1], Nick Hughes[6], Polona Itkin[1], Geir Johnsen[7,8], Jennifer A. King[1], Boris P. Koch[9], Zoe Koenig[10], Slawomir Kwasniewski[11], Samuel R. Laney[12], Marcel Nicolaus[9], Alexey K. Pavlov[1], Christopher M. Polashenski[13], Christine Provost[10], Anja Rösel[1], Marthe Sandbu[7], Gunnar Spreen[1,14], Lars H. Smedsrud[15,16], Arild Sundfjord[1], Torbjørn Taskjelle[17], Agnieszka Tatarek[11], Jozef Wiktor[11], Penelope M. Wagner[6], Anette Wold[1], Harald Steen[1] & Mats A. Granskog[1]

The Arctic icescape is rapidly transforming from a thicker multiyear ice cover to a thinner and largely seasonal first-year ice cover with significant consequences for Arctic primary production. One critical challenge is to understand how productivity will change within the next decades. Recent studies have reported extensive phytoplankton blooms beneath ponded sea ice during summer, indicating that satellite-based Arctic annual primary production estimates may be significantly underestimated. Here we present a unique time-series of a phytoplankton spring bloom observed beneath snow-covered Arctic pack ice. The bloom, dominated by the haptophyte algae *Phaeocystis pouchetii*, caused near depletion of the surface nitrate inventory and a decline in dissolved inorganic carbon by $16 \pm 6\,g\,C\,m^{-2}$. Ocean circulation characteristics in the area indicated that the bloom developed *in situ* despite the snow-covered sea ice. Leads in the dynamic ice cover provided added sunlight necessary to initiate and sustain the bloom. Phytoplankton blooms beneath snow-covered ice might become more common and widespread in the future Arctic Ocean with frequent lead formation due to thinner and more dynamic sea ice despite projected increases in high-Arctic snowfall. This could alter productivity, marine food webs and carbon sequestration in the Arctic Ocean.

Annual phytoplankton net primary production in the Arctic Ocean has increased by 30% since the late 1990's mainly due to the declining sea ice extent and an increasing phytoplankton growth season[1]. However, there is considerable uncertainty about the future change in Arctic Ocean primary productivity largely attributed to the

[1]Norwegian Polar Institute, Fram Centre, 9296 Tromsø, Norway. [2]Department of Arctic and Marine Biology, Faculty of Biosciences, Fisheries and Economics, UiT The Arctic University of Norway, 9037 Tromsø, Norway. [3]Centre for Earth Observation Science, University of Manitoba, Winnipeg, MB R3T 2N2, Canada. [4]Institute of Marine Research, 9019 Tromsø, Norway. [5]Department of Physics and Technology, Faculty of Science and Technology, UiT The Arctic University of Norway, 9037 Tromsø, Norway. [6]Norwegian Meteorological Institute, 9239 Tromsø, Norway. [7]Centre for Autonomous Marine Operations and Systems, Department of Biology, Norwegian University of Science and Technology, 7491 Trondheim, Norway. [8]University Centre in Svalbard, Post box 156, 9171 Longyearbyen, Norway. [9]Alfred Wegener Institute, Helmholtz Center for Polar and Marine Research, 27570 Bremerhaven, Germany. [10]LOCEAN, UMR 7159, CNRS/UPMC/MNHN/IRD, Pierre and Marie Curie University, Paris cedex, France. [11]Institute of Oceanology, Polish Academy of Sciences, 81-712 Sopot, Poland. [12]Biology Department, Woods Hole Oceanographic Institution, Woods Hole, MA 02543, USA. [13]U.S. Army, Cold Regions Research and Engineering Laboratory, Hanover, NH 03755, USA. [14]Institute of Environmental Physics, University of Bremen, 28334 Bremen, Germany. [15]Bjerknes Centre for Climate Research, 5007 Bergen, Norway. [16]Geophysical Institute, University of Bergen, 5007 Bergen, Norway. [17]Department of Physics and Technology, University of Bergen, 5007 Bergen, Norway. Correspondence and requests for materials should be addressed to P.A. (email: Philipp.Assmy@npolar.no)

different representation of the intricate balance between nutrient and light availability in coupled physical and biological ocean models[2,3]. The sea ice zone was identified as the area with largest model uncertainty[2]. Thus, a better understanding of the processes that control primary productivity in ice-covered waters will help to reduce this uncertainty.

Phytoplankton production beneath the ice-covered Arctic Ocean is assumed negligible because of the strong light attenuation properties of snow and sea ice, despite sporadic reports of phytoplankton growth beneath Arctic sea ice over the past decades[4–8]. This paradigm has recently been challenged by observations of under-ice phytoplankton blooms during the summer melt season[9–12]. In these studies, snowmelt onset and subsequent melt-pond formation permitted sufficient light transmission through the consolidated ice cover to trigger diatom-dominated phytoplankton blooms fuelled by underlying nutrient-rich waters[9–12]. In areas where extensive diatom blooms under thinning Arctic ice cover occur, current satellite-based estimates of annual primary production could be underestimated by an order of magnitude and change our perception of Arctic marine ecosystems[10]. In this study, we show for the first time that an under-ice phytoplankton bloom dominated by *Phaeocystis pouchetii* was actively growing beneath snow-covered pack ice at higher latitudes and earlier in the season than previously observed.

We studied the ice-associated ecosystem and the environmental factors shaping it in the Arctic Ocean north of Svalbard from 11 January to 24 June 2015 during the Norwegian young sea ICE (N-ICE2015) expedition[13]. Four ice camps were established during N-ICE2015[13], but herein we focus on drifts of ice floes 3 and 4 covering early spring to early summer (Fig. 1a). Chlorophyll (Chl *a*) concentrations in the water column were low ($<0.5\,\mu g\,L^{-1}$) until 25 May when we first drifted into an under-ice phytoplankton bloom over the Yermak Plateau (YP) 80 km north of the ice edge (Fig. 1a) and remained within it until the end of the expedition on 22 June (Fig. 1b). The onset of the bloom coincided with shallowing of the pycnocline (Fig. 1b) and reduction in turbulent mixing (Table S1). This resulted in an increased residence time in the surface layer and thus light exposure of phytoplankton. Maximum Chl *a* concentrations of $7.5\,\mu g\,L^{-1}$ were observed on 2 June and 50 m depth-integrated Chl *a* and particulate organic carbon (POC) standing stocks ranged between 109–233 mg Chl $a\,m^{-2}$ and 9–$22\,g\,C\,m^{-2}$. The under-ice bloom (10–80 km from open waters) nearly depleted the surface nitrate inventory (Fig. 1c) and reduced dissolved inorganic carbon (DIC) at depths down to 50 m (Fig. S1). The depth of nutrient depletion clearly indicates drawdown by phytoplankton rather than ice algal growth. Indeed, the ice algal community, dominated by pennate diatoms, was distinct from the under-ice bloom. The under-ice bloom was dominated by *P. pouchetii* (Fig. 2a), which accounted for 55–92% of phytoplankton abundance and 12–93% of phytoplankton biomass and occurred both in its flagellate stage (Fig. 2b) and as large colonies (Fig. 2c). Furthermore, ice algal standing stocks were low (<3 mg Chl $a\,m^{-2}$) throughout the drift indicating that contributions from the ice to water column stocks were negligible. A detailed list of protist plankton taxa observed during the bloom period can be found in the Supplementary Information (Table S2).

Regional ice thickness surveys with radius up to 50 km from the ice camp showed a total (ice plus snow) modal thickness of 1.8 m, with a secondary mode at 0.2 m, representing thin, lead ice (Fig. S2). Local surveys on floes 3 and 4 agreed, showing a modal ice thickness of 1.46 ± 0.66 m for the thick ice, covered by 0.39 ± 0.21 m of snow (Fig. S2), while snow thickness on the thin ice ranged from 0.01–0.06 m. Thus, for modelling of the under-ice light field and primary production, we treat all ice as being one of these two modal types either 'thick ice' with thick snow cover or 'thin ice' representative of recently refrozen leads with thin snow cover. The dominant snow-covered thick ice transmitted, on average, only $<1\%$ of the incident photosynthetic active radiation (E_{PAR}) to the underlying water column. On the other hand, E_{PAR} transmittance for thin ice examined near camp in a refrozen lead was 20% on average, ranging from 6.3–42.2%. Leads in the ice pack (Fig. S3) were frequently created by ice divergence events (Fig. S5) prior to and during the bloom period. This high lead fraction is characteristic of the pack ice north of Svalbard[14]. Satellite-based ice type classification (Fig. S4 and Table S3) indicated that open water and thin, newly formed ice covered 1–33% of the area during the bloom period (Fig. 3a). Melt ponds were not a major factor in light availability during this study. Snowmelt did not start until early June and melt ponds formed only towards the end of the study period, covering $<10\%$ of the ice surface. We combined the estimated aerial fractions of open water, thin ice and thick, snow-covered ice with E_{PAR} transmittance through these surfaces to estimate the aggregate light field (Fig. 3a and Figs S6 and S7) experienced by phytoplankton.

The growth potential of *P. pouchetii* was modelled based on ^{14}C photosynthesis-irradiance (PE) relationships obtained from a *P. pouchetii* bloom in the Greenland Sea[15], taking into account the underwater light field based on measured[16] and modelled irradiance through three different surface types (open water, thin ice with thin snow cover and thicker ice with thick snow cover) encountered during the study. The primary production (PP) model supports the observation that the bloom was actively growing beneath the ice despite the low irradiance (Fig. 3b). This is in accordance with previous studies showing that *Phaeocystis* is particularly well adapted to low light environments[17,18]. *In vivo* photosynthetic parameters, obtained with the Pulse Amplitude Modulation (PAM) method to assess the photo-acclimation status of the bloom, corroborate this finding (Table S5). High maximum quantum yields of charge separation in photosystem II (Chl *a* fluorescence of dark-acclimated cells) of 0.48–0.66 showed that the bloom-forming species were in good condition and actively growing. The maximum light utilization coefficient (α) of 0.188–0.295, obtained from Rapid Light Curves, also illustrates that the bloom exhibited high photosynthetic rates at low irradiances. Furthermore, the low POC/Chl *a* ratio of 31.4 in the upper 25 m of the under-ice water column suggests a relatively high investment in photosynthetic pigments, indicative of shade-acclimation. On the other hand, light saturation (E_k) values of 137–584 μmol photons $m^{-2}\,s^{-1}$ suggests that the phytoplankton community was at the same time acclimated to relatively high irradiances. This apparent inconsistency can be explained by the plasticity in photosynthetic performance of *P. pouchetii* that seems to be a characteristic feature of this species[15] promoting its dominance under the highly variable light regime encountered during this study. The relatively minor contribution of diatoms to the under-ice bloom (Fig. 2a), with the exception of 8 June, is supported by the PP model results (Table S4). Diatoms are usually a major component of the phytoplankton spring bloom in the marginal ice zone north of Svalbard[19] and have been reported to dominate
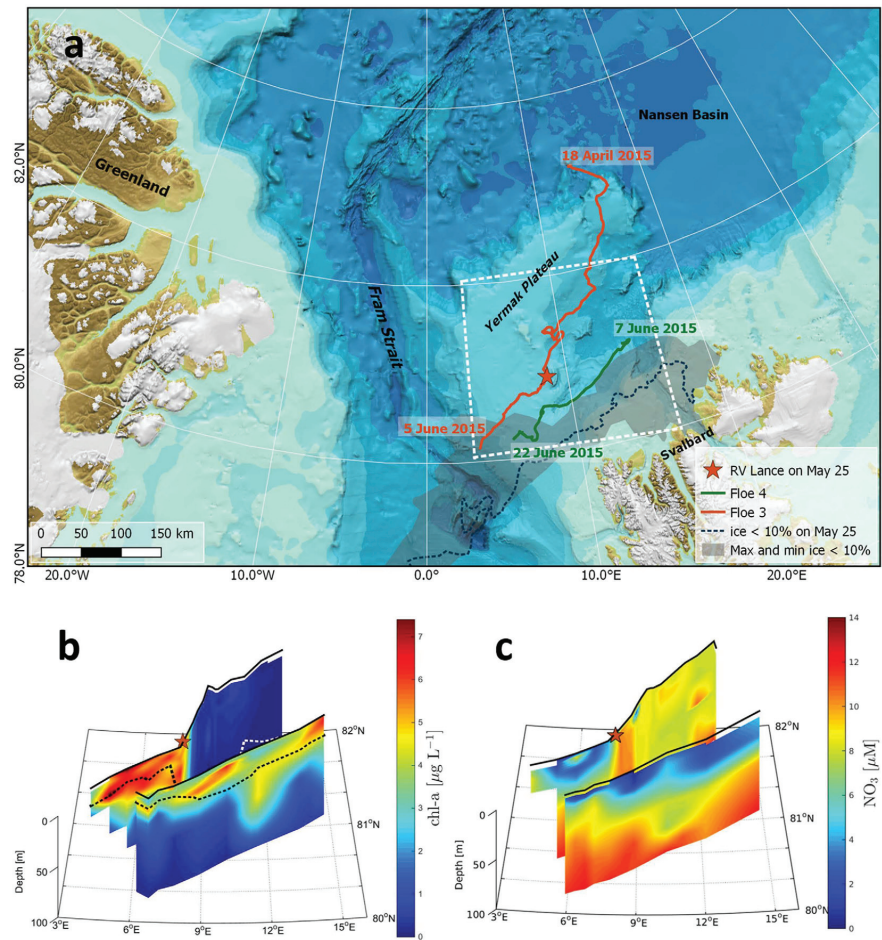
Figure 1. Study location and vertical and spatial extent of the under-ice bloom. (**a**) European Arctic with bathymetry. Orange and green lines are the drift trajectories of floes 3 and 4, respectively, with start and end dates. The location when we first drifted into the under-ice bloom on 25 May is indicated with an orange star. The area demarcating the ice-edge positions between April and June 2015 is shaded in grey. The ice-edge position on 25 May is indicated by the broken blue line and is representative for the bloom period. We define the ice edge as the outer perimeter of a polygon where ice concentration is >10%. The white outline demarcates the area shown in panels b and c. Map created by the Norwegian Polar Institute, Max König with permission from IBCAO[47]. Drift trajectories of floes 3 and 4 showing (**b**) Chlorophyll *a*, and (**c**), nitrate concentrations for the upper 100 m of the water column. The dashed line in (**b**) indicates depth of the pycnocline.

under-ice blooms below ponded ice in summer[9–12]. The dynamic light conditions beneath the snow-covered drifting pack ice interspersed with transparent leads were apparently not sufficient to sustain growth rates for diatom bloom build-up[20]. Silicic acid concentrations in the upper 50 m during the bloom period remained close to winter values at $4.0 \pm 0.4\,\mu mol\,L^{-1}$ (Fig. S8), suggesting that no substantial diatom growth had taken place in these waters.

Measurements made with a vessel-mounted profiling current meter during the drifts over the YP indicated that transport velocities in Polar Surface Water (PSW) were weak. Time-mean current velocity components in PSW at 20–30 m depth for the bloom period were $2.2\,cm\,s^{-1}$ heading nearly due west (Table S6). While these observations do not explicitly cover areas upstream of the drift itself, they indicate that advection over this part of YP was very weak during the expedition. An operational ocean model (PSY4, Mercator-Ocean, Table S6) shows similar, but smaller, net currents due west (Fig. 3c) at the same depth. These simulations do not contain tidal forcing and thus no tidal residual currents.
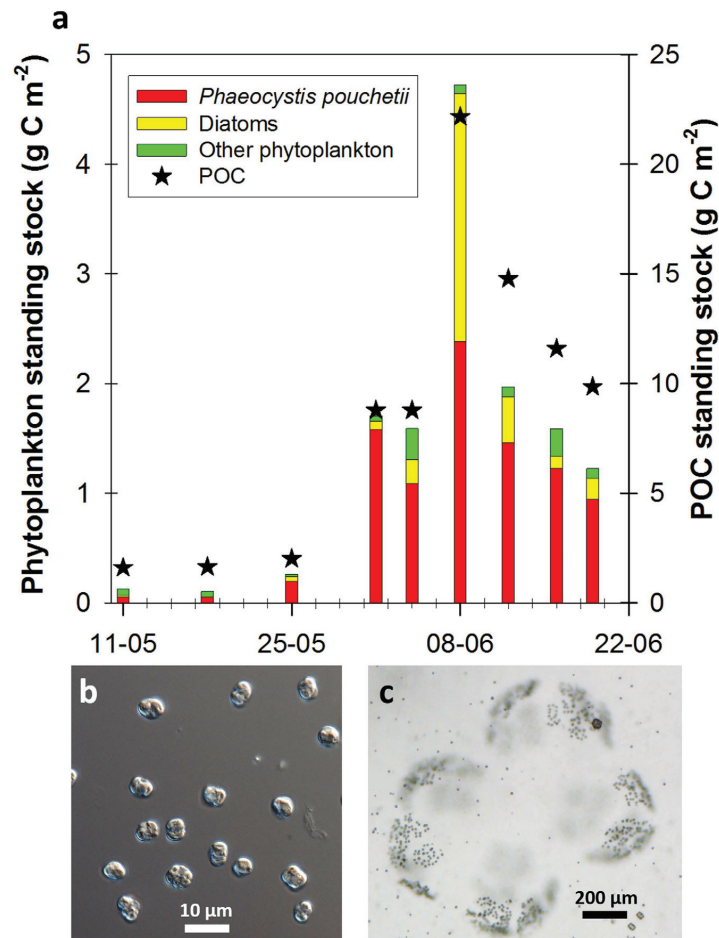
Figure 2. Composition of the under-ice phytoplankton bloom and particulate organic carbon standing stocks.
(**a**) Integrated stocks of phytoplankton carbon (coloured bars) with contributions of *Phaeocystis pouchetii*, diatoms and other phytoplankton and particulate organic carbon (black stars) for the upper 50 m surface layer. Micrographs of (**b**), solitary cells (600x magnification) and (**c**), a colony of *P. pouchetii* (100x magnification).

Model and observations both suggest that surface waters over the interior YP were not advected from open water regions. During the bloom, model and observations show the presence of Atlantic Water (AW) masses at greater depths (Fig. 3d). The overall circulation regime was not favourable for rapid advection of AW from the main branches of the West Spitsbergen Current into the interior part of the YP. Mean currents on the YP itself were weak and not capable of advecting substantial volumes of surface waters from the ice edge to the northern-most part of the observed bloom on time scales less than six weeks. Six weeks prior to the observed under-ice bloom (12 and 13 April), we measured Chl *a* concentrations of $<0.1 \mu g L^{-1}$ in open waters across the shelf slope north of Svalbard on transit to floe 3. Thus, the weak re-circulation pattern over YP implies that the bloom grew *in situ* beneath the ice pack. The area that floes 3 and 4 drifted over towards the end of their respective drifts in June was open water in mid-April when the ice edge was at its northern-most position during the period April to June 2015 (Fig. 1a and Supplementary Video). Considering the low Chl *a* concentration measured in April, our observations also discount the alternative explanation that the bloom developed in open waters and was subsequently covered by drifting sea ice. However, enhanced vertical mixing over the YP[21] supports the theory that *P. pouchetii* cells were likely mixed upwards from the sub-surface AW into the bloom in the PSW, thus contributing to the seeding of the bloom. This is consistent with observations that *P. pouchetii* is affiliated with AW[22]. Furthermore, in winter AW can be found close to the surface over the southern parts of YP providing another potential seeding mechanism.

The mean integrated drawdown of $16 \pm 6 \, g \, C \, m^{-2}$ in the DIC inventory and a nitrate uptake equivalent to $15 \pm 5 \, g \, C \, m^{-2}$ for the bloom period agreed well with the build-up in POC standing stocks. The biogeochemical footprint

Figure 3. Primary production model and water mass circulation over the Yermak Plateau. (a) Open water, thin and thick ice concentration an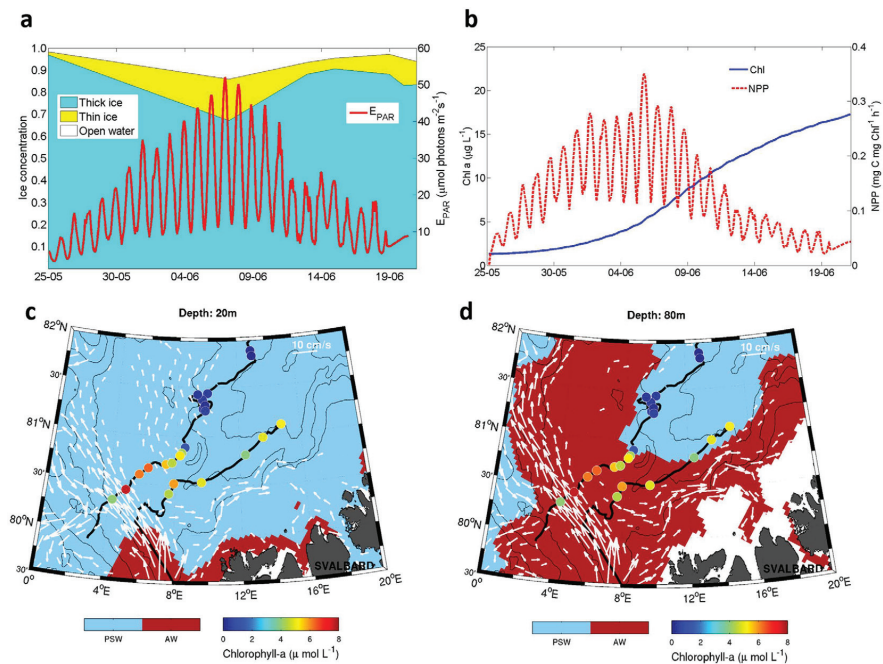d weight-averaged E_{PAR} right below the sea surface based on the aerial fractions of the three different surface types. The white and coloured areas represent the area fraction of open water and sea ice, respectively, derived from satellite data (Supplementary Fig. S4). E_{PAR} values are modelled from surface E_{PAR} measurements and taking into account the diurnal cycle, different fractions of ice and open water and their respective optical properties. **(b)** Temporal evolution of Chl *a* concentration and net primary production (NPP) during the bloom period predicted by the model. Map of **(c)**, surface (20 m) and **(d)**, subsurface (80 m) simulated currents from model outputs with currents $>2\,cm\,s^{-1}$. Current velocity is indicated by the size of the vectors (scale on figure). Black lines show drift trajectories. Colour dots show surface Chl *a* concentrations as measured along track indicating the bloom locations. Background colours show surface and subsurface water masses where blue is Polar Surface Water (PSW) and red is Atlantic Water (AW). Areas shallower than 20 m **(c)** and 80 m **(d)** are white. Topography of the Yermak Plateau is shown as thin black lines (500, 1000, 2000 and 3000 m). The maps in **(c)** and **(d)** were generated with the m-map package of Matlab 8.4 (https://www.eoas.ubc.ca/~rich/map.html).

of the bloom was comparable to a diatom bloom beneath ponded, more transparent sea ice at a lower latitude[12]. Carbon export rates at 100 m increased from 74 to 244 mg C m^{-2} d^{-1} during the bloom period. Inspection of 100 m depth sediment-trap material revealed that the bulk of vertical carbon export was mediated via *P. pouchetii* aggregates, while zooplankton faecal pellets accounted for <2%. Out of the 63 zooplankton taxa identified in 200 μm MultiNet samples taken during the bloom period, the three dominant *Calanus* species (*C. finmarchicus*, *C. glacialis* and *C. hyperboreus*) accounted for $89 \pm 8\%$ of the total zooplankton biomass. The apparently low grazing impact on the *P. pouchetii* bloom by the dominant *Calanus* copepods is supported by the finding that *P. pouchetii* does not significantly contribute to *Calanus* diet[23]. Daily export rates were low, corresponding to 0.9–2% of POC standing stocks in the upper 100 m. This is consistent with previous measurements from the Barents Sea[24] and supports the finding that *P. pouchetii* does not contribute much to deep carbon sequestration, which is generally mediated by diatoms[25,26]. This is corroborated by the dominance of fatty acid trophic markers from diatoms, rather than *Phaeocystis*, in benthic macrofauna[27]. Significant export of *P. pouchetii* biomass below 100 m has been reported previously[28,29], but has been attributed to downwelling[29], deep vertical mixing[26] or could potentially be attributed to other mechanisms facilitating deep export such as mineral ballasting.

Our observations extend the spatial and temporal domains of known under-ice blooms. High lead fraction provided sufficient light to initiate and sustain an under-ice spring bloom dominated by *P. pouchetii,* despite the thick snow cover and limited light transmission. High lead fractions in Fram Strait, the Barents Sea, and in other parts of the Arctic Ocean[14] suggest that early phytoplankton blooms under snow-covered sea ice might be widespread and become more prevalent in the future Arctic Ocean under an increasingly thinner and dynamic ice cover[30] and a projected increase in high-Arctic snowfall[31]. This trend could be reinforced by the recent increase in advective transport of AW into the European Arctic[32] seeding PSW with shade-adapted *P. pouchetii*, a conjecture

that is corroborated by a shift in dominance from diatoms towards *P. pouchetii* in Fram Strait since 2006[33–35]. Nutrient depletion by early *P. pouchetii* blooms under snow-covered sea ice would constrain diatom blooms during the melt season, with far-reaching repercussions on bloom timing and composition, strength of the biological carbon pump and energy flow through Arctic marine food webs.

Methods

Standard analytical procedures. Chl *a* samples were collected on 25-mm GF/F filters (Whatman), extracted in 100% methanol for 12 h at 5 °C on board the ship and measured fluorometrically with an AU10 Turner Fluorometer (Turner Design, Inc.). Phaeopigments were measured by fluorescence after acidification with 5% HCl. Calibration of the Turner Fluorometer was carried out following the JGOFS protocol[36]. Chl *a* measurement uncertainty (5.5% of measured values) was estimated from triplicate water samples taken from depths ranging between 5 and 100 m. Particulate organic carbon (POC) and particulate organic nitrogen (PON) samples were collected onto pre-combusted 25-mm GF/F filters (Whatman), dried at 60 °C and stored at room temperature in PALL filter slides until analysis with continuous-flow mass spectrometry (CF-IMRS) carried out with a Roboprep/tracermass mass spectrometer (Europa Scientific, UK). All POC/N values were corrected for instrument drift and blanks. Water samples for inorganic nutrients were collected in 20 mL scintillation vials, fixed with 0.2 mL chloroform and stored refrigerated until sample analysis approximately 6 months later. Nitrite, nitrate, phosphate and silicic acid were measured spectrophotometrically at 540, 540, 810 and 810 nm, respectively, on a modified Scalar autoanalyser. The measurement uncertainty for nitrite is $0.06 \mu mol \, L^{-1}$ and 10% or less for nitrate, phosphate and silicic acid. Seawater for DIC analyses was sampled in 250 mL borosilicate bottles, preserved with $60 \mu L$ saturated mercuric chloride solution and stored dark and cool. DIC was determined using gas extraction followed by colourometric detection[37]. Certified Reference Material (CRM from A. Dickson at Scripps Institution of Oceanography, USA) was used for calibration and to check the accuracy of the analysis. The integrated nutrient drawdown in the upper 50 m for the bloom period was estimated from salinity-normalized (34.33) nDIC and nNO_3^- (nitrate) for all stations and converted to carbon using the measured POC/PON ratio of 5.7 ± 1.3. The complete N-ICE2015 water column biogeochemical dataset has been published in the Norwegian Polar Data Centre[38].

Sediment traps. Ice-tethered sediment traps (KC Denmark) were deployed four times at 5, 25, 50 and 100 m depth during the bloom period. Deployment time varied between 36 and 72 h, but was usually close to 48 h. Before deployment, each trap cylinder was filled with a saturated NaCl solution to reduce microbial activity and thus increase the retention of organic matter. The traps were carefully deployed and retrieved to avoid loss of trap material. Swimmers (copepods and other zooplankton) were removed before sub-sampling for Chl *a*, POC, plankton taxonomy, and faecal pellets.

Phyto-PAM measurements. The maximum quantum yield of charge separation in photosystem II Chl *a* fluorescence ($\Phi PSII$-max), the light saturation parameter (E_k), the maximum light utilization coefficient (α) and the maximum relative electron transfer rate ($rETR_{max}$) were obtained using the Pulse Amplitude Modulated (PAM) fluorometry method with a Phyto-PAM (Walz, Germany) following established protocols[39].

Phyto- and zooplankton analysis. Phytoplankton samples were settled in 50 mL Utermöhl sedimentation chambers (HYDRO-BIOS©, Kiel, Germany) for 48 h. Phytoplankton was identified and enumerated at 100–600× magnification using an inverted Nikon Ti-S light and epifluorescence microscope. The organisms were identified to the lowest taxonomic level possible under inverted light microscopy, ideally to species level, otherwise to genus level or grouped into size-classes. Microscopic counts of the dominant organisms at each depth were always well above the recommended number of 50 per sample. Further, the water column stocks presented in Fig. 2 are integrations of 4 discrete samples from the upper 50 m of the water column, so the total number of specimens counted per predominating species per water column was >100 in most cases, reducing the error to <20%. Randomly chosen individuals of each phytoplankton species/group were measured and the average cell size was used to calculate the biovolume from equivalent geometrical shapes[40]. The biovolume was converted to cellular carbon content using published carbon conversion factors[41].

Mesozooplankton was sampled with a MultiNet (HYDRO-BIOS©, Kiel, Germany) consisting of five nets with a $0.25 m^2$ opening and $200 \mu m$ mesh size at the following depth strata: 0–20, 20–50, 50–200 and 200 m-bottom. Zooplankton were preserved using 4% formaldehyde solution in seawater buffered with hexamethylentetramine and identified to species and stage[42].

Irradiance measurements. Solar spectral planar irradiance (E_λ) was measured simultaneously with two upward-looking Ramses spectral radiometers with cosine collectors (Ramses ACC-VIS, Trios GmbH, Germany). One measured the incident and the second the transmitted irradiance at the bottom of the ice. These measurements were integrated over the wavelength band of photosynthetically active radiation (PAR, 400–700 nm) and then used to estimate the transmittance (fraction of transmitted to incident radiation) of E_{PAR}, photosynthetically active radiation (PAR, 400–700 nm) through the ice and snow. The measurements were conducted continuously during floes 3 and 4 at a site representative of the thick snow-covered ice[43]. The same type of sensors were used to determine the transmittance of E_{PAR} for thin ice (<0.25 m) in a refrozen lead. In addition, incident irradiance and irradiance under thick and thin ice was measured with Satlantic HyperOCR hyperspectral radiometers with cosine collectors, at the surface and mounted to a remotely operated vehicle (ROV) respectively. From these measurements, transmittance of E_{PAR} was calculated as with the Ramses data.

Primary production model. A simple primary production model was applied using photosynthesis versus irradiance data obtained during an Arctic *Phaeocystis*-dominated phytoplankton bloom[15] combined with measured[16] and modelled irradiance through thick ice with thick snow cover, thin ice with thin snow cover and open water taking into account the areal fractions of the three different surface types. A detailed description of the primary production model can be found in the Supplementary Information.

Ice and snow thickness measurements. Total ice and snow thickness was measured with a portable electromagnetic instrument (EM31, Geonics Ltd., Mississauga, Ontario, Canada) mounted on a sledge[44]. In addition, large-scale surveys of total ice and snow thickness were conducted with a helicopter-borne EM instrument (HEM, Ferra Dynamics Inc, Mississauga, Ontario, Canada)[45]. The EM31 and HEM measurements use the same principle. The height above the bottom of the ice is derived from the strength of electromagnetic induction in the conductive sea water under the ice. For the HEM measurements, the height of the instrument above the surface of the ice or snow is determined with a laser altimeter included in the HEM instrument. The EM31 conductivity values were calibrated with drill-hole measurements and post processed to derive total thickness of ice and snow. Snow thickness was measured with a GPS snow probe (Magnaprobe, Snow-Hydro, Fairbanks, AK, USA)[46]. When used together, these two instruments give the spatial distribution of both the total thickness of the ice and snow (from EM31) and the snow depth (from Magnaprobe). For direct comparison of the values, and to subtract' the snow from the EM31 data, we re-sampled the EM31 data on the Magnaprobe track and applied a Gaussian filter to the EM31 data. The EM31 and Magnaprobe datasets were median-sampled on a 5 m regular grid. Snow depth was subtracted from the EM31 values to derive sea-ice thickness.

References

1. Arrigo, K. R. & van Dijken, G. L. Continued increases in Arctic Ocean primary production. *Progr. Oceanogr.* **136,** 60–70 (2015).
2. Vancoppenolle, M. *et al.* Future Arctic Ocean primary productivity from CMIP5 simulations: Uncertain outcome, but consistent mechanisms. *Global Biogeochem. Cy.* **27,** 605–619 (2013).
3. Popova, E. E. *et al.* What controls primary production in the Arctic Ocean? Results from an intercomparison of five general circulation models with biogeochemistry. *J. Geophys. Res.* **117,** C00D12 (2012).
4. Michel, C., Legendre, L., Therriault, J. C., Demers, S. & Vandevelde, T. Springtime coupling between ice algal and phytoplankton assemblages in southeastern Hudson Bay, Canadian Arctic. *Polar Biol.* **13,** 441–449 (1993).
5. Strass, V. H. & Nöthig, E. M. Seasonal shifts in ice edge phytoplankton blooms in the Barents Sea related to the water column stability. *Polar Biol.* **16,** 409–422 (1996).
6. Pomeroy, L. R. Primary production in the Arctic Ocean estimated from dissolved oxygen. *J. Mar. Syst.* **10,** 1–8 (1997).
7. Gosselin, M. *et al.* New measurements of phytoplankton and ice algal production in the Arctic Ocean. *Deep Sea Res. PT II* **44,** 1623–1644 (1997).
8. Fortier, M., Fortier, L., Michel, C. & Legendre, L. Climatic and biological forcing of the vertical flux of biogenic particles under seasonal Arctic sea ice. *Mar. Ecol. Prog. Ser.* **225,** 1–16 (2002).
9. Arrigo, K. R. *et al.* Massive phytoplankton blooms under Arctic sea ice. *Science* **336,** 1408–1408 (2012).
10. Arrigo, K. R. *et al.* Phytoplankton blooms beneath the sea ice in the Chukchi Sea. *Deep-Sea Res. PT II* **105,** 1–16 (2014).
11. Mundy, C. J. *et al.* Contribution of under-ice primary production to an ice-edge upwelling phytoplankton bloom in the Canadian Beaufort Sea. *Geophys. Res. Lett.* **36,** L17601 (2009).
12. Mundy, C. J. *et al.* Role of environmental factors on phytoplankton bloom initiation under landfast sea ice in Resolute Passage, Canada. *Mar. Ecol. Prog. Ser.* **497,** 39–49 (2014).
13. Granskog, M. A. *et al.* Arctic research on thin ice: Consequences of Arctic sea ice loss. *EOS Trans. AGU* **97,** 22–26 (2016).
14. Willmes, S. & Heinemann, G. Sea-ice wintertime lead frequencies and regional characteristics in the Arctic, 2003–2015. *Remote Sens.* **8,** doi: 10.3390/rs8010004 (2016).
15. Cota, G. F., Smith, W. O. Jr. & Mitchell, B. G. Photosynthesis of *Phaeocystis* in the Greenland Sea. *Limnol. Oceanogr.* **39,** 948–953 (1994).
16. Taskjelle, T., Granskog, M. A., Pavlov, A. K., Hudson, S. R. & Hamre, B. Effects of an Arctic under-ice bloom on solar radiant heating of the water column. *J. Geophys. Res. Oceans*, doi: 10.1002/2016JC012187 (2016).
17. Palmisano, A. C. *et al.* Photoadaptation in *Phaeocystis pouchetii* advected beneath annual sea ice in McMurdo Sound, Antarctica. *J. Plankton Res.* **8,** 891–906 (1986).
18. Sakshaug, E. & Skjoldal, H. R. Life at the ice edge. *Ambio* **18,** 60–67 (1989).
19. Degerlund, M. & Eilertsen, H. C. Main species characteristics of phytoplankton spring blooms in NE Atlantic and Arctic Waters (68–80 degrees N). *Estuaries and Coasts* **33,** 242–269 (2010).
20. Hoppe, C. J. M., Holtz, L.-M., Trimborn, S. & Rost, B. Ocean acidification decreases the light-use efficiency in an Antarctic diatom under dynamic but not constant light. *New Phytol* **207,** 159–171 (2015).
21. Rippeth, T. P. *et al.* Tide-mediated warming of Arctic halocline by Atlantic heat fluxes over rough topography. *Nature Geosci.* **8,** 191–194 (2015).
22. Metfies, K., von Appen, W.-J., Kilias, E., Nicolaus, A. & Nöthig, E.-M. Biogeography and photosynthetic biomass of Arctic marine pico-eukaryotes during summer of the record sea ice minimum 2012. *PLoS ONE* **11,** e0148512, doi: 10.1371/journal.pone.0148512 (2016).
23. Ray, J. L. *et al.* Molecular gut content analysis demonstrates that *Calanus* grazing on *Phaeocystis pouchetii* and *Skeletonema marinoi* is sensitive to bloom phase but not prey density. *Mar. Ecol. Prog. Ser.* **542,** 63–77 (2016).
24. Reigstad, M., Wexels Riser, C., Wassmann, P. & Ratkova, T. Vertical export of particulate organic carbon: Attenuation, composition and loss rates in the northern Barents Sea. *Deep Sea Res. PT II* **55,** 2308–2319 (2008).
25. Wassmann, P., Vernet, M., Mitchell, B. G. & Rey, F. Mass sedimentation of *Phaeocystis pouchetii* in the Barents Sea. *Mar. Ecol. Prog. Ser.* **66,** 183–195 (1990).
26. Reigstad, M. & Wassmann, P. Does *Phaeocystis* spp. contribute significantly to vertical export of organic carbon? *Biogeochem.* **83,** 217–234 (2007).
27. Søreide, J. E. *et al.* Sympagic-pelagic-benthic coupling in Arctic and Atlantic waters around Svalbard revealed by stable isotopic and fatty acid tracers. *Mar. Biol. Res.* **9,** 831–850 (2013).
28. Le Moigne, F. A. C. *et al.* Carbon export efficiency and phytoplankton community composition in the Atlantic sector of the Arctic Ocean. *J. Geophys. Res.* **120,** 3896–3912 (2015).
29. Lalande, C., Bauerfeind, E. & Nothig, E.-M. Downward particulate organic carbon export at high temporal resolution in the eastern Fram Strait: influence of Atlantic Water on flux composition. *Mar. Ecol. Prog. Ser.* **440,** 127–136 (2011).
30. Kwok, R., Spreen, G. & Pang, S. Arctic sea ice circulation and drift speed: Decadal trends and ocean currents. *J. Geophys. Res.* **118,** 2408–2425 (2013).

31. Bintanja, R. & Selten, F. M. Future increases in Arctic precipitation linked to local evaporation and sea-ice retreat. *Nature* **509**, 479–484 (2014).
32. Carmack, E. *et al.* Towards quantifying the increasing role of oceanic heat in sea ice loss in the new Arctic. *B. Am. Meteorol. Soc.* **97**, 2079–2105 (2015).
33. Lasternas, S. & Agusti, S. Phytoplankton community structure during the record Arctic ice-melting of summer 2007. *Polar Biol.* **33**, 1709–1717 (2010).
34. Lalande, C., Bauerfeind, E., Nöthig, E.-M. & Beszczynska-Moller, A. Impact of a warm anomaly on export fluxes of biogenic matter in the eastern Fram Strait. *Progr. Oceanogr.* **109**, 70–7 (2013).
35. Nöthig, E.-M. *et al.* Summertime plankton in Fram Strait – a compilation of long- and short-term observations. *Polar Res.* **34**, 23349 (2015).
36. Knap, A., Michaels, A., Close, A., Ducklow, H. & Dickson, A. Measurement of Chlorophyll *a* and Phaeopigments by fluorometric analysis. *JGOFS Rep.* **19**, 118–122 (1996).
37. Dickson, A. G., Sabine, C. L. & Christian, J. R. Guide to best practices for ocean CO_2 measurements. *PICES Spec. Publ.* **3**, 191 pp (2007).
38. Assmy, P. *et al.* N-ICE2015 water column biogeochemistry (v1.0) [Data set]. Norwegian Polar Institute. doi: 10.21334/npolar.2016. 3ebb7f64 (2009).
39. Nymark, M. *et al.* An integrated analysis of molecular acclimation to high light in the marine diatom *Phaeodactylum tricornutum*. *PloS ONE* **11**, e7743 (2009).
40. Hillebrand, H., Duerselen, C. D., Kirschtel, D., Pollingher, U. & Zohary, T. Biovolume calculation for pelagic and benthic microalgae. *J Phycol* **35**, 403–424 (1999).
41. Menden-Deuer, S. & Lessard, E. J. Carbon to volume relationships for dinoflagellates, diatoms and other protist plankton. *Limnol. Oceanogr.* **45**, 569–579 (2000).
42. Kwasniewski, S., Hop, H., Falk-Petersen, S. & Pedersen, G. Distribution of *Calanus* species in Kongsfjorden, a glacial fjord in Svalbard. *J. Plankton. Res.* **25**, 1–20 (2003).
43. Taskjelle, T., Hudson, S. R., Pavlov, A. & Granskog, M. A. N-ICE2015 surface and under-ice spectral shortwave radiation data (v1.4) [*Data set*]. *Norwegian Polar Institute*, doi: 10.21334/npolar.2016.9089792e (2016).
44. Rösel, A. *et al.* N-ICE2015 total (snow and ice) thickness data from EM31 (v1.0) [Data set]. Norwegian Polar Institute. doi: 10.21334/npolar.2016.70352512 (2016).
45. King, J, Gerland, S., Spreen, G. & Bratrein, M. N-ICE2015 sea-ice thickness measurements from helicopter-borne electromagnetic induction sounding [Data set]. Norwegian Polar Institute. doi: 10.21334/npolar.2016.aa3a5232 (2016).
46. Rösel, A. *et al.* N-ICE2015 snow depth data with Magna Probe [Data set]. Norwegian Polar Institute. doi: 10.21334/npolar.2016.3d72756d (2016).
47. Jakobsson, M. *et al.* The International Bathymetric Chart of the Arctic Ocean (IBCAO) Version 3.0. *Geophys. Res. Lett.* **39**, L12609 (2012).

Acknowledgements

Author Contributions

H.S., M.A.G., S.R.H., S.G., G.S., L.H.S., N.H., A.S., P.A. and P.D. designed the field campaign. M.F.M., H.M.K., L.M.O., C.J.M., H.H., A.W., A.B., M.S., P.D., M.C., A.F., M.A.G., S.R.L., B.P.K. and P.A. collected and analysed the biogeochemical data. M.S., P.D., H.M.K. and G.J. performed the Phyto-PAM measurements and analysed the data. L.C., M.A.G. and S.R.H. conducted the atmospheric measurements. A.T. and J.W. performed the phytoplankton analysis and S.K. the zooplankton analysis. A.M., A.Ra., L.H.S. and Z.K. performed the oceanographic measurements. Z.K. and C.P. contributed with the operational model PSY4 from Mercator-Ocean. A.R., J.A.K., P.I., G.S., M.N., C.M.P. and S.G. contributed sea ice, snow and ice dynamics data. T.T., C.J.M., A.K.P., S.R.H., H.M.K., J.K.E. and M.A.G. conducted the irradiance measurements and analysed the data. P.M.W., N.H. and A.P.D. contributed remote sensing data and the sea ice classification. P.A. drafted the first manuscript; and all authors contributed to the final version.

Additional Information

Paper II

RESEARCH ARTICLE

Key Points:
- High PAR transmittance (up to 0.41) through a refrozen lead compared to thicker snow-covered ice (<0.003)
- Ice algal biomass was similar in both ice types, despite greater light availability in the lead ice, possibly hampered by high irradiance
- High total MAA concentrations in the CDOM-low lead ice due to high light exposure

Supporting Information:
- Supporting Information S1

Correspondence to:
H. M. Kauko,
hanna.kauko@npolar.no

Windows in Arctic sea ice: Light transmission and ice algae in a refrozen lead

Hanna M. Kauko[1,2] ![iD], Torbjørn Taskjelle[3] ![iD], Philipp Assmy[1] ![iD], Alexey K. Pavlov[1] ![iD], C. J. Mundy[4], Pedro Duarte[1] ![iD], Mar Fernández-Méndez[1], Lasse M. Olsen[1] ![iD], Stephen R. Hudson[1] ![iD], Geir Johnsen[2], Ashley Elliott[4], Feiyue Wang[4], and Mats A. Granskog[1] ![iD]

[1]Norwegian Polar Institute, Tromsø, Norway, [2]Trondhjem Biological Station, Department of Biology, Norwegian University of Science and Technology, Trondheim, Norway, [3]Department of Physics and Technology, University of Bergen, Bergen, Norway, [4]Centre for Earth Observation Science, University of Manitoba, Winnipeg, Manitoba, Canada

Abstract The Arctic Ocean is rapidly changing from thicker multiyear to thinner first-year ice cover, with significant consequences for radiative transfer through the ice pack and light availability for algal growth. A thinner, more dynamic ice cover will possibly result in more frequent leads, covered by newly formed ice with little snow cover. We studied a refrozen lead (≤0.27 m ice) in drifting pack ice north of Svalbard (80.5–81.8°N) in May–June 2015 during the Norwegian young sea ICE expedition (N-ICE2015). We measured downwelling incident and ice-transmitted spectral irradiance, and colored dissolved organic matter (CDOM), particle absorption, ultraviolet (UV)-protecting mycosporine-like amino acids (MAAs), and chlorophyll *a* (Chl *a*) in melted sea ice samples. We found occasionally very high MAA concentrations (up to 39 mg m^{-3}, mean 4.5 ± 7.8 mg m^{-3}) and MAA to Chl *a* ratios (up to 6.3, mean 1.2 ± 1.3). Disagreement in modeled and observed transmittance in the UV range let us conclude that MAA signatures in CDOM absorption spectra may be artifacts due to osmotic shock during ice melting. Although observed PAR (photosynthetically active radiation) transmittance through the thin ice was significantly higher than that of the adjacent thicker ice with deep snow cover, ice algal standing stocks were low (≤2.31 mg Chl *a* m^{-2}) and similar to the adjacent ice. Ice algal accumulation in the lead was possibly delayed by the low inoculum and the time needed for photoacclimation to the high-light environment. However, leads are important for phytoplankton growth by acting like windows into the water column.

1. Introduction

Arctic sea ice has changed rapidly over the last decades, from a predominantly thicker perennial to a seasonal and thinner ice cover, with implications for the whole Arctic marine system [e.g., *Meier et al.*, 2014]. The new ice-free areas have prompted an increase in phytoplankton primary production [*Arrigo and van Dijken*, 2015]. In ice-covered areas, thinning of the ice results in increased light availability in the visible range [*Nicolaus et al.*, 2012] and exposure to ultraviolet light [*Fountoulakis et al.*, 2014] for algae both associated with the ice (ice algae) and in the underlying water column (phytoplankton).

Dynamics of the Arctic ice cover are expected to increase, with accelerated motion of the thinner ice cover [*Kwok et al.*, 2013; *Itkin et al.*, 2017]. Leads are a ubiquitous feature of the Arctic ice cover, and the region north of Svalbard was identified as one with frequent occurrence of leads in the ice pack [*Willmes and Heinemann*, 2016], promoting formation of thin ice in the winter and spring. Despite relatively low coverage in the total ice pack, leads are important for the energy fluxes for the surrounding ice and the underlying water column [*Vivier et al.*, 2016; *Taskjelle et al.*, 2017]. Thin snow-free ice has high light transmittance: in an Arctic fjord (Kongsfjorden, Svalbard), 77–86% of incident light in the PAR range was transmitted through newly formed ice that accumulated ice algal biomass rapidly in a matter of days [*Taskjelle et al.*, 2016b].

Snow cover plays a critical role in the transparency of the sea ice cover and the resulting light field in and under the ice because it has a much stronger effect on light attenuation than the sea ice itself [*Grenfell and Maykut*, 1977; *Perovich*, 1990; *Hamre et al.*, 2004]. Thus, the snow cover influences the growth environment for sea ice algae. During early spring, primary production is light-limited and ice algal biomass is a negative function of snow depth [*Leu et al.*, 2015]. This relationship may reverse toward summer if the snow cover transmits enough light but delays bottom melt and the concomitant termination of the ice algal bloom and can protect ice algae from harmfully high irradiance levels [*Leu et al.*, 2015]. Under thin snow cover, the bottom ice community can

be sloughed off due to brine drainage and ice melt [*Mundy et al.*, 2005; *Campbell et al.*, 2014]. On the other hand, high ice algal standing stocks can increase ice melting due to increased energy absorption and heat dissipation, as shown in a modeling study by *Zeebe et al.* [1996]. The extent of algal-induced sea ice melting is dependent on the snow and ice thickness (i.e., the amount of light energy that reaches the algal layer) and the distribution of algae in the ice column. For example, an algal standing stock of 100 mg m^{-2} concentrated in bottom 4 cm of 140 cm thick ice could cause an ice thickness reduction exceeding the depth of the algal layer in just over a month, thus destroying the algal habitat [*Zeebe et al.*, 1996].

Light exposure can reach damaging levels and inhibit algal photosynthesis and growth. In snow removal experiments, decrease in ice algal biomass has been attributed to elevated light levels [*Juhl and Krembs*, 2010; *Campbell et al.*, 2015]. However, algae that were acclimated to high light (under initially thinner snow cover) coped well with the snow removal [*Juhl and Krembs*, 2010]. Algae have evolved several acclimation strategies to cope with and to utilize high irradiances, spanning different time scales (seconds to days). For example, several intracellular compounds, like photoprotective carotenoids of the rapid xanthophyll cycle, have been identified to shield excess light [*Brunet et al.*, 2011]. Protection from ultraviolet light (UVA: 320–400 nm, UVB: 280–320 nm) can be achieved with mycosporine-like amino acids (MAAs; reviewed in *Karentz* [2001], *Shick and Dunlap* [2002], and *Carreto et al.* [2011]).

MAAs are small water-soluble molecules that absorb in the UV range (in vitro absorption peaks range from 309 to 362 nm) and are efficient in dissipating the absorbed energy as heat. MAAs have also other roles in various organisms, like osmoregulation [cf. *Oren and Gunde-Cimerman*, 2007], but the photochemical and photophysical properties of, e.g., porphyra-334 support the suitability for photoprotection [*Conde et al.*, 2000]. Algae in sea ice with thin or no snow cover are potentially exposed to more harmful UV radiation than phytoplankton that is subject to vertical mixing in a deep water column. Antarctic diatoms have shown higher MAA production in an experimental light regime without mixing [*Hernando et al.*, 2011].

Composition of MAAs in sea ice algae has been reported to our knowledge only from two locations in the Northern Hemisphere: the Baltic Sea [*Uusikivi et al.*, 2010; *Piiparinen et al.*, 2015] and Allen Bay in the Canadian Arctic [*Elliott et al.*, 2015]. Reports from the Antarctic exist from McMurdo Sound [*Ryan et al.*, 2002] and Palmer station [*Karentz*, 1994]. MAA-like signatures have also been observed in particle absorption samples from sea ice [*Uusikivi et al.*, 2010; *Fritsen et al.*, 2011; *Mundy et al.*, 2011; *Piiparinen et al.*, 2015; *Taskjelle et al.*, 2016b]. Likewise, MAA-like absorption peaks in the UV range have been observed in the dissolved matter fraction of melted sea ice samples [*Uusikivi et al.*, 2010; *Xie et al.*, 2014; *Logvinova et al.*, 2016; *Taskjelle et al.*, 2016b]. Besides MAAs, other algal pigments and colored dissolved organic matter (CDOM) significantly affect light absorption in the ice [*Perovich et al.*, 1998; *Belzile et al.*, 2000; *Uusikivi et al.*, 2010].

Here we present a unique spring time series of bio-optical properties in young sea ice in a refrozen lead from the Norwegian young sea ICE expedition (N-ICE2015). The N-ICE2015 expedition consisted of a nearly half-year long field campaign with drifting ice stations between 80° and 83°N in the southern Nansen Basin of the Arctic Ocean [*Granskog et al.*, 2016], with the aim to study the energy fluxes and state of the ice-associated ecosystem in the new, thinner Arctic sea ice regime. Little is known about the radiative processes in newly formed sea ice [cf. *Taskjelle et al.*, 2016b] and the suitability of young ice as a habitat, which limits our understanding of how the Arctic marine ecosystem will respond to a thinner and more dynamic ice cover in the future Arctic Ocean. *Steiner et al.* [2016] pointed out that in biogeochemical sea ice modeling there is a need for better understanding of the radiative transfer processes. The striking feature of the young ice environment is the high irradiance due to thin ice and snow cover and its potential effects on ice algae. The objectives of this study were to investigate light transmission through young sea ice and to assess the optical properties of the algal biomass growing in this type of ice. For this we characterized the absorption properties and the UV-protecting pigments (MAAs) of ice algae. To determine and disentangle the role of dissolved and particulate matter in light absorption in thin ice, we conducted a case study on light transmittance with a radiative transfer model.

2. Materials and Methods

2.1. N-ICE2015 Expedition

During the N-ICE2015 expedition research vessel *Lance* was frozen into pack ice north of Svalbard between January and June 2015 [*Granskog et al.*, 2016]. In total, four ice floes were monitored during the study period
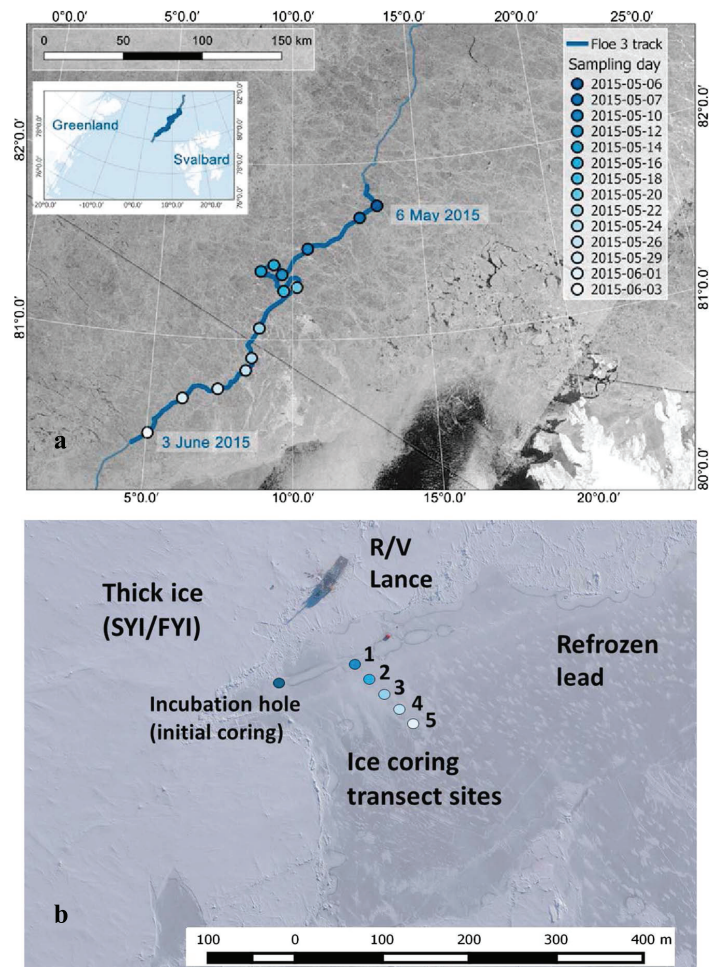
Figure 1. (a) Drift trajectory of Floe 3 of N-ICE2015 expedition north of Svalbard (satellite image taken on 25 May). The sampling period with start and end dates is marked in bold on the drift trajectory, and the sampling days are indicated with circles (see legend). Image source: RADARSAT-2 image provided by NSC/KSAT under the Norwegian-Canadian RADARSAT agreement. RADARSAT-2 Data and Products © MacDonald, Dettwiler and Associates Ltd (2013) All Rights Reserved. RADARSAT is an official mark of the Canadian Space Agency. Map created by the Norwegian Polar Institute/Max König. (b) Aerial image of the refrozen lead and R/V *Lance* (image taken on 23 May 2015) and location of sampling sites. Image: Vasily Kustov and Sergey Semenov (Arctic and Antarctic Research Institute, St. Petersburg, Russia).

to investigate the thinning Arctic ice pack. This paper presents data from the drift of Floe 3 [see *Granskog et al.*, 2016], studied from mid-April to early June, and specifically focuses on data from a refrozen lead during this part of the drift (80.5–81.8°N; Figure 1).

2.2. Sampling on the Refrozen Lead

A lead (approximately 400 m wide) that opened close to the vessel on 23 April began to refreeze on 26 April and was completely refrozen by 1 May. The young ice that formed in the lead was sampled from 6 May, when

ice had grown 15 cm thick and was safe to work on, until it broke up on 4 June. From 7 May onward, a 100 m long sampling transect was established from the edge of the lead toward its center (Figure 1b), when ice thicknesses were 17–24 cm. The transect was sampled every 2–3 days (13 times in total) between 7 May and 3 June 2015 (see Table S1; Figure 1a).

On the refrozen lead, incoming (planar downwelling) and ice-transmitted spectral irradiance ($E_d(\lambda)$) were simultaneously measured with two Ramses ACC-VIS spectroradiometers (TriOS Mess- und Datentechnik GmbH, Rastede, Germany) for the wavelength range 320–950 nm, at five locations along the transect, 25 m apart from each other (Figure 1b). Data are available in *Taskjelle et al*. [2016a]. On three occasions (see Table S1), measurements were repeated after snow was carefully removed with a shovel within a radius of about 1 m around the location of the under-ice sensor. The radius is a sufficient distance to avoid edge effects from snow cover, according to *Petrich et al*. [2012]. All sensors were factory calibrated shortly before the field campaign. Field comparisons of the different sensors suggest an uncertainty on the order of ±10% in measured energy fluxes in the UV range, due to calibration uncertainties under variable incident light fields. For under-ice measurements, a hinged arm placing the sensor 1 m away from the initial 9 cm hole was used. Measurements with a tilt less than 5° were used (3–10 spectra were averaged). Spectral irradiance was converted from W m^{-2} nm^{-1} to µmol photons m^{-2} s^{-1} for E_d(PAR). After the transmittance measurements snow depth was measured (an average of 5–10 locations within 1 m from the under-ice sensor site).

After snow depth recordings, two (until 16 May) or three (18 May onward) 9 cm diameter ice cores were collected with an ice corer (Mark II coring system, KOVACS enterprise, Roseburg, USA) at the site of the under-ice sensor and combined into one melting bucket. Occasionally, additional cores for ice stratigraphy and temperature were collected (Table S1). Ice temperature data are available in *Gerland et al*. [2017]. Brine salinity was calculated from ice temperatures based on *Cox and Weeks* [1986] for temperatures < -2°C and *Leppäranta and Manninen* [1988] for temperatures > -2°C. From 18 May onward, cores were cut into two sections: bottom 10 cm and the top (rest of the core: 9–17 cm). On a subsequent new sampling day, the transect was moved on average 2–3 m away from the earlier transect line, to measure transmittance and collect cores at an undisturbed location.

Ice cores were brought back onboard in darkness and melted overnight at room temperature without addition of filtered seawater [cf. *Rintala et al*., 2014]. The melting buckets were monitored to sample the buckets as soon as the ice had melted. Samples for fluorometric chlorophyll *a* (Chl *a*), particle absorption (a_p), and MAAs were filtered onto Whatman GF/F filters (diameter 25 mm; GE Healthcare, Little Chalfont, UK) under low vacuum pressure (ca -30 kPa) and shading from excess light. MAA and a_p samples were stored at -80°C until analysis. Colored dissolved organic matter (CDOM) samples were filtered through a 0.2 µm PALL Acrodisc syringe filter (PALL Corporation, Ann Arbor, USA) with acid-washed all-plastic syringes into precombusted amber glass vials and stored at $+4$°C in the dark. Salinity in the melted samples was measured with WTW Cond 3110 probe (WTW Wissenschaftlich-Technische Werkstätten GmbH, Weilheim, Germany). Ice core data (other than absorption spectra) are available in *Assmy et al*. [2017b].

For continuous incident spectral downwelling irradiance measurements Ramses ACC-VIS spectroradiometers (TriOS Mess- und Datentechnik GmbH, Rastede, Germany) were used [*Taskjelle et al*., 2016a]. Measurements were performed at a fixed location on the adjacent second-year ice (initial ice thickness 130 cm, snow depth 40 cm) throughout the period the refrozen lead was sampled. At the same site, another sensor recorded the under-ice irradiance [*Taskjelle et al*., 2016a].

2.3. Laboratory Analysis of Ice Core Samples

Chl *a* was extracted with 100% methanol at 5°C for 24 h [*Holm-Hansen and Riemann*, 1978] and measured fluorometrically using a Turner 10-AU Fluorometer (Turner Designs, San Jose, USA).

Particle absorbance was measured between 240 and 800 nm with a Shimadzu UV-2450 dual-beam spectrophotometer with an integrating sphere (ISR-2200, Shimadzu Corporation, Kyoto, Japan) following the modified method described in *Tassan and Ferrari* [2002] and recommendations in *Tilstone et al*. [2002] and *Mueller et al*. [2003]. The diameter of the colored area on the filter was measured on each sample individually. As a wet reference, an average of 20 blank filters, prepared with ultrapure water in the field throughout the campaign, was used to account for light scattering and absorption by the filter. Filters were bleached with

400 µL of sodium hypochlorite (NaClO with 1% active chlorine) for 10 min, with additional 20 min if first bleaching was not complete and rinsed with 30 mL of artificial seawater (60 g Na_2SO_4 in 1 L of ultrapure water). Optical density (absorbance) of particles on filters ($OD_s(\lambda)$) was converted to optical density of particles in suspension ($OD_{sus}(\lambda)$) following equation 10 in *Tassan and Ferrari* [2002]

$$OD_{sus}(\lambda) = 0.423 \times OD_s(\lambda) + 0.479 \times OD_s(\lambda)^2 \qquad (1)$$

$OD_{sus}(\lambda)$ was then converted to an absorption coefficient $a_p(\lambda)$:

$$a_p(\lambda) = 2.303 \times OD_{sus}(\lambda)/l \qquad (2)$$

where 2.303 is the natural logarithm of 10, and l is the hypothetical path length in meters, based on the ratio between the filtered sample volume and sample area diameter on the filter. A baseline correction was done relative to the mean absorption values at 750–800 nm.

Measurement before bleaching yields the total particle absorption (a_p, m^{-1}), whereas spectra after bleaching show detrital (nonpigmented particles) absorption (a_d, m^{-1}). Difference between these is the algal (pigment) absorption (a_ϕ, m^{-1}). Dividing a_ϕ by the corresponding Chl a values (in mg m^{-3}) gives Chl a-specific algal absorption (a_ϕ^*, m^2 (mg Chl)$^{-1}$). Particle spectral absorption coefficients are available in *Kauko et al.* [2017].

CDOM absorbance was measured between 240 and 700 nm with 0.5 nm resolution using a Shimadzu UV-2401PC spectrophotometer (Shimadzu Corporation, Kyoto, Japan) and 10 cm quartz cells with fresh ultrapure water as reference. Absorbance values were baseline corrected following *Stedmon et al.* [2000], using a constant that accounts for minor shifts at longer wavelengths. Absorbance values were then converted to an absorption coefficient a_{CDOM} (m^{-1}) following

$$a_{CDOM}(\lambda) = 2.303 \times A(\lambda)/l \qquad (3)$$

where $A(\lambda)$ is the absorbance at a given wavelength λ and l is the path length of the cuvette in meters. CDOM spectral absorption coefficients are available in *Pavlov et al.* [2017a].

MAA analysis by high-performance liquid chromatography (HPLC) in the Ultra-Clean Trace Elements Laboratory (UCTEL) at the University of Manitoba (Winnipeg, Canada) is described in *Elliott et al.* [2015] and based on the method by *Carreto et al.* [2005]. In short, samples were extracted with 100% methanol then evaporated to dryness and reconstituted with the starting mobile phase (0.2% formic acid in water adjusted to pH = 3.15). Analysis was done with a HPLC (Agilent 1200)-electrospray ionization (ESI)-triple quadrupole mass spectrometer (MS) (Agilent 6410b) (i.e., HPLC-ESI-MS) coupled with a diode array and multiple wavelength detector (Agilent 1100 series; Agilent technologies, Santa Clara, USA). Although a number of MAAs were detected in the samples, structural identification and quantification were only possible for shinorine, palythine, and porphyra-334 for which standards were available [*Elliott et al.*, 2015]. Total MAA concentration reported herein refers to the sum of these three components only and thus underestimates the total MAA concentration.

The procedure we used for the stratigraphy ice cores is described in more detail in *Olsen et al.* [2017] and based on the method described in *Lange* [1988]. In short, the vertical surface of the ice core section was smoothed with a microtome. Thick sections (5–7 mm) were photographed in normal light and thin sections (1 mm) in polarized light to examine air pockets, brine channels, and ice crystal structure.

2.4. Radiative Transfer Model

We applied the AccuRT radiative transfer model [*Hamre et al.*, 2017] to investigate the effect of various constituents on light attenuation in the UV and PAR range in the ice. AccuRT is a 1-D coupled atmosphere-snow-ice-ocean model based on DISORT [*Thomas and Stamnes*, 1999]. The model has been used successfully for atmosphere-snow-sea ice-ocean work by, e.g., *Hamre et al.* [2004] and on thin ice by *Taskjelle et al.* [2016b]. In this study, the atmosphere contained a 500 m thick cloud layer where volume fraction and particle size were adjusted so that the measured incident irradiance was reproduced well. The zenith angle was set to 60°, representative of time of day and location of irradiance measurements. Modeled albedo was somewhat higher (10% for snow-covered case, 20% for bare ice) than

Table 1. Descriptions of Model Components[a]

Model Component	Explanation
Observed with snow	Measured in situ transmittance
Observed without snow	Measured in situ transmittance after snow removal
Pure sea ice	Ice with brine and bubbles but without organic and inorganic matter (CDOM and particles)
Ice	Ice with brine, bubbles and matter (CDOM and/or particles) that is specified in the legend entry
Snow	The observed 2 cm snow cover
CDOM	Measured ice core sample CDOM absorption spectra
$CDOM_{exp}$	Exponential CDOM spectra; measured spectra without MAA peaks
$CDOM_{Baltic}$	CDOM absorption spectrum from Baltic Sea ice
Particles	Particle absorption (algal and nonalgal particles)

[a]Each modeling case was a combination of the different components listed.

measured, modeled absorption is thus a conservative estimate. Snow was represented by a layer of ice spheres with a radius of 170 μm and density of 205 kg m^{-3} added to the bottom of the atmosphere, with inherent optical properties (IOPs) computed using a parameterization based on Mie code [*Stamnes et al.*, 2011]. The values were chosen for optimal transmittance reproduction but are near what was measured on the refrozen lead (optical radius of snow grains 190 μm; no density measurements on 26 May but the density on 29 May was 160 kg m^{-3}; J.-C. Gallet, personal communication, 2016). The thickness of the layer was the same as the measured snow depth (2 cm). Layers containing ice in the model were specified based on the sectioning of the ice cores, i.e., a lower layer that is 10 cm thick and an upper layer that covers the remaining ice thickness. Absorption coefficients of pure ice are from *Warren and Brandt* [2008]. For pure water, absorption coefficients are from *Mason et al.* [2016] and *Pope and Fry* [1997]. Photos of thick sections indicated larger brine pockets and higher brine volume fraction in the granular ice than in the columnar ice. Brine is represented as spheres of water, and following the observations from the thick sections, we set the brine volume to 30% and 10% in the granular and columnar layers, respectively, and the radius to 1 mm and 0.3 mm. The air bubble radius was set to 0.1 mm in both layers, and the air volume fraction was adjusted until modeled transmittance had a good fit with the measured transmittance. It is assumed that the layers are uniform. With 0.85% air in the granular layer and 0.3% in the columnar layer, effective scattering coefficients ($b_{eff} = b(1 - g)$, where g is the average cosine of the scattering angle) were about 20 m^{-1} and 8 m^{-1}, respectively. As for the snow, IOPs are obtained using the parameterizations defined by *Stamnes et al.* [2011] based on the size and volume fraction of the inclusions. Absorption coefficients corresponding to the measured absorption by particulate and dissolved matter (Figure 3h) were added to the ice. Measured spectral absorption and scattering coefficients in the water column [*Pavlov et al.*, 2017b; *Taskjelle et al.*, 2017] were used for the layer describing the water column below the ice. The components used in and on the ice are listed in Table 1.

3. Results

3.1. Physical Environment

Subzero air temperatures and cloudy skies prevailed during the lead sampling period (6 May to 3 June) [*Hudson and Cohen*, 2015; *Cohen et al.*, 2017; *Walden et al.*, 2017]. Until 24 May, air temperature ranged between −20 and −10°C, except for two days (16 and 19 May) when temperatures rose to around 0°C. Both days were associated with a single large-scale storm event [*Cohen et al.*, 2017]. From 24 May onward, temperatures were between −10 and 0°C [*Cohen et al.*, 2017; *Hudson and Cohen*, 2015]. Cloud fraction was often >0.9 [*Walden et al.*, 2017]. On six days (6, 8, 12, and 22 to 24 May) lower fractions were observed (0–0.64). Ocean Conservative Temperature [*McDougall et al.*, 2012] under ice (2 m depth) was between −1.60 and −1.87°C during the sampling period, nearly at freezing temperature [*Meyer et al.*, 2017].

Ice thickness during transect sampling ranged between 17 and 27 cm (Figure 2a). Ice thickness at sites 2–5 was within a few centimeters of each other, while site 1 was the thinnest throughout. Ice growth was observed in the beginning of the sampling, but after 20 May a reduction in thickness due to ice melt was
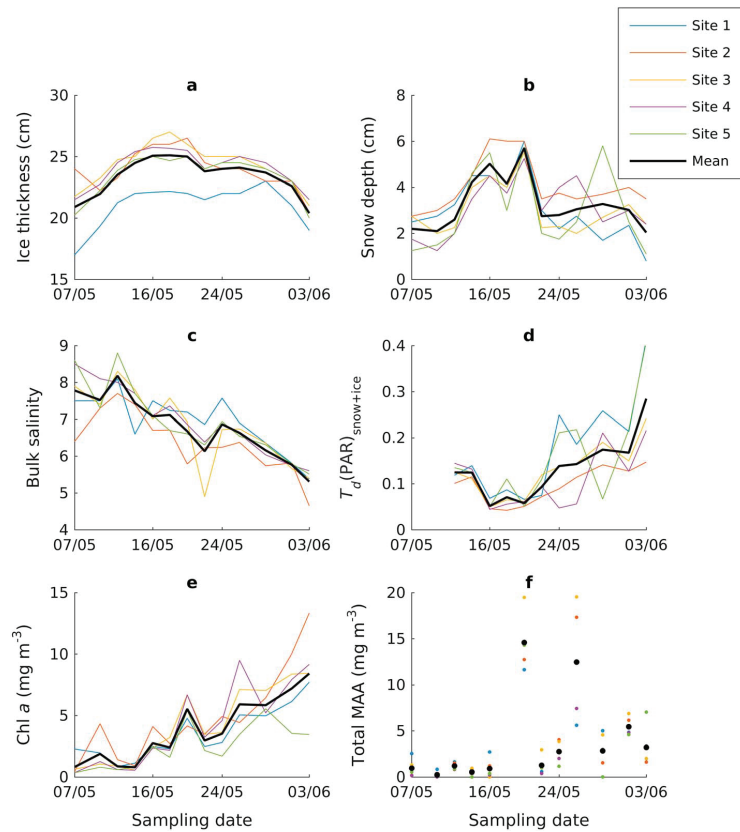
Figure 2. Time series of (a) ice thickness, (b) snow depth, (c) bulk salinity, (d) E_d(PAR) transmittance through snow and ice $(T_d(PAR)_{snow+ice})$, (e) Chl a, and (f) total MAA concentration (shinorine, palythine, and porphyra-334) for the five different coring sites on the refrozen lead, including the mean (black line or black dots). In the case of bulk salinity, Chl a, and MAAs the mean values after 18 May are volume-weighed means of the core top and bottom values. There are no data for transmittance for the first two days (7 and 10 May) and for MAA on 18 May.

observed at all sites. After 22 May ice grew slightly, but during the last week of sampling ice was continuously melting. The ice consisted of a granular ice layer on the top and columnar ice at the bottom (not shown), but the relation between granular and columnar ice was different between the sites. On 26 May, sites 1 and 5 had 4–5 cm granular ice and 17–19.5 cm of columnar ice, compared to 17 cm of granular and 5–8 cm of columnar ice at sites 2 and 3. Site 4 had 12 cm granular and 12.5 cm columnar ice.

Snow depth ranged from 1 to 6 cm (Figure 2b). The deepest snow cover (4 to 6 cm) was observed between 14 and 20 of May, concurrent with snowfall events during 16 and 19 May. After 20 May, snow depth decreased to 2–3 cm, likely due to wind redistribution. In the beginning, the refrozen lead was covered by frost flowers that were then covered by snow. Later in the sampling, the snow pack developed a surface crust of melt grain clusters and later a wind slab. The bottom of the snow pack was first characterized by loose snow, later wet, and salty depth hoar (possibly remnants of the frost flowers) or slush.

Mean sea ice bulk salinity decreased during transect sampling period from 7.8 to 5.3 (Figure 2c). Brine salinity (calculated from ice temperature) ranged between 23.9 and 52.2 during transect sampling (18 May to 1 June). On 6 May, before the transect sampling started, brine salinity was up to 78.9 in the top 3 cm of the ice core and ice temperature was −4.45°C.
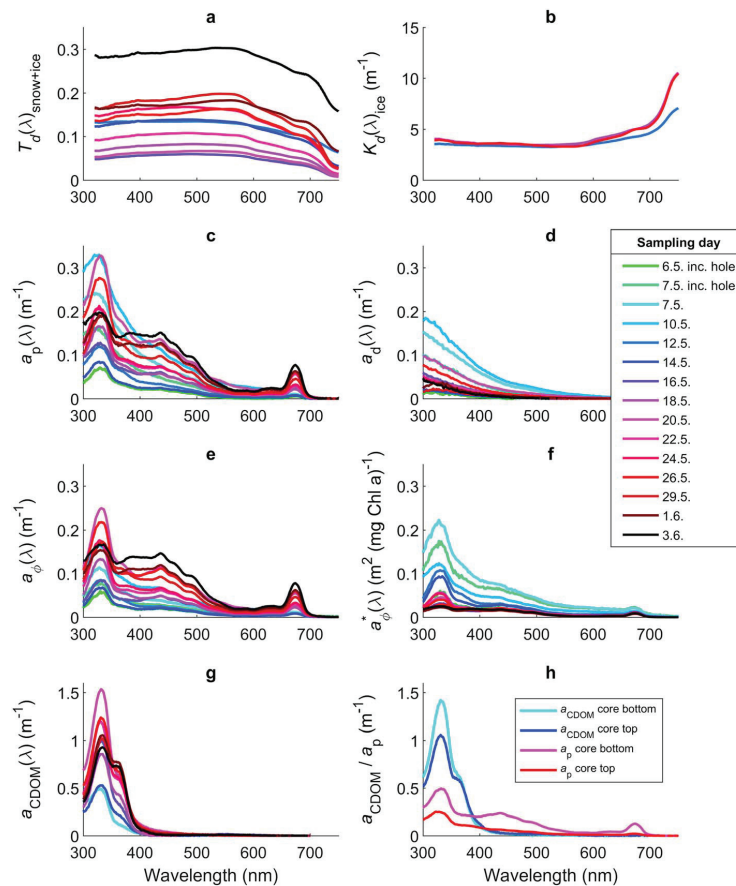
Figure 3. Absorption and diffuse attenuation coefficients and spectral transmittance in the refrozen lead. (a) Measured spectral transmittance through snow and ice. (b) Diffuse attenuation coefficients ($K_d(\lambda)_{ice}$) for ice, calculated from incoming and ice-transmitted irradiance measurements after snow removal. Absorption by particles, for (c) total (a_p), (d) detritus (a_d), and (e) algal (a_ϕ) particles. (f) Chl a-specific absorption of algae (a_ϕ^*). (g) CDOM absorption (a_{CDOM}). (h) CDOM and particle absorption spectra on 26 May on site 3. All transect spectra are averages of the five sites on the corresponding day, except in Figure 3h (only site 3). In Figures 3c–3f, the data labeled "inc. hole" (incubation hole) on 6 and 7 May are from another coring location on the lead that was sampled prior to the transect (see map in Figure 1b), with two cores averaged on 6 May and three cores averaged on 7 May. Other legend entries refer to transect sampling dates. Measurements from 12 May onward are included in Figure 3a, from 12, 18, and 26 May in Figure 3b, from all dates in Figures 3c–3f, and from all dates but 10 and 12 May in Figure 3g. From 18 May onward, values in Figures 3c–3g are volume-weighed means of the ice core top and bottom values.

Measured incoming E_d showed a distinct diurnal pattern and a slight increase from early May to early June (Figure S1), with maximum values of 1240 μmol photons m^{-2} s^{-1} for E_d(PAR) and 80 μmol photons m^{-2} s^{-1} for E_d(UV$_{350-400}$) (UV light integrated over 350–400 nm) [*Taskjelle et al.*, 2016a]. Mean E_d(PAR) values in the 48 h prior to sampling ranged between 450 and 730 μmol photons m^{-2} s^{-1} (Figure S2).

3.2. Light Transmission Measurements

Transmittance T_d(PAR)$_{snow+ice}$, the fraction of E_d(PAR) transmitted through snow and ice, was 0.05−0.41 and inversely related to snow depth (Figures 2b, 2d, and S3). Spectral transmittance, $T_d(\lambda)_{snow+ice}$, is shown in Figure 3a. Measured E_d(PAR) under the snow-covered thin ice ranged between 30 μmol photons m^{-2} s^{-1}

and 350 μmol photons m^{-2} s^{-1}. To study transmittance through bare ice, snow was carefully removed and the irradiance measurements were repeated for snow-free ice on three sampling days (12, 18, and 26 May). While it is impossible to completely remove the effect of a snow cover, the level and salty ice surface made the conditions on the lead as ideal as possible, and we are confident that any remaining snow had very little effect on the measurements. $T_d(\text{PAR})_{\text{ice}}$ for snow-free ice ranged from 0.28 to 0.49. Sites 1 and 5 had the highest snow-free transmittance on all days, and sites 2 and 3 the lowest. Transmittance after snow removal was 2.2–6.5 times higher than transmittance through snow-covered ice on the corresponding site and day. E_d (PAR) values under snow-free ice ranged between 225 and 420 μmol photons m^{-2} s^{-1}.

The diffuse attenuation coefficient $K_d(\text{PAR})_{\text{snow+ice}}$ for snow and ice was calculated from the downwelling and transmitted $E_d(\text{PAR})$ using the equation

$$K_d(\text{PAR})_{\text{snow+ice}} = \frac{1}{z} \ln\left[\frac{E_d(0,\text{PAR})}{E_d(z,\text{PAR})}\right] \quad (4)$$

where z is the total thickness of snow and ice, $E_d(0,\text{PAR})$ is downwelling irradiance above ice and snow, and E_d (z,PAR) downwelling irradiance right below the ice. $K_d(\text{PAR})_{\text{snow+ice}}$ ranged from 4.5 to 12.4 m^{-1}. Using the measurements after snow removal, we calculated K_d of the sea ice, both spectrally ($K_d(\lambda)_{\text{ice}}$) and for the PAR range (z is the total thickness of ice, and $E_d(0)$ downwelling irradiance above ice). Specular reflection of 5% ($R_s = 0.05$) was introduced following *Ehn et al.* [2004].

$$K_d = \frac{1}{z} \ln\left[(1-R_s)\frac{E_d(0)}{E_d(z)}\right] \quad (5)$$

Both $K_d(\lambda)_{\text{ice}}$ (Figure 3b) and $T_d(\lambda)_{\text{snow+ice}}$ (Figure 3a) show signs of algal pigment absorption at 674 nm especially later in the sampling period. $K_d(\text{PAR})_{\text{ice}}$ ranged between 2.9 and 4.7 m^{-1} (median and mean 3.7 m^{-1}). Based on the $K_d(\text{PAR})_{\text{ice}}$ and the $E_d(\text{PAR})$ measurements with snow, $K_d(\text{PAR})_{\text{snow}}$ for snow was calculated as follows:

$$K_d(\text{PAR})_{\text{snow}} = -\ln\left[\frac{E_d(z,\text{PAR})}{E_d(0,\text{PAR}) \times \exp\left(-K_d(\text{PAR})_{\text{ice}} \times z_{\text{ice}}\right)}\right]/z_{\text{snow}} \quad (6)$$

where z_{ice} and z_{snow} are the ice and snow thickness, respectively. $K_d(\text{PAR})_{\text{snow}}$ ranged between 21.2 and 63.7 m^{-1} (median 39.2 and mean 43.1 m^{-1}).

3.3. Biomass and Bio-optical Properties

The ice algal biomass, measured as Chl *a* standing stock, increased with time. Standing stocks in the lead were 0.06–2.31 mg Chl *a* m^{-2} and Chl *a* concentration 0.33–13.33 mg Chl *a* m^{-3} (Figure 2e). Between 20 and 22 May all sites experienced a distinct reduction in Chl *a*. Most ice algal biomass was concentrated in the ice core bottom sections (Figure 4a).

In general, total particle (a_p) and algal absorption (a_ϕ) in the PAR range increased during the study period (Figures 3c, 3e, 5a, and 5b). Values of a_ϕ at 440 nm (absorption peak of Chl *a* and contribution from other pigments) ranged between 0.015 and 0.390 m^{-1} for individual samples (Figure 3 shows averages of the five transect sites and after 18 May volume-weighed mean values of ice core top and bottom sections). In contrast, Chl *a*-specific algal absorption (a_ϕ^*) was highest in the beginning of the sampling period and then decreased (Figure 3f). Values of a_ϕ^* at 440 nm ranged between 0.013 and 0.099 m^2 (mg Chl *a*)$^{-1}$. Early days of the transect sampling show highest detrital absorption (a_d), up to almost 0.18 m^{-1} at 300 nm on average (Figure 3d). To assess the variability along the transect, we calculated the coefficient of variation (CV) at 440 nm for lead transect days: CV for a_p, a_d, a_ϕ, and a_ϕ^* was 10–63, 12–73, 11–67, and 10–61%, respectively. From 12 May onward, CV at 440 for a_p, a_ϕ, and a_ϕ^* was smaller, 10–34, 11–35, and 10–31%, respectively.

The samples collected on 20 and 26 May stand out with high absorption (and biomass, Figure 2e). All spectra show strong absorption in the near-UV range (300–400 nm). Especially in the core tops (Figures 5b and 5d), absorption in UV range is high compared to the PAR range. Toward the end of the sampling, the peak at 380 nm increased relative to the peak at 330 nm (Figure 4d).
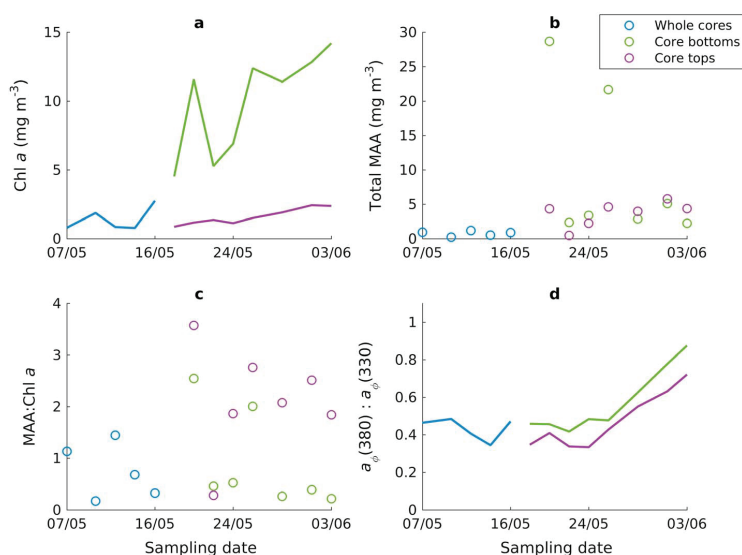
Figure 4. Time series of Chl a and MAA concentration for ice core bottom and top sections (average of five sites). Until 16 May, the ice core was sampled as one ("whole cores"). Core sectioning was started on 18 May, after which the ice core was sampled in two separate sections ("core bottoms" and "core tops"). (a) Chl a, (b) total MAA concentration, (c) MAA to Chl a ratio, and (d) ratio between algal absorption (a_{ϕ}) at 380 nm to that at 330 nm.

CDOM absorption at 295 nm ranged between 0.18 and 1.53 m^{-1} for individual samples. All CDOM samples show very high absorption in the near-UV range (peaks at 330 and 360 nm) (Figure 3g). Difference in the shape of the spectra between ice core bottom and top samples is visible (Figures 5e and 5f): a second peak, at 360 nm, becomes gradually more prominent in the core tops. Absorption values are otherwise similar.

In general, the total MAA concentration (shinorine, palythine, and porphyra-334) increased over time (Figure 2f). Two days, 20 and 26 May, stand out with high concentrations: up to almost 20 mg MAAs m^{-3} for the whole ice column (a volume-weighed mean of ice core bottom and top samples). The highest concentration (39 mg m^{-3}) was measured in an ice core bottom sample from 26 May. Mean concentration of all samples ($n = 92$) was 4.5 ± 7.8 mg m^{-3}. The difference between ice core bottom and top sections is shown in Figure 4b. The MAA to Chl a ratio (mg MAA m^{-3} to mg Chl a m^{-3}) was higher in the core tops with the exception of 22 May and ranged on average (average of five sites) up to 3.6 (Figure 4c) and for all samples up to 6.3 on 20 May (mean 1.2 ± 1.3, $n = 92$). The patterns in concentration were similar for the three individual MAAs (individual plots not shown). Shinorine was the most abundant compound, followed by porphyra-334 and then palythine. In addition to the three compounds that could be verified with standards, two unknown ones were observed: one with the absorption maximum at 331 nm and retention time of 18.0 min was abundantly present in most of the samples. This compound is likely mycosporine-serine-glycine methyl ester [*Carignan and Carreto*, 2013], based on mass spectrometer results. Based on estimated concentration using the molar extinction coefficient of the related shinorine [*Karentz*, 2001], this compound contributed on average 62 ± 25% to the total concentration of these four compounds. Another unknown compound that corresponds to U2 in *Elliott et al.* [2015], with the absorption maximum at 363 nm and a secondary peak at 337 nm, was present mainly on 20 and 29 May.

3.4. Contribution of the Different Components to Light Absorption

As a case study to investigate the role of particulate and dissolved matter for light transmittance, we used data from site 3 on 26 May and compared radiative transfer model results to measured transmittance. On this day and site, the measured snow cover was 2 cm and the observed T_d(PAR) was 0.15 and 0.32 for the ice with
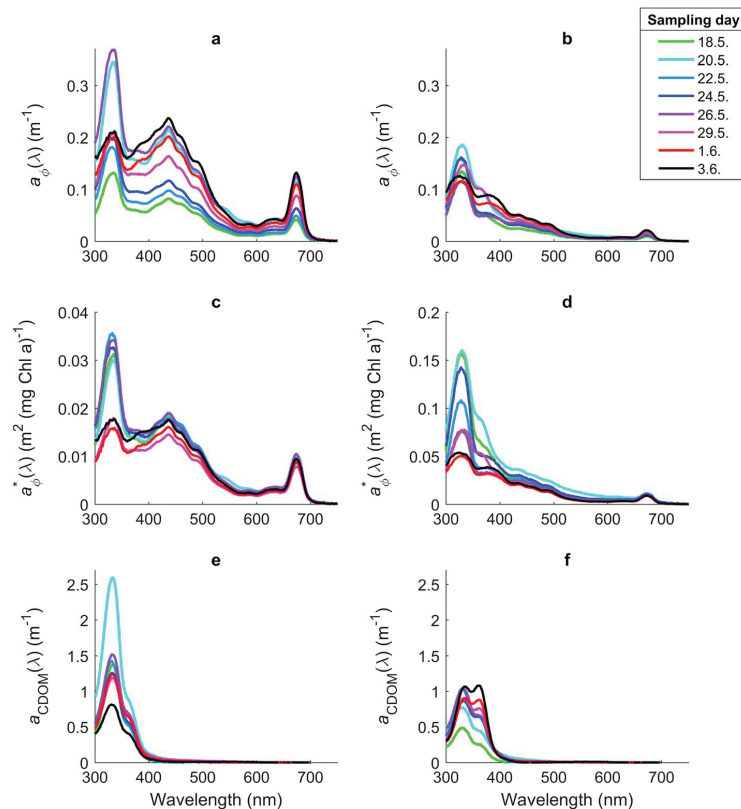
Figure 5. Absorption spectra in ice core bottoms (Figures 5a, 5c, and 5e) and tops (Figures 5b, 5d, and 5f). (a, b) Algal absorption (a_ϕ), (c, d) Chl a-specific algal absorption (a_ϕ^*), and (e, f) CDOM absorption (a_{CDOM}) coefficients. Note different scales on y axis between Figures 5c and 5d.

and without snow, respectively. Transmittance was largest at 558 nm in both cases. Modeled T_d(PAR) with all constituents was 0.15 and 0.33 with and without snow, respectively. Observed transmittance both with and without snow is contrasted with model results (Figures 6a and 6b) for four different cases: (1) pure sea ice including brine and bubbles; (2) sea ice with brine, bubbles, and measured CDOM absorption; (3) sea ice with brine, bubbles, and particle absorption (but without CDOM); and 4) sea ice with brine, bubbles, CDOM, and particle absorption. Transmittance, absorption, and bottom UV:PAR ratio values from the modeling are listed in supporting information Table S2.

The model run with pure sea ice (Figures 6a and 6b) clearly overestimated light transmission below 550 nm and between 600 and 700 nm, and peak transmittance was shifted from about 560 nm to about 500 nm compared to the observed transmittance. Likewise, the PAR range of the spectrum was overestimated in a run with measured CDOM absorption in addition to pure sea ice. Closest to the observed spectra were the runs that included particle absorption, showing that algae contributed to light attenuation in the ice. Observed PAR transmittance was 6 and 11% lower than modeling with pure sea ice with and without snow, respectively. In terms of fraction of absorbed energy in PAR, pure sea ice with 2 cm snow absorbed 25% less than ice with particles and 2 cm snow (0.03 compared to 0.04).

In the UV range the model runs with measured CDOM and particle absorption spectra gave clearly lower transmittance than observed. Modeling with all constituents resulted in 46 and 36% lower UVA transmittance for snow-covered and bare ice, respectively, than observed; e.g., for snow-covered ice, observed UVA
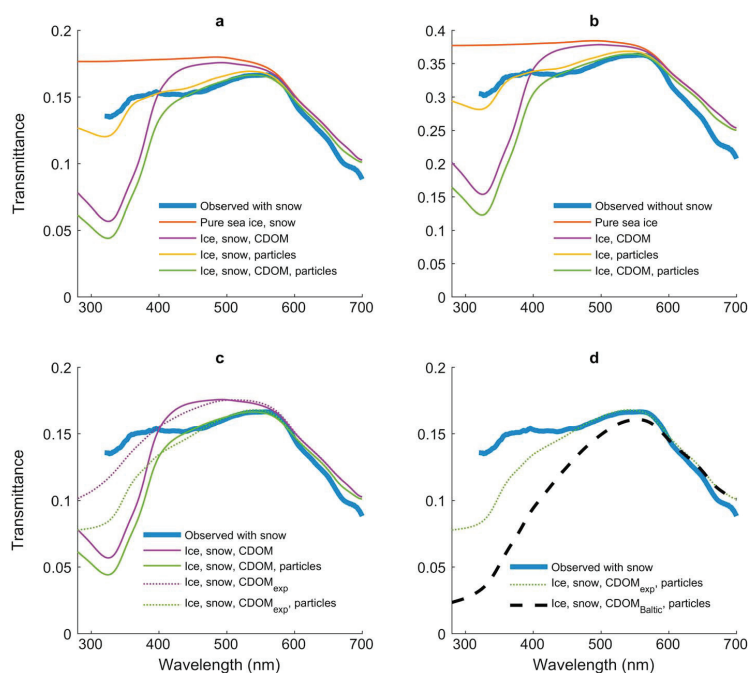
Figure 6. Contribution of the individual components to light transmission at site 3 on 26 May and comparison to Baltic Sea CDOM, examined with the radiative transfer model. Measurements and modeling (a) with snow cover (2 cm) and (b) after snow removal. (c) Modeling with CDOM spectra without MAA peaks ($CDOM_{exp}$). (d) High CDOM case equivalent to Baltic Sea ice [*Uusikivi et al.*, 2010]. Thick blue lines show observed transmittance, and other lines represent model cases with different optical components included (see Table 1 for explanations). "Snow" means the observed 2 cm snow cover. "Pure sea ice" and "ice" include brine and bubbles.

transmittance was 0.15 and modeled (with all constituents) 0.08 (due to the lower limit of the instrument, 320 nm, comparison can only be done for UVA range).

To overcome the model discrepancy in the UV range, an exponential CDOM spectrum, without the MAA peaks, was used in further modeling (see Figure S3). For the part of the spectrum that is affected by MAA absorption (300–425 nm), the spectral slope is calculated based on the values outside the MAA region [*Pavlov et al.*, 2014]. This modification was based on earlier reports of elevated absorption in the UV range after sample handling, caused by leakage of MAAs onto the filter and into the filtrate [*Laurion et al.*, 2003], and will be discussed in section 4.3.

UV transmittance for the exponential (ice and exponential CDOM spectra; without MAA peaks) and measured CDOM case (ice and measured CDOM spectra; with MAA peaks) was, respectively, 0.14 and 0.10 for snow-covered ice (Figure 6c). In other words, using exponential CDOM spectra resulted in 40% higher UV transmittance for snow-covered ice than using the measured spectra. Compared to in situ light measurements, using an exponential CDOM absorption spectrum (together with ice and particle absorption) resulted in 27% lower UVA transmittance for snow-covered ice. Therefore, modeled light attenuation spectrum with the exponential CDOM matched better with that observed but still overestimated attenuation in UV.

The effect of CDOM concentration was investigated by using a CDOM spectrum from Baltic Sea ice ($a_{CDOM} = a_{350} * \exp(-0.0165[\lambda-350])$, where $a_{350} = 1$ m^{-1}) [*Uusikivi et al.*, 2010], where CDOM concentrations are substantially higher. The observed N-ICE2015 UVA transmittance was 0.15, whereas modeled transmittance with Baltic Sea CDOM (with ice, snow, and particles) was 0.06 (Figure 6d). Compared to the exponential (without MAA peaks) CDOM spectra from N-ICE2015, Baltic Sea-like CDOM absorption resulted in

considerably lower UV transmittance. Compared to the $CDOM_{Baltic}$ case, UV transmittance increased by 0.05 (83%) when modeled with N-ICE2015 exponential CDOM spectra.

For energy accumulation calculations, we took the fraction of absorbed light energy on 26 May as a starting point and multiplied it with the incoming E_d(PAR) (mW m^{-2}) for the following week. The time after 26 May was chosen because the sky was overcast (cloud fraction >0.9) and radiative transfer modeling suggests that in cloudy conditions transmittance varies only very little with solar zenith angle. Biomass in the lead increased on average from 1.3 to 1.4 mg Chl a m^{-2} during the time (until 3 June). Incoming energy in PAR range during the time was 89 MJ m^{-2}. Difference in absorbed light energy in PAR between pure sea ice and ice with particles was 0.03 on 26 May; that is, 3% of incident light energy was absorbed by algae and other particles. If we assume that the fraction of light absorbed by particles remained the same (despite the moderate increase in biomass), particles absorbed 2.7 MJ m^{-2} in a week, or simplified, an algal biomass corresponding to 1.3 mg Chl a absorbed 2.7 MJ in a week. By using density and latent heat for pure ice we can calculate the theoretical maximum of pure ice melting caused by the energy absorbed by particles.

$$\mathrm{d}h = \frac{Q}{L \times \rho} \tag{7}$$

where dh is thickness change, Q = 2.7 MJ m^{-2} (absorbed energy), L = 0.335 MJ kg^{-1} (latent heat), and ρ = 918 kg m^{-3} (ice density). Based on this, the energy absorbed by algae and other particles could have melted 0.8 cm of pure ice in a week, assuming that all absorbed energy ended up as heat.

4. Discussion

4.1. Factors Regulating Light Transmission Through the Refrozen Lead

We assessed the contribution of different properties regulating light transmission through the refrozen lead based on direct irradiance measurements before and after snow removal and radiative transfer modeling to include the effects of particle and CDOM absorption. PAR transmittance T_d(PAR)$_{snow+ice}$ through the refrozen lead was 0.05–0.41 (Figure 2d) which is significantly higher than through the adjacent thicker ice (ice thickness 130 cm with 40 cm of snow, T_d(PAR)$_{snow+ice}$ < 0.003) illustrating its role as a window into the underlying ocean. The thick ice measurement site was representative of the study area with an average snow thickness of 43 cm [$Rösel\ et\ al.$, 2016]. Snow removal on the refrozen lead further increased PAR transmittance by about twofold to sevenfold (to 0.28–0.49), emphasizing the strong effect by even thin snow cover on PAR transmittance. The variation in transmittance between the lead sites after snow removal could be explained by differences in ice thickness and structure among sites. In particular, the ratio of columnar to granular ice had a strong impact on light transmission, with significantly lower transmittance in ice cores containing thicker granular section. This is consistent with studies showing that light scattering is considerably higher in granular ice than in columnar ice [$Grenfell\ and\ Maykut$, 1977; $Uusikivi\ et\ al.$, 2010]. This might also explain why T_d(PAR) of the snow-free refrozen lead was considerably lower than the 0.86 measured on snow-free new ice (<15 cm) in Kongsfjorden, Svalbard [$Taskjelle\ et\ al.$, 2016b]. The new ice in the study by $Taskjelle\ et\ al.$ [2016b] grew in very calm conditions and was thus likely free of granular ice. The variability in granular ice across the refrozen lead cores is likely a result of variable frazil accumulation at the initial stages of ice formation in the lead. Thus, conditions during freezeup, which determine the ice structure, and the amount of granular ice can have a significant impact on thin ice light transmittance.

Calculated K_d(PAR) values (mean 3.7 m^{-1} for ice and mean 43.1 m^{-1} for snow) are within the range of previous studies on thin snow and ice covers. $Ehn\ et\ al.$ [2004] report 3.1–4.7 m^{-1} for Baltic Sea ice of similar thickness. Modeling studies by $Hamre\ et\ al.$ [2004] showed that K_d for snow on sea ice increases with decreasing snow depth, and resulted in a K_d(PAR) of 88.2 m^{-1} for a 1 cm snow layer. Spectral extinction coefficients for temperate snow by $Perovich$ [2007] were between 20 and 40 m^{-1} for 2–4 cm depth range.

In addition to snow and ice properties, also, the organic constituents in the ice play a significant role in light attenuation and, e.g., protection from UV light [$Perovich\ et\ al.$, 1998; $Belzile\ et\ al.$, 2000; $Uusikivi\ et\ al.$, 2010]. We could not reproduce the observed transmittance without the inclusion of particles in the radiative transfer model. From the organic compounds, particles had higher contribution to PAR transmittance than CDOM: compared to pure sea ice (with snow), ice containing particles had 6% lower transmittance, whereas for

CDOM the effect was not visible (when transmittance is expressed with two-decimal accuracy). Removing snow cover increased transmittance by 120%. To investigate further the role of CDOM (Figure 6d) and algal absorption, additional calculations were made.

CDOM absorption coefficients in the surface water during the lead formation and sampling were generally low (below 0.2 m^{-1} at 350 nm) [*Pavlov et al.*, 2017b]. Therefore, absorption by CDOM in sea ice formed in these surface waters is relatively low as well and likely does not represent a significant factor of UV protection for organisms in the same way it does in waters with high CDOM concentration found in other Arctic locations influenced by terrigenous CDOM [*Granskog et al.*, 2012; *Pavlov et al.*, 2015]. In this regard, ice in the refrozen lead presented here is different from, e.g., the Baltic Sea, where similar studies were made on thin ice [*Uusikivi et al.*, 2010; *Piiparinen et al.*, 2015]. We show how CDOM at high concentration, like measured from Baltic Sea ice, has a larger contribution to total light attenuation than the lead ice CDOM and high concentrations of MAAs in the ice algae combined (Figure 6d). The reduced UV transmittance caused by high CDOM absorption in the Baltic Sea ice is a possible reason for large differences in total MAA concentration (see discussion in section 4.2) between the lead and the Baltic Sea studies. Ice algae living in low CDOM areas have to invest considerably more in UV protection.

The potential effect of algal absorption on ice melt was estimated. During the last week of sampling, energy absorption by particles could theoretically melt almost 1 cm sea ice. While this is a rough estimate and does not take into account ice thermodynamics or, e.g., the distribution of algae in the ice [*Zeebe et al.*, 1996], it demonstrates that even with low biomass, but under high irradiance, ice algae have the potential to affect ice growth and thickness in scales relevant for the ice algal habitat. In a modeling study, *Zeebe et al.* [1996] were operating with considerably higher ice algal standing stocks than in our study, but the ice was much thicker (>1.6 m), strongly limiting the available irradiance at the algal layer. Thickness of melted ice in the study by *Zeebe et al.* [1996] was on the order of centimeters over the course of the melting period (40 days). Further studies could conclude if this mechanism limits biomass buildup in thin ice covers, by causing melt-out when ice-algal biomass reaches a certain level.

4.2. MAA Production

The MAA concentrations in the lead ice were occasionally very high (up to 39 mg m^{-3} for individual samples), and the bulk MAA:Chl *a* ratios are, to our knowledge, the highest ever reported for sea ice (up to 6.3 mg MAA m^{-3} per mg Chl *a* m^{-3} for individual samples). The highest total MAA concentrations were recorded in the ice bottom on 20 and 26 May (Figure 4b), when increased Chl *a* concentration was also seen compared to the preceding days. Because of the lack of standards for all encountered MAA compounds, total MAA concentration in the cells was higher than what was measured, and our results are thus a conservative estimate of the MAA concentration. Total concentrations in Baltic Sea ice have been reported to be <2 mg m^{-3} [*Uusikivi et al.*, 2010] and <3.5 mg m^{-3} [*Piiparinen et al.*, 2015]. *Elliott et al.* [2015] reported relative concentrations (Canadian Arctic Archipelago) but estimated maximum concentrations of 21.9 and 19.9 mg m^{-3} for shinorine and porphyra-334, respectively (total concentration per sample not specified). When it comes to the bulk MAA: Chl *a* ratio, *Ryan et al.* [2002] refer mean ratios below 0.03 (volumetric concentrations not given), *Uusikivi et al.* [2010] and *Piiparinen et al.* [2015] obtained ratios below 1 (highest ratios at ice surface), and *Elliott et al.* [2015] up to 0.6 (based on the estimated total MAA concentration).

The most apparent explanation for the high MAA production in our case is the high light environment under thin snow and ice cover. MAAs can have many roles in a cell [*Oren and Gunde-Cimerman*, 2007], but the major function of MAAs in marine algae seems to be functioning as UV protection and antioxidants [*Carreto et al.*, 2011]. *Helbling et al.* [1996] observed clear reduction of algal photoinhibition when MAAs were present. Naturally, MAAs can simultaneously serve several purposes. Sea ice is a challenging environment regarding osmotic balance, but the very high MAA concentrations found in our study (e.g., 20 May) are unlikely a response to osmotic stress because brine salinities in the lead ice (32.9–45.0 on 20 May) were not exceptionally high and close to seawater salinity. In addition, bulk salinity decreased, whereas MAA concentration in general increased over the sampling period (Figure 2).

4.3. Absorption Patterns

Generally, particle and algal absorption increased during the sampling period, following the increase in ice algal biomass (Figures 2e, 3c, 3e, 5a, and 5b). Days with high biomass or detrital content did not strictly

follow the temporal trend. Chl *a*-specific absorption decreased during the period (Figures 3f, 5c, and 5d). Average specific absorption efficiency ("packaging effect," the ratio of Chl *a*-specific absorption at 674 nm to the theoretical maximum at this wavelength), calculated as in *Johnsen and Sakshaug* [2007], decreased from 0.64 to 0.28 over the study period. A higher value indicates lower packaging [*Johnsen and Sakshaug*, 2007] which can be attributed to small cell sizes or to low pigment content due to high-light acclimation [*Kirk*, 2011]. Because the algae likely acclimated from low light to high light over the study period (see discussion in section 4.5), the increasing packaging could possibly be explained by species succession in the lead ice and subsequent increase in cell size. Flagellates and small centric diatoms colonized the lead ice in the beginning [*Olsen et al.*, 2017]. Toward the end of the sampling period, the pennate diatoms *Nitzschia frigida* and *Navicula* spp., characteristic of ice bottom assemblages [*Leu et al.*, 2015], became dominant [*Olsen et al.*, 2017]. These findings highlight the complex relationship between absorption coefficients and pigment packaging in natural samples by showing that pigment packaging in this young ice environment was likely controlled by both light and species composition.

Distinct absorption peaks in the UV range were observed in both CDOM and particle absorption samples (Figures 3c, 3e–3g, and 5), likely caused by MAAs. However, the magnitude of the peaks has to be treated with caution. As *Laurion et al.* [2003] points out, MAAs can be released from cells, in this case dinoflagellates, during sampling procedures like thawing of frozen filters, which results in unpacked (exaggerated) absorption of the compounds spread on the filter. In sections 3 and 4 we therefore only concentrate on the location of the absorption peaks as we consider that aspect as uncompromised data. However, the MAA peaks in our particle absorption spectra are more in line with the peaks in the visible part, compared to the disproportionally high MAA peaks (up to almost 9 times higher than the blue peak at 440 nm) obtained in the above mentioned experiments by *Laurion et al.* [2003]. Likewise, CDOM absorption might be affected by sample handling. A field experiment we conducted in 2016 indicates that the ice core melting method affected the measured UV absorption in CDOM samples. MAA peaks (at 330 nm and 360 nm) were visible only in CDOM absorption spectra from samples melted directly (without addition of filtered seawater). In this study direct melting was used and thus CDOM spectra can be affected by the damage caused in the algal cells due to osmotic shock [*Miller et al.*, 2015]. Further, improvement in the model and observation agreement obtained by the removal of MAA peaks (Figure 6c) indicates that CDOM absorption coefficients in the MAA range were overestimated. This potential effect should be taken into consideration, and all sea ice studies should report the melting method to be able to assess possible artifacts. However, for CDOM samples buffered melting would not be straightforward because adding filtered seawater to the ice sample also introduces random CDOM from the water column. Melting with artificial seawater free of organics could possibly be an option, but further experiments are needed. Release of MAAs probably varies between algal species, some being more robust to handling (e.g., diatoms with hard silica frustules), and more studies are also needed to understand the consequences of other sampling procedures like filtration method.

4.4. Linking Algal Absorption Characteristics and Different MAA Compounds

The primary MAA peak in the particle absorption spectra is around 330 nm, where many different MAAs absorb, including the compounds we had standards for, shinorine (absorption maximum at 333 nm), palythine (320 nm), and porphyra-334 (334 nm) [*Carreto et al.*, 2011], and the fourth, unknown compound present in the samples (331 nm). The fifth, unknown compound ("U2") present in our samples, possibly a condensation product of euhalothece-362 and another MAA [*Elliott et al.*, 2015], had an absorption maximum at 363 nm. This fits well with particle absorption characteristics on two sampling days (20 and 29 May, secondary peak around 365 nm) and the presence of U2 compound (mainly 20 and 29 May). However, the second MAA peak in CDOM samples at around 360 nm (Figures 5e and 5f) was present in most samples (most notable in ice core tops samples). In particle absorption spectra, a second peak around 380 nm is visible especially in many ice core top samples (Figures 5b and 5d). All MAA components reported in literature have absorption peaks <362 nm [*Karentz*, 2001; *Carreto et al.*, 2011]. This second peak could be attributed to a UV-absorbing compound that is not a MAA and thus was not detected with the method used. The compound could also be responsible for the 360 nm peak in the CDOM absorption spectra, because of possibly different absorption characteristics for in vivo and in vitro, which is well known for chlorophylls and carotenoids, due to binding to different proteins when intact in cells [*Kirk*, 2011]. This unidentified compound becomes more important toward the end of the sampling, seen as increased absorption (Figure 4d). Also, its stronger role in the ice core

tops seems to indicate that it is produced in response to high light exposure. Likewise, the presence of the unknown U2 compound in our samples, as well as shinorine being abundant, agree with earlier studies [*Elliott et al.*, 2015] that connect these compounds with high light exposure.

4.5. Biomass Buildup in Young Ice

The ice algal standing stock in the lead ice was 0.06–2.31 mg Chl a m^{-2}. This is similar to previous estimates of ice algal standing stocks (summarized by *Leu et al.* [2015]) in the Atlantic sector of the Arctic during spring (March to May): 0.1–5.5 mg Chl a m^{-2} in Fram Strait and Greenland Sea pack ice, and 0.3–9.8 mg m^{-2} in pack ice around Svalbard. In areas affected by warm Atlantic water inflow, bottom ice ablation, which deteriorates the ice algal habitat, is suggested to be the limiting factor for ice algal biomass buildup [*Leu et al.*, 2015].

Interestingly, ice algal standing stock in the newly formed ice was similar to those of the surrounding thicker and older ice during the study time. The second-year ice (122–145 cm thick with 38–56 cm snow cover) contained 1.1–2.4 mg Chl a m^{-2} [*Olsen et al.*, 2017]. Thus, the algae in the newly formed ice reached comparable standing stocks to that of the surrounding older ice, despite thicker ice column and larger seeding stock of algae in the latter. However, considering the very low irradiance under the thick ice (1–2 μmol photons m^{-2} s^{-1} [*Olsen et al.*, 2017; *Taskjelle et al.*, 2016a], compared to 30–350 μmol photons m^{-2} s^{-1} in the lead), the thin ice environment was expected to be more productive.

Olsen et al. [2017] suggest that the refrozen lead was seeded by sea ice algae (specifically the dominant pennate diatom *Nitzschia frigida*) from the adjacent thick ice. The photoacclimation process from a low light environment (thick ice) to a high light environment (newly formed refrozen lead ice) might be similar to the one observed by *Juhl and Krembs* [2010]. They found that algal biomass response to snow removal was, in addition to physical processes, dependent on initial snow depth (i.e., light environment and therefore light acclimation status of algae). From laboratory experiments they concluded that photoacclimation of *Nitzschia frigida* from 1–2 to 110 μmol photons m^{-2} s^{-1} took between 3 and 6 days. In nonacclimated cells, growth rate decreased following transfer to high light intensities, but for high-light-acclimated cells no growth inhibition could be observed (at irradiances up to 110 μmol photons m^{-2} s^{-1}) [*Juhl and Krembs*, 2010]. Therefore, we hypothesize that the initial algal community of the refrozen lead might have undergone a similar photoacclimation process delaying its growth and resulting in the lower than expected algal biomass.

Over time, ice algae in the refrozen lead seem to become high-light acclimated. On 26 May, the optimal irradiance at which maximum photosynthetic rates occurred was 210–330 μmol photons m^{-2} s^{-1} and E_k (photoacclimation parameter) was 110–200 μmol photons m^{-2} s^{-1}, based on photosynthesis vs irradiance curves (M. Fernández-Méndez, unpublished data, 2015). Photoinhibition occurred above 250 to 350 μmol photons m^{-2} s^{-1}. Based on the in situ measurements, undertaken between 12 and 14 local time on the sampling days, highest E_d(PAR) average (average of five sites) was 240 μmol photons m^{-2} s^{-1}. Thus, irradiance was likely below photoinhibiting levels during the latter part of the study, but based on literature, the irradiance levels could cause photoinhibition for unacclimated cells [*Kühl et al.*, 2001; *Juhl and Krembs*, 2010]. This is supported by the fact that biomass was high on 20 May, when snow cover was the thickest and thus transmittance was among the lowest (Figure 2). Increasing biomass toward the end of the sampling despite increasing irradiance could be explained by the photoacclimation that had occurred by that time.

The high MAA production indicates the need for active photoprotection against damaging UV radiation levels and is possibly associated with a high metabolic cost, which could further explain the lower than expected biomass accumulation in the thin ice. *Hernando et al.*, [2002, 2011] observed lower cell numbers and higher MAA production in Antarctic diatom (*Thalassiosira* sp.) cultures that received higher UV exposure and suggested that growth was compromised by photoprotective compound synthesis. Initial growth inhibition in diatoms following elevated UV exposure was reported also by, e.g., *Zudaire and Roy* [2001]. However, MAA synthesis was not maintained over the whole experiment but replaced by elevated diatoxanthin levels, maybe because of the energetic costs of the MAA synthesis. This could be similar to our observations, where Chl a to MAA ratios declined toward the end of the study period. In the ice core tops, however, the ratios remained still high. According to *Shick and Dunlap* [2002] evidence on metabolic costs and growth effect of MAA production is inconclusive, but the cost of producing MAAs is estimated to be similar to Chl a synthesis. Considering the very high ratios of MAAs to Chl a in our samples, it seems likely that MAA production affected the growth rates negatively.

Phytoplankton growth clearly benefitted from the higher light transmittance through thin ice and open leads, resulting in an under-ice bloom with Chl a standing stocks (integrated for the upper 50 m) of up to 233 mg Chl a m^{-2} [*Assmy et al.*, 2017a]. Unlike the ice algae, phytoplankton is being vertically mixed through the water column, reducing the probability of photoinhibition and increasing nutrient replenishment. Silicate limitation was possibly one important factor restricting growth in the thin ice, as indicated by biogeochemical modeling [*Duarte et al.*, 2017]. Furthermore, in this particular case the water column bloom was dominated by *Phaeocystis pouchetii* which is a very plastic species with regard to photoacclimation, suggesting that it can acclimate to the alternating light field provided by the heterogenous ice cover [*Assmy et al.*, 2017a]. Further studies could show how the thin ice algal community evolves after the initial period described here—the lead ice broke up on June 4—but based on our observations, the leads in the area enhanced mainly the phytoplankton production.

5. Conclusions

Here we present unique bio-optical observations and PAR transmittance of newly formed Arctic sea ice in a lead in spring. While the dominating thicker ice with thicker snow cover transmitted very little E_d(PAR) ($<0.3\%$) to the bottom ice algal community and the underlying water column, leads act like windows into the water column with 5–40% transmittance in this study. We showed how even a thin snow cover and the conditions during refreezing of leads, affecting ice structure, are important for how effective these windows are in transmitting light. The water masses in the area and the lead ice were low in CDOM concentration, requiring the need for UV protection compounds (MAAs), which the algae synthetized in high concentrations.

Our results indicate that growth of shade-acclimated ice algae in newly formed thin ice may be compromised by the need for photoacclimation to a high light environment and investment in photoprotective pigments. In addition, ice bottom melt caused by algal absorption even at relatively low biomass has the potential to limit ice algal biomass accumulation in thin ice environments. Indeed, the growth of a large under-ice bloom supported by the added sunlight through open and refrozen leads indicates that phytoplankton rather than ice algae profited from an ice cover with frequent leads. The occurrence of leads may become more common in the future Arctic as the dynamics of the ice pack increases, which could have a profound impact on the sea ice-associated ecosystem.

References

Arrigo, K. R., and G. L. van Dijken (2015), Continued increases in Arctic Ocean primary production, *Prog. Oceanogr.*, *136*, 60–70, doi:10.1016/j.pocean.2015.05.002.

Assmy, P., et al. (2017a), Leads in Arctic pack ice enable early phytoplankton blooms below snow-covered sea ice, *Sci. Rep.*, *7*, 40850, doi:10.1038/srep40850.

Assmy, P., et al. (2017b), N-ICE2015 sea ice biogeochemistry, Norwegian Polar Institute, doi:10.21334/npolar.2017.d3e93b31.

Belzile, C., S. C. Johannessen, M. Gosselin, S. Demers, and W. L. Miller (2000), Ultraviolet attenuation by dissolved and particulate constituents of first-year ice during late spring in an Arctic polynya, *Limnol. Oceanogr.*, *45*(6), 1265–1273, doi:10.4319/lo.2000.45.6.1265.

Brunet, C., G. Johnsen, J. Lavaud, and S. Roy (2011), Pigments and photoacclimation processes, in *Phytoplankton Pigments—Characterization, Chemotaxonomy and Applications in Oceanography*, edited by S. Roy et al., pp. 445–471, Cambridge Univ. Press, Cambridge.

Campbell, K., C. J. Mundy, D. G. Barber, and M. Gosselin (2014), Remote estimates of ice algae biomass and their response to environmental conditions during spring melt, *Arctic*, *67*(3), 375–387, doi:10.14430/arctic4409.

Campbell, K., C. J. Mundy, D. G. Barber, and M. Gosselin (2015), Characterizing the sea ice algae chlorophyll *a*-snow depth relationship over Arctic spring melt using transmitted irradiance, *J. Mar. Syst.*, *147*, 76–84, doi:10.1016/j.jmarsys.2014.01.008.

Carignan, M. O., and J. I. Carreto (2013), Characterization of mycosporine-serine-glycine methyl ester, a major mycosporine-like amino acid from dinoflagellates: A mass spectrometry study, *J. Phycol.*, *49*(4), 680–688, doi:10.1111/jpy.12076.

Carreto, J. I., M. O. Carignan, and N. G. Montoya (2005), A high-resolution reverse-phase liquid chromatography method for the analysis of mycosporine-like amino acids (MAAs) in marine organisms, *Mar. Biol.*, *146*(2), 237–252, doi:10.1007/s00227-004-1447-y.

Carreto, J. I., S. Roy, K. Whitehead, C. A. LLewellyn, and M. O. Carignan (2011), UV-absorbing "pigments": Mycosporine-like amino acids, in *Phytoplankton Pigments—Characterization, Chemotaxonomy and Applications in Oceanography*, edited by S. Roy, C. A. Llewellyn, and E. S. Egeland, pp. 412–441, Cambridge Univ. Press, Cambridge.

Cohen, L., S. R. Hudson, V. P. Walden, R. M. Graham, and M. A. Granskog (2017), Meteorological conditions in a thinner Arctic sea ice regime from winter through summer during the Norwegian Young Sea ICE expedition (N-ICE2015), *J. Geophys. Res. Atmos.*, doi:10.1002/2016JD026034.

Conde, F. R., M. S. Churio, and C. M. Previtali (2000), The photoprotector mechanism of mycosporine-like amino acids. Excited-state properties and photostability of porphyra-334 in aqueous solution, *J. Photochem. Photobiol. B Biol.*, *56*(2–3), 139–144, doi:10.1016/S1011-1344(00)00066-X.

Cox, G. F. N., and W. F. Weeks (1986), Changes in the salinity and porosity of sea-ice samples during shipping and storage, *J. Glaciol.*, *32*(112), 371–375.

Duarte, P., et al. (2017), Sea ice thermodynamics and biogeochemistry in the Arctic Ocean: Empirical and model results, *J. Geophys. Res. Biogeosci.*, *122*, doi:10.1002/2016JG003660.

Ehn, J., M. A. Granskog, A. Reinart, and A. Erm (2004), Optical properties of melting landfast sea ice and underlying seawater in Santala Bay, Gulf of Finland, *J. Geophys. Res.*, *109*, C09003, doi:10.1029/2003JC002042.

Elliott, A., C. J. Mundy, M. Gosselin, M. Poulin, K. Campbell, and F. Wang (2015), Spring production of mycosporine-like amino acids and other UV-absorbing compounds in sea ice associated algae communities in the Canadian Arctic, *Mar. Ecol. Prog. Ser.*, *541*, 91–104, doi:10.3354/meps11540.

Fountoulakis, I., A. F. Bais, K. Tourpali, K. Fragkos, and S. Misios (2014), Projected changes in solar UV radiation in the Arctic and sub-Arctic oceans: Effects from changes in reflectivity, ice transmittance, clouds, and ozone, *J. Geophys. Res. Atmos.*, *119*, 8073–8090, doi:10.1002/2014JD021918.

Fritsen, C. H., E. D. Wirthlin, D. K. Momberg, M. J. Lewis, and S. F. Ackley (2011), Bio-optical properties of Antarctic pack ice in the early austral spring, *Deep Sea Res., Part II*, *58*(9–10), 1052–1061, doi:10.1016/j.dsr2.2010.10.028.

Gerland, S., M. A. Granskog, J. A. King, and A. Rösel (2017), N-ICE2015 ice core physics: Temperature, salinity and density [data set], Norwegian Polar Institute, doi:10.21334/npolar.2017.c3db82e3.

Granskog, M. A., C. A. Stedmon, P. A. Dodd, R. M. W. Amon, A. K. Pavlov, L. De Steur, and E. Hansen (2012), Characteristics of colored dissolved organic matter (CDOM) in the Arctic outflow in the Fram Strait: Assessing the changes and fate of terrigenous CDOM in the Arctic Ocean, *J. Geophys. Res.*, *117*, C12021, doi:10.1029/2012JC008075.

Granskog, M. A., P. Assmy, S. Gerland, G. Spreen, H. Steen, and L. H. Smedsrud (2016), Arctic research on thin ice: Consequences of Arctic sea ice loss, *Eos. Trans. AGU*, *97*(5), 22–26.

Grenfell, T. C., and G. A. Maykut (1977), The optical properties of ice and snow in the Arctic basin, *J. Glaciol.*, *18*(80), 445–463.

Hamre, B., J. G. Winther, S. Gerland, J. J. Stamnes, and K. Stamnes (2004), Modeled and measured optical transmittance of snow-covered first-year sea ice in Kongsfjorden, Svalbard, *J. Geophys. Res.*, *109*(C10006), doi:10.1029/2003JC001926.

Hamre, B., S. Stamnes, K. Stamnes, and J. Stamnes (2017), AccuRT: A versatile tool for radiative transfer simulations in the coupled atmosphere-ocean system, *AIP Conf. Proc.*, *1810*(1), 120002, doi:10.1063/1.4975576.

Helbling, E. W., B. E. Chalker, W. C. Dunlap, O. Holm-Hansen, and V. E. Villafañe (1996), Photoacclimation of antarctic marine diatoms to solar ultraviolet radiation, *J. Exp. Mar. Biol. Ecol.*, *204*(96), 85–101.

Hernando, M., J. I. Carreto, M. O. Carignan, G. A. Ferreyra, and C. Gross (2002), Effects of solar radiation on growth and mycosporine-like amino acids content in *Thalassiosira* sp., an Antarctic diatom, *Polar Biol.*, *25*, 12–20, doi:10.1007/s003000100306.

Hernando, M. P., J. I. Carreto, M. Carignan, and G. A. Ferreyra (2011), Effect of vertical mixing on short-term mycosporine-like amino acid synthesis in the Antarctic diatom, *Thalassiossira* sp, *Sci. Mar.*, *76*(1), 49–57, doi:10.3989/scimar.03203.16D.

Holm-Hansen, O., and B. Riemann (1978), Chlorophyll *a* determination: Improvements in methodology, *Oikos*, *30*(3), 438–447.

Hudson, S. R., and L. Cohen (2015), N-ICE2015 surface meteorology v2 [data set], Norwegian Polar Institute, doi:10.21334/npolar.2015.056a61d1.

Itkin, P., G. Spreen, B. Cheng, M. Doble, F. Girard-Ardhuin, J. Haapala, N. Hughes, L. Kaleschke, M. Nicolaus, and J. Wilkinson (2017), Thin ice and storms: A case study of sea ice deformation from buoy arrays deployed during N-ICE2015, *J. Geophys. Res. Oceans*, doi:10.1002/2016JC012403.

Johnsen, G., and E. Sakshaug (2007), Biooptical characteristics of PSII and PSI in 33 species (13 pigment groups) of marine phytoplankton, and the relevance for pulse-amplitude-modulated and fast-repetition-rate fluorometry, *J. Phycol.*, *43*(6), 1236–1251, doi:10.1111/j.1529-8817.2007.00422.x.

Juhl, A. R., and C. Krembs (2010), Effects of snow removal and algal photoacclimation on growth and export of ice algae, *Polar Biol.*, *33*(8), 1057–1065, doi:10.1007/s00300-010-0784-1.

Karentz, D. (1994), Ultraviolet tolerance mechanisms in Antarctic marine organisms, in *Ultraviolet Radiation in Antarctica: Measurements and Biological Effects. Antarctic Research Series*, edited by C. S. Weiler and P. A. Penhale, pp. 93–110, AGU, Washington, D. C.

Karentz, D. (2001), Chemical defenses of marine organisms against solar radiation exposure: UV-absorbing mycosporine-like amino acids and scytonemin, in *Marine Chemical Ecology*, edited by J. McClintock and W. Baker, pp. 481–520, CRC Press, Boca Raton, Fla.

Kauko, H. M., A. K. Pavlov, E. Nystedt, and M. A. Granskog (2017), N-ICE2015 particulate matter absorption spectra, Norwegian Polar Institute, doi:10.21334/npolar.2017.35978199.

Kirk, J. T. O. (2011), *Light and Photosynthesis in Aquatic Ecosystems*, 3d ed., pp. 292 & 311–319, Cambridge Univ. Press, Cambridge.

Kwok, R., G. Spreen, and S. Pang (2013), Arctic sea ice circulation and drift speed: Decadal trends and ocean currents, *J. Geophys. Res. Oceans*, *118*, 2408–2425, doi:10.1002/jgrc.20191.

Kühl, M., R. N. Glud, J. Borum, R. Roberts, and S. Rysgaard (2001), Photosynthetic performance of surface-associated algae below sea ice as measured with a pulse-amplitude-modulated (PAM) fluorometer and O_2 microsensors, *Mar. Ecol. Prog. Ser.*, *223*(1), 1–14, doi:10.3354/meps223001.

Lange, M. A. (1988), Basic properties of Antarctic sea ice as revealed by textural analysis of ice cores, *Ann. Glaciol.*, *10*, 95–101.

Laurion, I., F. Blouin, and S. Roy (2003), The quantitative filter technique for measuring phytoplankton absorption: Interference by MAAs in the UV waveband, *Limnol. Oceanogr. Methods*, *1*, 1–9, doi:10.4319/lom.2011.1.1.

Leppäranta, M., and T. Manninen (1988), The brine and gas content of sea ice with attention to low salinities and high temperatures, *Finnish Inst. Mar. Res. Intern. Rep.*, *2*, 1–14.

Leu, E., C. J. Mundy, P. Assmy, K. Campbell, T. M. Gabrielsen, M. Gosselin, T. Juul-Pedersen, and R. Gradinger (2015), Arctic spring awakening—Steering principles behind the phenology of vernal ice algal blooms, *Prog. Oceanogr.*, *139*, 151–170, doi:10.1016/j.pocean.2015.07.012.

Logvinova, C. L., K. E. Frey, and L. W. Cooper (2016), The potential role of sea ice melt in the distribution of chromophoric dissolved organic matter in the Chukchi and Beaufort seas, *Deep Sea Res., II*, *130*, 28–42, doi:10.1016/j.dsr2.2016.04.017.

Mason, J. D., M. T. Cone, and E. S. Fry (2016), Ultraviolet (250–550 nm) absorption spectrum of pure water, *Appl. Opt.*, *55*(25), 7163–7172, doi:10.1364/AO.55.007163.

McDougall, T. J., D. R. Jackett, F. J. Millero, R. Pawlowicz, and P. M. Barker (2012), A global algorithm for estimating Absolute Salinity, *Ocean Sci.*, *8*(6), 1123–1134, doi:10.5194/os-8-1123-2012.

Meier, W. N., et al. (2014), Arctic sea ice in transformation: A review of recent observed changes and impacts on biology and human activity, *Rev. Geophys.*, *51*, 185–217, doi:10.1002/2013RG000431.

Meyer, A., et al. (2017), Winter to summer oceanographic observations in the Arctic Ocean north of Svalbard, *J. Geophys. Res. Oceans*, doi:10.1002/2016JC012391.

Miller, L. A., et al. (2015), Methods for biogeochemical studies of sea ice: The state of the art, caveats, and recommendations, *Elem. Sci. Anthr.*, *3*, 38, doi:10.12952/journal.elementa.000038.

Mueller, J. L., G. S. Fargion, C. R. McClain, S. Pegau, J. R. V. Zanefeld, B. G. Mitchell, M. Kahru, J. Wieland, and M. Stramska (2003), Ocean optics protocols for satellite ocean color sensor validation, revision 4, volume IV: Inherent optical properties: Instruments, characterizations, field measurements and data analysis protocols, NASA Tech. Rep., NASA Goddard Space Flight Center, Greenbelt, Md.

Mundy, C. J., D. G. Barber, and C. Michel (2005), Variability of snow and ice thermal, physical and optical properties pertinent to sea ice algae biomass during spring, *J. Mar. Syst.*, *58*, 107–120, doi:10.1016/j.jmarsys.2005.07.003.

Mundy, C. J., et al. (2011), Characteristics of two distinct high-light acclimated algal communities during advanced stages of sea ice melt, *Polar Biol.*, *34*(12), 1869–1886, doi:10.1007/s00300-011-0998-x.

Nicolaus, M., C. Katlein, J. Maslanik, and S. Hendricks (2012), Changes in Arctic sea ice result in increasing light transmittance and absorption, *Geophys. Res. Lett.*, *39*, L24501, doi:10.1029/2012GL053738.

Olsen, L. M., et al. (2017), The seeding of ice algal blooms in Arctic pack ice: The multiyear ice seed repository hypothesis, *J. Geophys. Res. Biogeosci.*, *122*, doi:10.1002/2016JG003668.

Oren, A., and N. Gunde-Cimerman (2007), Mycosporines and mycosporine-like amino acids: UV protectants or multipurpose secondary metabolites?, *FEMS Microbiol. Lett.*, *269*(1), 1–10, doi:10.1111/j.1574-6968.2007.00650.x.

Pavlov, A. K., A. Silyakova, M. A. Granskog, R. G. J. Bellerby, A. Engel, K. G. Schulz, and C. P. D. Brussaard (2014), Marine CDOM accumulation during a coastal Arctic mesocosm experiment: No response to elevated pCO$_2$, *J. Geophys. Res. Biogeosci.*, *119*, 1216–1230, doi:10.1002/2013JG002587.

Pavlov, A. K., M. A. Granskog, C. A. Stedmon, B. V. Ivanov, S. R. Hudson, and S. Falk-Petersen (2015), Contrasting optical properties of surface waters across the Fram Strait and its potential biological implications, *J. Mar. Syst.*, *143*, 62–72, doi:10.1016/j.jmarsys.2014.11.001.

Pavlov, A. K., H. M. Kauko, C. Stedmon, and M. A. Granskog (2017a), N-ICE2015 colored dissolved organic matter absorption spectra, Norwegian Polar Institute, doi:10.21334/npolar.2017.f46970ba.

Pavlov, A. K., T. Taskjelle, B. Hamre, H. M. Kauko, S. R. Hudson, P. Assmy, P. Duarte, M. Fernández Méndez, C. J. Mundy, and M. A. Granskog (2017b), Altered inherent optical properties and estimates of the underwater light field during an Arctic under-ice bloom of *Phaeocystis pouchetii*, *J. Geophys. Res. Oceans*, *122*, doi:10.1002/2016JC012471.

Perovich, D. K. (1990), Theoretical estimates of light reflection and transmission by spatially complex and temporally varying sea ice covers, *J. Geophys. Res.*, *95*(C6), 9557–9567, doi:10.1029/JC095iC06p09557.

Perovich, D. K. (2007), Light reflection and transmission by a temperate snow cover, *J. Glaciol.*, *53*(181), 201–210, doi:10.3189/172756507782202919.

Perovich, D. K., C. S. Roesler, and W. S. Pegau (1998), Variability in Arctic sea ice optical properties, *J. Geophys. Res.*, *103*, 1193–1208, doi:10.1029/97JC01614.

Petrich, C., M. Nicolaus, and R. Gradinger (2012), Sensitivity of the light field under sea ice to spatially inhomogeneous optical properties and incident light assessed with three-dimensional Monte Carlo radiative transfer simulations, *Cold Reg. Sci. Technol.*, *73*, 1–11, doi:10.1016/j.coldregions.2011.12.004.

Piiparinen, J., S. Enberg, J.-M. Rintala, R. Sommaruga, M. Majaneva, R. Autio, and A. Vähätalo (2015), The contribution of mycosporine-like amino acids, chromophoric dissolved organic matter and particles to the UV protection of sea-ice organisms in the Baltic Sea, *Photochem. Photobiol. Sci.*, doi:10.1039/C4PP00342J.

Pope, R. M., and E. S. Fry (1997), Absorption spectrum (380–700 nm) of pure water. II. Integrating cavity measurements, *Appl. Opt.*, *36*(33), 8710–8723.

Rintala, J.-M., J. Piiparinen, J. Blomster, M. Majaneva, S. Müller, J. Uusikivi, and R. Autio (2014), Fast direct melting of brackish sea-ice samples results in biologically more accurate results than slow buffered melting, *Polar Biol.*, *37*(12), 1811–1822, doi:10.1007/s00300-014-1563-1.

Ryan, K. G., A. McMinn, K. A. Mitchel, and L. Trenerry (2002), Mycosporine-like amino acids in Antarctic sea ice algae, and their response to UVB radiation, *Z. Naturforsch.*, *57c*, 471–477.

Rösel, A., et al. (2016), N-ICE2015 snow depth data with Magnaprobe, Norwegian Polar Institute, doi:10.21334/npolar.2016.3d72756d.

Shick, J. M., and W. C. Dunlap (2002), Mycosporine-like amino acids and related gadusols: Biosynthesis, accumulation, and UV-protective functions in aquatic organisms, *Annu. Rev. Physiol.*, *64*(1), 223–262, doi:10.1146/annurev.physiol.64.081501.155802.

Stamnes, K., B. Hamre, J. J. Stamnes, G. Ryzhikov, M. Biryulina, R. Mahoney, B. Hauss, and A. Sei (2011), Modeling of radiation transport in coupled atmosphere-snow-ice-ocean systems, *J. Quant. Spectrosc. Radiat. Transf.*, *112*(4), 714–726, doi:10.1016/j.jqsrt.2010.06.006.

Stedmon, C. A., S. Markager, and H. Kaas (2000), Optical properties and signatures of chromophoric dissolved organic matter (CDOM) in Danish coastal waters, *Estuar. Coast. Shelf Sci.*, *51*(2), 267–278, doi:10.1006/ecss.2000.0645.

Steiner, N., C. Deal, D. Lannuzel, D. Lavoie, F. Massonnet, L. A. Miller, S. Moreau, E. Popova, J. Stefels, and L. Tedesco (2016), What sea-ice biogeochemical modellers need from observers, *Elem. Sci. Anthr.*, *4*, 84, doi:10.12952/journal.elementa.000084.

Taskjelle, T., S. R. Hudson, A. K. Pavlov, and M. A. Granskog (2016a), N-ICE2015 surface and under-ice spectral shortwave radiation data [data set], Norwegian Polar Institute, doi:10.21334/npolar.2016.9089792e.

Taskjelle, T., S. R. Hudson, M. A. Granskog, M. Nicolaus, R. Lei, S. Gerland, J. J. Stamnes, and B. Hamre (2016b), Spectral albedo and transmittance of thin young Arctic sea ice, *J. Geophys. Res. Oceans*, *121*, 540–553, doi:10.1002/2015JC011254.

Taskjelle, T., M. A. Granskog, A. K. Pavlov, S. R. Hudson, and B. Hamre (2017), Effects of an Arctic under-ice bloom on solar radiant heating of the water column, *J. Geophys. Res. Oceans*, *122*, 126–138, doi:10.1002/2016JC012187.

Tassan, S., and G. M. Ferrari (2002), A sensitivity analysis of the "transmittance–reflectance" method for measuring light absorption by aquatic particles, *J. Plankton Res.*, *24*(8), 757–774.

Thomas, G. E., and K. Stamnes (1999), *Radiative Transfer in the Atmosphere and Ocean*, 548 pp., Cambridge Univ. Press, Cambridge.

Tilstone, G. H., G. F. Moore, K. Sørensen, R. Doerffer, R. Røttgers, K. G. Ruddick, R. Pasterkamp, and P. V Jørgensen (2002), Regional validation of MERIS chlorophyll products in North Sea coastal waters, REVAMP methodologies – EVG1 – CT – 2001 - 00049.

Uusikivi, J., A. Vähätalo, M. A. Granskog, and R. Sommaruga (2010), Contribution of mycosporine-like amino acids and colored dissolved and particulate matter to sea ice optical properties and ultraviolet attenuation, *Limnol. Oceanogr.*, *55*(2), 703–713, doi:10.4319/lo.2009.55.2.0703.

Vivier, F., J. K. Hutchings, Y. Kawaguchi, T. Kikuchi, J. H. Morison, A. Lourenco, and T. Noguchi (2016), Sea ice melt onset associated with lead opening during the spring/summer transition near the North Pole, *J. Geophys. Res. Oceans*, *121*, 2499–2522, doi:10.1002/2015JC011588.

Walden, V. P., L. Cohen, S. Y. Murphy, S. R. Hudson, and M. A. Granskog (2017), Atmospheric components of the surface energy budget over young sea ice: Results from the N-ICE2015 campaign, *J. Geophys. Res. Atmos.*, doi:10.1002/2016JD026091.

Warren, S. G., and R. E. Brandt (2008), Optical constants of ice from the ultraviolet to the microwave: A revised compilation, *J. Geophys. Res.*, *113*, D14220, doi:10.1029/2007JD009744.

Willmes, S., and G. Heinemann (2016), Sea-ice wintertime lead frequencies and regional characteristics in the Arctic, 2003–2015, *Remote Sens.*, *8*(4), doi:10.3390/rs8010004.

Xie, H., C. Aubry, Y. Zhang, and G. Song (2014), Chromophoric dissolved organic matter (CDOM) in first-year sea ice in the western Canadian Arctic, *Mar. Chem.*, *165*, 25–35, doi:10.1016/j.marchem.2014.07.007.

Zeebe, R. E., H. Eicken, D. H. Robinson, D. Wolf-Gladrow, and G. S. Dieckmann (1996), Modeling the heating and melting of sea ice through light absorption by microalgae, *J. Geophys. Res.*, *101*(C1), 1163–1181, doi:10.1029/95JC02687.

Zudaire, L., and S. Roy (2001), Photoprotection and long-term acclimation to UV radiation in the marine diatom *Thalassiosira weissflogii*, *J. Photochem. Photobiol.*, *62*, 26–34, doi:10.1016/S1011-1344(01)00150-6.

Paper III

Algal Colonization of Young Arctic Sea Ice in Spring

Hanna M. Kauko [1,2*], Lasse M. Olsen [1], Pedro Duarte [1], Ilka Peeken [3], Mats A. Granskog [1], Geir Johnsen [4,5], Mar Fernández-Méndez [1], Alexey K. Pavlov [1], Christopher J. Mundy [6] and Philipp Assmy [1]

[1] Norwegian Polar Institute, Fram Centre, Tromsø, Norway, [2] Trondheim Biological Station, Department of Biology, Norwegian University of Science and Technology, Trondheim, Norway, [3] Alfred Wegener Institute Helmholtz Centre for Polar and Marine Research, Bremerhaven, Germany, [4] Centre for Autonomous Marine Operations and Systems, Trondheim Biological Station, Department of Biology, Norwegian University of Science and Technology, Trondheim, Norway, [5] University Centre in Svalbard, Longyearbyen, Norway, [6] Centre for Earth Observation Science, University of Manitoba, Winnipeg, MB, Canada

The importance of newly formed sea ice in spring is likely to increase with formation of leads in a more dynamic Arctic icescape. We followed the ice algal species succession in young ice (≤0.27 m) in spring at high temporal resolution (sampling every second day for 1 month in May–June 2015) in the Arctic Ocean north of Svalbard. We document the early development of the ice algal community based on species abundance and chemotaxonomic marker pigments, and relate the young-ice algal community to the communities in the under-ice water column and the surrounding older ice. The seeding source seemed to vary between algal groups. Dinoflagellates were concluded to originate from the water column and diatoms from the surrounding older ice, which emphasizes the importance of older ice as a seeding source over deep oceanic regions and in early spring when algal abundance in the water column is low. In total, 120 taxa (80 identified to species or genus level) were recorded in the young ice. The protist community developed over the study period from a ciliate, flagellate, and dinoflagellate dominated community to one dominated by pennate diatoms. Environmental variables such as light were not a strong driver for the community composition, based on statistical analysis and comparison to the surrounding thicker ice with low light transmission. The photoprotective carotenoids to Chl *a* ratio increased over time to levels found in other high-light habitats, which shows that the algae were able to acclimate to the light levels of the thin ice. The development into a pennate diatom-dominated community, similar to the older ice, suggests that successional patterns tend toward ice-associated algae fairly independent of environmental conditions like light availability, season or ice type, and that biological traits, including morphological and physiological specialization to the sea ice habitat, play an important role in colonization of the sea ice environment. However, recruitment of ice-associated algae could be negatively affected by the ongoing loss of older ice, which acts as a seeding repository.

Keywords: sea-ice algae, young ice, Arctic, N-ICE2015, pigments, succession

INTRODUCTION

The Arctic icescape is changing rapidly, which affects the whole marine system (Meier et al., 2014). Primary production or algal species dynamics and habitats are altered for example by a shorter ice season (Arrigo and van Dijken, 2015) and likely by the reduction of multi-year ice (Lange et al., 2017; Olsen et al., 2017b). The sea ice is also more dynamic and vulnerable to wind forcing (Itkin et al., 2017), which can alter the habitat of ice algae. In the Arctic, ice algae contribute to the annual primary production to a varying degree (<1–60%) depending on season and region (Gosselin et al., 1997; Rysgaard and Nielsen, 2006; Fernández-Méndez et al., 2015). Based on modeling, an estimated 7.5% of annual Arctic primary production is attributed to ice algae (Dupont, 2012). Ice algae also constitute a highly concentrated food source early in the growth season (e.g., Søreide et al., 2010), and thus are a crucial part of Arctic marine foodwebs.

Algae are incorporated into sea ice when it forms through, for example, sieving by growing (Syvertsen, 1991; Lund-Hansen et al., 2017) or rising ice crystals (Reimnitz et al., 1990). Waves, currents, vertical mixing, and other physical factors enhance the entrainment: encounter rates between particles and ice crystals are increased by mixing of crystals into water and water movement through forming ice (Weissenberger and Grossmann, 1998) and along irregularities in bottom-ice topography(Krembs et al., 2002; Lund-Hansen et al., 2017). Frazil ice, which is formed under turbulent conditions (Petrich and Eicken, 2010), was observed to have higher foraminifera abundance than congelation ice (Dieckmann et al., 1990). Also active migration of motile species, and growth even under low irradiances contribute to inhabiting the ice and may be important under calm conditions (Melnikov, 1995; Weissenberger, 1998). In field studies, ice formation has been observed to preferentially retain larger cells (Gradinger and Ikävalko, 1998; Riedel et al., 2007; Rózanska et al., 2008). Further, exopolymeric substances produced by the algae make the cell surfaces sticky and may enhance their incorporation into the ice (Meiners et al., 2003; Riedel et al., 2007).

The main sources of algal species in newly formed sea ice are cells in the water column (pelagic), the sea floor (benthic), or the surrounding older ice (sympagic). Some studies have compared sea ice and water column communities during autumn freeze-up and concluded that the communities differ already during the initial phase of ice formation, suggesting that the seeding community was present in the water column only intermittently (Tuschling et al., 2000; Werner et al., 2007; Niemi et al., 2011). Differences in sea ice communities were observed based on proximity to land i.e., benthic habitats (Ratkova and Wassmann, 2005). Olsen et al. (2017b) suggested that multi-year ice can act as a seed repository, harboring algal cells from a previous growing season that can colonize new ice. In a Greenland fjord the bottom ice algal bloom was formed via spring colonization by phytoplankton, facilitated by increased surface roughness in growing ice crystals (Lund-Hansen et al., 2017). The algal assemblage in new sea ice (ice thickness ≤0.03 m) from the Beaufort Sea was similar to the one in the water column, but became different in older stages of ice (Rózanska et al., 2008).

Both ice melting and freezing seem to trigger increased species exchange between the water column and sea ice (Hardge et al., 2017). Thus the ice algal community apparently can have many origins, but their relative importance for ice algal recruitment is still not well-known.

Community development can be investigated in light of characteristics of the species present and environmental conditions affecting the species. Further, the number of observed species and how evenly abundance is distributed among the species describe communities (Peet, 1974). Succession refers to changes in species composition and abundance over time. Concepts of species succession (reviewed in McCook, 1994) are derived from work with plant and rocky bottom communities and aim to explain the mechanisms that lead to a certain type of community after disturbance of a site, such as modification of the site by early-colonizing species.

Previous sea ice colonization studies of new and young ice have been conducted in autumn or winter, or in mesocosm experiments (see references above). However, with the ongoing changes in the Arctic icescape, new ice formation during the main algal growth season will possibly increase and offer new habitats for the sympagic communities. Contrary to autumn, light intensity increases during spring, and in spring young ice is a high-light environment compared to older ice with thick snow cover (Kauko et al., 2017), or new ice formed in autumn or winter. Algae in general face an ever-fluctuating light climate, altered e.g., by changing cloud and snow covers. To balance incoming irradiance with the capacity of the photosynthetic apparatus, algae need photoacclimation mechanisms such as adjustment of the cellular pigment pool (reviewed in Brunet et al., 2011). In response to increasing irradiance, changes in the fraction of light-harvesting pigments (LHP) and photoprotective carotenoids (PPC) occur. The latter do not channel the absorbed energy to photosynthesis but dissipate it as heat, thus protecting the photosystems from excess light. The ratios of PPCs to LHP give information on physiology and light history of cells. In addition, many LHP are specific to certain algal groups and can serve as a proxy for taxonomic composition (reviewed in Jeffrey et al., 2011), including those of ice algal communities (Alou-Font et al., 2013).

Increasing light availability due to sea ice retreat has been shown to alter phytoplankton dynamics in the Arctic Ocean using ocean color remote sensing (Arrigo and van Dijken, 2015), but similar large-scale studies are not yet possible for the sea ice habitat due to lack of suitable methods. We have made an effort to understand physical and biological processes in a high-light, young sea ice environment in a refrozen lead during Arctic spring. In a previous study, we have shown that the biomass in the young ice in the refrozen lead was similar to the surrounding older and thicker ice while the light climate was very different, and that algae in the young ice had high concentrations of ultraviolet (UV)-protecting pigments (Kauko et al., 2017). In this paper, we investigate the colonization of the young ice by ice algae and how that relates both to the possible seeding sources, and to the light environment and other environmental conditions. We further examine light acclimation by investigating the photoprotective carotenoids synthetized by

the algae. The objectives of the study were to describe the succession of ice algal species and algal pigment concentrations in young sea ice formed in spring, identify the most important drivers for the algal succession, and compare the young ice community with the surrounding older ice and water column to identify the seeding source.

METHODS

Field Sampling

Young ice (thickness 0.17–0.27 m; Petrich and Eicken, 2010) in a recently refrozen lead was sampled during the Norwegian young sea ICE (N-ICE2015) expedition in the pack ice north of Svalbard at 80.5–82.4°N (**Figure 1A**) in spring 2015 (Granskog et al., 2016, 2018). Ice coring was conducted from early May, a few days after ice reformed over the whole lead, to the beginning of June (Supplementary Table 1) when the ice in the lead broke up. Ice cores for biological samples were first collected close to the edge of the lead (4 and 6 May) and thereafter 13 times (7 May−3 June; approximately every second day) along a transect (five coring sites, three cores pooled at each site) toward the center of the lead (**Figure 1B**). On subsequent sampling days, the transect was moved 2–3 m to the side in order to sample undisturbed ice. Ice cores were melted onboard overnight in the dark at room temperature and unbuffered (Rintala et al., 2014). After 18 May, the ice cores were divided into two sections, where the bottom section was always 0.10 m thick and the top section constituted the remaining part of the core (0.09–0.17 m thick). Salinity of the melted ice cores was measured with a WTW Cond 3110 probe (WTW Wissenschaftlich-Technische Werkstätten GmbH, Weilheim, Germany). Brine salinity was calculated from ice temperature (Cox and Weeks, 1986; Leppäranta and Manninen, 1988). The method for ice core stratigraphy studies is described in Olsen et al. (2017b) and based on Lange (1988). Incoming and ice-transmitted planar downwelling spectral irradiance was measured with two Ramses ACC-VIS spectroradiometers (TriOS Mess- und Datentechnik GmbH, Rastede, Germany) for the wavelength range 320–950 nm (irradiance data are available from Taskjelle et al., 2016). Sampling on the lead is described in detail in Kauko et al. (2017) and biochemical and basic physical data can be found in Assmy et al. (2017a). First-year ice (FYI) and second-year ice (SYI) were sampled weekly and melted by the same procedure (Olsen et al., 2017b). Two cores were pooled and the bottom 0.20 m were cut into 0.10 m long sections and the remaining ice core into 0.20 m sections (all SYI and first FYI coring) or two equal sections (rest of FYI). The water column was sampled via CTD rosettes (one operated from the ship and one through a hole on the adjacent ice floe) twice per week (Assmy et al., 2017b).

Laboratory Methods

From the melted ice core sections 190 mL samples were fixed with glutaraldehyde and 20% hexamethylenetetramine-buffered formaldehyde at final concentrations of 0.1 and 1%, respectively. The samples were stored dark and cool in 200 mL brown glass bottles. Sub-samples were settled in 10 mL Utermöhl sedimentation chambers (HYDRO-BIOS©, Kiel, Germany) for

48 h. Subsequently, protists were identified and counted on a Nikon Ti-U inverted light microscope by the Utermöhl method (Edler and Elbrächter, 2010). Cells were counted in transects. At least 50 cells of the dominant species were counted in each sample (error of ±28% according to Edler and Elbrächter, 2010). Microscopy count data can be found in Olsen et al. (2017a). Abundances (cells L^{-1}) were converted to biomass (mg carbon m^{-3}) using biovolume calculations (Hillebrand et al., 1999) and carbon conversion factors (Menden-Deuer and Lessard, 2000).

Additional samples from the melted ice cores were taken to analyze the algal pigment composition, including diagnostic marker pigments and pigments related to the xanthophyll cycle. For this 100–300 mL melted ice was filtered through 25 mm GF/F filters and shock frozen in liquid nitrogen. The samples were stored at −80°C until analysis. Pigments were analyzed by reverse-phase high performance liquid chromatography (HPLC) using a VARIAN Microsorb-MV3 C8 column (4.6 × 100 mm) and HPLC-grade solvents (Merck), a Waters 1,525 binary pump equipped with an auto sampler (OPTIMAS™), a Waters photodiode array detector (2,996) and the EMPOWER software. For further details see Tran et al. (2013). The ice core samples were melted overnight in darkness and therefore the ratios of the pigments involved in the xanthophyll cycle do not strictly resemble the sampling moment, but together represent a pool of photoprotective carotenoids and are here reported as a sum concentration. HPLC data can be found in Assmy et al. (2017a). An overview of marker pigments and chemotaxonomy can be found in Jeffrey et al. (2011), Higgins et al. (2011), and in the data sheets of Roy et al. (2011). A review of pigments involved in the photoacclimation process can be found in Brunet et al. (2011).

Statistical Methods

Statistical analyses were performed with R (R Core Team, 2017). Data from young ice (including all coring sites and vertical sections, 110 samples) were compared to water column data down to 50 m (23 April−4 June, 69 samples from 17 CTD casts) and to data from the surrounding SYI/FYI (all vertical sections, 22 April−5 June, 74 samples from 11 cores).

Non-metric multidimensional scaling (NMDS), performed with the function *isoMDS* in the MASS package (Venables and Ripley, 2002), was used to investigate the algal community similarity between the different environments based on algal abundance (counts). The count data were first square-root transformed and Bray-Curtis dissimilarity was used for the scaling (calculated with the vegan package; Oksanen et al., 2017).

Shannon's diversity indices (H) were calculated for the species count data with the function *diversity* in the vegan package, defined as H = −sum (p_i ln p_i), where p_i is the proportion of individuals of species i. Pielou's species evenness (J) was calculated as J = H/H_{max}, where H_{max} is a maximum diversity index. Further, H_{max} = $\log_2$(S), where S is the species richness (species number).

To relate the ice algal species abundance in the young ice to environmental variables, canonical correspondence analysis (CCA; suitable for count data) was performed and additionally function *envfit* was used to fit the environmental variables on NMDS analysis of the young ice. Both were performed with the

FIGURE 1 | (A) Study area with the drift trajectory of R/V Lance and sampling location on each sampling day. (B) Ice coring locations on the young ice in the lead. In (A) satellite image (taken on 25 May 2015) source: RADARSAT-2 image provided by NSC/KSAT under the Norwegian-Canadian RADARSAT agreement. RADARSAT-2 Data and Products © MacDonald, Dettwiler and Associates Ltd (2013). All Rights Reserved. RADARSAT is an official mark of the Canadian Space Agency. Map created by the Norwegian Polar Institute/Max König. Aerial image in (B) (taken on 23 May 2015): Vasily Kustov and Sergey Semenov (Arctic and Antarctic Research Institute, St. Petersburg, Russia). Maps modified from Kauko et al. (2017).

vegan package and all samples (110) and species were included in the analysis. Environmental variables included snow thickness (indicative also for light intensity) and bulk salinity. Surface water column nitrate concentration (silicate did not change over the sampling period) correlated strongly with bulk salinity of the sea ice and was excluded from further analysis. Bulk salinity therefore also represents the water column nitrate dynamics.

There were unfortunately no nutrient samples from the lead ice. Likewise, temperature values, which enable calculation of brine salinity, were not available for the whole period, thus bulk salinity was used. Ice thickness could indicate ice melting events and therefore changes in the physical habitat, but because of strong correlation with snow thickness it was not included in the analysis. The variable snow thickness thus represents several

environmental variables that co-vary, including average in-ice irradiance of the past 48 h, which was calculated for the sampling events. The environmental data were standardized prior to usage by subtracting the mean and then dividing by standard deviation.

The function *anosim* in the vegan package was used to test if variation in the count data was higher between the sampling days than between the ice coring sites on the young ice, to justify the use of averages of the five coring sites.

In time series figures for the days when ice cores were sectioned in two, first a volumetric average of the ice core bottom and top section values (biomass and pigment concentrations) was calculated, and thereafter an average of the five ice coring sites. For 4 and 6 May, averages could be calculated from four and two ice cores, respectively. In the case of pigment to Chl *a* ratios (w: w), the ratio was calculated before averaging the ice core bottom and top sections.

RESULTS

Environmental Conditions

A lead next to the research vessel Lance opened on 23 April. Within the next 3 days, the lead was opening and closing, until it got gradually frozen over by 1 May (width ∼400 m). New ice formed first on the side closest to the vessel, on which the ice coring transect was located. Initially, the edge of the lead was characterized by windblown slush and small ice pieces that congealed to a solid ice cover. By the time of sampling, the ice had reached young ice stage and was thick enough to safely work on. The first ice cores for physical measurements were taken on 1 May at the very edge of the lead (same site as on 4 May; **Figure 1B**). At this site on 1 May, the ice was composed of 0.09 m granular ice in the top half and 0.07 m columnar ice in the bottom. Ice temperatures ranged from −2.0 to −4.2°C and bulk salinities from 9.3 to 10.0. On the site that was sampled on 6 May, the ice consisted of 0.03 m granular ice at the top and 0.14 m columnar ice below. Temperatures ranged from −2.1 to −4.5°C and bulk salinities from 10.3 to 14.9. Brine salinity was up to 78.9 at 0.03 m below the ice core top. For the ice coring transect (7 May onwards; **Figure 1B**), ice structure and other physical properties are reported in detail by Kauko et al. (2017). In short, ice thicknesses ranged from 0.17 to 0.27 m, and increased until 20 May after which a reduction was observed. Sites 2 and 3 had the highest proportion of granular ice (0.17 m on 26 May, compared to 0.05–0.08 m columnar ice) and sites 1 and 5 the lowest (0.04–0.05 m granular ice on 26 May, compared to 0.17–0.195 m columnar ice). Snow thicknesses ranged from 0.01 to 0.06 m. Bulk salinity decreased on average (average of 5 sites) from 7.8 to 5.3 during the sampling period and brine salinities ranged from 23.9 to 52.2 (18 May−1 June). Under-ice downwelling irradiance E_d(PAR) in the photosynthetically active radiation range (PAR, 400–700 nm) was on average 114 µmol photons m^{-2} s^{-1} and ranged from 30 to 350 µmol photons m^{-2} s^{-1} for the period from 12 May to 3 June.

The surrounding ice floe was a composite ice floe consisting of SYI and FYI with a modal ice thickness of 1.2 m and modal snow thickness of 0.45 m (Rösel et al., 2018). Ice temperature and other physical properties are described in Olsen et al. (2017b).

Snow depths at the SYI coring site ranged from 0.40 to 0.50 m and at the FYI coring site they were 0.20 m (Olsen et al., 2017b). Irradiance was an order of magnitude lower under FYI than under young ice, and under SYI compared to FYI, with measured irradiances of 0.1–1 µmol photons m^{-2} s^{-1} under SYI and calculated irradiances of 1–20 µmol photons m^{-2} s^{-1} under FYI (Olsen et al., 2017b). Oceanographic conditions of the study area, with Polar Surface Water in the surface, are described in Meyer et al. (2017). Bottom depths during the young ice sampling period varied between 600 and 1,932 m, with shallowest depths occurring toward the end of the study when the ice floe drifted over the Yermak Plateau.

Ice Algal Succession
Temporal Trends in Young Ice

In total, 120 taxa (including e.g., different size categories of flagellates, but excluding cysts) comprising 80 species (including protists identified to species or genus level) were recorded in the young ice samples over the study period. The taxa for all environments are listed in Supplementary Table 2. The community in young ice comprised 54 diatom taxa (45 species), 20 dinoflagellate taxa (15 species), 35 flagellate taxa (15 species), and 11 ciliate taxa (5 species). In this section and section Temporal Trends in Xanthophyll Cycle Pigments, presented values are averages of four ice cores (4 May), two ice cores (6 May), or five coring sites (unless site is specified) where three cores were pooled at each site (transect sampling 7 May onwards; see map in **Figure 1B**). For 18 May and onwards, volumetric averages of ice core bottom and top section values are shown (see section Methods).

In the beginning of the study period, the young ice protist biomass (mg C m^{-3}) and abundance were largely dominated by the ciliate *Mesodinium rubrum* and the cryptophyte chloroplasts (called symbionts hereafter) it had incorporated (**Figure 2** and Supplementary Figure 1). Ciliate cells were presumably damaged during sampling causing release of the symbionts. From 12 May onwards diatoms and dinoflagellates became more prevalent, and together made up almost 70% of the biomass on 12 May. Biomass of ciliates and symbionts decreased thereafter, except on 16 and 20 May. Both flagellates and dinoflagellates biomass increased from early May, but diatoms exponentially increased to over 90% of the total biomass by 3 June, whereas dinoflagellates generally comprised <10% of the biomass. Maximum diatom biomass was 600 mg C m^{-3} on 1 June.

Fucoxanthin, indicative of diatoms, was the most abundant chemotaxonomic marker pigment and increased over the sampling period from 0.01 to 1.26 mg m^{-3} (**Figure 3B**). In terms of marker pigment to Chl *a* ratios, fucoxanthin, and peridinin (a marker for dinoflagellates) showed a contrasting picture during the transect sampling (**Figures 4A,B**). Initially, the peridinin to Chl *a* ratio was high at 0.22 on 7 May, and declined to 0.01 on 1 June. The fucoxanthin to Chl *a* ratio showed the opposite trend, increasing from 0.04 to 0.27.

Species succession was also observed within the diatom community. At the beginning of the transect sampling (7 May onwards) centric diatoms were dominant (**Figure 5A**) and comprised more than 70% of the diatom biomass until

FIGURE 2 | (A) Absolute and **(B)** relative protist biomass in young ice estimated from microscopy counts.
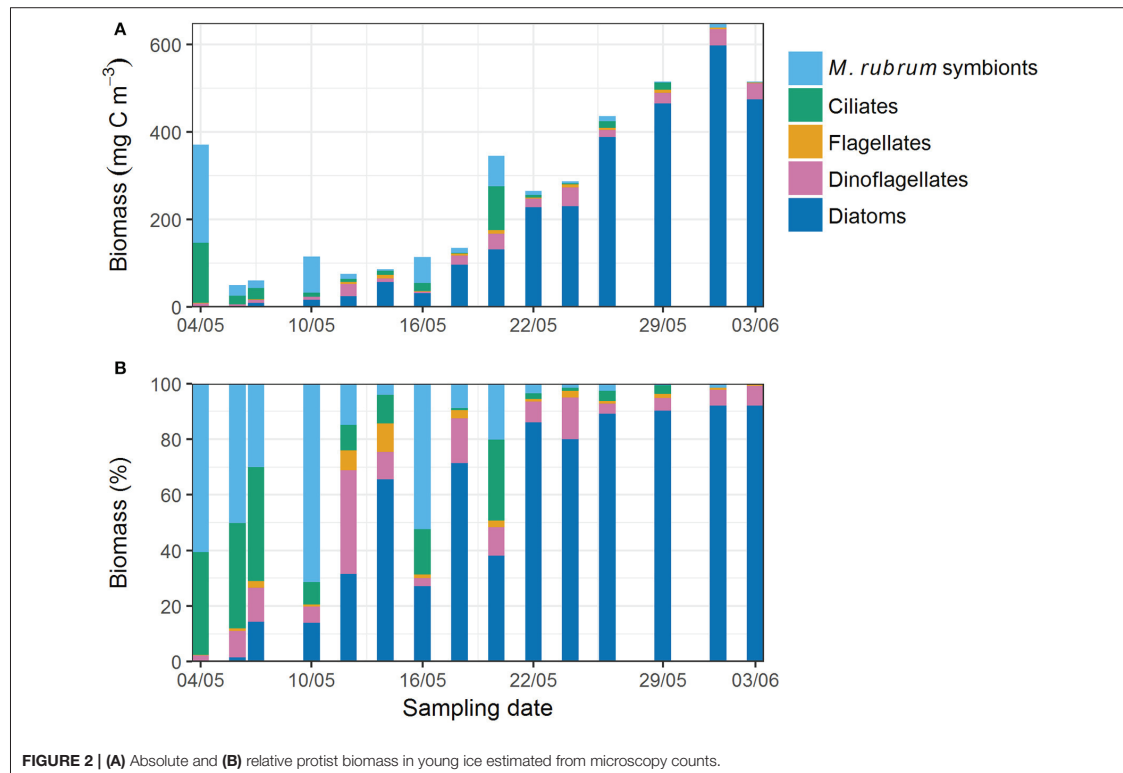
14 May. From 22 May onwards, centric diatoms generally accounted for <60% of diatom biomass, while pennate diatoms increased and dominated (>80% of diatom biomass) from 29 May onwards. The most prevalent taxa among the centric diatoms were *Porosira glacialis* and *Thalassiosira gravida/antarctica* var. *borealis*, and among the pennate diatoms *Nitzschia frigida/neofrigida* (**Figure 6A**), *Fragilariopsis cylindrus* (**Figure 6B**), *Navicula* spp. (**Figure 6C**), and *Pseudo-nitzschia* spp. *Navicula pelagica* appeared in the samples after 18 May. *Fragilariopsis cylindrus* was especially abundant in the middle of the sampling period in terms of cell numbers (Supplementary Figure 2a). On the last two sampling days, *N. frigida/neofrigida* accounted for the highest biomass (ca. 30%) of any individual species.

Cysts accounted for more than 60% of the dinoflagellate biomass on 9 of the 15 sampling days. Cysts of *Polarella glacialis* (**Figure 6E**) occurred throughout the sampling period (**Figure 5B**, Supplementary Figure 2b) and comprised more than 90% of the dinoflagellate biomass on 3 June (35 mg C m^{-3}). Besides cysts, *Gymnodinium* spp. and unidentified dinoflagellates in the size range 10–20 μm were the most prevalent groups among the dinoflagellates.

Unidentified flagellates in the size categories 3–7 and 7–10 μm comprised more than 50% of the flagellate biomass on

most sampling days (**Figure 5C**). Prymnesiophytes, consisting of mainly unidentified Coccolithales, peaked on 14 May but were observed on most sampling days. *Phaeocystis pouchetii* was observed from 16 May onwards to a varying degree (biomass <1 mg C m^{-3}). Prasinophytes (**Figure 6F**) and cryptophytes (other than the *M. rubrum* symbionts) were present at low biomass on most sampling days. Chlorophytes were observed only on 4 sampling days. Statocysts of the chrysophyte algae *Dinobryon* sp. were present especially in the latter half of the sampling period (Supplementary Figure 2c).

For Chl *b*, which is found in chlorophytes, prasinophytes, and euglenophytes, concentrations were generally low, up to 0.11 mg m^{-3} on 26 May (**Figure 3D**) and before the transect sampling on 4 May (not shown). The Chl *b* to Chl *a* ratio was highest on 18 May (0.05; **Figure 4C**) and before the coring transect sampling on 6 May (0.07; Supplementary Figure 3c). Alloxanthin (a cryptophyte marker pigment) concentration was at times high: up to 1.72 mg m^{-3} on site 5 on 20 May (**Figure 3E**), and 1.5 mg m^{-3} in one of the ice cores on 4 May. The alloxanthin to Chl *a* ratio was highest on 6 May (Supplementary Figure 3d). Also gyroxanthin diester (found mainly in dinoflagellates) and β,ε-carotene (α-carotene; found in cryptophytes) had marked peaks on site 5 on 20 May (0.15 and 0.84 mg m^{-3}, respectively; **Figures 3F,G**) and before the transect sampling, but otherwise

FIGURE 3 | Concentrations of main algal pigments in young ice during the ice coring transect study (7 May onwards). **(A)** Chlorophyll (Chl) *a*, **(B)** fucoxanthin, **(C)** peridinin, **(D)** chlorophyll *b*, **(E)** alloxanthin, **(F)** gyroxanthin diester, and **(G)** α carotene.
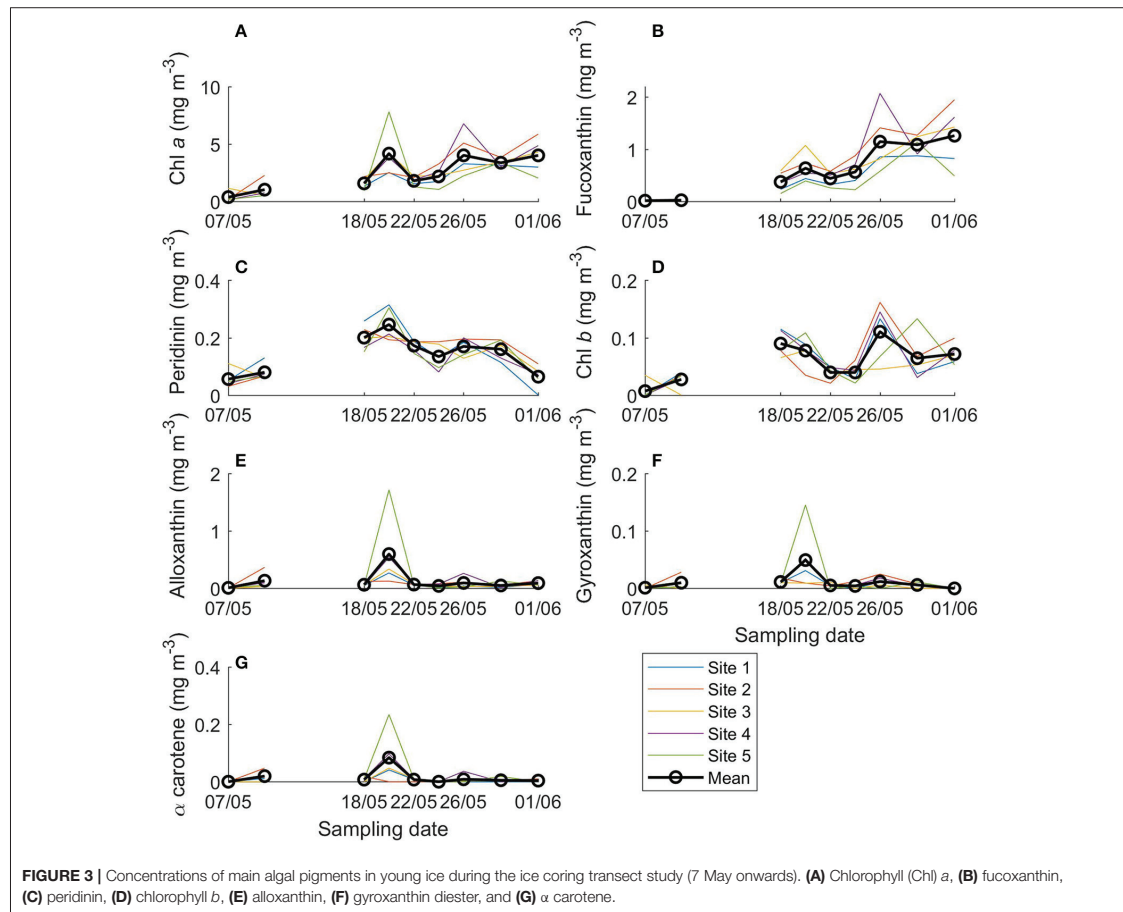
had low concentrations during the transect sampling period. The patterns were similar for ratios of these pigments to Chl *a*, but the ratios were low after 24 May (**Figures 4D–F**). Other pigments are shown in Supplementary Figures 4–6 (they were low in concentration or without taxonomic information). No chlorophyll degradation products such as chlorophyllide *a* (algae senescence) or phaeopigments (e.g., phaeophorbide *a*, indicative of grazing) were detected in the samples.

Differences Between Ice Core Bottom and Top Sections in Young Ice

In the previous paragraphs, values were reported for the ice core bottom and top section together (volumetric mean of the values) to be able to investigate the sampling period as a whole (ice core sectioning started on 18 May). In general, abundance and biomass of the species and groups were higher in the ice core bottom sections than in top sections. There were some exceptions, most notably for cysts of the dinoflagellate *Polarella glacialis* and the *Dinobryon* sp. statocysts (**Figure 7**). In terms

of relative biomass (Supplementary Figure 7), centric diatoms had a higher contribution in the ice core top sections than in bottom sections. Pennate diatoms had a higher contribution in bottom sections than in top sections, although these also increased and dominated over time in the top sections. For flagellates and dinoflagellates, biomass was low and patterns were not as clear (except for the cysts). Pigment concentrations were likewise in general higher in bottom sections than in top sections. Differences in pigment to Chl *a* ratio between the bottom and top sections are shown in Supplementary Figures 3, 6. Fucoxanthin had higher ratios to Chl *a* in the bottom sections. Gyroxanthin diester, α-carotene, dinoxanthin, and neoxanthin were absent from the top sections, whereas Chl c_3 was only found in top sections.

Comparison of Community Structure Between Habitats

Ice algal community patterns in SYI and FYI are described in Olsen et al. (2017b) and reveal the dominance of pennate

FIGURE 4 | Ratios of main algal pigments to Chl *a* in young ice during the ice coring transect study (7 May onwards). **(A)** Fucoxanthin: Chl *a*, **(B)** peridinin: Chl *a*, **(C)** Chl *b*: Chl *a*, **(D)** alloxanthin: Chl *a*, **(E)** gyroxanthin diester: Chl *a*, and **(F)** α carotene: Chl *a*.
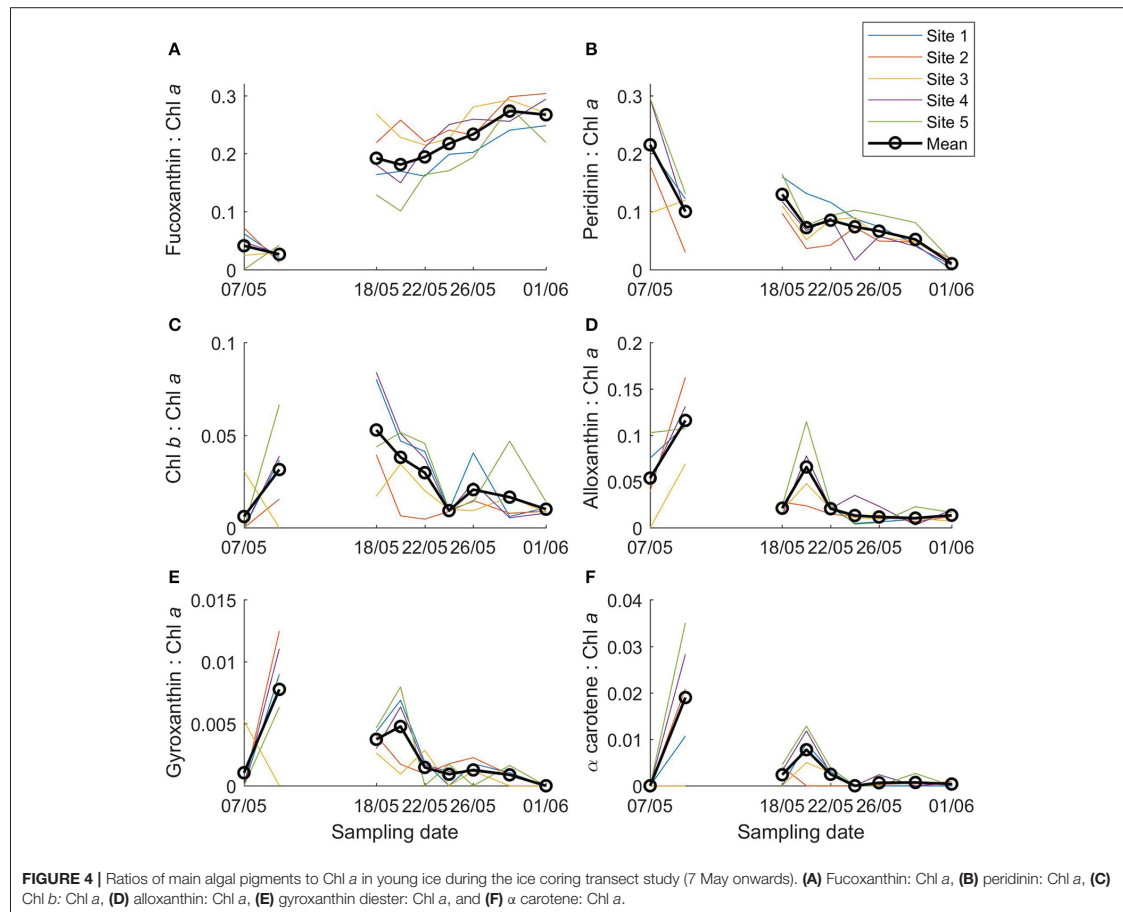
diatoms, especially *N. frigida*, and show that resting cysts were also prominent. In the water column, Chl *a* concentration was low (<0.5 mg m^{-3}) until 25 May when we encountered an under-ice phytoplankton bloom (maximum Chl *a* concentration 7.5 mg m^{-3}) dominated by the haptophyte *P. pouchetii* (Assmy et al., 2017b).

The count data are available in Olsen et al. (2017a). These show that during the early sampling period (22 April−7 May), dinoflagellate abundance in the water column was on average 14-fold higher (average ± standard deviation 1,391 ± 1,217%) compared to diatom abundance. In the surrounding SYI (no FYI sampled at this time period), dinoflagellate abundance was one fourth (24 ± 53%) of diatom abundance. In SYI, 42 diatom, 8 dinoflagellate, and 16 other flagellate taxa (taxonomic level ranging from single species to size categories of flagellates) were identified during this time. In the water column, 8 diatom, 17 dinoflagellate, and 12 other flagellate taxa were identified (Olsen et al., 2017a).

In the early young ice samples (4 May−7 May), 15 diatom (11 of them being pennate species), 12 dinoflagellate, and 9 other

flagellate taxa were found, but most taxa were present only in one or two samples. Of these taxa we identified those that were also found in either the water column (samples from 26 April−5 May), SYI (30 April and 7 May) or in both habitats during the re-freezing of the lead and early sampling. Of these, nearly all the dinoflagellates were only found in the water column except for three taxa that were in addition found in four SYI samples. Cysts were found only in SYI and not in the water column. All diatoms were found only in SYI except for two taxa that were also found in one water column sample each, and *N. frigida/neofrigida* in several samples. *N. frigida/neofrigida* was however 1,500 times more abundant in SYI than in the water column.

Temporal Trends in Xanthophyll Cycle Pigments

The photoprotective pigments diadinoxanthin and diatoxanthin increased in both concentration and ratio to Chl *a* over the sampling period, especially compared to the early transect sampling (7 and 10 May; **Figures 8A,C**). The combined concentration increased from 0.01 to 0.87 mg m^{-3} and the ratio

FIGURE 5 | **(A)** Diatom, **(B)** dinoflagellate, and **(C)** flagellate biomass in young ice. In **(A)**, *Porosira glacialis* and *Thalassiosira gravida/antarctica* are centric diatoms, and the remaining species are pennate diatoms. Note the varying y-axis scale.
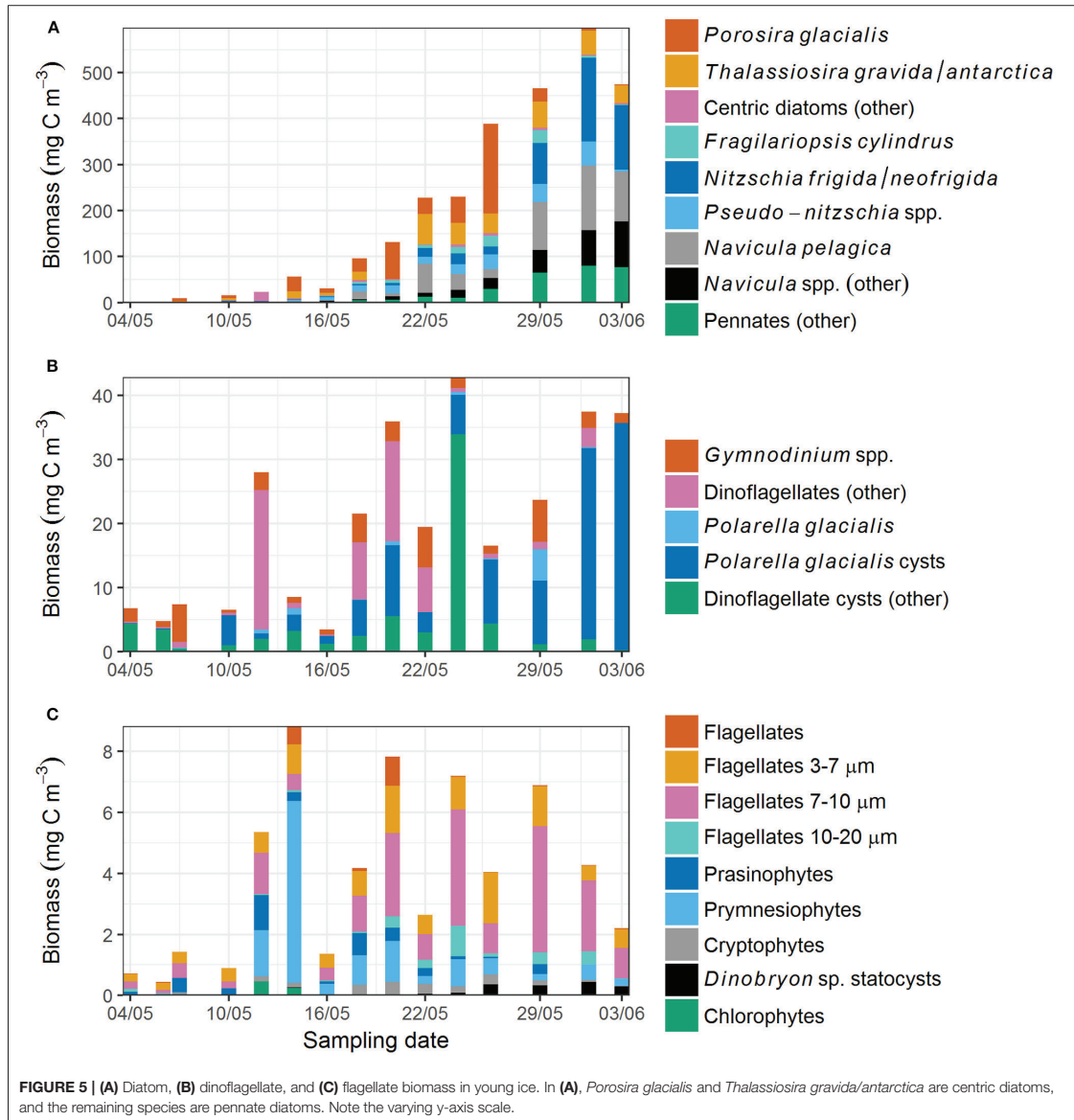
of diadinoxanthin+diatoxanthin to Chl *a* from 0.05 to 0.20 over the transect sampling period. Ratios were similar between the ice bottom and top sections (average ± standard deviation for bottom sections 0.19 ± 0.06 and for top sections 0.20 ± 0.07; Supplementary Figure 8a).

Violaxanthin+zeaxanthin concentration and ratio to Chl *a* varied greatly with peaks around 6, 18–20 and 24–29 May (**Figures 8B,D**, Supplementary Figure 8b). The concentration was on average below 0.03 mg m^{-3} and the ratio to Chl *a* was mostly below 0.02.

Statistical Analysis of Community Similarity and Succession

Each habitat—young ice, SYI/FYI, and water column— formed distinct clusters in the NMDS analysis investigating community similarity (**Figure 9**). In the young ice, a temporal shift in species composition is evident (indicated by the coloring) and the samples approach the SYI/FYI group. Ice core bottom and top section samples are on different sides of the young ice samples group (symbols not shown). For thick ice or water column, neither consistent
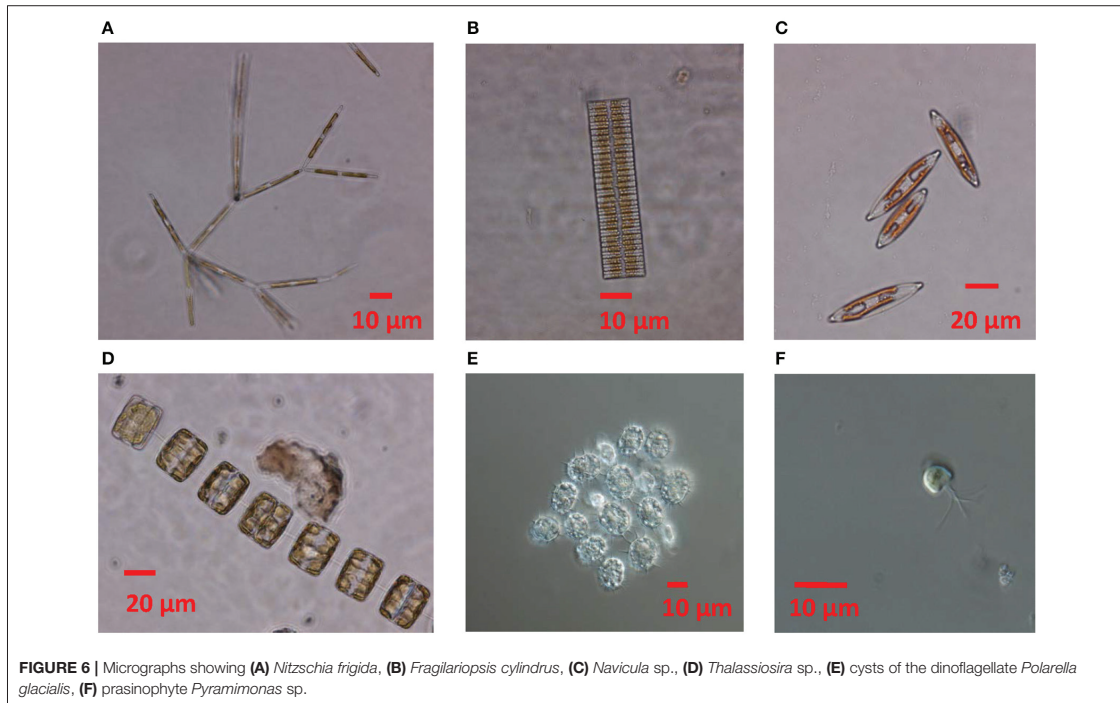
FIGURE 6 | Micrographs showing **(A)** *Nitzschia frigida*, **(B)** *Fragilariopsis cylindrus*, **(C)** *Navicula* sp., **(D)** *Thalassiosira* sp., **(E)** cysts of the dinoflagellate *Polarella glacialis*, **(F)** prasinophyte *Pyramimonas* sp.

vertical (symbols not shown) nor temporal patterns were seen.

The range of Shannon's diversity indices, calculated from species abundance data, was similar in all three environments: 0.01–2.73, 0–2.72, and 0–2.86 for young ice, SYI/FYI and water column, respectively (Supplementary Table 3). When SYI and FYI were treated separately, SYI had a lower diversity range of 0.32–2.46. The young ice had the lowest indices at the beginning of the sampling period whereas the water column samples with lowest diversity were from the latter half of the period (Supplementary Figure 9a). In the SYI/FYI samples, no clear temporal pattern was visible in the diversity index. In general, there was large variation in the indicators (species diversity, richness, and evenness), but species richness increased over time in all habitats (Supplementary Figures 9c,d) and evenness decreased in the water column (Supplementary Figures 9e,f). When the taxon *M. rubrum* symbionts was removed from the dataset (their abundance was likely affected by bursting of *M. rubrum* cells during sampling), evenness had a decreasing trend also in young ice. Furthermore, the early low diversity indices of the young ice disappeared (Supplementary Figure 9b) and the range shifted to 0.84–2.74. Diversity in the young ice was not significantly higher in the ice core top sections than in the bottom sections after removal of the symbionts.

The environmental variables snow thickness and bulk ice salinity (representing several co-varying environmental variables, see section Methods) accounted for 17% of the variance in ice algal abundance in the young ice (CCA in Supplementary Figure 10). The first axis accounted for 16.7% and the second for 0.6% of the variation. The variable bulk salinity aligned close to the first axis and snow thickness close to the second axis. The first axis is parallel to the temporal gradient of the samples (indicated by color in the figure). When the environmental variables were fitted on unconstrained ordination (NMDS for young ice), the patterns were similar and bulk salinity was significantly correlated but snow thickness was not significant.

The sampling days in the young ice differed significantly from each other ($p = 0.001$, $R = 0.41$) for the algal count data, whereas the ice coring sites did not ($p = 0.98$, $R = -0.02$). It is therefore valid to use averages of the coring sites to show the temporal patterns in the young ice biomass and abundance figures.

DISCUSSION

Origin of the Young Ice Community

When new ice forms, cells present in the water column are incorporated into the sea ice. Previous studies have however suggested that not only phytoplankton but also benthic habitats and possibly surrounding ice are sources of ice algae (Ratkova and Wassmann, 2005; Olsen et al., 2017b). In our study, the most probable seeding sources were the water column and surrounding SYI/FYI communities, since the bottom depths at the time of re-freezing were between 1,300 and 2,000 m.

FIGURE 7 | Differences in cyst biomass between ice core bottom and top sections. Ice cores were sectioned from 18 May onwards.
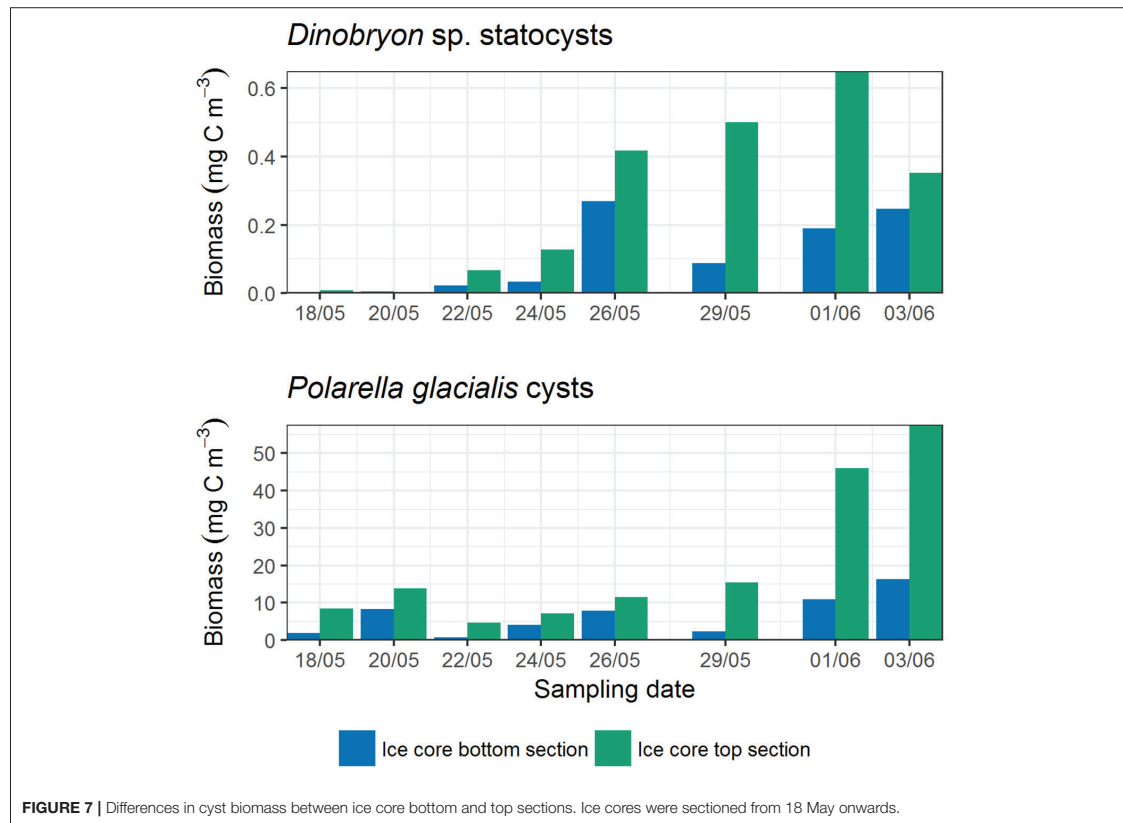
Transport of algae from the shelf waters was not likely as the ice floe was drifting on Polar Surface Water (Meyer et al., 2017). During the re-freezing of the lead and early sampling of the young ice, the algal community in SYI consisted mainly of diatoms and the water column community mainly of dinoflagellates.

The dinoflagellates present in the early young ice samples were in addition found mainly in the water column (and not in SYI). The diatoms, by contrast, were found almost exclusively in SYI except for *N. frigida/neofrigida*. This species is tightly associated with ice, and considering the difference in abundance between SYI and water column, the cells in the water column likely originated from the ice. Olsen et al. (2017b) presented a seeding repository hypothesis for *N. frigida*, suggesting that ice algae from the previous growing season are trapped in the ice and survive over the winter in multi-year ice (MYI), and in the following growing season are able to seed the surrounding new ice. Given our findings, we suggest that the majority of the diatoms in the young ice originated from the surrounding thick ice, although most likely transported via the under-ice water column, while the main source of dinoflagellates was the water column. An additional route for ice-associated species might have

been the wind-blown ice pieces that were observed in the lead and were incorporated in the young ice cover. The granular ice that was observed in the ice core top may in turn indicate that the initial ice formed in turbulent conditions, which are favorable for cell harvesting (Dieckmann et al., 1990; Weissenberger and Grossmann, 1998).

In the NMDS analysis each of the habitats (young ice, SYI/FYI, and water column) formed distinct clusters (**Figure 9**). As discussed above, the cells in the young ice are likely to have initially originated from both the water column and older ice. The separation from water column samples means that algae are either selectively incorporated into ice as found in previous studies (Gradinger and Ikävalko, 1998; Riedel et al., 2007; Rózanska et al., 2008), or that community changes happened almost immediately during the first week after ice formation. It was observed that the ice algal community resembled the water column community in new ice (≤0.03 m) but differed in young ice (0.17–0.21 m; Rózanska et al., 2008). Survival in the new habitat may be different; changes for example in salinity and light regime are substantial when moving from the water column to the ice. Brine salinity in the young ice on 6 May was up to 79, and when in ice, algae are subject to a more stable and

FIGURE 8 | Photoprotective xanthophyll cycle pigments concentration **(A,B)** and ratio to Chl *a* **(C,D)** in young ice during the ice coring transect study (7 May onwards).

FIGURE 9 | Results of the NMDS analysis showing the grouping of young ice, SYI/FYI, and water column groups. The stress value of the plot is 16.6%.
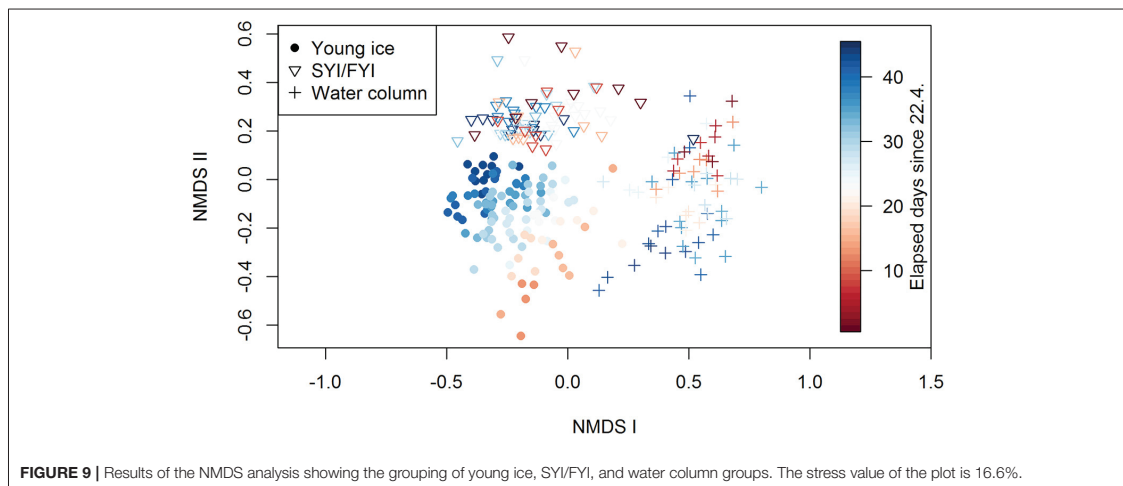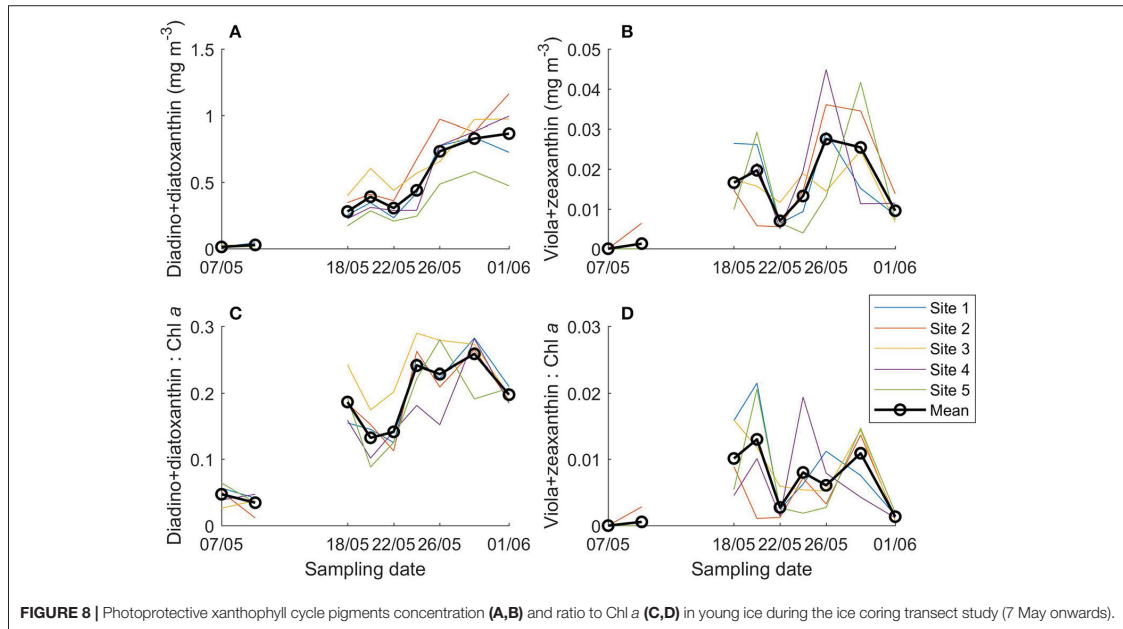
intense light exposure than in the water column. Niemi et al. (2011) observed higher average number of taxa in new ice (1–6 days old) compared to older stages of ice (35+ days old), which could indicate that several species did not survive as the ice grew older. However, considering the long time gap other processes might have also played a role. Our water column taxonomy samples may also have missed the uppermost water layer, where the transport between ice habitats possibly occurs. Hardge et al. (2017) showed that the algal community at 1 m depth below ice

was more similar to the deeper water column than to the FYI and MYI in the Central Arctic Ocean.

Separation of young ice from the SYI/FYI in the ordination (**Figure 9**) shows that the community in the young ice was not identical to the older ice. In the SYI/FYI group, no temporal patterns and thus succession was observed. In contrast, the young ice samples displayed a temporal trend in community composition, indicating that we were able to report the species succession in this habitat. The late young ice samples started to

resemble the SYI/FYI samples and became increasingly distinct from the water column samples, indicating that the young ice community evolved toward a more mature ice algal community.

This study indicates that surrounding ice is an important seeding source at a time of year when the water column has low algal, and especially low diatom, abundance. Ratkova and Wassmann (2005) observed that land-fast sea ice in the White Sea was dominated by pennate diatoms, whereas pack-ice communities in northern Barents Sea were dominated by flagellates, dinoflagellates and centric diatoms, pointing to the importance of sediments as another source for pennate diatoms. As Olsen et al. (2017b) suggest, MYI has an important role as a source in deep areas where the sediment repository is distant. Thus for the ice algal communities to mature to the typical pennate diatom community (Leu et al., 2015; van Leeuwe et al., 2018), contact with previous seasons' populations seems important, and in large parts of the Arctic, particularly the Central Basin, older ice likely plays a crucial role. This is further supported by the observations of Niemi et al. (2011), who found that the timing of ice formation did not determine the community composition in Cape Bathurst flaw lead in the Beaufort Sea, where new ice forms in leads throughout the winter and is surrounded by older first-year land-fast and pack ice. Two thirds of the taxa found in new ice (<6 days old) were not found in the water column but in older ice in their study. Even when phytoplankton is present during sea ice freezing in autumn, the sea ice community differs from the water column, showing that phytoplankton may not be the main source (Werner et al., 2007). In conclusion, timing of freezing (e.g., climate change caused later sea ice freezing in autumn) would be less important than proximity to sediments or older ice (i.e., existence of MYI) for the colonization of future ice algal assemblages.
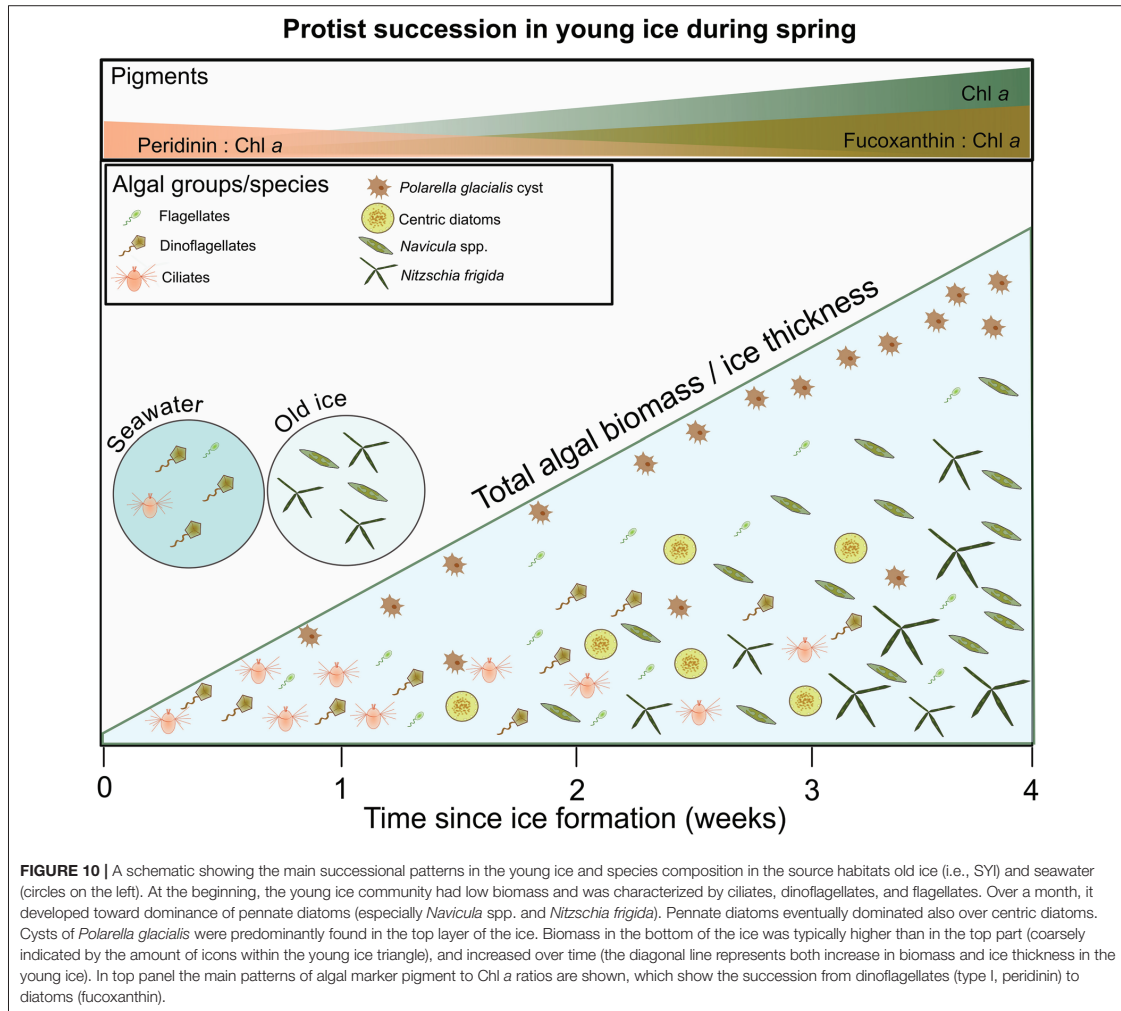
Ice Algal Succession
From Ciliates and Flagellates to Pennate Diatoms
Biomass in the young ice increased over time but the species composition also changed considerably. On the first sampling days the protist community consisted mainly of ciliates, flagellates, and dinoflagellates, which gradually changed to dominance of pennate diatoms. The most prominent early colonizer of the young ice was the ciliate *M. rubrum*. Cryptophyte chloroplast symbionts of the ciliate (for review on the acquired phototrophy see Hansen et al., 2013) dominated in the young ice at the beginning of the study. *M. rubrum* was also found in the water column in the study region. The high abundance of the free symbionts is an artifact caused by disintegration of *M. rubrum* cells during sampling and fixation (Crawford, 1989), but it shows that *M. rubrum* was not limited to the under-ice water column but some cells also actively entered the ice. The symbionts contributed to a high concentration of the cryptophyte marker pigment alloxanthin, thus in this case alloxanthin indicates *M. rubrum* rather than free-living cryptophytes. The biomass of other cryptophytes was less than 6% of the symbiont biomass (not shown). In the first sampling days, alloxanthin had the highest marker pigment to Chl a ratios, confirming a high contribution of *M. rubrum* to the protist community.

The pigment gyroxanthin diester is usually associated with dinoflagellates and is also reported from one pelagophyte and two coccolithophore species (Table 14.2 in Johnsen et al., 2011). In the Arctic, it has previously been associated with the coccolithophore *Emiliana huxleyi* (Pettersen et al., 2011). In our samples, however, gyroxanthin diester seemed to be mainly associated with cryptophytes: temporal patterns of gyroxanthin diester were nearly identical to those of alloxanthin and α carotene, the marker pigments usually associated with cryptophytes (see **Figures 3E–G**, Supplementary Figures 3d–f). In contrast, neither pigments found in dinoflagellates (peridinin, dinoxanthin), pelagophytes (19′-butanoyloxyfucoxanthin; but-fuco), or haptophytes (Chl c_3 found for example in coccolithophores) had similar patterns to gyroxanthin diester. Moreover, Chl c_3 was only found in ice core top sections, whereas gyroxanthin diester only occurred in bottom sections (after ice core sectioning started), which shows that these two pigments were not co-located. Considering that most of the cryptophyte biomass originated from the *M. rubrum* symbionts, gyroxanthin diester seems to be associated with the cryptophyte-*M. rubrum* complex. In the samples where alloxanthin was present but gyroxanthin diester was not, other cryptophytes could be the alloxanthin source. This new observation has implications for using this pigment as an indicator for toxic dinoflagellates or *E. huxleyi* (Pettersen et al., 2011), but more studies are needed to confirm the findings.

Besides *M. rubrum*, dinoflagellates were initially important in the young ice. In terms of marker pigment to Chl a ratios, peridinin-containing dinoflagellates were relatively as important in the beginning of the transect sampling as fucoxanthin containing algae (e.g., diatoms) at the end of the study. Fucoxanthin is considered to originate mainly from diatoms because the microscopy analysis confirmed the high abundance of diatoms and another source of fucoxanthin, haptophytes, can be considered to be of minor importance due to the low concentration of the associated pigment Chl c_3. Dinoflagellates have been shown to increase in a post-bloom situation in FYI (Alou-Font et al., 2013) but our study shows that they can also contribute substantially to the young ice community at the beginning of its formation when the total algal biomass in the ice is still low. Total biomass of diatoms was much higher at the end of the study period than the initial dinoflagellate biomass. Diatom biomass was low at the beginning and mainly formed by centric diatoms, but from mid-May diatoms had a higher contribution to biomass than dinoflagellates and the fucoxanthin to Chl a ratio also increased over the sampling period. Centric diatoms were not very abundant (Supplementary Figure 2a), and throughout the sampling less abundant than pennate diatoms, but because of their relatively high biomass per cell they were prominent in biomass time series. At the end of the sampling, pennate diatoms clearly dominated also in terms of biomass and in the ice core top sections. The successional patterns are summarized in **Figure 10**. The group composition of the ice algal community is also reflected in the algal absorption spectra (Kauko et al., 2017 their Figure 3). The shoulders in the absorption spectra at 460 and 490 nm, caused by carotenoids and chlorophylls c_1 and c_2,

FIGURE 10 | A schematic showing the main successional patterns in the young ice and species composition in the source habitats old ice (i.e., SYI) and seawater (circles on the left). At the beginning, the young ice community had low biomass and was characterized by ciliates, dinoflagellates, and flagellates. Over a month, it developed toward dominance of pennate diatoms (especially *Navicula* spp. and *Nitzschia frigida*). Pennate diatoms eventually dominated also over centric diatoms. Cysts of *Polarella glacialis* were predominantly found in the top layer of the ice. Biomass in the bottom of the ice was typically higher than in the top part (coarsely indicated by the amount of icons within the young ice triangle), and increased over time (the diagonal line represents both increase in biomass and ice thickness in the young ice). In top panel the main patterns of algal marker pigment to Chl *a* ratios are shown, which show the succession from dinoflagellates (type I, peridinin) to diatoms (fucoxanthin).

and the exact wavelength of the *in vivo* red peak of Chl *a* (672–674 nm) are typical for diatoms and dinoflagellates (Johnsen and Sakshaug, 2007).

Chl *b* was the most prominent of the flagellate marker pigments, in addition to the cryptophyte pigments mentioned earlier. In our study Chl *b* likely originated mainly from prasinophytes since they were more abundant and frequent than chlorophytes based on microscopy counts (euglenophytes were not observed). Both based on biomass and low marker pigment concentrations (neoxanthin and lutein), these groups were rare. A fraction of the flagellate group was probably heterotrophic and therefore did not contribute to the marker pigments concentrations, which would also explain why dinoflagellates were relatively more prominent in pigment than count data in

the early sampling period. Flagellate abundance could have been underestimated due to the unbuffered melting method used in this study (Garrison and Buck, 1986), but the concomitantly low flagellate marker pigment concentrations also indicate that they had a minor contribution to the ice algal biomass in the young ice, given that chloroplasts are retained on the sample filter.

Species succession from flagellates to diatoms was also observed over a few months in a mesocosm experiment where sea ice was formed from artificial sea water enriched with brine collected in Fram Strait (Weissenberger, 1998). Rózanska et al. (2008) observed that pennate diatoms were more abundant than centric diatoms or dinoflagellates in young ice (0.17–0.21 m thick) formed in fall in the Beaufort Sea, whereas the opposite was observed for new ice and nilas (thickness <0.08 m). Likewise,

Hegseth (1992) observed a succession from centric to pennate diatoms by studying pack ice floes of different age in Barents Sea, but the age of the different floes differed more than the time span of our sampling period. In some studies, however, new ice was already dominated by pennate diatoms (Okolodkov, 1992; Niemi et al., 2011) or centric diatoms became more abundant than pennates over the growth season (Galindo et al., 2017; Campbell et al., 2018). In general, pennate diatom dominance is a main succession stage during blooming bottom ice algal communities (Leu et al., 2015; van Leeuwe et al., 2018).

Cyst Formation

Cyst or resting stage formation are a part of the life cycle of many algae and are among others an adaptation to survive variable environmental conditions (Von Dassow and Montresor, 2011). In our study, cysts of the dinoflagellate *Polarella glacialis* and statocysts of the chrysophyte *Dinobryon* sp. were more abundant in the ice core top sections than in the bottom sections. The higher abundance of cysts from these groups in the upper ice was also found in previous studies (Stoecker et al., 1992, 1997; Garrison and Close, 1993; Gradinger, 1999; Werner et al., 2007). The cyst abundance and biomass increased over the sampling period, whereas vegetative cells were observed to a far lesser extent. This suggest that these species, after a short growth period in the ice, respond with rapid encystment. The pattern was observed throughout the entire sampling period, which means that algae encyst at the top of the ice core already before the main melting season in spring. This encystment seems to have occurred somewhat earlier than in studies from Antarctica (Stoecker et al., 1992; Garrison and Close, 1993), however, conditions in the young ice with thin snow cover and high irradiance may resemble a melting ice environment thus triggering encystment. The strong increase of *P. glacialis* cysts on the two last sampling days could also be a response to ice melt (ice thickness decreased). This encystment pattern over the whole period may however suggest that cysts are used as a dispersion strategy in addition to overwintering, as suggested by Stoecker et al. (1998). Inhabiting the ice surface would maximize dispersal distance, as that is the most likely part to survive longest and travel furthest. The mechanism to seek the surface could simply be controlled by light, as light intensity is higher further up in the ice. Cysts do not seem to have active Chl *a* (Stoecker et al., 1997) and presumably the photosynthetic apparatus is reduced, which explains the decline in peridinin concentration in our samples (**Figure 3C**) although biomass of the *P. glacialis* cysts increased (**Figure 5B**), and that peaks in dinoflagellate biomass and peridinin concentration do not always match (for *P. glacialis* pigments see Thomson et al., 2004). Thus for understanding survival strategies of sea ice biota, microscopic observations are important.

Species Diversity

Species richness increased over time in all habitats, and cumulative species number (Supplementary Figure 11) showed that the young ice community did not reach a plateau in species richness (if only species that were found on all days after they appeared were taken into account). In the ice habitats there were however no clear diversity changes over time (after removal of the symbionts) despite the increase in species richness. Shannon's diversity index indicates how difficult it is to predict the identity of a specimen taken randomly from the community, and Pielou's evenness describes how similar the abundances of the different species are (Peet, 1974), thus both species richness and evenness affect diversity. The low diversity indices and species evenness in the water column co-occur with the *P. pouchetii* under-ice bloom (Assmy et al., 2017b). The diversity pattern in the young ice case can be explained by the decrease in the species evenness: there are more species present, but some also become more dominant. Furthermore, in SYI the dominance seems to be stronger, because of lower evenness (and diversity) than in young ice or FYI. Thus ice algal communities seem to move in the course of succession toward lower diversity because of lower evenness at least during the bloom season. Alou-Font et al. (2013) observed that diversity did not vary between FYI sites with different snow cover (and thus light), but was lowest during peak bloom and highest during post bloom. MYI seems however to be important for the ice algal diversity: in a molecular study in Central Arctic Ocean, highest proportions of unique taxa (unique to ice as compared to melt ponds and water column) were found in MYI (Hardge et al., 2017). Compared to other studies of newly formed ice (that had less frequent sampling events than this study), the number of taxa was much higher in our case, spring young ice (120 taxa and 80 species), than in Beaufort Sea in autumn new ice ($\leq$6 days old; 46 taxa and 21 species; Niemi et al., 2011) or in autumn new ice, nilas, and young ice (ice thickness $\leq$ 0.21 m; 32–48 taxa and 18–26 species; Rózanska et al., 2008).

Drivers of Ice Algal Succession in Young Ice

In the young ice, there was a clear species succession as seen both in biomass and pigment concentration and also in the NMDS analysis. The main abiotic factors did not explain the variation in ice algal abundance to a great degree (17% of variation accounted for in constrained ordination; Supplementary Figure 10). Thus irradiance (indicated by snow thickness) does not seem to be a strong controlling factor of species succession. The significant correlation of bulk salinity with the unconstrained ordination (NMDS) is likely affected by the clear temporal patterns of bulk salinity caused by desalinization of the ice (Figure 2 in Kauko et al., 2017). The alignment of the first axis (in both ordinations) with the temporal gradient in the samples indicates that the main axis, along which the community varies is a temporal axis. Likewise, the correlation of water column nitrate with bulk salinity is likely caused by the temporal patterns, including strong nitrate drawdown during the under-ice phytoplankton bloom encountered in the latter half of the sampling period (Assmy et al., 2017b). Furthermore, bulk (<15; <9 during transect sampling) or brine salinities (<79; <52 during transect sampling) were not extreme in the young ice (this study and Kauko et al., 2017). Absence of grazing marker pigments (e.g., phaeophorbide *a*) indicate low grazing pressure. This and the weak control by the abiotic factors included here suggest that biotic factors, and moreover species traits and interactions advantageous for the sea ice environment, were likely important in community development (see Section Adaptation to Environmental Conditions and Morphology). This

conclusion is consistent with that the general pattern of diatom dominance (particularly pennate diatoms) in sea ice is similar across the Arctic (Poulin et al., 2011; Leu et al., 2015), despite a wide range in environmental conditions.

Irradiance

It should be noted that irradiance levels in our young ice case (on average 114 and range 30–350 μmol photons m^{-2} s^{-1}) were relatively high throughout the study period (Kauko et al., 2017). Light has been observed to impact community composition when experimentally perturbed (Enberg et al., 2015) or under different snow cover (Rózanska et al., 2009; Alou-Font et al., 2013). Alou-Font et al. (2013) observed no dinoflagellates under thick snow cover (lower light), but in our case they were found in both ice types. It has been suggested that higher abundance of centric compared to pennate diatoms in sea ice was due to higher light availability (Majaneva et al., 2017; Campbell et al., 2018). Exclusion of UV radiation led to biomass increase of *N. fridiga* in experiments (Enberg et al., 2015). In our samples, however, pennate diatoms dominated toward the end also in the young ice and in ice core top sections, i.e., under high irradiance. Thus in our study, this comparison, in addition to the statistical analysis, does not point to an important role of light in terms of community composition.

Nevertheless, photoacclimation is needed for the algae to be able to colonize new ice in spring. High irradiance can inhibit growth in non-acclimated cells (Mangoni et al., 2009; Juhl and Krembs, 2010). On the other hand, high irradiance likely enables more rapid growth in acclimated communities and dispersion in the ice in spring than in autumn. Ice algae have been considered to be highly shade adapted (Thomas and Dieckmann, 2002) and they can grow in very low light (<0.17 μmol photons m^{-2} s^{-1}; Hancke et al., 2018). Detailed studies on the photoacclimation capacities of ice algae conclude however that they have high plasticity regarding growth irradiance, aided to a large degree by the photoprotective xanthophyll cycle (Robinson et al., 1997; Petrou et al., 2011; Galindo et al., 2017). In our study, the xanthophyll cycle pigments diadino- and diatoxanthin showed an increasing trend both in concentration and ratio to Chl *a*, and thus show a response to increasing irradiance levels (Kauko et al., 2017 and Supplementary Figure 12). Diadino- and diatoxanthin are found in for example diatoms, dinoflagellates, and haptophytes (see Table 11.1 in Brunet et al., 2011) and thus represent the photoprotective mechanism of the majority of algae found in our samples. Other xanthophyll cycle pigments (violaxanthin and zeaxanthin, found e.g., in chlorophytes) were detected in our samples but in low concentrations and with a variable pattern, reflecting the low biomass of these algae in the samples in addition to the light exposure history. A similar seasonal increase in the photoprotective pigment pool in ice algae was also observed in FYI in the Canadian Arctic (Alou-Font et al., 2013; Galindo et al., 2017). The diadinoxanthin + diatoxanthin to Chl *a* ratios in our samples were in the range of what has been previously reported for surface habitats (ponds and slush) on Antarctic sea ice (Arrigo et al., 2014) or under thin snow cover in the Arctic (Alou-Font et al., 2013; Galindo et al., 2017). The average ratio was however similar in the surrounding FYI (data now shown) with much lower light levels [E_d(PAR) 1–20 μmol

photons m^{-2} s^{-1}] than in the young ice (Olsen et al., 2017b). The ratios found in surrounding SYI [E_d(PAR) <1 μmol photons m^{-2} s^{-1}] were on average lower and similar to those in interior and bottom ice habitats in Arrigo et al. (2014).

The photoprotective pigment to Chl *a* ratios were not significantly different between the ice core top and bottom sections despite higher light exposure in the former. Based on radiative transfer modeling for 26 May (Kauko et al., 2017), the E_d(PAR) difference between the bottom and top 0.01 m of ice was >450 μmol photons m^{-2} s^{-1}. Alou-Font et al. (2013) found differences in photoprotective pigment to Chl *a* ratios already for irradiance levels of 26 and <10 μmol photons m^{-2} s^{-1} (between different snow covers). In our case the surrounding thick SYI had diadino- + diatoxanthin to Chl *a* ratios that were significantly lower in the bottom 0.20 m of the ice column, despite thick snow cover and thus high light attenuation also at the top of the ice column. These seemingly contradictory results suggest that the photoprotective pigment expression is controlled by more factors than purely light intensity, or that in many cases the expression is not fine-tuned but rather responds to broad categories or thresholds in light intensity (consider also the similarity between young ice and FYI in our case), or temporally integrated doses. When it comes to the photosynthetic pigments in our samples, differences between the young ice sections were again visible. Fucoxanthin to Chl *a* and Chl c_2 to Chl *a* ratios (the most prominent light harvesting pigments in our samples) were higher in ice core bottom sections. In lower light, algae increase the amount of photosynthetic pigments to effectively harvest the available light (Brunet et al., 2011).

Adaptation to Environmental Conditions and Morphology

The succession of the ice algal community, from a flagellate-dinoflagellate to a diatom dominated community, and within the diatoms from centric to pennate diatoms, indicates that sea ice communities evolve toward a more ice-adapted species community over time during a bloom. This was also suggested by Syvertsen (1991), based on changes in ice algal community composition from the ice edge northwards in the Barents Sea, i.e., from younger to older ice. The temporal patterns thus can be affected by the traits of the different species. When ice is formed, the species composition reflects what was present in the water column at the time of ice formation. Over time, selection occurs based on adaptation to the conditions in the ice and competition between species. *N. frigida* with the arborescent colonies, and other pennate species with attaching and gliding capabilities, are well adapted to life in brine channels, which to a certain degree resemble benthic habitats. Furthermore, they are adapted to the growth conditions: for example *N. frigida* grows exponentially even at very low temperatures and high salinities (Aletsee and Jahnke, 1992). *Fragilariopsis* species were in experiments found to be more tolerant to high salinities than a chlorophyte species (Søgaard et al., 2011) and are known to produce antifreeze proteins (Bayer-Giraldi et al., 2010). Additional biotic factors might also play a role in species succession; abundance of *F. cylindrus* (formerly *Nitzschia cylindrus*) was observed to decrease in connection with parasitic infection in the Beaufort Sea (Horner and

Schrader, 1982). The exponential increase of the major pennate diatoms in our study indicates that the growth conditions were favorable for them. However, when the seeding stock is low, they and especially *N. frigida* needed time to become dominant even at close to maximum growth rates (Olsen et al., 2017b).

Dinoflagellates in general are not considered as typical ice algae, but the brine community in upper ice in Antarctic land-fast ice can be dominated by dinoflagellates (Stoecker et al., 1992). Stoecker et al. (1997) reported that dinoflagellates and chrysophytes excysted and started photosyntethizing under extreme conditions (in terms of salinity and temperature) in the upper ice layers early in the season. Stoecker et al. (1998) observed that as the ice warmed, flagellates were replaced by pennate diatoms also in the upper ice. Dinoflagellates seem to be outcompeted by diatoms in the lower parts of ice and during more favorable growth conditions, but some species have evolved capacities to survive and find a niche. Resting cysts are a major component of the life cycle of ice-associated dinoflagellates (see discussion and references in section Cyst formation).

The pennate diatom *F. cylindrus* was, in terms of cell counts, an important species and had an exponential apparent growth rate until 29 May. Thereafter cell numbers declined strongly, possibly due to melting of ice (ice thickness began to decrease), which may have flushed the cells out. The ribbon shaped colonies may not be as optimal for attaching to the ice matrix as e.g., colonies of *N. frigida*. Otherwise it is well-adapted: Petrou et al. (2012) studied the photophysiology of *F. cylindrus* under temperature and nutrient stress and noticed that cell division rates decreased under nitrogen depletion, but physiological changes allowed for greater photoprotective capacity and photosynthetic efficiency was maintained. *Fragiolariopsis* species are also prominent ice algal species throughout the Arctic (Leu et al., 2015). However, *F. cylindrus* (and other small diatoms) in Antarctica was observed in experiments to synthetize mycosporine-like amino acids (MAAs) only in trace amounts that were not sufficient for effective UV protection (Riegger and Robinson, 1997), which could be a competitive disadvantage compared to species with higher amounts of MAAs. Judging by the high MAA to Chl *a* ratios found in the young ice in our case (Kauko et al., 2017), algae were investing strongly in UV protection. Thus both physical changes in the ice (melting) as well as physiological reasons (UV protection) could be responsible for the decline in this species during the study period. Likewise, centric diatoms (morphology shown in **Figure 6D**) were possibly affected by ice melting at the end of the study period.

In summary, the ice algal succession in young ice appears to start in a stochastic manner and then follows patterns that are dependent on the traits of the species present, resulting in differential adaptation to the ice habitat and its conditions (different succession concepts reviewed in McCook, 1994). Initially, species are likely to arrive in ice in a relatively random order based on abundances in the water column, which again are based on proximity to suitable source habitats such as older ice and water column bloom status. Once in ice, traits that provide a competitive advantage in the ice habitat determine the success of species to further grow and spread. Since the diatoms that

were found in our early young ice were rarely observed in the water column, it suggests that the relatively few cells that came into contact with the young ice were successful in inhabiting and growing in the ice. Facilitation of the later arrivals by the early colonizers (see Connell and Slatyer, 1977) could occur as biologically produced extracellular polysaccharide substances have been observed to change the microstructure of growing ice (Krembs et al., 2011). Some degree of inhibition of later arrivals by early colonizers could also occur based on nutrient consumption, and in some cases because of allelopathy.

CONCLUSIONS

Our study provides the first observations of algal species succession in newly formed sea ice in spring. By following the same ice floe over an extended period of time we could observe the species succession at a high temporal resolution. The ice algal community originated both from the underlying water column and surrounding older ice, pointing to the importance of older ice as a seeding source. The community developed from a more mixed community toward dominance by ice-adapted pennate diatoms such as *N. frigida*. Overall the succession seemed to be determined more by the traits of the species than by variable abiotic factors. The colonization of the high light environment of young ice in spring is further aided by photoprotective carotenoids. The main trends in community succession were revealed also with marker pigment concentrations, with a fucoxanthin to Chl *a* ratio (indicative of diatoms) increase from 0.04 to 0.27 over the sampling period and low flagellate marker pigment concentrations. The pigment approach misses, however, the species succession within diatoms due to similar pigments, and patterns in cyst biomass due to lack of active photosynthesis in cysts. Cysts dominated the dinoflagellate biomass (>60%) on the majority of the sampling days. Cysts of the dinoflagellate *P. glacialis* were predominantly found in the top layers of the ice and were more prominent than the vegetative cells already in early May, which points to an important role of ice as a cyst repository and suggests that cysts may be used as a dispersion mechanism. With the decline in Arctic sea ice cover, loss of MYI and as ice retreats further away from the shelves, dispersal of ice algal species may be compromised, which could lead to changes in the relative importance of the dominant ice algal species. Based on this and previous studies, the source of pennate diatoms in new ice often seems to derive from surface sediments or older ice, whereas the time of freezing or environmental conditions play a smaller role in determining the community composition. In conclusion, the springtime young-ice algal community developed in less than a month into a typical, pennate diatom dominated community, when surrounding older sea ice can act as a seeding source.

AUTHOR CONTRIBUTIONS

PA, PD, MG, and CM planned the field work; PA, PD, MG, CM, HK, LO, MF-M, and AP conducted the field work; HK and

SUPPLEMENTARY MATERIAL

The Supplementary Material for this article can be found online at: https://www.frontiersin.org/articles/10.3389/fmars.2018.00199/full#supplementary-material

REFERENCES

Aletsee, L., and Jahnke, J. (1992). Growth and productivity of the psychrophilic marine diatoms *Thalassiosira antarctica* Comber and *Nitzschia frigida* Grunow in batch cultures at temperatures below the freezing point of sea water. *Polar Biol.* 11, 643–647. doi: 10.1007/BF00237960

Alou-Font, E., Mundy, C. J., Roy, S., Gosselin, M., and Agustí. S. (2013). Snow cover affects ice algal pigment composition in the coastal Arctic Ocean during spring. *Mar. Ecol. Prog. Ser.* 474, 89–104. doi: 10.3354/meps10107

Arrigo, K. R., Brown, Z. W., and Mills, M. M. (2014). Sea ice algal biomass and physiology in the Amundsen Sea, Antarctica. *Elem. Sci. Anthr.* 2:28. doi: 10.12952/journal.elementa.000028

Arrigo, K. R., and van Dijken, G. L. (2015). Continued increases in Arctic ocean primary production. *Prog. Oceanogr.* 136, 60–70. doi: 10.1016/j.pocean.2015.05.002

Assmy, P., Duarte, P., Dujardin, J., Fernández-Méndez, M., Fransson, A., Hodgson, R., et al. (2017a). *N-ICE2015 sea ice biogeochemistry [Data set]*. Tromsø: Norwegian Polar Data Centre. doi: 10.21334/npolar.2017.d3e93b31

Assmy, P., Fernández-Méndez, M., Duarte, P., Meyer, A., Randelhoff, A., Mundy, C. J., et al. (2017b). Leads in Arctic pack ice enable early phytoplankton blooms below snow-covered sea ice. *Sci. Rep.* 7:40850. doi: 10.1038/srep40850

Bayer-Giraldi, M., Uhlig, C., John, U., Mock, T., and Valentin, K. (2010). Antifreeze proteins in polar sea ice diatoms: diversity and gene expression in the genus Fragilariopsis. *Environ. Microbiol.* 12, 1041–1052. doi: 10.1111/j.1462-2920.2009.02149.x

Brunet, C., Johnsen, G., Lavaud, J., and Roy, S. (2011). "Pigments and photoacclimation processes," in *Phytoplankton Pigments - Characterization, Chemotaxonomy and Applications in Oceanography*, eds S. Roy, C. A. L. Lewellyn, E. S. Egeland, and G. Johnsen (Cambridge: Cambridge University Press), 445–471.

Campbell, K., Mundy, C. J., Belzile, C., Delaforge, A., and Rysgaard, S. (2018). Seasonal dynamics of algal and bacterial communities in Arctic sea ice under variable snow cover. *Polar Biol.* 41, 41–58. doi: 10.1007/s00300-017-2168-2

Connell, J., and Slatyer, R. O. (1977). Mechanisms of succession in natural communities and their role in community stability and organization. *Am. Nat.* 111, 1119–1144.

Cox, G. F. N., and Weeks, W. F. (1986). Changes in the salinity and porosity of sea-ice samples during shipping and storage. *J. Glaciol.* 32, 371–375.

Crawford, D. W. (1989). *Mesodinium rubrum*: the phytoplankter that wasn't. *Mar. Ecol. Prog. Ser.* 58, 161–174. doi: 10.3354/meps058161

Dieckmann, G. S., Spindler, M., Lange, M. A., Ackley, S. F., and Eicken, H. (1990). "Sea ice. a habitat for the foraminifer *Neogloboquadrina pachyderma*? in sea ice properties and processes," in *Proceedings of the W. F. Weeks Sea Ice Symposium, CRREL Monograph 90-1*, eds S. F. Ackley and W. F. Weeks (Hanover, NH: Cold Regions Research Engineering Laboratory), 86–92.

Dupont, F. (2012). Impact of sea-ice biology on overall primary production in a biophysical model of the pan-Arctic Ocean. *J. Geophys. Res. Oceans* 117, 1–18. doi: 10.1029/2011JC006983

Edler, L., and Elbrächter, M. (2010). "The Utermöhl method for quantitative phytoplankton analysis," in *Microscopic and Molecular Methods for Quantative Phytoplankton analysis*, eds B. Karlson, C. Cusack, and E. Bresnan (Paris: Intergovernmental Oceanographic Commission of UNESCO), 13–20.

Enberg, S., Piiparinen, J., Majaneva, M., Vähätalo, A. V., Autio, R., and Rintala, J.-M. (2015). Solar PAR and UVR modify the community composition and photosynthetic activity of sea ice algae. *FEMS Microbiol. Ecol.* 91, 1–11. doi: 10.1093/femsec/fiv102

Fernández-Méndez, M., Katlein, C., Rabe, B., Nicolaus, M., Peeken, I., Bakker, K., et al. (2015). Photosynthetic production in the central Arctic Ocean during the record sea-ice minimum in 2012. *Biogeosciences* 12, 3525–3549. doi: 10.5194/bg-12-3525-2015

Galindo, V., Gosselin, M., Lavaud, J., Mundy, C. J., Else, B., Ehn, J., et al. (2017). Pigment composition and photoprotection of Arctic sea ice algae during spring. *Mar. Ecol. Prog. Ser.* 585, 49–69. doi: 10.3354/meps1239

Garrison, D. L., and Buck, K. R. (1986). Organism losses during ice melting: a serious bias in sea ice community studies. *Polar Biol.* 6, 237–239. doi: 10.1007/BF00443401

Garrison, D. L., and Close, A. R. (1993). Winter ecology of the sea-ice biota in Weddell sea pack ice. *Mar. Ecol. Ser.* 96, 17–31.

Gosselin, M., Levasseur, M., Wheeler, P. A., Horner, R. A., and Booth, B. C. (1997). New measurements of phytoplankton and ice algal production in the Arctic Ocean. *Deep. Res. Part II Top. Stud. Oceanogr.* 44, 1623–1644. doi: 10.1016/S0967-0645(97)00054-4

Gradinger, R. (1999). Vertical fine structure of the biomass and composition of algal communities in Arctic pack ice. *Mar. Biol.* 133, 745–754.

Gradinger, R., and Ikävalko, J. (1998). Organism incorporation into newly forming Arctic sea ice in the Greenland Sea. *J. Plankton Res.* 20, 871–886. doi: 10.1093/plankt/20.5.871

Granskog, M. A., Assmy, P., Gerland, S., Spreen, G., Steen, H., and Smedsrud, L. H. (2016). Arctic research on thin ice: consequences of Arctic sea ice loss. *Eos. Trans. AGU* 97, 22–26. doi: 10.1029/2016EO044097

Granskog, M. A., Fer, I., Rinke, A., and Steen, H. (2018). Atmosphere-ice-ocean-ecosystem processes in a thinner Arctic sea ice regime: the Norwegian young sea ICE (N-ICE2015) expedition. *J. Geophys. Res. Ocean* 123, 1586–1594. doi: 10.1002/2017JC013328

Hancke, K., Lund-Hansen, L. C., Lamare, M. L., Pedersen, S. H., King, M. D., Andersen, P., et al. (2018). Extreme low light requirement for algae growth underneath sea ice : a case study from Station Nord, NE Greenland. *J. Geophys. Res. Oceans* 123, 985–1000. doi: 10.1002/2017JC013263

Hansen, P. J., Nielsen, L. T., Johnson, M., Berge, T., and Flynn, K. J. (2013). Acquired phototrophy in *Mesodinium* and *Dinophysis* - a review of cellular organization, prey selectivity, nutrient uptake and bioenergetics. *Harmful Algae* 28, 126–139. doi: 10.1016/j.hal.2013.06.004

Hardge, K., Peeken, I., Neuhaus, S., Lange, B. A., Stock, A., Stoeck, T., et al. (2017). The importance of sea ice for exchange of habitat-specific protist communities in the Central Arctic Ocean. *J. Mar. Syst.* 165, 124–138. doi: 10.1016/j.jmarsys.2016.10.004

Hegseth, E. N. (1992). Sub-ice algal assemblages of the Barents Sea: species composition, chemical composition, and growth rates. *Polar Biol.* 12, 485–496.

Higgins, H. W., Wright, S. W., and Schlüter, L. (2011). "Quantative interpretation of chemotaxonomic pigment data," in *Phytoplankton Pigments - Characterization, Chemotaxonomy and Applications in Oceanography*, eds S. Roy, C. A. LLewellyn, E. S. Egeland, and G. Johnsen (Cambridge: Cambridge University Press), 257–313.

Hillebrand, H., Dürselen, C.-D., Kirschtel, D., Pollingher, U., and Zohary, T. (1999). Biovolume calculation for pelagic and benthic microalgae. *J. Phycol.* 35, 403–424. doi: 10.1046/j.1529-8817.1999.3520403.x

Horner, R., and Schrader, G. C. (1982). Relative contributions of ice algae, phytoplankton, and benthic microalgae to primary production in nearshore regions of the Beaufort Sea. *Arctic* 35, 485–503. doi: 10.14430/arctic2356

Itkin, P., Spreen, G., Cheng, B., Doble, M., Girard-Ardhuin, F., Haapala, J., et al. (2017). Thin ice and storms: a case study of sea ice deformation from buoy arrays deployed during N-ICE2015. *J. Geophys. Res. Ocean.* 122, 4661–4674. doi: 10.1002/2016JC012403

Jeffrey, S. W., Wright, S. W., and Zapata, M. (2011). "Microalgal classes and their signature pigments," in *Phytoplankton Pigments - Characterization, Chemotaxonomy and Applications in Oceanography*, eds S. Roy, C. A. LLewellyn, E. S. Egeland, and G. Johnsen (Cambridge: Cambridge University Press), 3–77.

Johnsen, G., Moline, M. A., Pettersson, L. H., Pinckney, J., Pozdnyakov, D. V., Egeland, E. S., et al. (2011). "Optical monitoring of phytoplankton bloom pigment signatures," in *Phytoplankton Pigments - Characterization, Chemotaxonomy and Applications in Oceanography*, eds S. Roy, C. A. LLewellyn, E. S. Egeland, and G. Johnsen (Cambridge, UK: Cambridge University Press), 538–581.

Johnsen, G., and Sakshaug, E. (2007). Biooptical characteristics of PSII and PSI in 33 species (13 pigment groups) of marine phytoplankton, and the relevance for pulse-amplitude-modulated and fast-repetition-rate fluorometry. *J. Phycol.* 43, 1236–1251. doi: 10.1111/j.1529-8817.2007.00422.x

Juhl, A. R., and Krembs, C. (2010). Effects of snow removal and algal photoacclimation on growth and export of ice algae. *Polar Biol.* 33, 1057–1065. doi: 10.1007/s00300-010-0784-1

Kauko, H. M., Taskjelle, T., Assmy, P., Pavlov, A. K., Mundy, C. J., Duarte, P., et al. (2017). Windows in Arctic sea ice: light transmission and ice algae in a refrozen lead. *J. Geophys. Res. Biogeosci.* 122, 1486–1505. doi: 10.1002/2016JG003626

Krembs, C., Eicken, H., and Deming, J. W. (2011). Exopolymer alteration of physical properties of sea ice and implications for ice habitability and biogeochemistry in a warmer Arctic. *Proc. Natl. Acad. Sci. U.S.A.* 108, 3653–3658. doi: 10.1073/pnas.1100701108

Krembs, C., Tuschling, K., and von Juterzenka, K. (2002). The topography of the ice-water interface - its influence on the colonization of sea ice by algae. *Polar Biol.* 25, 106–117. doi: 10.1007/s003000100318

Lange, B. A., Flores, H., Michel, C., Beckers, J. F., Bublitz, A., Casey, J. A., et al. (2017). Pan-Arctic sea ice-algal chl *a* biomass and suitable habitat are largely underestimated for multiyear ice. *Glob. Chang. Biol.* 23, 4581–4597. doi: 10.1111/gcb.13742

Lange, M. A. (1988). Basic properties of Antarctic sea ice as revealed by textural analysis of ice cores. *Ann. Glaciol.* 10, 95–101.

Leppäranta, M., and Manninen, T. (1988). The brine and gas content of sea ice with attention to low salinities and high temperatures. *Finnish Inst. Mar. Res. Intern. Rep.* 2, 1–14.

Leu, E., Mundy, C. J., Assmy, P., Campbell, K., Gabrielsen, T. M., Gosselin, M., et al. (2015). Arctic spring awakening–steering principles behind the phenology of vernal ice algal blooms. *Prog. Oceanogr.* 139, 151–170. doi: 10.1016/j.pocean.2015.07.012

Lund-Hansen, L. C., Hawes, I., Nielsen, M. H., and Sorrell, B. K. (2017). Is colonization of sea ice by diatoms facilitated by increased surface roughness in growing ice crystals? *Polar Biol.* 40, 593–602. doi: 10.1007/s00300-016-1981-3

Majaneva, M., Blomster, J., Müller, S., Autio, R., Majaneva, S., Hyytiäinen, K., et al. (2017). Sea-ice eukaryotes of the Gulf of Finland, Baltic Sea, and evidence for herbivory on weakly shade-adapted ice algae. *Eur. J. Protistol.* 57, 1–15. doi: 10.1016/j.ejop.2016.10.005

Mangoni, O., Carrada, G. C., Modigh, M., Catalano, G., and Saggiomo, V. (2009). Photoacclimation in Antarctic bottom ice algae: an experimental approach. *Polar Biol.* 32, 325–335. doi: 10.1007/s00300-008-0517-x

McCook, L. J. (1994). Understanding ecological community succession: causal models and theories, a review. *Vegetatio* 110, 115–147.

Meier, W. N., Hovelsrud, G. K., van Oort, B. E. H., Key, J. R., Kovacs, K. M., Michel, C., et al. (2014). Actic sea ice in transformation: a review of recent observed changes and impacts on biology and human activity. *Rev. Geophys.* 51, 185–217. doi: 10.1002/2013RG000431

Meiners, K., Gradinger, R., Fehling, J., Civitarese, G., and Spindler, M. (2003). Vertical distribution of exopolymer particles in sea ice of the Fram Strait (Arctic) during autumn. *Mar. Ecol. Prog. Ser.* 248, 1–13. doi: 10.3354/meps248001

Melnikov, I. A. (1995). An *in situ* experimental study of young sea ice formation on an Antarctic lead. *J. Geophys. Res.* 100, 4673–4680.

Menden-Deuer, S., and Lessard, E. J. (2000). Carbon to volume relationship for dinoflagellates, diatoms and other protist plankton. *Limnol. Oceanogr.* 45, 569–579. doi: 10.4319/lo.2000.45.3.0569

Meyer, A., Sundfjord, A., Fer, I., Provost, C., Villacieros Robineau, N., Koenig, Z., et al. (2017). Winter to summer oceanographic observations in the Arctic Ocean north of Svalbard. *J. Geophys. Res. Ocean.* 122, 6218–6237. doi: 10.1002/2016JC012391

Niemi, A., Michel, C., Hille, K., and Poulin, M. (2011). Protist assemblages in winter sea ice: setting the stage for the spring ice algal bloom. *Polar Biol.* 34, 1803–1817. doi: 10.1007/s00300-011-1059-1

Okolodkov, Y. B. (1992). Cryopelagic flora of the Chukchi, East Siberian and Laptev Seas. *Proc. NIPR Symp. Polar Biol.* 5, 28–43.

Oksanen, J., Blanchet, F. G., Friendly, M., Kindt, R., Legendre, P., McGlinn, D., et al. (2017). *Vegan: Community Ecology Package*. Available online at: https://cran.r-project.org/package=vegan

Olsen, L. M., Assmy, P., Duarte, P., Laney, S. R., Fernández-Méndez, M., Kauko, H. M., et al. (2017a). *N-ICE2015 Phytoplankton and Ice Algae Taxonomy and Abundance [Data set]*. Tromsø: Norwegian Polar Data Centre. doi: 10.21334/npolar.2017.dc61cb24

Olsen, L. M., Laney, S. R., Duarte, P., Kauko, H. M., Fernández-Méndez, M., Mundy, C. J., et al. (2017b). The seeding of ice algal blooms in Arctic pack ice: the multiyear ice seed repository hypothesis. *J. Geophys. Res. Biogeosci.* 122, 1–20. doi: 10.1002/2016JG003668

Peet, R. K. (1974). The measurement of species diversity. *Annu. Rev. Ecol. Syst.* 5, 285–307.

Petrich, C., and Eicken, H. (2010). "Growth, structure and properties of sea ice," in *Sea Ice*, eds D. N. Thomas and G. S. Dieckmann (Oxford, UK: Wiley-Blackwell), 23–77.

Petrou, K., Hill, R., Doblin, M. A., McMinn, A., Johnson, R., Wright, S. W., et al. (2011). Photoprotection of sea-ice microalgal communities from the east Antarctic pack ice. *J. Phycol.* 47, 77–86. doi: 10.1111/j.1529-8817.2010.00944.x

Petrou, K., Kranz, S. A., Doblin, M. A., and Ralph, P. J. (2012). Photophysiological responses of *Fragilariopsis cylindrus* (Bacillariophyceae) to nitrogen depletion at two temperatures. *J. Phycol.* 48, 127–136. doi: 10.1111/j.1529-8817.2011.01107.x

Pettersen, R., Johnsen, G., Berge, J., and Hovland, E. K. (2011). Phytoplankton chemotaxonomy in waters around the Svalbard archipelago reveals high amounts of Chl *b* and presence of gyroxanthin-diester. *Polar Biol.* 34, 627–635. doi: 10.1007/s00300-010-0917-6

Poulin, M., Daugbjerg, N., Gradinger, R., Ilyash, L., Ratkova, T., and von Quillfeldt, C. (2011). The pan-Arctic biodiversity of marine pelagic and sea-ice unicellular eukaryotes: a first-attempt assessment. *Mar. Biodivers.* 41, 13–28. doi: 10.1007/s.12526-010-0058-8

R Core Team (2017). *R: A Language and Environment for Statistical Computing.* Vienna: R Foundation for Statistical Computing. Available online at: https://www.R-project.org/

Ratkova, T. N., and Wassmann, P. (2005). Sea ice algae in the White and Barents seas: composition and origin. *Polar Res.* 24, 95–110. doi: 10.1111/j.1751-8369.2005.tb00143.x

Reimnitz, E., Kempema, E. W., Weber, W. S., Clayton, J. R., and Payne, J. R. (1990). "Suspended-matter scavenging by rising frazil ice," in *Sea Ice Properties and Processes, Proceedings of the W. F. Weeks Sea Ice Symposium, CRREL Monograph 90-1*, eds S. F. Ackley and W. F. Weeks (Hanover, NH: Cold Regions Research Engineering Laboratory), 97–100.

Riedel, A., Michel, C., Gosselin, M., and LeBlanc, B. (2007). Enrichment of nutrients, exopolymeric substances and microorganisms in newly formed sea ice on the Mackenzie shelf. *Mar. Ecol. Prog. Ser.* 342, 55–67. doi: 10.3354/meps342055

Riegger, L., and Robinson, D. (1997). Photoinduction of UV-absorbing compounds in Antarctic diatoms and *Phaeocystis antarctica*. *Mar. Ecol. Prog. Ser.* 160, 13–25. doi: 10.3354/meps160013

Rintala, J.-M., Piiparinen, J., Blomster, J., Majaneva, M., Müller, S., Uusikivi, J., et al. (2014). Fast direct melting of brackish sea-ice samples results in biologically more accurate results than slow buffered melting. *Polar Biol.* 37, 1811–1822. doi: 10.1007/s00300-014-1563-1

Robinson, D. H., Kolber, Z., and Sullivan, C. W. (1997). Photophysiology and photoacclimation in surface sea ice algae from McMurdo Sound, Antarctica. *Mar. Ecol. Prog. Ser.* 147, 243–256. doi: 10.3354/meps147243

Rösel, A., Itkin, P., King, J., Divine, D., Wang, C., Granskog, M. A., et al. (2018). Thin sea ice, thick snow and widespread negative freeboard observed during N-ICE2015 north of Svalbard. *J. Geophys. Res. Ocean* 123, 1–21. doi: 10.1002/2017JC012865

Roy, S., Lewellyn, C. A., Egeland, E. S., and Johnsen, G., (eds) (2011). *Phytoplankton Pigments - Characterization, Chemotaxonomy and Applications in Oceanography, 1st Edn.* Cambridge: Cambridge University Press.

Rózanska, M., Gosselin, M., Poulin, M., Wiktor, J. M., and Michel, C. (2009). Influence of environmental factors on the development of bottom ice protist communities during the winter-spring transition. *Mar. Ecol. Prog. Ser.* 386, 43–59. doi: 10.3354/meps08092

Rózanska, M., Poulin, M., and Gosselin, M. (2008). Protist entrapment in newly formed sea ice in the Coastal Arctic Ocean. *J. Mar. Syst.* 74, 887–901. doi: 10.1016/j.jmarsys.2007.11.009

Rysgaard, S., and Nielsen, T. G. (2006). Carbon cycling in a high-arctic marine ecosystem-Young Sound, NE Greenland. *Prog. Oceanogr.* 71, 426–445. doi: 10.1016/j.pocean.2006.09.004

Søgaard, D. H., Hansen, P. J., Rysgaard, S., and Glud, R. N. (2011). Growth limitation of three Arctic sea ice algal species: effects of salinity, pH, and inorganic carbon availability. *Polar Biol.* 34, 1157–1165. doi: 10.1007/s00300-011-0976-3

Søreide, J. E., Leu, E., Berge, J., Graeve, M., and Falk-Petersen, S. (2010). Timing of blooms, algal food quality and *Calanus glacialis* reproduction

and growth in a changing Arctic. *Glob. Chang. Biol.* 16, 3154–3163. doi: 10.1111/j.1365-2486.2010.02175.x

Stoecker, D. K., Buck, K. R., and Putt, M. (1992). Changes in the sea-ice brine community during the spring- summer transition, McMurdo Sound, Antarctica. I. Photosynthetic protists. *Mar. Ecol. Prog. Ser. Ser.* 84, 265–278.

Stoecker, D. K., Gustafson, D. E., Black, M. M. D., and Baier, C. T. (1998). Population dynamics of microalgae in the upper land-fast sea ice at a snow-free location. *J. Phycol.* 34, 60–69. doi: 10.1046/j.1529-8817.1998.340060.x

Stoecker, D. K., Gustafson, D. E., Merrell, J. R., Black, M. M. D., and Baier, C. T. (1997). Excystment and growth of chrysophytes and dinoflagellates at low temperatures and high salinities in Antarctic sea-ice. *J. Phycol.* 33, 585–595. doi: 10.1111/j.0022-3646.1997.00585.x

Syvertsen, E. E. (1991). Ice algae in the Barents Sea: types of assemblages, origin, fate and role in the ice-edge phytoplankton bloom. *Polar Res.* 10, 277–288. doi: 10.1111/j.1751-8369.1991.tb00653.x

Taskjelle, T., Hudson, S. R., Pavlov, A. K., and Granskog, M. A. (2016). *N-ICE2015 Surface and Under-Ice Spectral Shortwave Radiation Data [Data set].* Tromsø: Norwegian Polar Data Centre. doi: 10.21334/npolar.2016.9089792e

Thomas, D. N., and Dieckmann, G. S. (2002). Antarctic sea ice - a habitat for extremophiles. *Science* 295, 641–644. doi: 10.1126/science.1063391

Thomson, P. G., Wright, S. W., Bolch, C. J. S., Nichols, P. D., Skerratt, J. H., and McMinn, A. (2004). Antarctic distribution, pigment and lipid composition, and molecular identification of the brine dinoflagellate *Polarella glacialis* (Dinophyceae). *J. Phycol.* 40, 867–873. doi: 10.1111/j.1529-8817.2004.03169.x

Tran, S., Bonsang, B., Gros, V., Peeken, I., Sarda-Esteve, R., Bernhardt, A., et al. (2013). A survey of carbon monoxide and non-methane hydrocarbons in the Arctic Ocean during summer 2010. *Biogeosciences* 10, 1909–1935. doi: 10.5194/bg-10-1909-2013

Tuschling, K. V., Juterzenka, K., Okolodkov, Y. B., and Anoshkin, A. (2000). Composition and distribution of the pelagic and sympagic algal assemblages in the Laptev Sea during autumnal freeze-up. *J. Plankton Res.* 22, 843–864. doi: 10.1093/plankt/22.5.843

van Leeuwe, M. A., Tedesco, L., Arrigo, K. R., Assmy, P., Campbell, K., Meiners, K. M., et al. (2018). Microalgal community structure and primary production in Arctic and Antarctic sea ice: a synthesis. *Elem. Sci. Anthr.* 6:4. doi: 10.1525/elementa.267

Venables, W. N., and Ripley, B. D. (2002). *Modern Applied Statistics With S, 4th Edn.* New York, NY: Springer.

Von Dassow, P., and Montresor, M. (2011). Unveiling the mysteries of phytoplankton life cycles: patterns and opportunities behind complexity. *J. Plankton Res.* 33, 3–12. doi: 10.1093/plankt/fbq137

Weissenberger, J. (1998). Arctic Sea ice biota: design and evaluation of a mesocosm experiment. *Polar Biol.* 19, 151–159.

Weissenberger, J., and Grossmann, S. (1998). Experimental formation of sea ice: importance of water circulation and wave action for incorporation of phytoplankton and bacteria. *Polar Biol.* 20, 178–188. doi: 10.1007/s003000050294

Werner, I., Ikävalko, J., and Schünemann, H. (2007). Sea-ice algae in Arctic pack ice during late winter. *Polar Biol.* 30, 1493–1504. doi: 10.1007/s00300-007-0310-2

Paper IV

Assessing photoacclimation state of an Arctic under-ice phytoplankton bloom using in situ absorption measurements

Hanna M. Kauko[1,2], Alexey K. Pavlov[1,3,4], Geir Johnsen[5,6], Mats A. Granskog[1], Ilka Peeken[7], Philipp Assmy[1]

[1]Norwegian Polar Institute, Fram Centre, Tromsø, Norway

[2]Trondheim Biological Station, Department of Biology, Norwegian University of Science and Technology, Trondheim, Norway

[3]Institute of Oceanology Polish Academy of Sciences, Sopot, Poland

[4]Akvaplan-niva, Fram Centre, Tromsø, Norway

[5]Centre for Autonomous Marine Operations and Systems, Trondheim Biological Station, Department of Biology, Norwegian University of Science and Technology, Trondheim, Norway

[6]University Centre in Svalbard, Longyearbyen, Norway

[7]Alfred Wegener Institute Helmholtz Centre for Polar and Marine Research, Bremerhaven, Germany

Abstract

Recent reports on Arctic under-ice phytoplankton blooms have directed attention to primary production below the ice cover, yet studying these blooms is difficult and often requires ship-based campaigns because ocean colour remote sensing cannot be used to monitor the under-ice water column. Methods for autonomous under-ice measurements are thus critically needed to extend observations beyond research vessel surveys. Here we investigate the possibility to use in situ absorption measurements to gain information about the photoacclimation state of phytoplankton during an under-ice bloom of *Phaeocystis pouchetii*. The slope of absorption between 488 and 532 nm, affected by both photoprotective (PPC) and photosynthetic carotenoids (PSC), was calculated from in situ absorption profiles and related to ratios of pigment concentrations (PPC:PSC) obtained from high performance liquid chromatography (HPLC) measurements. There was a significant linear relationship between these two, which would allow predicting the PPC:PSC ratio from in situ absorption measurements. We also explored different ways of processing the in situ absorption data of total non-water absorption to obtain phytoplankton absorption, and of grouping the photoprotective and photosynthetic pigments. Detrital absorption was low in our study area whereas absorption by coloured dissolved organic matter (CDOM) had to be subtracted from the in situ absorption measurements in order to achieve good results. The different pigment groupings had all significant linear relationships with the absorption slopes, but including only xanthophyll cycle pigments in PPC performed best. We found similarities in the linear regressions compared to earlier studies, but a validation dataset or extensive studies of the variability in

the relationship (affected e.g. by pigment packaging in algal cells) are likely needed for future studies to be able to use the method. Our study shows the potential for using in situ absorption measurements to gain information about phytoplankton physiology.

1. Introduction

The Arctic region, and the Arctic marine ecosystem receive high attention in the wake of the substantial environmental changes taking place (Wassmann et al. 2011; Meier et al. 2014). Primary production by algae (phytoplankton and ice algae) sustains the ecosystem, therefore being able to understand and monitor primary production is essential for sustainable ecosystem management.

In recent years, several reports of under-ice phytoplankton blooms in the Arctic Ocean (Fortier et al. 2002; Mundy et al. 2009, 2014, Arrigo et al. 2012, 2014b; Assmy et al. 2017) have enhanced our understanding of Arctic Ocean primary production. The growth of under-ice blooms was enabled by light transmitted either through melt ponds in summer (Arrigo et al. 2014b), early snow melt (Fortier et al. 2002) or open or refrozen leads in spring (Assmy et al. 2017). The conditions conducive to late summer under-ice blooms are becoming more favourable under the changing Arctic sea ice regime (Horvat et al. 2017) and it is important to include different types of under-ice blooms in future scenarios of Arctic primary production (Johnsen et al. 2018). In contrary to phytoplankton blooms in open waters, these blooms cannot be monitored from space by means of ocean colour remote sensing, and therefore, information about them is sparse. Efforts towards increasing the use of autonomous sampling platforms in ice-covered waters are underway, for example demonstrated by adding bio-optical sensors to e.g. ice-tethered buoys (Laney et al. 2014, 2017) or the use of autonomous underwater vehicles (Johnsen et al. 2018). In general, large-scale efforts to monitor the water column ecosystems are emerging, like increasing glider facilities and the biogeochemical Argo float program (Johnson and Claustre 2016), which carry various biogeochemical and optical instruments to study biological processes. Argo floats have also been deployed in seasonally ice covered waters and efforts continue to further expand the latitudinal range and possibilities of Argo float deployment (http://www.argo.ucsd.edu/Polar_Argo.html).

Thus, it is crucial to develop applications for data delivered by new platforms to extract more information on the state of the ecosystem. Here we study whether in situ spectral absorption measurements can be used to assess the photoacclimation state of an under-ice phytoplankton bloom by using a modification of a method originally developed in coastal waters off the West Coast of the United States (Eisner et al. 2003). They found that in situ absorption measurements enabled estimating the ratio of photoprotective (PPC) to photosynthetic (PSC) carotenoids. To protect the photosynthetic apparatus from excess light, algae can synthesize and alter the fraction of PPC, that dissipate the excess energy as heat instead of channelling it to photosynthesis (Brunet et al. 2011). Main examples of these pigments include some of the xanthophyll cycle carotenoids, where with increasing light intensity diadinoxanthin is de-epoxidized to diatoxanthin (e.g. in diatoms, haptophytes and dinoflagellates) or violaxanthin is de-epoxidized to zeaxanthin via antheraxanthin (e.g. in chlorophytes and chrysophytes) (Brunet et al. 2011). Several studies have previously examined the possibilities in e.g. studying the mixing properties of the water column by using photoprotective carotenoid ratios from water samples (Claustre et al. 1994; Moline 1998) or other photoprotective indices

(Falkowski 1983; Lewis et al. 1984), suggesting a potential use of these measurements beyond physiological studies.

In this study we examine the photoacclimation state, using the PPC:PSC ratio as a proxy, of an arctic under-ice phytoplankton bloom and attempt to validate a method to monitor pigment ratios by in situ absorption measurements.

2. Methods

2.1 Study area and water sampling

The samples and measurements in this study were obtained during the Norwegian young sea ICE (N-ICE2015) expedition (Granskog et al. 2016, 2018) in the pack ice north of Svalbard in May–June 2015. The research vessel Lance was anchored to and drifting along in total four different ice floes during the nearly half-year long expedition. In this study we use data from Floe 3 and 4 (Figure 1; 26.5.–18.6. for the in situ absorption data and 18.5.–21.6. for pigment data). Field sampling is described in detail in Assmy et al. (2017) and Pavlov et al. (2017). In short, the water column was typically sampled twice a week with a water sampler rosette operated from the RV Lance or with a rosette deployed from a hut on the ice ca. 400 m away from the vessel. Water samples for pigment and particle absorption measurements were filtered on 25 mm Whatman GF/F glass fiber filters (GE Healthcare, Little Chalfont, UK) and then stored at -80 degrees C until analysis. Coloured dissolved organic matter (CDOM) samples were filtered through 0.2 μm syringe filters and stored at +4 ℃ until analysis.
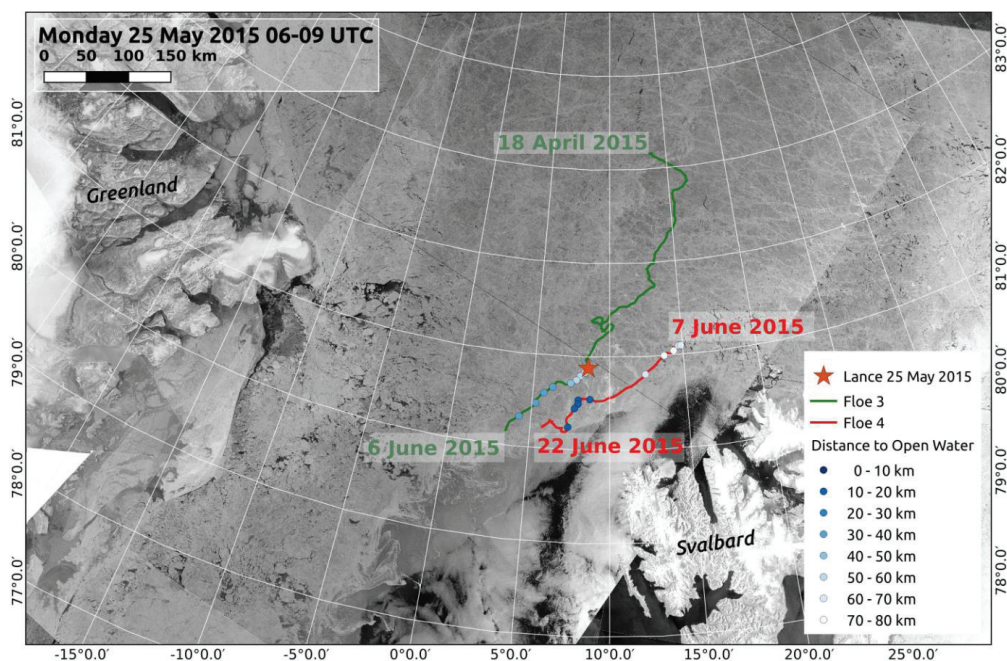
Figure 1. Satellite image (RADARSAT-2) of the study area with location of RV Lance (orange star) on 25 May 2015 and drift tracks for Floes 3 and 4 (start and end dates of tracks

indicated). Circles on tracks correspond to dates when the distance (see legend) between the position of RV Lance and open water could be estimated (satellite images were available). RADARSAT-2 images are provided by NSC/KSAT under the Norwegian-Canadian agreement. RADARSAT-2 data and products © MacDonald, Dettwiler, and Associates Ltd (2013). All rights reserved. RADARSAT is an official mark of the Canadian Space Agency. Map from Pavlov et al. (2017).

2.2 In situ absorption measurements with ac-9

In situ absorption measurements were made with an ac-9 absorption and light beam attenuation meter (WET Labs, Philomath, OR, USA) from a heated tent on the sea ice ca. 400 m away from the RV Lance, during the drifts of Floes 3 and 4 (Pavlov et al. 2016; Taskjelle et al. 2016). The ac-9 measured absorption ($a(\lambda)$, excluding absorption by pure water) and light beam attenuation ($c(\lambda)$, excluding attenuation by pure water) at nine distinct wavelengths: 412, 440, 488, 510, 532, 555, 650, 676, and 715 nm.

The majority of ac-9 measurements were restricted to the upper 20 m of the water column (due to cable length limitations). A Seabird 911 CTD sensor, calibrated before and after the expedition, was used to obtain vertical profiles of seawater temperature and salinity prior to or immediately after ac-9 casts. Data from corresponding CTD casts were used for temperature and salinity correction of spectral absorption data following Röttgers et al. (2014). Absorption data were also corrected for scattering effects by subtracting the measured absorption at the wavelength of minimum absorption (715 nm) (Zaneveld et al. 1994).

2.3 HPLC measurements and grouping of pigments

Pigment samples were measured with reverse-phase high performance liquid chromatography (HPLC) with a VARIAN Microsorb-MV3 C8 column (4.6x100 mm), using HPLC-grade solvents (Merck), Waters 1525 binary pump equipped with an autosampler (OPTIMAS™), a Waters 2996 PDA (photodiode array detector) and the EMPOWER software. For further details see Tran et al. (2013). Data down to 50 m depth from the time period 18.5.–21.6.2015 are shown in Figures 2 and 3.

Photoacclimation state is here investigated through the ratio (mg m^{-3} : mg m^{-3}) between PPC and PSC. To explore the method and to be able to compare to previous studies, we included several different ways of grouping the pigments. First, we followed the grouping used in Eisner et al. (2003). Pigments included in the PPC$_1$ category were diadinoxanthin (DD), diatoxanthin (DT), violaxanthin, zeaxanthin, alloxanthin, lutein and β,β-carotene. PSC$_1$ pigments included peridinin, fucoxanthin, 19'-butanoyloxyfucoxanthin (but-fuco), 19'-hexanoyloxyfucoxanthin (hex-fuco), neoxanthin and prasinoxanthin (Table 1). However, because alloxanthin is likely to be light-harvesting (Johnsen et al. 2011) we also show and discuss the analysis with alloxanthin relocated to PSC (PPC$_2$:PSC$_2$; consistent with Roy et al. (2008) and Alou-Font et al. (2013, 2016)). We also followed a more strict grouping of the PPCs (see discussion in section 3.3.1) where we calculated the ratio of the pigments involved in the photoprotective xanthophyll cycle (XC) to PSC (XC:PSC$_2$; XC included diadinoxanthin, diatoxanthin, violaxanthin and zeaxanthin). β,ε-carotene (α-carotene) and gyroxanthin diester were not included in the analysis because of uncertain pigment function.

Antheraxanthin was not observed. For a review on photoprotective patterns, see Brunet et al. (2011).

2.4 CDOM and particle absorption filter measurements

CDOM absorption ($a_{CDOM}(\lambda)$, m^{-1}) was measured with a Shimadzu UV-2401PC spectrophotometer (Shimadzu Corporation, Kyoto, Japan) using 10 cm quartz cuvettes. Total particle absorption ($a_p(\lambda)$, m^{-1}) was measured on a Shimadzu UV-2450 dual-beam spectrophotometer with an integrating sphere (ISR-2200) following the method by Tassan and Ferrari (2002). Particle absorption filters were bleached for 10–30 minutes with sodium hypochlorite (NaClO with 1 % active chlorine) and rinsed with 30 ml of artificial seawater (60 g Na_2SO_4 in 1 L of ultrapure water). Absorption measurements after bleaching provided information about detrital absorption ($a_d(\lambda)$, m^{-1}). At a processing stage we smoothed $a_{CDOM}(\lambda)$ and $a_d(\lambda)$ spectra with a low-pass (Savitzky–Golay) filter to increase signal-to-noise ratio, particularly at longer wavelengths (> 488 nm) used in this study (see section 2.5 below). Details of CDOM and particle absorption measurements are given in Kauko et al. (2017).

2.5 Slope calculations based on ac-9 absorption data

Normalized absorption slope values were calculated based on ac-9 data at three wavelengths (488, 532, and 676 nm) following Eisner et al. (2003) (Equation 1). The ac-9 instrument measured total non-water absorption by seawater, which includes not only phytoplankton, but also CDOM and detrital matter. We subtracted CDOM absorption from ac-9 absorption values at the three corresponding wavelengths (Equation 2). To match high vertical resolution (1 m bins) ac-9 profiles and discrete CDOM samples we selected ac-9 bins above the corresponding CDOM sample (e.g. for CDOM sample collected at 5 m, we used ac-9 data binned between 4 and 5 m). Taking CDOM absorption into account from discrete water samples is a slightly different approach compared to Eisner et al. (2003), who used two ac-9 instruments one of which was equipped with a 0.2 μm filter, allowing quantifying CDOM absorption in situ. Detrital absorption at 488, 532, and 676 nm was very low and did not change substantially during the bloom period (Pavlov et al. 2017). Therefore, we took the average of $a_d(\lambda)$ at 488, 532 and 676 nm during the whole period of observations, and subtracted them from absorption values measured by the ac-9 (Equation 2).

$$a_{ph} \text{ slope} = (a_{ph}(488) - a_{ph}(532)) / ((488-532) \, a_{ph}(676)) \qquad (1)$$

$$a_{ph}(\lambda) = a(\lambda) - a_{CDOM}(\lambda) - <a_d(\lambda)> \qquad (2)$$

where $<a_d(\lambda)>$ is the average detrital absorption at 488, 532, and 676 nm.

The a_{ph} slope varies with the light-acclimation state of a cell (e.g. Johnsen et al. 1994): in high light, algal cells produce more PPC (Brunet et al. 2011) and have a lower pigment packaging effect (Johnsen et al. 2011), which results in a steeper slope. Absorption at 488 nm has a high contribution from PPC and at 532 nm from PSC.

Overall, matching the ac-9 profiles and the water sampling from CTD profiles gave 15 data pairs in the upper 15 meters in the time period 26.5.–18.6.2015.

3. Results and discussion

3.1 Under-ice phytoplankton bloom

On 25 May 2015, when the ice camp was approximately 80 km (Figure 1) into the ice pack from open water, we drifted into an under-ice phytoplankton bloom on the Yermak Plateau and followed the bloom until the end of the campaign on 22 June. The bloom was dominated by the colony-forming haptophyte *Phaeocystis pouchetii* with Chl *a* concentrations up to 7.5 mg m^{-3} and a maximum standing stock in the upper 50 m of 233 mg Chl *a* m^{-2} (Assmy et al. 2017). The upper 50 to 100 m were characterized by Polar Surface Water, underlain by Atlantic Water with an average mixed layer depth of 6 m after 25 May (Meyer et al. 2017). The bloom was not advected from open water areas or covered by ice after growth in open water, based on current patterns in the area and ice cover history from ice charts (Assmy et al. 2017). In situ growth under the ice cover was possible with the light provided through open and refrozen leads (Assmy et al. 2017). Further, physiological measurements of in vivo Chl *a* fluorescence obtained using the Pulse Amplitude Modulated (PAM) fluorometry method showed that the bloom was in a healthy condition (maximum quantum yields of photosystem II fluorescence in dark-acclimated cells were 0.48–0.66) (Assmy et al. 2017).

3.2 Photoprotective carotenoids and photoacclimation

The highest PPC concentrations and PPC:PSC and XC:PSC ratios occurred in the upper water column towards the end of the sampling period (Figures 2 and 3). The initial increase in the PPC concentration on 26 May coincides with the bloom and shallowing of mixed layer from 64 to 6 m (averages before and after 25 May) (Meyer et al. 2017). The CTD cast on 25 May was taken before the bloom was encountered later that day. Over the whole bloom sampling period (26 May to 21 June) in the upper 50 m the XC:PSC$_2$ ranged between 0.04 and 0.29 and was on average (± standard deviation) 0.15 ±0.05 (Table 1). The high ratios at 50 m depth especially on 11 and 14 June, and at 5 m on 25 May (Figures 2 and 3) are possibly affected by the very low pigment concentrations prior the bloom and at depth, which introduced uncertainty in ratios. PPC:PSC ratios ranged between 0.13 and 0.56 and 0.13 and 0.44 for PPC$_1$:PSC$_1$ and PPC$_2$:PSC$_2$, respectively. The average was 0.30 ±0.10 and 0.25 ±0.07, respectively. This is similar to the ice-covered stations observed by Alou-Font et al. (2016) in the Beaufort Sea and to sea ice algal samples subject to lower incident irradiance levels (<50 mol photons m^{-2} d^{-1}) in the same area (Table 1; Alou-Font et al. 2013). Similar values were also observed in Oregon coastal waters (Eisner and Cowles 2005), in samples from >5 m depth from Washington coast (Eisner et al. 2003) and in fjord and estuary samples adjacent to the Gulf of St. Lawrence (Roy et al. 2008). In conclusion, the ratios observed in our study are at the lower range of those from the previous studies, when compared to their complete dataset, and indicate low-light acclimation of our under-ice bloom. It needs to be noted that diatoms were the dominant group in all previous studies while our under-ice bloom was dominated by *P. pouchetii*.

The above conclusion is in line with the other light acclimation parameters studied for the under-ice bloom of this study, like the light utilization coefficient (α; 0.188–0.295) from rapid light curves from PAM measurements, and the low particulate organic carbon to Chl *a* ratio (31.4 in the upper 25 m) (Assmy et al. 2017). The DD+DT to Chl *a* ratio, a commonly used light acclimation indicator for chromophytes, was on average 0.03 ±0.01 (range 0.02–0.06) in

the upper 50 m during the bloom (26 May to 21 June). This is somewhat lower than found for diatoms in ice-covered waters of the Beaufort Sea (Alou-Font et al. 2016) or in under-ice water samples from the Amundsen Sea in Antarctica (Arrigo et al. 2014a) with averages of 0.07–0.08. Likewise, in experiments *Phaeocystis antarctica* was observed to have a lower (DD+DT):Chl *a* ratio than the diatom *Fragilariopsis cylindrus* under the same growth irradiance (Kropuenske et al. 2009), whereas *P. globosa* had higher ratios compared to the diatom *Thalassiosira* sp. (Meyer et al. 2000). The light acclimation experiments showed in addition that (DD+DT):Chl *a* was mainly below 0.05 for *P. antarctica* (Kropuenske et al. 2009) and *P. globosa* (Meyer et al. 2000) under irradiances of <65 μmol photons $m^{-2} s^{-1}$. Thus also this pigment indicator points to low-light acclimation of the under-ice bloom, which is consistent with the light conditions prevailing under the ice. Downwelling planar irradiance in the PAR range (E_d(PAR), photosynthetically active radiation, 400-700 nm) under the studied second-year ice in the study ice floe was mainly below 1 μmol photons $m^{-2} s^{-1}$ (Olsen et al. 2017) and the aggregate light regime in the study area (an average taking into account the fraction of different ice types like thin ice in leads with higher light transmittance) was <52 μmol photons $m^{-2} s^{-1}$ (Assmy et al. 2017). It is noteworthy though that light saturation of photosynthesis (electron transport rate) was not reached early in rapid light curves conducted with a Phyto-PAM (light saturation parameter E_k was 137–584 μmol photons $m^{-2} s^{-1}$; Assmy et al. 2017), showing that photosynthesis was efficient at low light (α) but not saturated in high light (E_k). This gave the *P. pouchetii* under-ice bloom high flexibility regarding growth irradiance, which is typical for this species (Schoemann et al. 2005).
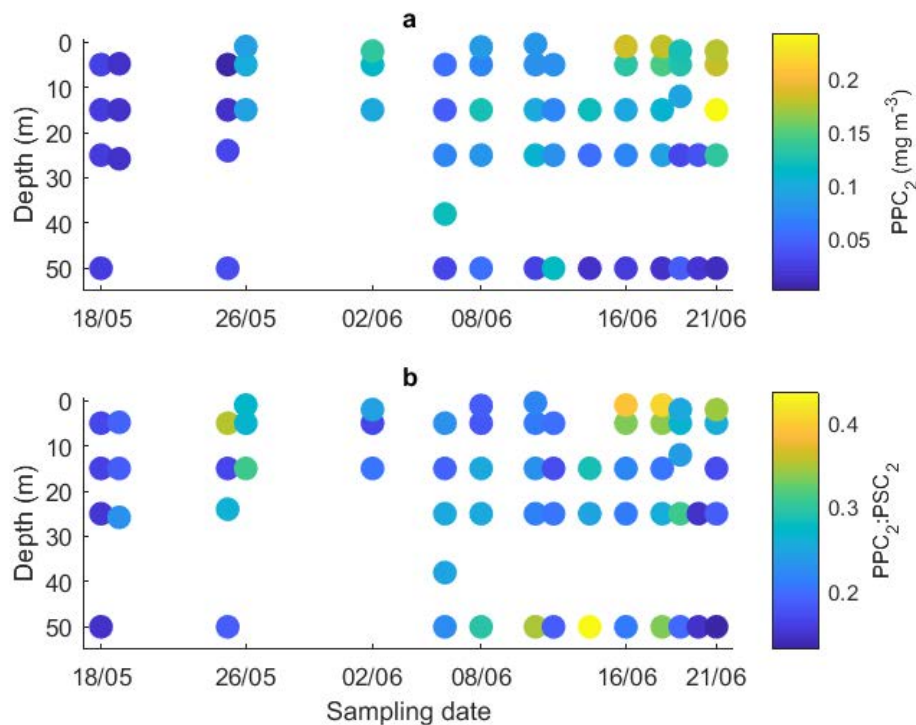
Figure 2. a) Concentration of photoprotective carotenoids (PPC_2) and b) ratio of PPC_2 to photosynthetic carotenoids (PSC_2) a week before and during the bloom.
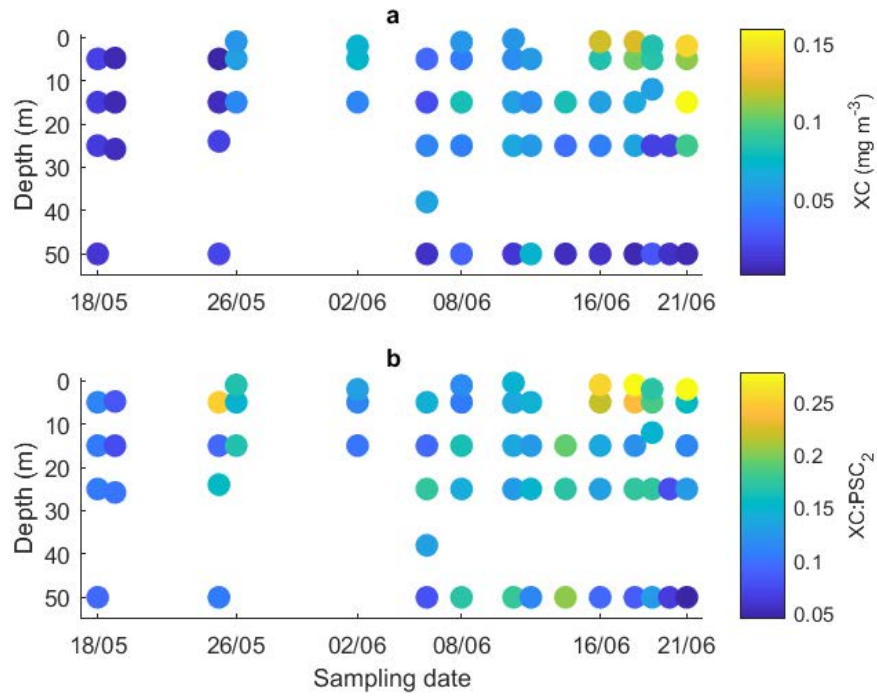
Figure 3. a) Concentration of xanthophyll cycle carotenoids (XC) and b) ratio of XC to photosynthetic carotenoids (PSC_2) a week before and during the bloom.

Table 1. Description of study areas and pigment ratios in this and related studies. For comparison with Eisner et al. (2003) and Eisner and Cowles (2005), use the first row. For comparison with Roy et al. (2008) and Alou-Font et al. (2013, 2016), use the second row. DD: diadinoxanthin, DT: diatoxanthin, viola: violaxanthin, zea: zeaxanthin, allo: alloxanthin, fuco: fucoxanthin, neo: neoxanthin, prasino: prasinoxanthin, anthera: antheraxanthin. * based on ice types and open water fraction in the study area (see Assmy et al. 2017)

Source	Dominant algal group/ species	Area	Habitat	PPC:PSC			Relationship between PPC:PSC (x) and a_{ph} slope (y)	PPC pigments	PSC pigments	Irradiance (E(PAR), different units)	Irradiance (description)
				Mean	SE	Range					
This study	*Phaeocystis pouchetii*	Yermak plateau	ice covered (100%)	0.30	0.01	0.13–0.56	-0.0168x - 0.0087	DD, DT, viola, zea, lutein, β,β-carotene, allo (PPC₁)	fuco, peridinin, hex-fuco, but-fuco, neo, prasino (PSC₁)	2–52	aggregate light regime right below sea or sea-ice surface * (µmol photons m⁻² s⁻¹)
This study	*Phaeocystis pouchetii*	Yermak plateau	ice covered (100%)	0.25	0.01	0.13–0.44	-0.0264x - 0.0072	DD, DT, viola, zea, lutein, β,β-carotene (PPC₂)	fuco, peridinin, hex-fuco, but-fuco, neo, prasino, allo (PSC₂)	2–52	aggregate light regime right below sea or sea-ice surface * (µmol photons m⁻² s⁻¹)
This study	*Phaeocystis pouchetii*	Yermak plateau	ice covered (100%)	0.14	0.01	0.04–0.27	-0.0407x - 0.0073	DD, DT, viola, zea (XC)	fuco, peridinin, hex-fuco, but-fuco, neo, prasino, allo (PSC₂)	2–52	aggregate light regime right below sea or sea-ice surface * (µmol photons m⁻² s⁻¹)
Eisner et al. (2003)	Diatoms	Orcas Island (Washington USA)	open water			ca. 0.05-1	-0.0174x - 0.0054	DD, DT, viola, zea, lutein, β,β-carotene, allo	fuco, peridinin, hex-fuco, but-fuco		
Eisner and Cowles (2005)	Diatoms	Oregon coast	open water			ca. 0.13–0.47		DD, DT, viola, zea, lutein, β,β-carotene, allo	fuco, peridinin, hex-fuco, but-fuco	30–350	mean of the hour prior to sampling at 5 m depth (µmol photons m⁻² s⁻¹)
Roy et al. (2008)	Diatoms	Saguenay fjord and estuary (Canada)	open water			ca. 0.1–0.4	-0.024x - 0.003	DD, DT, viola, anthera, zea, β,β-carotene	fuco, peridinin, but-fuco, prasino, allo		

Reference	Taxa	Location	Condition			Range		Pigments (photoprotective)	Pigments (photosynthetic)	Irradiance	Irradiance description
Roy et al. (2008)	Mixed	Gulf of St. Lawrence (Canada)	open water			ca. 0.15–1.4	-0.006x - 0.014	DD, DT, viola, anthera, zea, β,β-carotene	fuco, peridinin, but-fuco, prasino, allo		
Alou-Font et al. (2016)	Diatoms and prasinophytes	Beaufort Sea	ice covered (10–95%)	0.36	0.03	0.09–0.77		DD, DT, viola, zea, lutein, β,β-carotene	fuco, peridinin, hex-fuco, but-fuco, neo, prasino, allo	7.4 ±2.0	irradiance at sampling depth (μmol photons m^{-2} s^{-1})
Alou-Font et al. (2016)	Diatoms and prasinophytes	Beaufort Sea	open water	0.53	0.14	0.16–2.52		DD, DT, viola, zea, lutein, β,β-carotene	fuco, peridinin, hex-fuco, but-fuco, neo, prasino, allo	418.7 ± 82.6	irradiance at sampling depth (μmol photons m^{-2} s^{-1})
Alou-Font et al. (2013)	Diatoms (ice algae)	Beaufort Sea	sea ice			0.13–0.45		DD, DT, viola, zea, lutein, β,β-carotene	fuco, peridinin, neo, allo	<50	daily incident irradiance (mol photons m^{-2} d^{-1})
Alou-Font et al. (2013)	Diatoms (ice algae)	Beaufort Sea	sea ice			0.97–3.50		DD, DT, viola, zea, lutein, β,β-carotene	fuco, peridinin, neo, allo	>50	daily incident irradiance (mol photons m^{-2} d^{-1})

3.3 Relationship between in situ absorption and pigment ratios

3.3.1 Different grouping of photoprotective and photosynthetic carotenoids

In the studies by Eisner et al. (2003) and Eisner and Cowles (2005), alloxanthin was grouped in PPC, and to compare to their studies we have reported the values for $PPC_1:PSC_1$ as well. Analysis of in vivo absorption and in vivo fluorescence excitation spectra of alloxanthin containing algae (Johnsen et al. 2011) indicates however that this pigment is light-harvesting. Thus we have also followed the grouping by Roy et al. (2008) and Alou-Font et al. (2013, 2016) where alloxanthin is included in PSC ($PPC_2:PSC_2$). Both pigment groupings resulted with linear relationships between the pigment ratios and slopes of the in situ absorption measurements, with R^2 of 0.52 and 0.57 (for $PPC_1:PSC_1$ and $PPC_2:PSC_2$, respectively), but statistically different regression line slopes (-0.0168 and -0.0264, respectively; $p=4*10^{-6}$) and y-intercept values (Figure 4, Table 1).

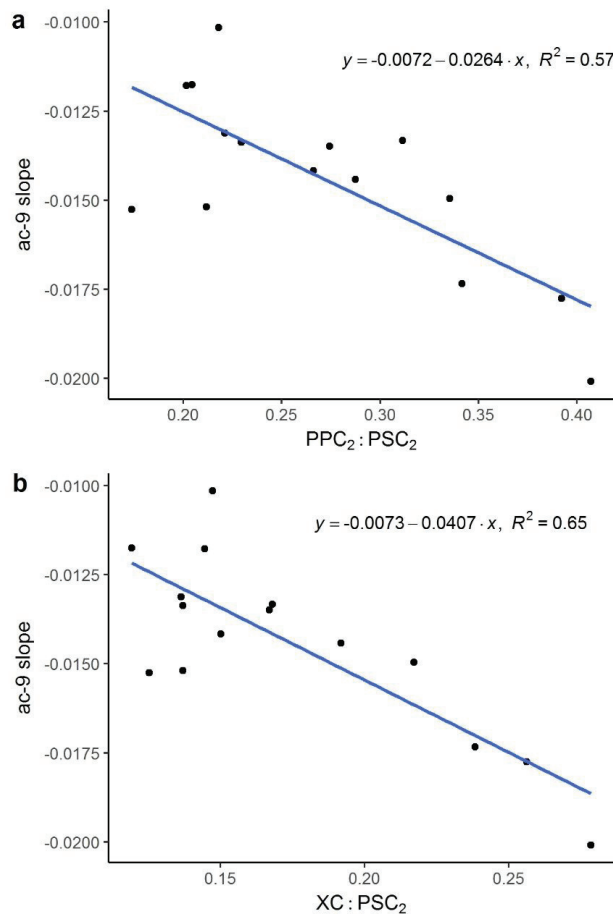

Figure 4. Relationship between the normalized absorption (a_{ph}) slopes from ac-9 measurements and the ratio of a) photoprotective (PPC_2) to photosynthetic carotenoids (PSC_2) b) xanthophyll cycle pigments (XC) to PSC_2.

Furthermore, violaxanthin is part of the photoprotective xanthophyll cycle (violaxanthin–antheraxanthin–zeaxanthin), but in the violaxanthin form the pigment is light-harvesting (Owens et al. 1987; Brunet et al. 2011). Our sampling procedures would however not allow for preserving the in situ xanthophyll cycle dynamics because of the handling time and dark sampling bottles allowing epoxidation of zeaxanthin back to violaxanthin. Therefore we include the pool of all xanthophyll cycle pigments (XC: diadinoxanthin, diatoxanthin, violaxanthin, zeaxanthin) in the analysis. In general, many PPC have light-harvesting capability but the energy transfer efficiency to Chl a is very low, making them primarily photoprotective (Johnsen et al. 2011). β,β-carotene has lower energy transfer efficiency than e.g. fucoxanthin and peridinin (Siefermann-Harms 1987) and lutein can in some cases have a photoprotective role (Dall'Osto et al. 2006), but also these pigments can have a light-harvesting function (Siefermann-Harms 1987). To limit the analysis to the xanthophyll cycle carotenoids, we have included results from the pigment ratio $XC:PSC_2$, where R^2 was 0.65 and the equation describing the relationship $y = -0.0407x - 0.0073$ (Figure 4, Table 1).

It should however be noted that we had a limited number of data points because of the depth limitation of the ac-9 data and water sample collection at standard depths only. Furthermore, due to logistical reasons the time difference between sampling and ac-9 measurements reached sometimes several hours (in most cases < 2.5 hrs). Single points and associated measurement uncertainties can thus have a relatively large impact on the regression, and the differences between approaches and which approach performs best should be taken with caution. Despite the limitations mentioned above, all pigment grouping approaches yielded a strong linear relationship between the pigment ratios and slopes of in situ absorption measurements (significance of regression line slopes for $PPC_1:PSC_1$ and $PPC_2:PSC_2$ $p<0.003$ and for $XC: PSC_2$ $p<0.0003$). This may suggest that future studies could concentrate on the xanthophyll cycle carotenoids to study this relationship. The slope of the regression line relating these measurements differed however between the approaches, thus caution is needed when e.g. comparing to other studies to make sure that the same pigment grouping is used. The relative importance of pigment classification will depend on the abundance of the pigment and thus species composition, because certain pigments are specific for different algal groups (Jeffrey et al. 2011) and also the type of xanthophyll cycle (diadino- and diatoxanthin, or viola-, anthera- and zeaxanthin) varies between algal groups (Brunet et al. 2011). The most abundant of the PPC_2 in our samples were diadinoxanthin and lutein with average concentration of 0.04 mg m^{-3} and 0.025 mg m^{-3}, respectively (others <0.004 mg m^{-3} – but see discussion above about sampling procedures enabling epoxidation to happen).

3.3.2 Performance of the method

As mentioned above, we found a linear relationship between the in situ absorption measurements (the normalised slope in the blue region) and the ratio of PPC to PSC. We chose the $XC:PSC_2$ ratio for further analysis (see discussion above) and tested additional ways of processing the ac-9 absorption data. In the figures and the section above, both $a_{CDOM}(\lambda)$ and $a_d(\lambda)$ were subtracted from the ac-9 absorption measurements (a) to obtain $a_{ph}(\lambda)$. For $a_{CDOM}(\lambda)$ subtraction, each $a_{CDOM}(\lambda)$ data point was matched with an ac-9 measurement taken within 1 m above the water sampling depth. For $a_d(\lambda)$ subtraction, an average of the bloom period was used (see Methods). Using the in situ absorption measurements without

subtractions (i.e. a, total non-water absorption) did not yield good results (R^2=0.15). Next, we tried omitting $a_d(\lambda)$ subtraction, but results remained good (no change in R^2 values compared to including both corrections). Using $a_d(\lambda)$ values from matching sample measurements did not cause large changes (R^2=0.67). In summary, $a_{CDOM}(\lambda)$ subtraction was needed, but $a_d(\lambda)$ did not have a large impact on the in situ absorption measurements in our case.

Both the absorption by CDOM and detrital matter did not change greatly during the bloom and especially $a_d(\lambda)$ was low (Pavlov et al. 2017), which facilitates the retrieval of phytoplankton absorption from bulk absorption measurements. In many parts of the Arctic CDOM makes a substantial contribution to the absorption budget (Granskog et al. 2007; Pavlov et al. 2015; Gonçalves-Araujo et al. 2018) and thus would require quantifying upfront this type of monitoring. We estimated CDOM absorption from distinct water samples for this method assessment, but another option especially for high-resolution measurements is the approach followed by Eisner et al. (2003), having two simultaneous ac-9 measurements, where the other instrument was equipped with a filter and thus allowed quantifying absorption by CDOM. This approach would however require a substantial investment in instrumentation and may not be feasible for long-term deployments.

To assess the significance of a_d contribution to a_p, Eisner et al. (2003) looked at the ratio $a_p(412):a_p(440)$ of in situ absorption spectra, with values above 0.96 indicating presence of detritus (in our case, the corresponding value was 0.91 for samples associated with ac-9 measurements). In our study, such ratio based on $a_p(\lambda)$ filter measurements from water samples ranged from 0.86 to 0.94, with average value of 0.90 (±0.02) for samples associated with ac-9 measurements. Therefore, this provides additional evidence for the insignificant contribution of detritus to total particle and total non-water absorption in our study. Another factor that likely facilitates the usability of the method in our case is the fairly homogenous species composition, reducing the variability in the relation between the pigments and the absorption characteristics. Furthermore, we were sampling in the upper 20 m of the water column (see Methods) and thus in the same water mass (Meyer et al. 2017), i.e. in a fairly homogenous environment.

We found that the relationship (i.e., the slope of the regression line) in our study was similar to that of Eisner et al. (2003) when using the same pigment grouping (-0.0168 compared to -0.0174, respectively). This indicates robustness of the method, despite the difference in dominating bloom species (diatoms vs. *P. pouchetii*). The regional and oceanographic settings were also very different, Pacific coastal water compared to ice-covered Atlantic-influenced Arctic waters. The y-intercepts of the regression lines differed between these studies. Similarly, Eisner and Cowles (2005) found similar slopes between different sample groups, but with different intercepts. For a given PPC:PSC ratio, the slope of ac-9 measurements was shallower (lower) in Eisner et al. (2003) compared to our measurements, which could indicate a stronger packaging effect in the former.

The relationship was calculated also by Roy et al. (2008) for samples from the Gulf of St. Lawrence and an adjacent estuary in Canada using filter pad absorption measurements. They found very different slopes compared to the study of Eisner et al. (2003) and between their sampling areas (Table 1). When using the same pigment grouping than in the study by Roy et al. (2008), we found a similar slope compared to the estuary and fjord stations (-0.0264 compared to -0.024), which had diatoms as the dominating group. The Gulf of St. Lawrence

stations had a larger (ca. 60 %) contribution of dinoflagellates, flagellates and "other" taxa than diatoms, whereas the estuary and fjord stations were dominated (>70 %) by diatoms. Thus the differences in slopes are possibly due to the different species compositions. The community composition determines the cell sizes in the bloom and therefore affects the pigment packaging. It is though remarkable that results obtained from a bloom dominated by the flagellate *P. pouchetii* fit together with results from diatom-dominated blooms (both having the colony-forming *Chaetoceros socialis* as one dominating species; Eisner et al. 2003; Roy et al. 2008). The reason could be that the colony form of *P. pouchetii* (which were ample during the bloom in our study; Assmy et al. 2017; Figure 5) strengthens the packaging effect, giving similar absorption efficiency as large diatoms. The areas in the study by Roy et al. 2008 also had a different light regime. The Gulf stations had less suspended matter and consequently higher light penetration, and the algae were high-light acclimated, which also affects pigment packaging. A difference to our method was that no in situ absorption measurements were used, but Eisner et al. (2003) found more similar regression line slopes between in situ and filter pad absorption measurements (-0.0174x vs. -0.0126x) than the variation in the study by Roy et al. (2008).

In conclusion, a validation dataset is likely required to accompany the in situ absorption measurements, allowing quantifying detrital and CDOM absorption, validating the relationship with a set of pigment samples, and possibly giving an indication of species composition and cell size. The method applicability will also benefit from more work investigating the variability in the relationship between absorption measurements and the pigment ratios, and factors affecting them. Our results are promising and suggest that this method could be applied to follow the photoacclimation state of phytoplankton in diverse environments.
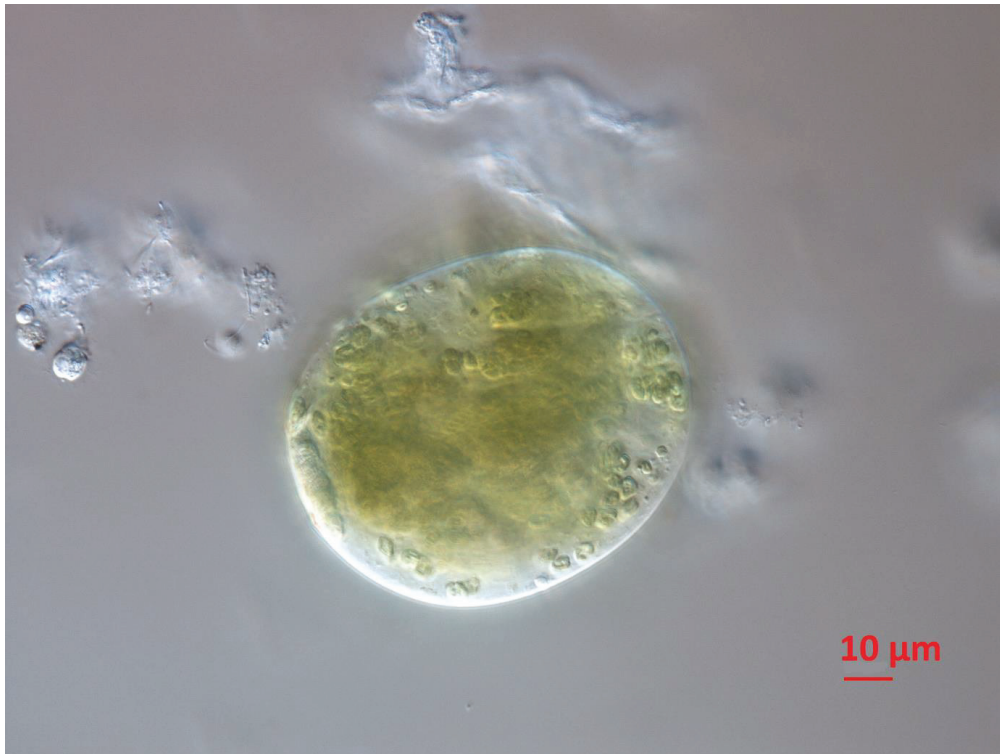
Figure 5 Micrograph of a *Phaeocystis pouchetii* colony from the under-ice phytoplankton bloom observed during the N-ICE2015 expedition. Micrograph taken by Jozef Wiktor, Institute of Oceanology Polish Academy of Sciences.

3.4 Ecological significance

Being able to extract in situ data on distribution, rates (e.g. primary production) and physiology of algae from autonomous measurements will improve data coverage and advance our understanding of ecosystem functioning. Especially ice-covered waters require applications for autonomous platforms other than satellites. Chl *a* fluorescence measurements, a proxy for phytoplankton biomass and distribution, are routinely done from ships or autonomous platforms, but other continuous in situ biological or bio-optical measurements are rare. Recently, Briggs et al. (2018) validated primary productivity measurements from an autonomous float by comparing simultaneous measurements of diel cycles of dissolved oxygen and particulate organic carbon from beam attenuation, and modelled primary productivity from irradiance and Chl *a* measurements. Here we venture into physiology by looking at the ratio of photoprotective to photosynthetic carotenoids and hence photoacclimation. The method, first developed in temperate waters (Eisner et al. 2003), worked well also in our case, which suggest that there is potential in these simple calculations and the further applicability of the method should be examined.

Here the main focus was to validate the method and all measurements used here were taken from the ship or the ice camp during the N-ICE2015 expedition, but with a robust method the pigment ratio could be predicted from absorption measurements conducted e.g. with a glider. Besides describing the bloom as such, the photoacclimation state of under-ice blooms could also provide information on their possible advective history. High-light acclimation indicates advective origin, whereas low-light acclimation indicates that the bloom has been growing in the low-light conditions under the ice pack, i.e. local bloom – similar to how pigment ratios could be used to indicate mixing and water mass characteristics of the water body in the case when mixing is faster than pigment acclimation. The time scales of the photoprotective mechanism can be related to the estimated time the advection from open water areas would take. The bloom in our case was shown to be low-light acclimated (see section 3.2) which supports the conclusion that it was growing under the ice pack.

Johnsen et al. (2018) demonstrated how using multiple platforms, like autonomous underwater vehicles (AUV) and ocean colour remote sensing in addition to ship-based sampling, can give a comprehensive picture of phytoplankton dynamics in the marginal ice zone. They concluded that the observed under-ice bloom north of Svalbard was of advective origin based on the ocean current patterns in the area, similar species composition in the open-water bloom adjacent to the area, and the photoacclimation state of the bloom. High-light acclimation of the bloom (indicated by high E_k (10–100 times the ambient under-ice irradiance) and high values of DD+DT to Chl a ratios) suggested that it had developed in higher light conditions than what was available below the sea ice. AUVs were used under the sea ice to extend physical (salinity, temperature) and biomass (Chl a fluorescence) observations in time and space.

While absorption meters are not part of the standard instrument package of e.g. bio-Argo floats, in situ absorption measurements have already been used in monitoring studies. In the study by Robbins et al. (2006), the extent of an harmful algal bloom (HAB) formed by the dinoflagellate *Karenia brevis* was mapped with the help of absorbance measurements collected from an AUV. In New Jersey, USA, ac-9 instruments were included in autonomous, cabled profiling platforms of a coastal observing network (Schofield et al. 2002). Adding sensors in long-term or autonomous deployments requires sufficient battery power and carrying capacity of the platform, which has to be evaluated against the added value of the measurements. Another operational challenge for the method we discuss here is obtaining the validation dataset for the pigment ratios and information on other optically active substances in seawater (detritus, CDOM) and possibly phytoplankton species composition and/or cell size. As we showed, even with relatively low background CDOM absorption during the study, CDOM absorption needs to be taken into consideration for robust results. To obtain concurrent information about CDOM, unless two ac-9 instruments are used simultaneously (the other one equipped with a filter) which is not always feasible especially in long-term deployments, one could add a CDOM fluorometer to the autonomous platform. Studies have shown that $a_{CDOM}(370)$ can be estimated from CDOM fluorometry measurements (Belzile et al. 2006), and by having knowledge on the slope parameter in the study region (e.g. Stedmon and Markager 2001) the spectral absorption can be calculated from absorption values at a single wavelength. While particle (cell) size could also be quantified from in situ measurements using laser diffraction particle size analyzers (e.g. LISST, Sequoia Scientific), some of the other variables (especially the pigment validation dataset) would need concurrent water sampling in the area covering different water masses. Combined with instrument

measurements, however, that cover a larger area and can sample with high temporal resolution, this approach can potentially give ample new information on phytoplankton blooms.

4. Conclusions

In this study we assess a simple bio-optical method to estimate algal pigment ratios from in situ absorption measurements of an Arctic under-ice bloom. We found a linear relationship between the slope calculated from in situ measurements, and the PPC to PSC ratio. The bloom was dominated by the haptophyte *Phaeocystis pouchetii* and it was low-light acclimated based on several light acclimation indicators (e.g., diadinoxanthin + diatoxanthin to Chl *a*). Slopes of linear regressions between the absorption measurement slopes and pigment ratios were similar to previous studies from diatom-dominated algal communities with low-light acclimation. This could possibly be explained with the additional packaging (intercellular self-shading) caused by the colony form of *P. pouchetii*, causing it to resemble the much bigger diatoms.

Further studies including several different types of algal communities would further elucidate the dependence of the linear regressions on pigment packaging. The slope of the linear regression was also sensitive to which pigments were included in the different functional pigment categories (photoprotective or photosynthetic), as this changes the pigment ratio. Detrital matter had little impact on non-water absorption in our study area, whereas subtraction of CDOM absorption from the bulk non-water absorption measurements was required to obtain algal absorption. Our results indicate that this method could be used to monitor the photoacclimation state of phytoplankton blooms. By using autonomous platforms to carry the required instruments it could give valuable information on under-ice blooms that cannot be observed from space.

analysis, Colin Stedmon for CDOM absorption measurements and Elina Nystedt for particle absorption measurements.

References

Alou-Font E, Mundy CJ, Roy S, et al (2013) Snow cover affects ice algal pigment composition in the coastal Arctic Ocean during spring. Mar Ecol Prog Ser 474:89–104. doi: 10.3354/meps10107

Alou-Font E, Roy S, Agustí S, Gosselin M (2016) Cell viability, pigments and photosynthetic performance of Arctic phytoplankton in contrasting ice-covered and open-water conditions during the spring-summer transition. Mar Ecol Prog Ser 543:89–106. doi: 10.3354/meps11562

Arrigo K, Perovich D, Pickart R, et al (2012) Massive phytoplankton blooms under Arctic sea ice. Science 336:1408. doi: 10.1007/BF02390423

Arrigo KR, Brown ZW, Mills MM (2014a) Sea ice algal biomass and physiology in the Amundsen Sea, Antarctica. Elem Sci Anthr 2:28. doi: 10.12952/journal.elementa.000028

Arrigo KR, Perovich DK, Pickart RS, et al (2014b) Phytoplankton blooms beneath the sea ice in the Chukchi sea. Deep Res Part II 105:1–16. doi: 10.1016/j.dsr2.2014.03.018

Assmy P, Fernández-méndez M, Duarte P, et al (2017) Leads in Arctic pack ice enable early phytoplankton blooms below snow-covered sea ice. Sci Rep 7:40850. doi: 10.1038/srep40850

Belzile C, Roesler CS, Christensen JP, et al (2006) Fluorescence measured using the WETStar DOM fluorometer as a proxy for dissolved matter absorption. Estuar Coast Shelf Sci 67:441–449. doi: 10.1016/j.ecss.2005.11.032

Briggs N, Guðmundsson K, Cetinić I, et al (2018) A multi-method autonomous assessment of primary productivity and export efficiency in the springtime North Atlantic. Biogeosciences Discuss. doi: https://doi.org/10.5194/bg-2017-534

Brunet C, Johnsen G, Lavaud J, Roy S (2011) Pigments and photoacclimation processes. In: Roy S, LLewellyn CA, Egeland ES, Johnsen G (eds) Phytoplankton Pigments - Characterization, Chemotaxonomy and Applications in Oceanography, 1. edition. Cambridge University Press, Cambridge, pp 445–471

Claustre H, Kerhervé P, Marty J-C, Prieur L (1994) Phytoplantkon photoadaptation related to some frontal physical processes. J Mar Syst 5:251–265

Dall'Osto L, Lico C, Alric J, et al (2006) Lutein is needed for efficient chlorophyll triplet quenching in the major LHCII antenna complex of higher plants and effective photoprotection *in vivo* under strong light. BMC Plant Biol 6:32. doi: 10.1186/1471-2229-6-32

Eisner LB, Cowles TJ (2005) Spatial variations in phytoplankton pigment ratios, optical properties, and environmental gradients in Oregon coast surface waters. 110: C10S14. doi: 10.1029/2004JC002614

Eisner LB, Twardowski MS, Cowles TJ, Perry MJ (2003) Resolving phytoplankton photoprotective : photosynthetic carotenoid ratios on fine scales using in situ spectral absorption measurements. Limnol Oceanogr 48:632–646. doi: 10.4319/lo.2003.48.2.0632

Falkowski PG (1983) Light-shade adaptation and vertical mixing of marine phytoplankton: A comparative field study. J Mar Res 41:215–237. doi: 10.1357/002224083788520199

Fortier M, Fortier L, Michel C, Legendre L (2002) Climatic and biological forcing of the vertical flux of biogenic particles under seasonal Arctic sea ice. Mar Ecol Prog Ser 225:1–16. doi: 10.3354/meps225001

Gonçalves-Araujo R, Rabe B, Peeken I, Bracher A (2018) High colored dissolved organic matter (CDOM) absorption in surface waters of the central-eastern Arctic Ocean: Implications for biogeochemistry and ocean color algorithms. PLoS One 13:e0190838. doi: 10.1371/journal.pone.0190838

Granskog MA, Assmy P, Gerland S, et al (2016) Arctic research on thin ice: Consequences of Arctic sea ice loss. Eos Trans AGU 97:22–26

Granskog MA, Fer I, Rinke A, Steen H (2018) Atmosphere-ice-ocean-ecosystem processes in a thinner Arctic sea ice regime: the Norwegian young sea ICE (N-ICE2015) expedition. J Geophys Res Ocean 123:1586–1594. doi: 10.1002/2017JC013328

Granskog MA, Macdonald RW, Mundy CJ, Barber DG (2007) Distribution, characteristics and potential impacts of chromophoric dissolved organic matter (CDOM) in Hudson Strait and Hudson Bay, Canada. Cont Shelf Res 27:2032–2050. doi: 10.1016/j.csr.2007.05.001

Horvat C, Jones DR, Iams S, et al (2017) The frequency and extent of sub-ice phytoplankton blooms in the Arctic Ocean. Sci Adv 3:e1601191. doi: 10.1126/sciadv.1601191

Jeffrey SW, Wright SW, Zapata M (2011) Microalgal classes and their signature pigments. In: Roy S, LLewellyn CA, Egeland ES, Johnsen G (eds) Phytoplankton Pigments - Characterization, Chemotaxonomy and Applications in Oceanography, 1. edition. Cambridge University Press, Cambridge, pp 3–77

Johnsen G, Bricaud A, Nelson N, et al (2011) In vivo bio-optical properties of phytoplankton pigments. In: Roy S, LLewellyn CA, Egeland ES, Johnsen G (eds) Phytoplankton Pigments - Characterization, Chemotaxonomy and Applications in Oceanography, 1. edition. Cambridge University Press, Cambridge, pp 496–537

Johnsen G, Norli M, Moline M, et al (2018) The advective origin of an under-ice spring bloom in the Arctic Ocean using multiple observational platforms. Polar Biol. doi: 10.1007/s00300-018-2278-5

Johnsen G, Samset O, Granskog L, Sakshaug E (1994) In vivo absorption characteristics in 10 classes of bloom-forming phytoplankton - Taxonomic characteristics and responses to photoadaptation by means of discriminant and HPLC analysis. Mar Ecol Prog Ser 105:149–158. doi: Doi 10.3354/Meps105149

Johnson KS, Claustre H (2016) Bringing biogeochemistry into the Argo age. Eos 97. doi: 10.1029/2016EO062427

Kauko HM, Taskjelle T, Assmy P, et al (2017) Windows in Arctic sea ice: Light transmission and ice algae in a refrozen lead. J Geophys Res Biogeosciences 122:1486–1505. doi: 10.1002/2016JG003626

Kropuenske LR, Mills MM, van Dijken GL, et al (2009) Photophysiology in two major Southern Ocean phytoplankton taxa: photoprotection in *Phaeocystis antarctica* and *Fragilariopsis cylindrus*. Limnol Oceanogr 54:1176–1196. doi: 10.4319/lo.2009.54.4.1176

Laney SR, Krishfield RA, Toole JM, et al (2014) Assessing algal biomass and bio-optical

distributions in perennially ice-covered polar ocean ecosystems. Polar Sci 8:73–85. doi: 10.1016/j.polar.2013.12.003

Laney SR, Krishfield RA, Toole JM (2017) The euphotic zone under Arctic Ocean sea ice: Vertical extents and seasonal trends. Limnol Oceanogr 62:1910–1934. doi: 10.1002/lno.10543

Lewis MR, Cullen JJ, Platt T (1984) Relationships between vertical mixing and photoadaptation of phytoplankton: similarity criteria. Mar Ecol Prog Ser 15:141–149. doi: 10.3354/meps015141

Meier WN, Hovelsrud GK, van Oort BEH, et al (2014) Actic sea ice in transformation: A review of recent observed changes and impacts on biology and human activity. Rev Geophys 51:185–217. doi: 10.1002/2013RG000431

Meyer AA, Tackx M, Daro N (2000) Xanthophyll cycling in *Phaeocystis globosa* and *Thalassiosira* sp.: a possible mechanism for species succession. J Sea Res 43:373–384

Meyer A, Sundfjord A, Fer I, et al (2017) Winter to summer hydrographic and current observations in the Arctic Ocean north of Svalbard. J Geophys Res Ocean 122:6218–6237. doi: 10.1002/2016JC012391

Moline MA (1998) Photoadaptive response during the development of a coastal Antarctic diatom bloom and relationship to water column stability. Limnol Oceanogr 43:146–153

Mundy CJ, Gosselin M, Ehn J, et al (2009) Contribution of under-ice primary production to an ice-edge upwelling phytoplankton bloom in the Canadian Beaufort Sea. Geophys Res Lett 36:L17601. doi: 10.1029/2009GL038837

Mundy CJ, Gosselin M, Gratton Y, et al (2014) Role of environmental factors on phytoplankton bloom initiation under landfast sea ice in Resolute Passage, Canada. Mar Ecol Prog Ser 497:39–49. doi: 10.3354/meps10587

Olsen LM, Laney SR, Duarte P, et al (2017) The seeding of ice algal blooms in Arctic pack ice: The multiyear ice seed repository hypothesis. J Geophys Res Biogeosciences 122:1–20. doi: 10.1002/2016JG003668

Owens TG, Gallagher JC, Alberte RS (1987) Photosynthetic light-harvesting function of violaxanthin in *Nannochloropsis* spp. (Eustigmatophyceae). J Phycol 23:79–85

Pavlov AK, Granskog MA, Stedmon CA, et al (2015) Contrasting optical properties of surface waters across the Fram Strait and its potential biological implications. J Mar Syst 143:62–72. doi: 10.1016/j.jmarsys.2014.11.001

Pavlov AK, Taskjelle T, Hudson SR, et al (2016) N-ICE2015 total absorption profiles from water column [Data set]. doi: 10.21334/npolar.2017.7dce5c52

Pavlov AK, Taskjelle T, Kauko HM, et al (2017) Altered inherent optical properties and estimates of the underwater light field during an Arctic under-ice bloom of *Phaeocystis pouchetii*. J Geophys Res Ocean 122:4939–4961. doi: 10.1002/2016JC012471

Robbins IC, Kirkpatrick GJ, Blackwell SM, et al (2006) Improved monitoring of HABs using autonomous underwater vehicles (AUV). Harmful Algae 5:749–761. doi: 10.1016/j.hal.2006.03.005

Roy S, Blouin F, Jacques A, Therriault J-C (2008) Absorption properties of phytoplankton in the Lower Estuary and Gulf of St. Lawrence (Canada). Can J Fish Aquat Sci 65:1721–1737. doi: 10.1139/F08-089

Röttgers R, McKee D, Utschig C (2014) Temperature and salinity correction coefficients for

light absorption by water in the visible to infrared spectral region. Opt Express 22:25093–25108. doi: 10.1364/OE.22.025093

Schoemann V, Becquevort S, Stefels J, et al (2005) *Phaeocystis* blooms in the global ocean and their controlling mechanisms: a review. J Sea Res 53:43–66. doi: 10.1016/j.seares.2004.01.008

Schofield O, Bergmann T, Bissett P, et al (2002) The long-term ecosystem observatory: an integrated coastal observatory. IEEE J Ocean Eng 27:146–154

Siefermann-Harms D (1987) The light-harvesting and protective functions of carotenoids in photosynthetic membranes. Physiol Plant 69:561–568. doi: 10.1111/j.1399-3054.1987.tb09240.x

Stedmon CA, Markager S (2001) The optics of chromophoric dissolved organic matter (CDOM) in the Greenland Sea: An algorithm for differentiation between marine and terrestrially derived organic matter. Limnol Oceanogr 46:2087–2093. doi: 10.4319/lo.2001.46.8.2087

Taskjelle T, Granskog MA, Pavlov AK, et al (2016) N-ICE2015 total attenuation and absorption profiles from water column with AC-9 [Data set]. doi: 10.21334/npolar.2016.114bfaaa

Tassan S, Ferrari GM (2002) A sensitivity analysis of the "Transmittance–Reflectance" method for measuring light absorption by aquatic particles. J Plankton Res 24:757–774

Tran S, Bonsang B, Gros V, et al (2013) A survey of carbon monoxide and non-methane hydrocarbons in the Arctic Ocean during summer 2010. Biogeosciences 10:1909–1935. doi: 10.5194/bg-10-1909-2013

Wassmann P, Duarte CM, Agustí S, Sejr MK (2011) Footprints of climate change in the Arctic marine ecosystem. Glob Chang Biol 17:1235–1249. doi: 10.1111/j.1365-2486.2010.02311.x

Zaneveld JR V., Kitchen JC, Moore CC (1994) Scattering error correction of reflecting-tube absorption meters. In: Proc. SPIE 2258, Ocean Optics XII. International Society for Optics and Photonics, pp 44–56

Doctoral theses in Biology
Norwegian University of Science and Technology
Department of Biology

Year	Name	Degree	Title
1974	Tor-Henning Iversen	Dr. philos Botany	The roles of statholiths, auxin transport, and auxin metabolism in root gravitropism
1978	Tore Slagsvold	Dr. philos Zoology	Breeding events of birds in relation to spring temperature and environmental phenology
1978	Egil Sakshaug	Dr. philos Botany	"The influence of environmental factors on the chemical composition of cultivated and natural populations of marine phytoplankton"
1980	Arnfinn Langeland	Dr. philos Zoology	Interaction between fish and zooplankton populations and their effects on the material utilization in a freshwater lake
1980	Helge Reinertsen	Dr. philos Botany	The effect of lake fertilization on the dynamics and stability of a limnetic ecosystem with special reference to the phytoplankton
1982	Gunn Mari Olsen	Dr. scient Botany	Gravitropism in roots of *Pisum sativum* and *Arabidopsis thaliana*
1982	Dag Dolmen	Dr. philos Zoology	Life aspects of two sympartic species of newts (*Triturus, Amphibia*) in Norway, with special emphasis on their ecological niche segregation
1984	Eivin Røskaft	Dr. philos Zoology	Sociobiological studies of the rook *Corvus frugilegus*
1984	Anne Margrethe Cameron	Dr. scient Botany	Effects of alcohol inhalation on levels of circulating testosterone, follicle stimulating hormone and luteinzing hormone in male mature rats
1984	Asbjørn Magne Nilsen	Dr. scient Botany	Alveolar macrophages from expectorates – Biological monitoring of workers exosed to occupational air pollution. An evaluation of the AM-test
1985	Jarle Mork	Dr. philos Zoology	Biochemical genetic studies in fish
1985	John Solem	Dr. philos Zoology	Taxonomy, distribution and ecology of caddisflies (*Trichoptera*) in the Dovrefjell mountains
1985	Randi E. Reinertsen	Dr. philos Zoology	Energy strategies in the cold: Metabolic and thermoregulatory adaptations in small northern birds
1986	Bernt-Erik Sæther	Dr. philos Zoology	Ecological and evolutionary basis for variation in reproductive traits of some vertebrates: A comparative approach
1986	Torleif Holthe	Dr. philos Zoology	Evolution, systematics, nomenclature, and zoogeography in the polychaete orders *Oweniimorpha* and *Terebellomorpha*, with special reference to the Arctic and Scandinavian fauna
1987	Helene Lampe	Dr. scient Zoology	The function of bird song in mate attraction and territorial defence, and the importance of song repertoires
1987	Olav Hogstad	Dr. philos Zoology	Winter survival strategies of the Willow tit *Parus montanus*
1987	Jarle Inge Holten	Dr. philos Botany	Autecological investigations along a coust-inland transect at Nord-Møre, Central Norway

1987	Rita Kumar	Dr. scient Botany	Somaclonal variation in plants regenerated from cell cultures of *Nicotiana sanderae* and *Chrysanthemum morifolium*
1987	Bjørn Åge Tømmerås	Dr. scient Zoology	Olfaction in bark beetle communities: Interspecific interactions in regulation of colonization density, predator - prey relationship and host attraction
1988	Hans Christian Pedersen	Dr. philos Zoology	Reproductive behaviour in willow ptarmigan with special emphasis on territoriality and parental care
1988	Tor G. Heggberget	Dr. philos Zoology	Reproduction in Atlantic Salmon (*Salmo salar*): Aspects of spawning, incubation, early life history and population structure
1988	Marianne V. Nielsen	Dr. scient Zoology	The effects of selected environmental factors on carbon allocation/growth of larval and juvenile mussels (*Mytilus edulis*)
1988	Ole Kristian Berg	Dr. scient Zoology	The formation of landlocked Atlantic salmon (*Salmo salar* L.)
1989	John W. Jensen	Dr. philos Zoology	Crustacean plankton and fish during the first decade of the manmade Nesjø reservoir, with special emphasis on the effects of gill nets and salmonid growth
1989	Helga J. Vivås	Dr. scient Zoology	Theoretical models of activity pattern and optimal foraging: Predictions for the Moose *Alces alces*
1989	Reidar Andersen	Dr. scient Zoology	Interactions between a generalist herbivore, the moose *Alces alces*, and its winter food resources: a study of behavioural variation
1989	Kurt Ingar Draget	Dr. scient Botany	Alginate gel media for plant tissue culture
1990	Bengt Finstad	Dr. scient Zoology	Osmotic and ionic regulation in Atlantic salmon, rainbow trout and Arctic charr: Effect of temperature, salinity and season
1990	Hege Johannesen	Dr. scient Zoology	Respiration and temperature regulation in birds with special emphasis on the oxygen extraction by the lung
1990	Åse Krøkje	Dr. scient Botany	The mutagenic load from air pollution at two work-places with PAH-exposure measured with Ames Salmonella/microsome test
1990	Arne Johan Jensen	Dr. philos Zoology	Effects of water temperature on early life history, juvenile growth and prespawning migrations of Atlantic salmon (*Salmo salar*) and brown trout (*Salmo trutta*): A summary of studies in Norwegian streams
1990	Tor Jørgen Almaas	Dr. scient Zoology	Pheromone reception in moths: Response characteristics of olfactory receptor neurons to intra- and interspecific chemical cues
1990	Magne Husby	Dr. scient Zoology	Breeding strategies in birds: Experiments with the Magpie *Pica pica*
1991	Tor Kvam	Dr. scient Zoology	Population biology of the European lynx (*Lynx lynx*) in Norway
1991	Jan Henning L'Abêe Lund	Dr. philos Zoology	Reproductive biology in freshwater fish, brown trout *Salmo trutta* and roach *Rutilus rutilus* in particular
1991	Asbjørn Moen	Dr. philos Botany	The plant cover of the boreal uplands of Central Norway. I. Vegetation ecology of Sølendet nature reserve; haymaking fens and birch woodlands
1991	Else Marie Løbersli	Dr. scient Botany	Soil acidification and metal uptake in plants
1991	Trond Nordtug	Dr. scient Zoology	Reflectometric studies of photomechanical adaptation in superposition eyes of arthropods

1991	Thyra Solem	Dr. scient Botany	Age, origin and development of blanket mires in Central Norway
1991	Odd Terje Sandlund	Dr. philos Zoology	The dynamics of habitat use in the salmonid genera *Coregonus* and *Salvelinus*: Ontogenic niche shifts and polymorphism
1991	Nina Jonsson	Dr. philos Zoology	Aspects of migration and spawning in salmonids
1991	Atle Bones	Dr. scient Botany	Compartmentation and molecular properties of thioglucoside glucohydrolase (myrosinase)
1992	Torgrim Breiehagen	Dr. scient Zoology	Mating behaviour and evolutionary aspects of the breeding system of two bird species: the Temminck's stint and the Pied flycatcher
1992	Anne Kjersti Bakken	Dr. scient Botany	The influence of photoperiod on nitrate assimilation and nitrogen status in timothy (*Phleum pratense* L.)
1992	Tycho Anker-Nilssen	Dr. scient Zoology	Food supply as a determinant of reproduction and population development in Norwegian Puffins *Fratercula arctica*
1992	Bjørn Munro Jenssen	Dr. philos Zoology	Thermoregulation in aquatic birds in air and water: With special emphasis on the effects of crude oil, chemically treated oil and cleaning on the thermal balance of ducks
1992	Arne Vollan Aarset	Dr. philos Zoology	The ecophysiology of under-ice fauna: Osmotic regulation, low temperature tolerance and metabolism in polar crustaceans.
1993	Geir Slupphaug	Dr. scient Botany	Regulation and expression of uracil-DNA glycosylase and O^6-methylguanine-DNA methyltransferase in mammalian cells
1993	Tor Fredrik Næsje	Dr. scient Zoology	Habitat shifts in coregonids.
1993	Yngvar Asbjørn Olsen	Dr. scient Zoology	Cortisol dynamics in Atlantic salmon, *Salmo salar* L.: Basal and stressor-induced variations in plasma levels ans some secondary effects.
1993	Bård Pedersen	Dr. scient Botany	Theoretical studies of life history evolution in modular and clonal organisms
1993	Ole Petter Thangstad	Dr. scient Botany	Molecular studies of myrosinase in Brassicaceae
1993	Thrine L. M. Heggberget	Dr. scient Zoology	Reproductive strategy and feeding ecology of the Eurasian otter *Lutra lutra*.
1993	Kjetil Bevanger	Dr. scient Zoology	Avian interactions with utility structures, a biological approach.
1993	Kåre Haugan	Dr. scient Botany	Mutations in the replication control gene trfA of the broad host-range plasmid RK2
1994	Peder Fiske	Dr. scient Zoology	Sexual selection in the lekking great snipe (*Gallinago media*): Male mating success and female behaviour at the lek
1994	Kjell Inge Reitan	Dr. scient Botany	Nutritional effects of algae in first-feeding of marine fish larvae
1994	Nils Røv	Dr. scient Zoology	Breeding distribution, population status and regulation of breeding numbers in the northeast-Atlantic Great Cormorant *Phalacrocorax carbo carbo*
1994	Annette-Susanne Hoepfner	Dr. scient Botany	Tissue culture techniques in propagation and breeding of Red Raspberry (*Rubus idaeus* L.)
1994	Inga Elise Bruteig	Dr. scient Botany	Distribution, ecology and biomonitoring studies of epiphytic lichens on conifers

1994	Geir Johnsen	Dr. scient Botany	Light harvesting and utilization in marine phytoplankton: Species-specific and photoadaptive responses
1994	Morten Bakken	Dr. scient Zoology	Infanticidal behaviour and reproductive performance in relation to competition capacity among farmed silver fox vixens, *Vulpes vulpes*
1994	Arne Moksnes	Dr. philos Zoology	Host adaptations towards brood parasitism by the Cockoo
1994	Solveig Bakken	Dr. scient Botany	Growth and nitrogen status in the moss *Dicranum majus* Sm. as influenced by nitrogen supply
1994	Torbjørn Forseth	Dr. scient Zoology	Bioenergetics in ecological and life history studies of fishes.
1995	Olav Vadstein	Dr. philos Botany	The role of heterotrophic planktonic bacteria in the cycling of phosphorus in lakes: Phosphorus requirement, competitive ability and food web interactions
1995	Hanne Christensen	Dr. scient Zoology	Determinants of Otter *Lutra lutra* distribution in Norway: Effects of harvest, polychlorinated biphenyls (PCBs), human population density and competition with mink *Mustela vision*
1995	Svein Håkon Lorentsen	Dr. scient Zoology	Reproductive effort in the Antarctic Petrel *Thalassoica antarctica*; the effect of parental body size and condition
1995	Chris Jørgen Jensen	Dr. scient Zoology	The surface electromyographic (EMG) amplitude as an estimate of upper trapezius muscle activity
1995	Martha Kold Bakkevig	Dr. scient Zoology	The impact of clothing textiles and construction in a clothing system on thermoregulatory responses, sweat accumulation and heat transport
1995	Vidar Moen	Dr. scient Zoology	Distribution patterns and adaptations to light in newly introduced populations of *Mysis relicta* and constraints on Cladoceran and Char populations
1995	Hans Haavardsholm Blom	Dr. philos Botany	A revision of the *Schistidium apocarpum* complex in Norway and Sweden
1996	Jorun Skjærmo	Dr. scient Botany	Microbial ecology of early stages of cultivated marine fish; inpact fish-bacterial interactions on growth and survival of larvae
1996	Ola Ugedal	Dr. scient Zoology	Radiocesium turnover in freshwater fishes
1996	Ingibjørg Einarsdottir	Dr. scient Zoology	Production of Atlantic salmon (*Salmo salar*) and Arctic charr (*Salvelinus alpinus*): A study of some physiological and immunological responses to rearing routines
1996	Christina M. S. Pereira	Dr. scient Zoology	Glucose metabolism in salmonids: Dietary effects and hormonal regulation
1996	Jan Fredrik Børseth	Dr. scient Zoology	The sodium energy gradients in muscle cells of *Mytilus edulis* and the effects of organic xenobiotics
1996	Gunnar Henriksen	Dr. scient Zoology	Status of Grey seal *Halichoerus grypus* and Harbour seal *Phoca vitulina* in the Barents sea region
1997	Gunvor Øie	Dr. scient Botany	Eevalution of rotifer *Brachionus plicatilis* quality in early first feeding of turbot *Scophtalmus maximus* L. larvae
1997	Håkon Holien	Dr. scient Botany	Studies of lichens in spurce forest of Central Norway. Diversity, old growth species and the relationship to site and stand parameters

1997	Ole Reitan	Dr. scient Zoology	Responses of birds to habitat disturbance due to damming
1997	Jon Arne Grøttum	Dr. scient Zoology	Physiological effects of reduced water quality on fish in aquaculture
1997	Per Gustav Thingstad	Dr. scient Zoology	Birds as indicators for studying natural and human-induced variations in the environment, with special emphasis on the suitability of the Pied Flycatcher
1997	Torgeir Nygård	Dr. scient Zoology	Temporal and spatial trends of pollutants in birds in Norway: Birds of prey and Willow Grouse used as
1997	Signe Nybø	Dr. scient Zoology	Impacts of long-range transported air pollution on birds with particular reference to the dipper *Cinclus cinclus* in southern Norway
1997	Atle Wibe	Dr. scient Zoology	Identification of conifer volatiles detected by receptor neurons in the pine weevil (*Hylobius abietis*), analysed by gas chromatography linked to electrophysiology and to mass spectrometry
1997	Rolv Lundheim	Dr. scient Zoology	Adaptive and incidental biological ice nucleators
1997	Arild Magne Landa	Dr. scient Zoology	Wolverines in Scandinavia: ecology, sheep depredation and conservation
1997	Kåre Magne Nielsen	Dr. scient Botany	An evolution of possible horizontal gene transfer from plants to sail bacteria by studies of natural transformation in *Acinetobacter calcoacetius*
1997	Jarle Tufto	Dr. scient Zoology	Gene flow and genetic drift in geographically structured populations: Ecological, population genetic, and statistical models
1997	Trygve Hesthagen	Dr. philos Zoology	Population responces of Arctic charr (*Salvelinus alpinus* (L.)) and brown trout (*Salmo trutta* L.) to acidification in Norwegian inland waters
1997	Trygve Sigholt	Dr. philos Zoology	Control of Parr-smolt transformation and seawater tolerance in farmed Atlantic Salmon (*Salmo salar*) Effects of photoperiod, temperature, gradual seawater acclimation, NaCl and betaine in the diet
1997	Jan Østnes	Dr. scient Zoology	Cold sensation in adult and neonate birds
1998	Seethaledsumy Visvalingam	Dr. scient Botany	Influence of environmental factors on myrosinases and myrosinase-binding proteins
1998	Thor Harald Ringsby	Dr. scient Zoology	Variation in space and time: The biology of a House sparrow metapopulation
1998	Erling Johan Solberg	Dr. scient Zoology	Variation in population dynamics and life history in a Norwegian moose (*Alces alces*) population: consequences of harvesting in a variable environment
1998	Sigurd Mjøen Saastad	Dr. scient Botany	Species delimitation and phylogenetic relationships between the Sphagnum recurvum complex (Bryophyta): genetic variation and phenotypic plasticity
1998	Bjarte Mortensen	Dr. scient Botany	Metabolism of volatile organic chemicals (VOCs) in a head liver S9 vial equilibration system in vitro
1998	Gunnar Austrheim	Dr. scient Botany	Plant biodiversity and land use in subalpine grasslands. – A conservtaion biological approach
1998	Bente Gunnveig Berg	Dr. scient Zoology	Encoding of pheromone information in two related moth species
1999	Kristian Overskaug	Dr. scient Zoology	Behavioural and morphological characteristics in Northern Tawny Owls *Strix aluco*: An intra- and interspecific comparative approach

1999	Hans Kristen Stenøien	Dr. scient Botany	Genetic studies of evolutionary processes in various populations of nonvascular plants (mosses, liverworts and hornworts)
1999	Trond Arnesen	Dr. scient Botany	Vegetation dynamics following trampling and burning in the outlying haylands at Sølendet, Central Norway
1999	Ingvar Stenberg	Dr. scient Zoology	Habitat selection, reproduction and survival in the White-backed Woodpecker *Dendrocopos leucotos*
1999	Stein Olle Johansen	Dr. scient Botany	A study of driftwood dispersal to the Nordic Seas by dendrochronology and wood anatomical analysis
1999	Trina Falck Galloway	Dr. scient Zoology	Muscle development and growth in early life stages of the Atlantic cod (*Gadus morhua* L.) and Halibut (*Hippoglossus hippoglossus* L.)
1999	Marianne Giæver	Dr. scient Zoology	Population genetic studies in three gadoid species: blue whiting (*Micromisistius poutassou*), haddock (*Melanogrammus aeglefinus*) and cod (*Gradus morhua*) in the North-East Atlantic
1999	Hans Martin Hanslin	Dr. scient Botany	The impact of environmental conditions of density dependent performance in the boreal forest bryophytes *Dicranum majus*, *Hylocomium splendens*, *Plagiochila asplenigides*, *Ptilium crista-castrensis* and *Rhytidiadelphus lokeus*
1999	Ingrid Bysveen Mjølnerød	Dr. scient Zoology	Aspects of population genetics, behaviour and performance of wild and farmed Atlantic salmon (*Salmo salar*) revealed by molecular genetic techniques
1999	Else Berit Skagen	Dr. scient Botany	The early regeneration process in protoplasts from *Brassica napus* hypocotyls cultivated under various g-forces
1999	Stein-Are Sæther	Dr. philos Zoology	Mate choice, competition for mates, and conflicts of interest in the Lekking Great Snipe
1999	Katrine Wangen Rustad	Dr. scient Zoology	Modulation of glutamatergic neurotransmission related to cognitive dysfunctions and Alzheimer's disease
1999	Per Terje Smiseth	Dr. scient Zoology	Social evolution in monogamous families:
1999	Gunnbjørn Bremset	Dr. scient Zoology	Young Atlantic salmon (*Salmo salar* L.) and Brown trout (*Salmo trutta* L.) inhabiting the deep pool habitat, with special reference to their habitat use, habitat preferences and competitive interactions
1999	Frode Ødegaard	Dr. scient Zoology	Host spesificity as parameter in estimates of arhrophod species richness
1999	Sonja Andersen	Dr. scient Zoology	Expressional and functional analyses of human, secretory phospholipase A2
2000	Ingrid Salvesen	Dr. scient Botany	Microbial ecology in early stages of marine fish: Development and evaluation of methods for microbial management in intensive larviculture
2000	Ingar Jostein Øien	Dr. scient Zoology	The Cuckoo (*Cuculus canorus*) and its host: adaptions and counteradaptions in a coevolutionary arms race
2000	Pavlos Makridis	Dr. scient Botany	Methods for the microbial econtrol of live food used for the rearing of marine fish larvae
2000	Sigbjørn Stokke	Dr. scient Zoology	Sexual segregation in the African elephant (*Loxodonta africana*)
2000	Odd A. Gulseth	Dr. philos Zoology	Seawater tolerance, migratory behaviour and growth of Charr, (*Salvelinus alpinus*), with emphasis on the high Arctic Dieset charr on Spitsbergen, Svalbard

2000	Pål A. Olsvik	Dr. scient Zoology	Biochemical impacts of Cd, Cu and Zn on brown trout (*Salmo trutta*) in two mining-contaminated rivers in Central Norway
2000	Sigurd Einum	Dr. scient Zoology	Maternal effects in fish: Implications for the evolution of breeding time and egg size
2001	Jan Ove Evjemo	Dr. scient Zoology	Production and nutritional adaptation of the brine shrimp *Artemia* sp. as live food organism for larvae of marine cold water fish species
2001	Olga Hilmo	Dr. scient Botany	Lichen response to environmental changes in the managed boreal forset systems
2001	Ingebrigt Uglem	Dr. scient Zoology	Male dimorphism and reproductive biology in corkwing wrasse (*Symphodus melops* L.)
2001	Bård Gunnar Stokke	Dr. scient Zoology	Coevolutionary adaptations in avian brood parasites and their hosts
2002	Ronny Aanes	Dr. scient Zoology	Spatio-temporal dynamics in Svalbard reindeer (*Rangifer tarandus platyrhynchus*)
2002	Mariann Sandsund	Dr. scient Zoology	Exercise- and cold-induced asthma. Respiratory and thermoregulatory responses
2002	Dag-Inge Øien	Dr. scient Botany	Dynamics of plant communities and populations in boreal vegetation influenced by scything at Sølendet, Central Norway
2002	Frank Rosell	Dr. scient Zoology	The function of scent marking in beaver (*Castor fiber*)
2002	Janne Østvang	Dr. scient Botany	The Role and Regulation of Phospholipase A_2 in Monocytes During Atherosclerosis Development
2002	Terje Thun	Dr. philos Biology	Dendrochronological constructions of Norwegian conifer chronologies providing dating of historical material
2002	Birgit Hafjeld Borgen	Dr. scient Biology	Functional analysis of plant idioblasts (Myrosin cells) and their role in defense, development and growth
2002	Bård Øyvind Solberg	Dr. scient Biology	Effects of climatic change on the growth of dominating tree species along major environmental gradients
2002	Per Winge	Dr. scient Biology	The evolution of small GTP binding proteins in cellular organisms. Studies of RAC GTPases in *Arabidopsis thaliana* and the Ral GTPase from *Drosophila melanogaster*
2002	Henrik Jensen	Dr. scient Biology	Causes and consequenses of individual variation in fitness-related traits in house sparrows
2003	Jens Rohloff	Dr. philos Biology	Cultivation of herbs and medicinal plants in Norway – Essential oil production and quality control
2003	Åsa Maria O. Espmark Wibe	Dr. scient Biology	Behavioural effects of environmental pollution in threespine stickleback *Gasterosteus aculeatur* L.
2003	Dagmar Hagen	Dr. scient Biology	Assisted recovery of disturbed arctic and alpine vegetation – an integrated approach
2003	Bjørn Dahle	Dr. scient Biology	Reproductive strategies in Scandinavian brown bears
2003	Cyril Lebogang Taolo	Dr. scient Biology	Population ecology, seasonal movement and habitat use of the African buffalo (*Syncerus caffer*) in Chobe National Park, Botswana
2003	Marit Stranden	Dr. scient Biology	Olfactory receptor neurones specified for the same odorants in three related Heliothine species (*Helicoverpa armigera, Helicoverpa assulta* and *Heliothis virescens*)
2003	Kristian Hassel	Dr. scient Biology	Life history characteristics and genetic variation in an expanding species, *Pogonatum dentatum*

2003	David Alexander Rae	Dr. scient Biology	Plant- and invertebrate-community responses to species interaction and microclimatic gradients in alpine and Artic environments
2003	Åsa A Borg	Dr. scient Biology	Sex roles and reproductive behaviour in gobies and guppies: a female perspective
2003	Eldar Åsgard Bendiksen	Dr. scient Biology	Environmental effects on lipid nutrition of farmed Atlantic salmon (*Salmo Salar* L.) parr and smolt
2004	Torkild Bakken	Dr. scient Biology	A revision of Nereidinae (Polychaeta, Nereididae)
2004	Ingar Pareliussen	Dr. scient Biology	Natural and Experimental Tree Establishment in a Fragmented Forest, Ambohitantely Forest Reserve, Madagascar
2004	Tore Brembu	Dr. scient Biology	Genetic, molecular and functional studies of RAC GTPases and the WAVE-like regulatory protein complex in *Arabidopsis thaliana*
2004	Liv S. Nilsen	Dr. scient Biology	Coastal heath vegetation on central Norway; recent past, present state and future possibilities
2004	Hanne T. Skiri	Dr. scient Biology	Olfactory coding and olfactory learning of plant odours in heliothine moths. An anatomical, physiological and behavioural study of three related species (*Heliothis virescens, Helicoverpa armigera* and *Helicoverpa assulta*)
2004	Lene Østby	Dr. scient Biology	Cytochrome P4501A (CYP1A) induction and DNA adducts as biomarkers for organic pollution in the natural environment
2004	Emmanuel J. Gerreta	Dr. philos Biology	The Importance of Water Quality and Quantity in the Tropical Ecosystems, Tanzania
2004	Linda Dalen	Dr. scient Biology	Dynamics of Mountain Birch Treelines in the Scandes Mountain Chain, and Effects of Climate Warming
2004	Lisbeth Mehli	Dr. scient Biology	Polygalacturonase-inhibiting protein (PGIP) in cultivated strawberry (*Fragaria* x *ananassa*): characterisation and induction of the gene following fruit infection by *Botrytis cinerea*
2004	Børge Moe	Dr. scient Biology	Energy-Allocation in Avian Nestlings Facing Short-Term Food Shortage
2005	Matilde Skogen Chauton	Dr. scient Biology	Metabolic profiling and species discrimination from High-Resolution Magic Angle Spinning NMR analysis of whole-cell samples
2005	Sten Karlsson	Dr. scient Biology	Dynamics of Genetic Polymorphisms
2005	Terje Bongard	Dr. scient Biology	Life History strategies, mate choice, and parental investment among Norwegians over a 300-year period
2005	Tonette Røstelien	PhD Biology	Functional characterisation of olfactory receptor neurone types in heliothine moths
2005	Erlend Kristiansen	Dr. scient Biology	Studies on antifreeze proteins
2005	Eugen G. Sørmo	Dr. scient Biology	Organochlorine pollutants in grey seal (*Halichoerus grypus*) pups and their impact on plasma thyrid hormone and vitamin A concentrations
2005	Christian Westad	Dr. scient Biology	Motor control of the upper trapezius
2005	Lasse Mork Olsen	PhD Biology	Interactions between marine osmo- and phagotrophs in different physicochemical environments
2005	Åslaug Viken	PhD Biology	Implications of mate choice for the management of small populations

2005	Ariaya Hymete Sahle Dingle	PhD Biology	Investigation of the biological activities and chemical constituents of selected *Echinops* spp. growing in Ethiopia
2005	Anders Gravbrøt Finstad	PhD Biology	Salmonid fishes in a changing climate: The winter challenge
2005	Shimane Washington Makabu	PhD Biology	Interactions between woody plants, elephants and other browsers in the Chobe Riverfront, Botswana
2005	Kjartan Østbye	Dr. scient Biology	The European whitefish *Coregonus lavaretus* (L.) species complex: historical contingency and adaptive radiation
2006	Kari Mette Murvoll	PhD Biology	Levels and effects of persistent organic pollutans (POPs) in seabirds, Retinoids and α-tocopherol – potential biomakers of POPs in birds?
2006	Ivar Herfindal	Dr. scient Biology	Life history consequences of environmental variation along ecological gradients in northern ungulates
2006	Nils Egil Tokle	PhD Biology	Are the ubiquitous marine copepods limited by food or predation? Experimental and field-based studies with main focus on *Calanus finmarchicus*
2006	Jan Ove Gjershaug	Dr. philos Biology	Taxonomy and conservation status of some booted eagles in south-east Asia
2006	Jon Kristian Skei	Dr. scient Biology	Conservation biology and acidification problems in the breeding habitat of amphibians in Norway
2006	Johanna Järnegren	PhD Biology	Acesta Oophaga and Acesta Excavata – a study of hidden biodiversity
2006	Bjørn Henrik Hansen	PhD Biology	Metal-mediated oxidative stress responses in brown trout (*Salmo trutta*) from mining contaminated rivers in Central Norway
2006	Vidar Grøtan	PhD Biology	Temporal and spatial effects of climate fluctuations on population dynamics of vertebrates
2006	Jafari R Kideghesho	PhD Biology	Wildlife conservation and local land use conflicts in western Serengeti, Corridor Tanzania
2006	Anna Maria Billing	PhD Biology	Reproductive decisions in the sex role reversed pipefish *Syngnathus typhle*: when and how to invest in reproduction
2006	Henrik Pärn	PhD Biology	Female ornaments and reproductive biology in the bluethroat
2006	Anders J. Fjellheim	PhD Biology	Selection and administration of probiotic bacteria to marine fish larvae
2006	P. Andreas Svensson	PhD Biology	Female coloration, egg carotenoids and reproductive success: gobies as a model system
2007	Sindre A. Pedersen	PhD Biology	Metal binding proteins and antifreeze proteins in the beetle *Tenebrio molitor* - a study on possible competition for the semi-essential amino acid cysteine
2007	Kasper Hancke	PhD Biology	Photosynthetic responses as a function of light and temperature: Field and laboratory studies on marine microalgae
2007	Tomas Holmern	PhD Biology	Bushmeat hunting in the western Serengeti: Implications for community-based conservation
2007	Kari Jørgensen	PhD Biology	Functional tracing of gustatory receptor neurons in the CNS and chemosensory learning in the moth *Heliothis virescens*
2007	Stig Ulland	PhD Biology	Functional Characterisation of Olfactory Receptor Neurons in the Cabbage Moth, (*Mamestra brassicae* L.) (Lepidoptera, Noctuidae). Gas Chromatography

			Linked to Single Cell Recordings and Mass Spectrometry
2007	Snorre Henriksen	PhD Biology	Spatial and temporal variation in herbivore resources at northern latitudes
2007	Roelof Frans May	PhD Biology	Spatial Ecology of Wolverines in Scandinavia
2007	Vedasto Gabriel Ndibalema	PhD Biology	Demographic variation, distribution and habitat use between wildebeest sub-populations in the Serengeti National Park, Tanzania
2007	Julius William Nyahongo	PhD Biology	Depredation of Livestock by wild Carnivores and Illegal Utilization of Natural Resources by Humans in the Western Serengeti, Tanzania
2007	Shombe Ntaraluka Hassan	PhD Biology	Effects of fire on large herbivores and their forage resources in Serengeti, Tanzania
2007	Per-Arvid Wold	PhD Biology	Functional development and response to dietary treatment in larval Atlantic cod *(Gadus morhua* L.) Focus on formulated diets and early weaning
2007	Anne Skjetne Mortensen	PhD Biology	Toxicogenomics of Aryl Hydrocarbon- and Estrogen Receptor Interactions in Fish: Mechanisms and Profiling of Gene Expression Patterns in Chemical Mixture Exposure Scenarios
2008	Brage Bremset Hansen	PhD Biology	The Svalbard reindeer (*Rangifer tarandus platyrhynchus*) and its food base: plant-herbivore interactions in a high-arctic ecosystem
2008	Jiska van Dijk	PhD Biology	Wolverine foraging strategies in a multiple-use landscape
2008	Flora John Magige	PhD Biology	The ecology and behaviour of the Masai Ostrich (Struthio camelus massaicus) in the Serengeti Ecosystem, Tanzania
2008	Bernt Rønning	PhD Biology	Sources of inter- and intra-individual variation in basal metabolic rate in the zebra finch, (*Taeniopygia guttata*)
2008	Sølvi Wehn	PhD Biology	Biodiversity dynamics in semi-natural mountain landscapes - A study of consequences of changed agricultural practices in Eastern Jotunheimen
2008	Trond Moxness Kortner	PhD Biology	"The Role of Androgens on previtellogenic oocyte growth in Atlantic cod (*Gadus morhua*): Identification and patterns of differentially expressed genes in relation to Stereological Evaluations"
2008	Katarina Mariann Jørgensen	Dr. scient Biology	The role of platelet activating factor in activation of growth arrested keratinocytes and re-epithelialisation
2008	Tommy Jørstad	PhD Biology	Statistical Modelling of Gene Expression Data
2008	Anna Kusnierczyk	PhD Biology	*Arabidopsis thaliana* Responses to Aphid Infestation
2008	Jussi Evertsen	PhD Biology	Herbivore sacoglossans with photosynthetic chloroplasts
2008	John Eilif Hermansen	PhD Biology	Mediating ecological interests between locals and globals by means of indicators. A study attributed to the asymmetry between stakeholders of tropical forest at Mt. Kilimanjaro, Tanzania
2008	Ragnhild Lyngved	PhD Biology	Somatic embryogenesis in *Cyclamen persicum.* Biological investigations and educational aspects of cloning
2008	Line Elisabeth Sundt-Hansen	PhD Biology	Cost of rapid growth in salmonid fishes

2008	Line Johansen	PhD Biology	Exploring factors underlying fluctuations in white clover populations – clonal growth, population structure and spatial distribution
2009	Astrid Jullumstrø Feuerherm	PhD Biology	Elucidation of molecular mechanisms for pro-inflammatory phospholipase A2 in chronic disease
2009	Pål Kvello	PhD Biology	Neurons forming the network involved in gustatory coding and learning in the moth *Heliothis virescens*: Physiological and morphological characterisation, and integration into a standard brain atlas
2009	Trygve Devold Kjellsen	PhD Biology	Extreme Frost Tolerance in Boreal Conifers
2009	Johan Reinert Vikan	PhD Biology	Coevolutionary interactions between common cuckoos *Cuculus canorus* and *Fringilla* finches
2009	Zsolt Volent	PhD Biology	Remote sensing of marine environment: Applied surveillance with focus on optical properties of phytoplankton, coloured organic matter and suspended matter
2009	Lester Rocha	PhD Biology	Functional responses of perennial grasses to simulated grazing and resource availability
2009	Dennis Ikanda	PhD Biology	Dimensions of a Human-lion conflict: Ecology of human predation and persecution of African lions (*Panthera leo*) in Tanzania
2010	Huy Quang Nguyen	PhD Biology	Egg characteristics and development of larval digestive function of cobia (*Rachycentron canadum*) in response to dietary treatments - Focus on formulated diets
2010	Eli Kvingedal	PhD Biology	Intraspecific competition in stream salmonids: the impact of environment and phenotype
2010	Sverre Lundemo	PhD Biology	Molecular studies of genetic structuring and demography in *Arabidopsis* from Northern Europe
2010	Iddi Mihijai Mfunda	PhD Biology	Wildlife Conservation and People's livelihoods: Lessons Learnt and Considerations for Improvements. Tha Case of Serengeti Ecosystem, Tanzania
2010	Anton Tinchov Antonov	PhD Biology	Why do cuckoos lay strong-shelled eggs? Tests of the puncture resistance hypothesis
2010	Anders Lyngstad	PhD Biology	Population Ecology of *Eriophorum latifolium*, a Clonal Species in Rich Fen Vegetation
2010	Hilde Færevik	PhD Biology	Impact of protective clothing on thermal and cognitive responses
2010	Ingerid Brænne Arbo	PhD Medical technology	Nutritional lifestyle changes – effects of dietary carbohydrate restriction in healthy obese and overweight humans
2010	Yngvild Vindenes	PhD Biology	Stochastic modeling of finite populations with individual heterogeneity in vital parameters
2010	Hans-Richard Brattbakk	PhD Medical technology	The effect of macronutrient composition, insulin stimulation, and genetic variation on leukocyte gene expression and possible health benefits
2011	Geir Hysing Bolstad	PhD Biology	Evolution of Signals: Genetic Architecture, Natural Selection and Adaptive Accuracy
2011	Karen de Jong	PhD Biology	Operational sex ratio and reproductive behaviour in the two-spotted goby (*Gobiusculus flavescens*)
2011	Ann-Iren Kittang	PhD Biology	*Arabidopsis thaliana* L. adaptation mechanisms to microgravity through the EMCS MULTIGEN-2 experiment on the ISS:– The science of space experiment integration and adaptation to simulated microgravity

2011	Aline Magdalena Lee	PhD Biology	Stochastic modeling of mating systems and their effect on population dynamics and genetics
2011	Christopher Gravningen Sørmo	PhD Biology	Rho GTPases in Plants: Structural analysis of ROP GTPases; genetic and functional studies of MIRO GTPases in Arabidopsis thaliana
2011	Grethe Robertsen	PhD Biology	Relative performance of salmonid phenotypes across environments and competitive intensities
2011	Line-Kristin Larsen	PhD Biology	Life-history trait dynamics in experimental populations of guppy (*Poecilia reticulata*): the role of breeding regime and captive environment
2011	Maxim A. K. Teichert	PhD Biology	Regulation in Atlantic salmon (*Salmo salar*): The interaction between habitat and density
2011	Torunn Beate Hancke	PhD Biology	Use of Pulse Amplitude Modulated (PAM) Fluorescence and Bio-optics for Assessing Microalgal Photosynthesis and Physiology
2011	Sajeda Begum	PhD Biology	Brood Parasitism in Asian Cuckoos: Different Aspects of Interactions between Cuckoos and their Hosts in Bangladesh
2011	Kari J. K. Attramadal	PhD Biology	Water treatment as an approach to increase microbial control in the culture of cold water marine larvae
2011	Camilla Kalvatn Egset	PhD Biology	The Evolvability of Static Allometry: A Case Study
2011	AHM Raihan Sarker	PhD Biology	Conflict over the conservation of the Asian elephant (*Elephas maximus*) in Bangladesh
2011	Gro Dehli Villanger	PhD Biology	Effects of complex organohalogen contaminant mixtures on thyroid hormone homeostasis in selected arctic marine mammals
2011	Kari Bjørneraas	PhD Biology	Spatiotemporal variation in resource utilisation by a large herbivore, the moose
2011	John Odden	PhD Biology	The ecology of a conflict: Eurasian lynx depredation on domestic sheep
2011	Simen Pedersen	PhD Biology	Effects of native and introduced cervids on small mammals and birds
2011	Mohsen Falahati-Anbaran	PhD Biology	Evolutionary consequences of seed banks and seed dispersal in *Arabidopsis*
2012	Jakob Hønborg Hansen	PhD Biology	Shift work in the offshore vessel fleet: circadian rhythms and cognitive performance
2012	Elin Noreen	PhD Biology	Consequences of diet quality and age on life-history traits in a small passerine bird
2012	Irja Ida Ratikainen	PhD Biology	Foraging in a variable world:adaptions to stochasticity
2012	Aleksander Handå	PhD Biology	Cultivation of mussels (*Mytilus edulis*):Feed requirements, storage and integration with salmon (*Salmo salar*) farming
2012	Morten Kraabøl	PhD Biology	Reproductive and migratory challenges inflicted on migrant brown trour (*Salmo trutta* L) in a heavily modified river
2012	Jisca Huisman	PhD Biology	Gene flow and natural selection in Atlantic salmon
2012	Maria Bergvik	PhD Biology	Lipid and astaxanthin contents and biochemical post-harvest stability in *Calanus finmarchicus*
2012	Bjarte Bye Løfaldli	PhD Biology	Functional and morphological characterization of central olfactory neurons in the model insect *Heliothis virescens*.

2012	Karen Marie Hammer	PhD Biology	Acid-base regulation and metabolite responses in shallow- and deep-living marine invertebrates during environmental hypercapnia
2012	Øystein Nordrum Wiggen	PhD Biology	Optimal performance in the cold
2012	Robert Dominikus Fyumagwa	Dr. Philos Biology	Anthropogenic and natural influence on disease prevalence at the human –livestock-wildlife interface in the Serengeti ecosystem, Tanzania
2012	Jenny Bytingsvik	PhD Biology	Organohalogenated contaminants (OHCs) in polar bear mother-cub pairs from Svalbard, Norway. Maternal transfer, exposure assessment and thyroid hormone disruptive effects in polar bear cubs
2012	Christer Moe Rolandsen	PhD Biology	The ecological significance of space use and movement patterns of moose in a variable environment
2012	Erlend Kjeldsberg Hovland	PhD Biology	Bio-optics and Ecology in *Emiliania huxleyi* Blooms: Field and Remote Sensing Studies in Norwegian Waters
2012	Lise Cats Myhre	PhD Biology	Effects of the social and physical environment on mating behaviour in a marine fish
2012	Tonje Aronsen	PhD Biology	Demographic, environmental and evolutionary aspects of sexual selection
2012	Bin Liu	PhD Biology	Molecular genetic investigation of cell separation and cell death regulation in *Arabidopsis thaliana*
2013	Jørgen Rosvold	PhD Biology	Ungulates in a dynamic and increasingly human dominated landscape – A millennia-scale perspective
2013	Pankaj Barah	PhD Biology	Integrated Systems Approaches to Study Plant Stress Responses
2013	Marit Linnerud	PhD Biology	Patterns in spatial and temporal variation in population abundances of vertebrates
2013	Xinxin Wang	PhD Biology	Integrated multi-trophic aquaculture driven by nutrient wastes released from Atlantic salmon (*Salmo salar*) farming
2013	Ingrid Ertshus Mathisen	PhD Biology	Structure, dynamics, and regeneration capacity at the sub-arctic forest-tundra ecotone of northern Norway and Kola Peninsula, NW Russia
2013	Anders Foldvik	PhD Biology	Spatial distributions and productivity in salmonid populations
2013	Anna Marie Holand	PhD Biology	Statistical methods for estimating intra- and inter-population variation in genetic diversity
2013	Anna Solvang Båtnes	PhD Biology	Light in the dark – the role of irradiance in the high Arctic marine ecosystem during polar night
2013	Sebastian Wacker	PhD Biology	The dynamics of sexual selection: effects of OSR, density and resource competition in a fish
2013	Cecilie Miljeteig	PhD Biology	Phototaxis in *Calanus finmarchicus* – light sensitivity and the influence of energy reserves and oil exposure
2013	Ane Kjersti Vie	PhD Biology	Molecular and functional characterisation of the IDA family of signalling peptides in *Arabidopsis thaliana*
2013	Marianne Nymark	PhD Biology	Light responses in the marine diatom *Phaeodactylum tricornutum*
2014	Jannik Schultner	PhD Biology	Resource Allocation under Stress - Mechanisms and Strategies in a Long-Lived Bird
2014	Craig Ryan Jackson	PhD Biology	Factors influencing African wild dog *(Lycaon pictus)* habitat selection and ranging behaviour: conservation and management implications

2014	Aravind Venkatesan	PhD Biology	Application of Semantic Web Technology to establish knowledge management and discovery in the Life Sciences
2014	Kristin Collier Valle	PhD Biology	Photoacclimation mechanisms and light responses in marine micro- and macroalgae
2014	Michael Puffer	PhD Biology	Effects of rapidly fluctuating water levels on juvenile Atlantic salmon (*Salmo salar* L.)
2014	Gundula S. Bartzke	PhD Biology	Effects of power lines on moose *(Alces alces)* habitat selection, movements and feeding activity
2014	Eirin Marie Bjørkvoll	PhD Biology	Life-history variation and stochastic population dynamics in vertebrates
2014	Håkon Holand	PhD Biology	The parasite *Syngamus trachea* in a metapopulation of house sparrows
2014	Randi Magnus Sommerfelt	PhD Biology	Molecular mechanisms of inflammation – a central role for cytosolic phospholiphase A2
2014	Espen Lie Dahl	PhD Biology	Population demographics in white-tailed eagle at an on-shore wind farm area in coastal Norway
2014	Anders Øverby	PhD Biology	Functional analysis of the action of plant isothiocyanates: cellular mechanisms and in vivo role in plants, and anticancer activity
2014	Kamal Prasad Acharya	PhD Biology	Invasive species: Genetics, characteristics and trait variation along a latitudinal gradient.
2014	Ida Beathe Øverjordet	PhD Biology	Element accumulation and oxidative stress variables in Arctic pelagic food chains: Calanus, little auks (alle alle) and black-legged kittiwakes (Rissa tridactyla)
2014	Kristin Møller Gabrielsen	PhD Biology	Target tissue toxicity of the thyroid hormone system in two species of arctic mammals carrying high loads of organohalogen contaminants
2015	Gine Roll Skjervø	Dr. philos Biology	Testing behavioral ecology models with historical individual-based human demographic data from Norway
2015	Nils Erik Gustaf Forsberg	PhD Biology	Spatial and Temporal Genetic Structure in Landrace Cereals
2015	Leila Alipanah	PhD Biology	Integrated analyses of nitrogen and phosphorus deprivation in the diatoms *Phaeodactylum tricornutum* and *Seminavis robusta*
2015	Javad Najafi	PhD Biology	Molecular investigation of signaling components in sugar sensing and defense in *Arabidopsis thaliana*
2015	Bjørnar Sporsheim	PhD Biology	Quantitative confocal laser scanning microscopy: optimization of in vivo and in vitro analysis of intracellular transport
2015	Magni Olsen Kyrkjeeide	PhD Biology	Genetic variation and structure in peatmosses (*Sphagnum*)
2015	Keshuai Li	PhD Biology	Phospholipids in Atlantic cod (*Gadus morhua* L.) larvae rearing: Incorporation of DHA in live feed and larval phospholipids and the metabolic capabilities of larvae for the de novo synthesis
2015	Ingvild Fladvad Størdal	PhD Biology	The role of the copepod *Calanus finmarchicus* in affecting the fate of marine oil spills
2016	Thomas Kvalnes	PhD Biology	Evolution by natural selection in age-structured populations in fluctuating environments
2016	Øystein Leiknes	PhD Biology	The effect of nutrition on important life-history traits in the marine copepod *Calanus finmarchicus*

2016	Johan Henrik Hårdensson Berntsen	PhD Biology	Individual variation in survival: The effect of incubation temperature on the rate of physiological ageing in a small passerine bird
2016	Marianne Opsahl Olufsen	PhD Biology	Multiple environmental stressors: Biological interactions between parameters of climate change and perfluorinated alkyl substances in fish
2016	Rebekka Varne	PhD Biology	Tracing the fate of escaped cod (*Gadus morhua* L.) in a Norwegian fjord system
2016	Anette Antonsen Fenstad	PhD Biology	Pollutant Levels, Antioxidants and Potential Genotoxic Effects in Incubating Female Common Eiders (*Somateria mollissima*)
2016	Wilfred Njama Marealle	PhD Biology	Ecology, Behaviour and Conservation Status of Masai Giraffe (***Giraffa camelopardalis tippelskirchi***) in Tanzania
2016	Ingunn Nilssen	PhD Biology	Integrated Enviromental Mapping and Monitoring: A Methodological approach for endusers.
2017	Konika Chawla	PhD Biology	Discovering, analysing and taking care of knowledge.
2017	Øystein Hjorthol Opedal	PhD Biology	The Evolution of Herkogamy: Pollinator Reliability, Natural Selection, and Trait Evolvability.
2017	Ane Marlene Myhre	PhD Biology	Effective size of density dependent populations in fluctuating environments
2017	Emmanuel Hosiana Masenga	PhD Biology	Behavioural Ecology of Free-ranging and Reintroduced African Wild Dog (Lycaon pictus) Packs in the Serengeti Ecosystem, Tanzania
2017	Xiaolong Lin	PhD Biology	Systematics and evolutionary history of Tanytarsus van der Wulp, 1874 (Diptera: Chironomidae)
2017	Emmanuel Clamsen Mmassy	PhD Biology	Ecology and Conservation Challenges of the Kori bustard in the Serengeti National Park
2017	Richard Daniel Lyamuya	PhD Biology	Depredation of Livestock by Wild Carnivores in the Eastern Serengeti Ecosystem, Tanzania
2017	Katrin Hoydal	PhD Biology	Levels and endocrine disruptive effects of legacy POPs and their metabolites in long-finned pilot whales of the Faroe Islands
2017	Berit Glomstad	PhD Biology	Adsorption of phenanthrene to carbon nanotubes and its influence on phenanthrene bioavailability/toxixity in aquatic organism
2017	Øystein Nordeide Kielland	PhD Biology	Sources of variation in metabolism of an aquatic ectotherm
2017	Narjes Yousefi	PhD Biology	Genetic divergence and speciation in northern peatmosses (*Sphagnum*)
2018	Signe Christensen-Dalgaard	PhD Biology	Drivers of seabird spatial ecology - implications for development of offshore wind-power in Norway
2018	Janos Urbancsok	PhD Biology	Endogenous biological effects induced by externally supplemented glucosinolate hydrolysis products (GHPs) on Arabidopsis thaliana
2018	Alice Mühlroth	PhD Biology	The influence of phosphate depletion on lipid metabolism of microalgae
2018	Franco Peniel Mbise	PhD Biology	Human-Carnivore Coexistence and Conflict in the Eastern Serengeti, Tanzania